TOUGHNESS AND ABRASION RESISTANCE OF HIGH ALLOY CAST IRON.

David William John Elwell.

Submitted for the degree of Doctor
of
Philosophy.

Aston University.

March 1986

Title:	Toughness and abrasion resistance of high alloy cast iron.
Name:	David William John Elwell.
Degree:	Ph.D.
Year:	1986.

Summary.

High chromium cast irons have been recognised as a hard, wear resistant alloy for use in crushing, grinding and material handling applications. The successful operation of these wear resistant components has been limited by their inherent brittleness and failure to withstand impact conditions.

Laboratory work has shown that the fracture toughness of a molybdenum alloyed high chromium cast iron can be significantly increased by carrying out a specialised high temperature heat treatment which modifies the eutectic carbide morphology.

Trial swing hammer castings have been produced and treated to attain a suitably modified carbide morphology. Microstructural examination of the alloy together with fracture toughness evaluation at specific specimen locations have been carried out. A matrix leeching technique has been used to observe the changes in carbide morphology. After 16 months service a returned casting was examined as described and in addition the wear damage was analysed and micro mechanisms suggested. Conventionally heat treated material was also examined in the unused condition and the results compared with the specially processed alloy.

High temperature heat treatments have been observed to have a significant effect in modifying eutectic carbide morphology and a less angular, more spheroidised carbide has been produced. The short bar fracture toughness specimen has been found to be capable of descriminating between austenitic and martensitic matrix alloys, the austenitic material having the higher toughness. Two distinctly different wear regimes have been identified as operating during service. The characteristics of these regimes have been related to the mechanics of the particular size reduction process studied.

Key words: High chromium cast irons, fracture,
abrasion resistance, carbide morphology.

CONTENTS.

List of Figures.

List of Tables.

List of Plates.

Appendix:

Acknowledgements.

I would like to express my appreciation to Professor J.T.Barnby of Aston University and Dr.R.W.Durman of Bradley and Foster Limited for their guidance and comments throughout this research. I would also like to record my gratitude to Dr.R.S.Jackson of Aston University and Dr.J.T.H.Pearce of West Bromwich College of Commerce and Technology for their helpful discussions. My thanks to the staff of Aston University and Bradley and Foster Limited for their assistance and especially Mrs.V.Shore for the typing of this thesis.

I must also express my gratitude to the Management of Blue Circle Industries, Weardale Works for their interest and willingness to participate in the service trials of the developed components.

-o-o-o-o-o-o-

Toughness and abrasion resistance of high alloy cast iron.

Summary.

High chromium cast irons have been recognised as a hard, wear resistant alloy for use in crushing, grinding and material handling applications. The successful operation of these wear resistant components has been limited by their inherent brittleness and failure to withstand impact conditions.

Laboratory work has shown that the fracture toughness of a molybdenum alloyed high chromium cast iron can be significantly increased by carrying out a specialised high temperature heat treatment which modifies the eutectic carbide morphology.

Trial swing hammer castings have been produced and treated to attain a suitably modified carbide morphology. Microstructural examination of the alloy together with fracture toughness evaluation at specific specimen locations have been carried out. A matrix leeching technique has been used to observe the changes in carbide morphology. After 16 months service a returned casting was examined as described and in addition the wear damage was analysed and micro mechanisms suggested. Conventionally heat treated material was also examined in the unused condition and the results compared with the specially processed alloy.

High temperature heat treatments have been observed to have a significant effect in modifying eutectic carbide morphology and a less angular, more spheroidised carbide has been produced. The short bar fracture toughness specimen has been found to be capable of descriminating between austenitic and martensitic matrix alloys, the austenitic material having the higher toughness. Two distinctly different wear regimes have been identified as operating during service. The characteristics of these regimes have been related to the mechanics of the particular size reduction process studied.

Key words: High chromium cast irons, fracture,
abrasion resistance, carbide morphology.

Introduction.

The material processing industry has a demand for abrasion resistant castings and for many years high chromium white cast irons have been used in the less arduous situations. The combined effects of the users trend towards larger plant and the casting producers search for new markets has resulted in the requirement for a tougher chromium cast iron.

Whereas the laboratory classification of wear resistance is a subjective procedure and possibly not representative of service conditions, toughness can be measured in terms of a critical stress intensity factor. This is a material property and often denoted by K_{IC} or referred to as fracture toughness. Failure of a component will occur when the factor at a crack tip exceeds this value. Conventional fracture toughness measurements involve protracted and expensive testing but a new fracture toughness specimen configuration, the short rod/short bar has been developed together with a suitable test machine, the Fractometer II. This equipment permits the relatively rapid and inexpensive assessment of fracture toughness.

Previous work has produced a high chromium white cast iron specification whose toughness can be significantly improved by a specialised high temperature heat treatment.

This research project, jointly sponsored by the Science and Engineering Research Council and Staveley Industries PLC, (represented by Bradley and Foster Limited) will 'extent and develop the previous work.

Trial castings subjected to the specialised high temperature vacuum process have been examined metallographically and for fracture toughness assessment both before and after service. In addition, a study of the abrasive wear mechanisms operating in the service environment and the interrelationship with microstructural features have been investigated.

1.0 WEAR.

1.1 Introduction

The significance of wear together with the more general topic of tribology must never be minimised. The definitions of the two terms provide an indication of their importance in any technologically orientated society.

> Tribology: "study of friction, wear, lubrication and design of bearings science of interacting surfaces in relative motion" (1)
>
> Wear: "the progressive loss of substance from the operating surface of a body occuring as a result of relative motion at the surface" (2)

It is therefore apparent that wear need not necessarily be a detrimental process as its definition also encompasses grinding and polishing.

The history of tribology has been comprehensively surveyed by Dowson (3) who related the chronological development of tribology (or perhaps more generally, technology) with the prevailing societies and cultures. The economic aspects of tribology have been rationalised by Jost (4) who estimated that by the better application of tribological principles and practices, industry in the U.K. could save about £515 M. annually (1965 values.) Halling (5) has since reported that experience has suggested that this figure was not unduly optimistic and in addition anticipated even greater savings as research activities expanded.

1.2 Classification of Wear.

The types of wear may be classified by describing either the results or the physical nature of the wear process. In general four mechanisms have been proposed (6) namely:

- i) Adhesive wear.
- ii) Abrasive wear.
- iii) Corrosive wear.
- iv) Fatigue wear.

While other groupings have also listed as "Minor types".

- v) Erosive wear.
- vi) Cavitation wear.

and more recently delamination has been proposed. (7)

Furthermore, each classification may contain a number of sub divisions.

1.2.1 The Adhesive Theory of Wear.

The model for the adhesive theory of wear has been based on asperity contact, deformation and subsequent shearing of two surfaces, (8) see Figure 1a. Initially only a small number of asperities are in contact and the application of a normal load, P, resulted in localised high pressures being achieved. Plastic deformation occurred until the real contact area was able to support the applied load. In the absence of surface films, or under the action of relative movement to disperse films, the surfaces adhered (sometimes referred to as pseudo-welding) continued sliding sheared these initial junctions and allowed new ones to form. In such a model, the wear rate would naturally depend on the location of the failed segment and their tendency to detach from the surface to form wear debris.

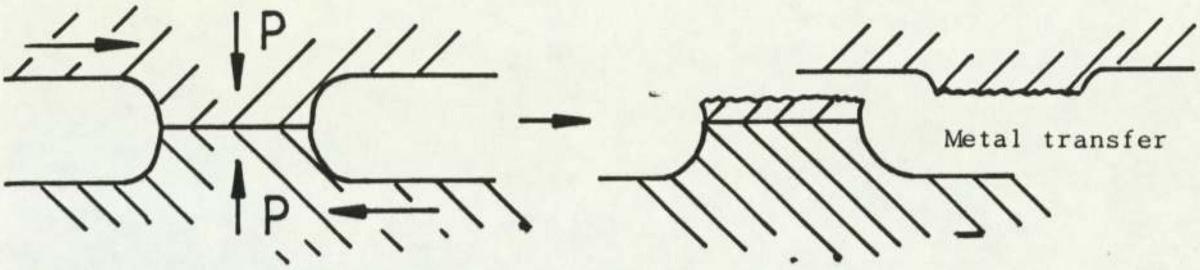

1.1 (a)
Adhesive Wear.

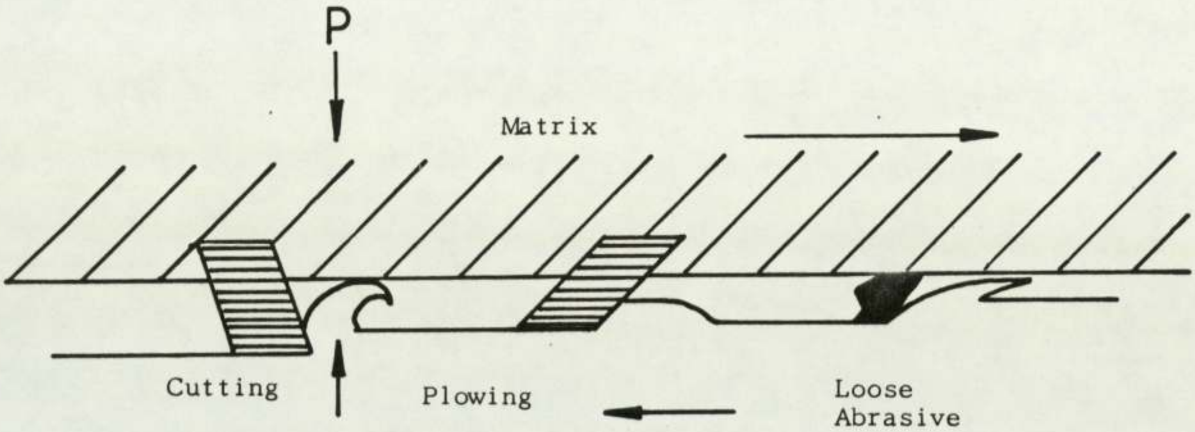

1.1 (b)
Abrasive Wear.

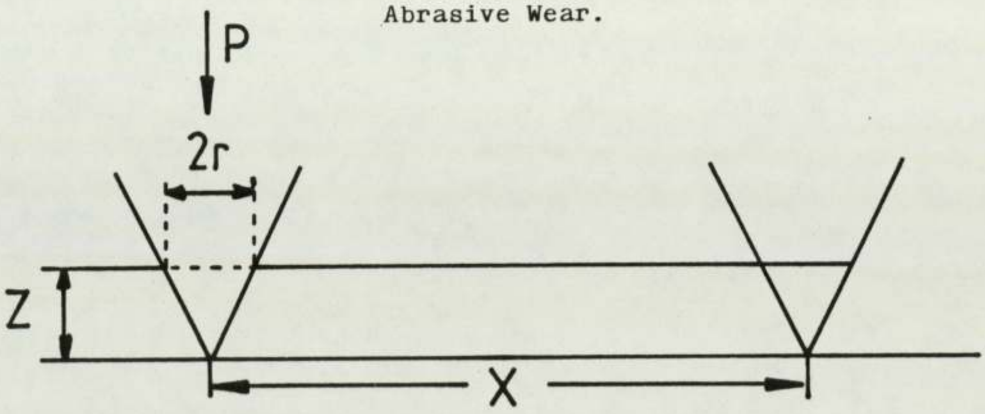

1.1 (c)
Abrasive Wear

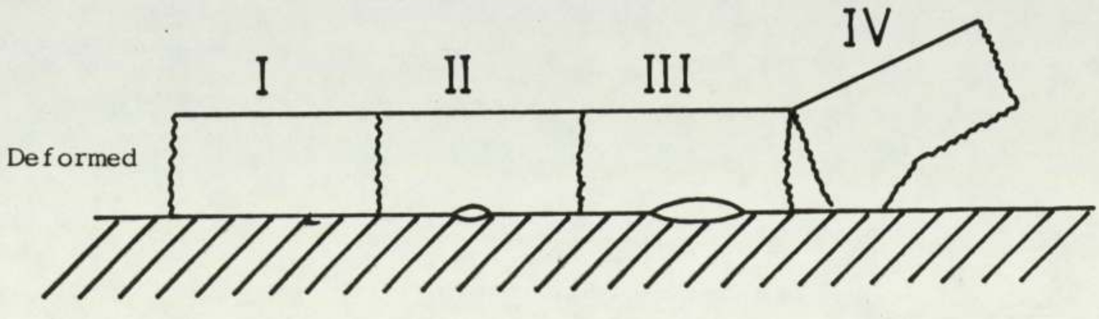

1.1 (d)
FIGURE 1.1.
Delamination Wear.

Wear Models (10)

Archard (9) quantified this model and proposed the relationship:

$$V = K \frac{(P x)}{(3H)} \qquad \_1.1$$

where V = volume of material removed by wear.

P = normal load.

x = sliding distance.

H = hardness of softer material

K = dimensionless wear coefficient representing the probability of an interaction between a pair of asperities forming a wear particle.

Values of K have been reported as being typically 10^{-3} to 10^{-7}. (10) Hence the relatively small number of wear particles produced and the inefficiency of the process. Further work by Archard et al (11) proposed the "severe wear" and "mild wear" regimes depending on applied load. Rowe (12) subsequently extended Archard's basic theory to include the effect of surface films and presented a modified wear equation.

$$V = Km\,(1 + \alpha\,\mu^{2})^{\frac{1}{2}} \quad \beta\,{}^{P}/_{H} \qquad \_1.2$$

where Km = constant for the materials

β = characteristic of the lubricant

α = constant

μ = the coefficient of friction.

The analysis of adhesive wear has produced three 'laws of wear'.

The volume of wear material being proportional to:

i) load

ii) distance of travel

and iii) inversely proportional to the hardness (or yield strength) of the softer material.

1.2.2 The Abrasive Theory of Wear.

Abrasive wear has been defined as "the removal of material from a surface by mechanical action of hard abrasive particles in contact with the surface". (13) However, in an attempt to further classify abrasive wear processes specific categories have been identified by Avery (14) as:

i) Gouging abrasion
ii) High stress grinding abrasion
iii) Low stress scratching abrasion (or erosion)

Gouging abrasion has been reported as resulting in the loss of large particles from a metal surface which then exhibited characteristic heavy gouges. This type of wear has been observed on the digger teeth of earth moving machinery and on the hammers of rotary impact machines. High stress grinding abrasion has been recognised as the fragmentation of abrasive particles by the rubbing together of two working surfaces. Figure 1.1b This form of wear has long been reported as the predominant mechanism in material comminution by ball milling. Low stress abrasion (which has also been referred to as scratching abrasion (15)) occurred by the removal of metal due to the relative movement of abrasive particles. This has been experienced in material handling environments such as ore delivery chutes. The terms high and low stress apply to the abrasive particle and not the wear resisting component. In high stress conditions the abrasive particles become fragmented by the action of localised compressive stresses developed during the process while in low stress grinding no comminution of the abrasive particle occurred.

An alternative approach to distinguish between the different regimes encountered in abrasive wear has been based on the two-body or three-body models. The two-body concept used a hard, rough body ploughing into a softer body, for example the filing process. As an extension of this idea three-body abrasion takes place when a third material (usually hard and granular) becomes trapped between the two sliding surfaces. When embedded into one surface grooves were cut into the opposite one.

The model suggested by Rabinowicz for abrasive wear (8) consisted of a cone shaped asperity of a hard material ploughing horizontally through a softer material and thereby causing plastic deformation. (see Figure 1.1c) An analysis of this condition enabled an equation for abrasive wear situations to be developed.

$$V = K_A \frac{Px}{3H} \qquad \_1.3$$

It is obvious that this equation is of the same form as that developed for adhesive wear conditions and hence the "laws of wear" also apply to abrasive conditions.

1.2.3 Corrosive Wear Theory.

Corrosive wear requires the synergistic effects of rubbing and corrosion. The sequence of events necessitates the production of a poorly adherent surface layer which subsequently becomes removed by rubbing. If for example the surface layer was a hard oxide film these particles may then further participate in three body abrasive wear. The contaminated surface layer reformed and the process was repeated. Such a process which continually removes a surface reaction product has inevitably been associated with accelerated wear. However, if a soft, ductile surface layer should be formed then wear rates would be reduced.

1.2.4 Fatigue Wear.

In adhesive or abrasive wear direct contact between surfaces took place but during fatigue wear these surfaces may be separated by a lubricant. This would be typical of a roller bearing. Fatigue conditions arise due to the reversing (during rolling) of maximum shear stresses occurring below the surface of the materials. If the amplitude of the stresses was above the endurance limit then fatigue failure will occur. Unlike the preceeding forms of wear which exhibit continued metal removal fatigue wear can be characterised by the sudden production of relatively large wear particles. Palmgren (15) has established an empirical relationship of the form

$$P^3 N = \text{constant} \qquad \_1.4$$

which related the number of cycles, N, to failure at load P. This mechanism was highly stress dependent. The problems of rolling contact fatigue have been succinctly reviewed elsewhere. (16)

Fatigue has also been reported as operating during sliding wear. (17) If asperities plastically deformed as two surfaces slide past each other then after a critical number of contacts the asperity would fail by fatigue. It had been suggested by Archard and Hirst (11) that fatigue may be responsible for the final detachment of material during adhesion. Subsequent work at I.B.M. produced a theory for sliding contact which involved contributions due to 'zero' wear and 'measurable' wear. (18, 19) This model for a low wear regime was based on mechanisms of fatigue and corrosion. The term 'zero' wear appears to have been a slight misnomer since this condition was defined as "wear less than the surface finish".

1.2.5 Erosion and Cavitation Erosion.

Erosion damage was reported to occur by the impingement of a fluid on the surface of a solid body. (5) Two predominant forms of erosive wear have been identified ,namely cavitation erosion and solid particle erosion. Cavitation erosion resulting from the relative motion of solid and fluid mediums are typified by samples such as slurry pump impellors or ships propellors. Damage is reported as being produced by the implosion of unstable bubbles against the solid body. This form of wear has been described as pitting damage (16) suggestive of a fatigue problem. Material resiliance, the dissipation of energy before deformation or cracking has occurred has been put forward as an important property in design against cavitation erosion. Work on erosion by Bitter (20) has shown that two different mechanisms operate depending on the ductile or brittle tendency of the eroded solid. (see Figure 1.2) Brittle materials are believed to wear by the coalescence of surface cracks which produced wear particles. The erosive mechanism of ductile material changed from abrasion at the maximum condition to predominantly fatigue as the angle of attack approached 90°. Bitter stated that in both forms of erosion the wear rate was proportional to the kinetic energy of the impinging particles.

Electro discharge machining is the beneficial effect of spark erosion, the damage resulting from an electrical spark between two surfaces. Bucklow and Cole (21) have reviewed the E.D.M. process and proposed erosion mechanisms. Current E.D.M. technology has been comprehensively surveyed elsewhere. (22)

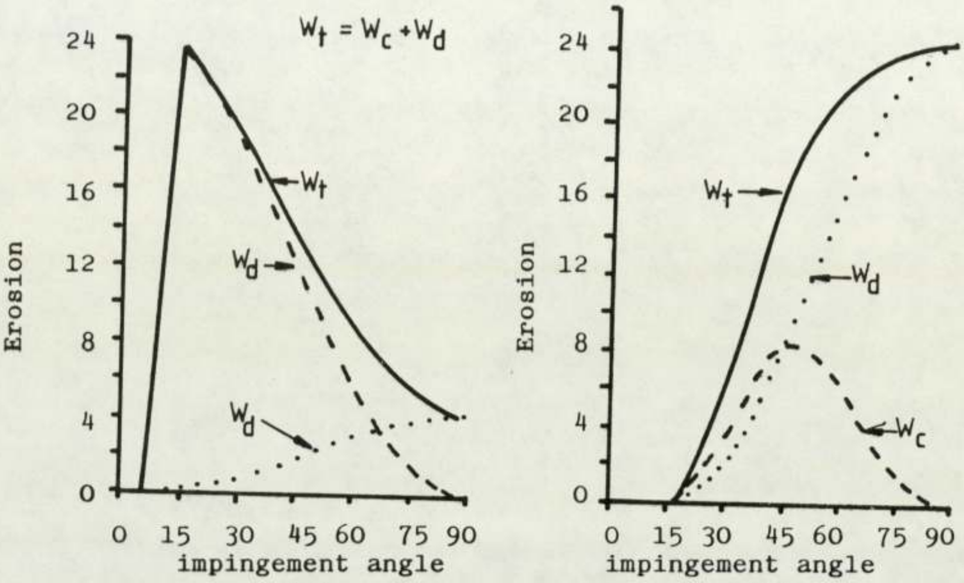

(a)

(b)

Figure 1.2

Material Erosion

Wt. = total wear
Wc. = cutting wear
Wd. = wear due to repeated deformation.

(a) Erosion of a soft and ductile material
(b) Erosion of a hardened brittle material.

1.2.6 Delamination Theory.

The work of Suh and his colleagues (7, 23) has lead to the delamination theory of wear (Figure 1.1d)or as some authors refer a "unified debris formation model." Suh proposed that during sliding wear subsurface deformation generated both dislocations and vacancies. Continued deformaton produced voids (which subsequently coalesced) resulting in the formation of subsurface cracks parallel to the wear surface. When the cracks attained a critical size shearing of the material between crack and surface produced a 'sheet' or flake' like wear particle. It has been further suggested that the wear processes of fretting, fatigue and adhesion are the products of this same mechanism. Shu (7) proposed a 'wear' equation for the determination theory which was of the form:

$$V = K'PX \qquad - 1.5$$

where P = the applied load

x = the sliding distance

K' = a wear factor given by

$$K' = \frac{b}{4\pi} \left[\frac{K_1 G_1}{\sigma_{f1} S_{02} (1 - \nu_1)} + \frac{K_2 G_2}{\sigma_{f2} S_{02} (1 - \nu_2)} \right] \qquad - 1.6$$

where K_1 and K_2 = constants related to surface topography

G = shear modulus

S_o = critical sliding distance.

ν = Poisson's Ratio

Equation [1.5] differed from Archard wear equation by not having a direct dependence on hardness.

1.3 The Assessment of Wear Resistance.

Wear resistance is not a material property but a system property. Some authors have reported that wear resistance can only be accurately determined by carrying out service trials. However the use of laboratory scale tests remain a common and frequently reported procedure. No universally accepted wear test exists but many of the wide variety of procedures fall within one of two broad categories.

i) reduced scale laboratory size machines which are 'models' of industrial plant.

ii) apparatus which simulates a specific wear regime.

Sare (24) questioned the ability of tests to precisely simulate the wear mechanisms encountered in real-world applications. However, Ludema (25) considered the production of similar wear debris to be an indicator of validity and Bayer (26) has stipulated the need for similarity between wear mechanisms.

Long term tests using full scale plant has undoubtably been the most thorough technique for obtaining wear data. For example, the interior of ball mills have been lined with a range of different alloys (27) and material handling chutes have been covered with a variety of materials. (28) These situations represented an 'ideal' test condition but such studies have been infrequently reported probably because of lack of plant availability and high costs. A compromise has been reached in the area of grinding media where useful data has been generated by employing 'marked ball' trials. (29) A relatively small number of marked, i.e. drilled, grinding balls of close weight tolerance have been added to the charge of a tumbling mill. By retrieving even one or two balls at periodic intervals the wear rate of the grinding media was monitored.

1.3.1 Laboratory Controlled Wear Tests.

There can be no doubt that an innumerable number of wear test machines have been produced to assist with alloy and process development. Some of the more frequently encountered machines will be reviewed.

Borik (30) has used a modified Fargo abrasion machine to assess the relative wear resistance of a number of materials under low stress abrasion conditions. This test, more commonly known as the rubber wheel abrasion test, was an extension of several other experimenters experiences. (31, 32) A sample approximately 6 mm x 25 mm x 56 mm under a load of about 22kg. was run for 5000 revolutions against a 175 mm diameter rubber rimmed wheel in an abrasive slurry environment. For each material a running-in test was performed prior to the actual measured test. Three hardnesses of rubber wheels nominally 45, 55 and 65 Durometer were used and the results normalised to provide a volume loss at 55 Durometer hardness. Borik concluded that this test exhibited considerably better reproducibility than other previously reported rubber wheel tests. This work was reiterated by Borik in 1972 (33) and the same test used by Diesburg and Borik. (34) A rubber wheel abrasion test has now been incorporated into an A.S.T.M. specification. (35)

Muscara and Sinnott (36) have developed an apparatus to determine the resistance of ferrous alloys to high stress grinding abrasion. The machine was a converted vertical milling machine which rotated a 6 mm diameter pin sample under a predetermined load against a moving abrasive cloth. This equipment enabled eight parameters to be controlled during a wear test. The data generated from this test was in the form of a weight loss but for many samples this was presented as a wear ratio. This ratio being given by the weight loss of a test material divided by the weight loss of a standard alloy . It was found that if the experimental parameters were correctly defined then results correlated well with particular service conditions e.g. ball milling and ploughing through soil. An important point was highlighted by these workers who emphasised that a wear ratio could not be used to rank materials under changing abrasive conditions. A wear ratio may only be used to compare different materials under similar abrasive conditions.

When considering gouging abrasion it was perhaps obvious to investigate laboratory sized equipment. Borik and Sponseller (37) used a laboratory sized jaw crusher to investigate the effect of metallurgical variables on the gouging wear of ore and rock crushing materials. A characteristic feature of the jaw crusher was to utilise twojaw plates these authors were able to quote a wear ratio for each test. The ratio was calculated by dividing the weight loss of the stationary test plate by the weight loss of the movable reference plate. However, as each test required 908kg. of rock and duplicate tests were always carried out then considerable problems regarding rock availability and disposal could be envisaged.

The abrasive wear resistance of fifteen materials including cast iron, glass and polyurethane in an agressive steel work slurry environment has been studied by Hocke and Wilkinson. (38) The aim of this exercise was to determine the suitability of materials for use in slurry pipeline transport. Initially this was carried out using an actual pipeline but after three years of operation it became apparent that a much longer test period would be necessary. The test rig was modified to accept 50 mm long, 6 mm diameter samples for an accelerated wear test. While recognising the limitations of their test facility these authors concluded that of the fifteen materials tested 5, i.e. polyurethane, rubber and 3 grades of high chromium cast iron, would be most likely to resist abrasive wear by steel work slurries.

A further abrasion test has been developed by Boyes. (39) This used a wedge shaped sample rotating under load against an annealed steel track covered with fresh, dry silica sand. Although of relatively simple design this apparatus permitted the control of several important parameters. Boyes generally represented his results as a volume loss although the studied materials would have exhibited a narrow range of density values compared with the investigation by Hocke.

A test which simulated repeated impact/spalling wear conditions such as experienced in ball milling has been reported by several authors. (40, 41, 42) Cast iron grinding media in excess of 60 mm diameter was repeatedly dropped from a predetermined height on to an anvil. This type of test was generally continued until failure occurred or some specified number of cycles had been completed.

There also exists a number of relatively simple wear test machines and specimens, such as Falex, four ball machine and pin on disc.

The falex test used two 'V' shaped test pieces mechanically forced together from diametrically opposed directions against a rotating pin. This type of test produced a line contact situation and has been used to assess material-lubricant combinations. The Alumer test was similar to the Falex differing mainly in the specimen geometry. (16)

The four ball test, for example that developed byShell, has generally been used to assess lubricant quality. Three 12.7 mm diameter balls were clamped to form a nest into which a fourth ball was forced and rotated. The rotational speed was within the range 1450 - 1500 r.p.m. and incremental loads could be applied up to 800 kg. By carrying out a number of tests, each using a new set of balls and determining the diameter of the wear scar, a lubricant characteristic was identified. The principle disadvantage of this type of test has been that the results apply to a particular system (i.e. the ball material and lubricant combination) which may not occur in service. Baldwin (43) has shown that when the same lubricants were tested in both four ball and Falex machines different relative rankings were produced. However, when the specimen materials were standardised then both tests produced the same lubricant ranking. This point was later confirmed by de Gee. (44)

The pin on disc or pin on cylinder machines have employed a stationary pin loaded against a revolving surface. A number of alternatives to this basic combination are possible as discussed elsewhere with particular reference to escape of wear debris. (5)

1.4 The Effect of Structural Variables on Material Wear.

The wear resistance of various materials will be reviewed with reference to structural parameters. In this way the more significant and tribologically important features can be identified and developed.

1.4.1 Wear of Steel.

There has been an extensive amount of literature published on specific steel and steel/environment systems. This section will therefore, only consider the general metallurgical variables in relation to some of the wear regimes mentioned earlier (see section 1.2). Austenitic manganese steel will be discussed separately in more detail.

Miller (10) has reported that while the presence of carbides in steel influence all types of wear the effect was most significant during abrasive wear. As a generalisation the wear rate was found to be inversely proportional to the size of both the carbides and pearlite colonies. The formation of carbides brought about two competing effects, an increase in hardness and an increase in potential void sites. However, the increased resistance to plastic deformation off-set the possible decrease in toughness.

The formation of a hard, brittle, continuous pro-eutectoid cementite phase enabled void nucleation and propagation thereby reducing wear resistance. The work of Kruschov and Babichev (45) and Kruschov (46) related the wear resistance of different materials to bulk hardness has been summarised diagramatically by Zum-Gahr. (47) see Figure 1.3It can be appreciated from this diagram that the wear resistance of commercially pure metals was a linear function of bulk hardness , as described by Archards law see equation 1 - 1. It was also apparent that steels of the same hardness as pure metals exhibited reduced wear resistance. Furthermore, steels

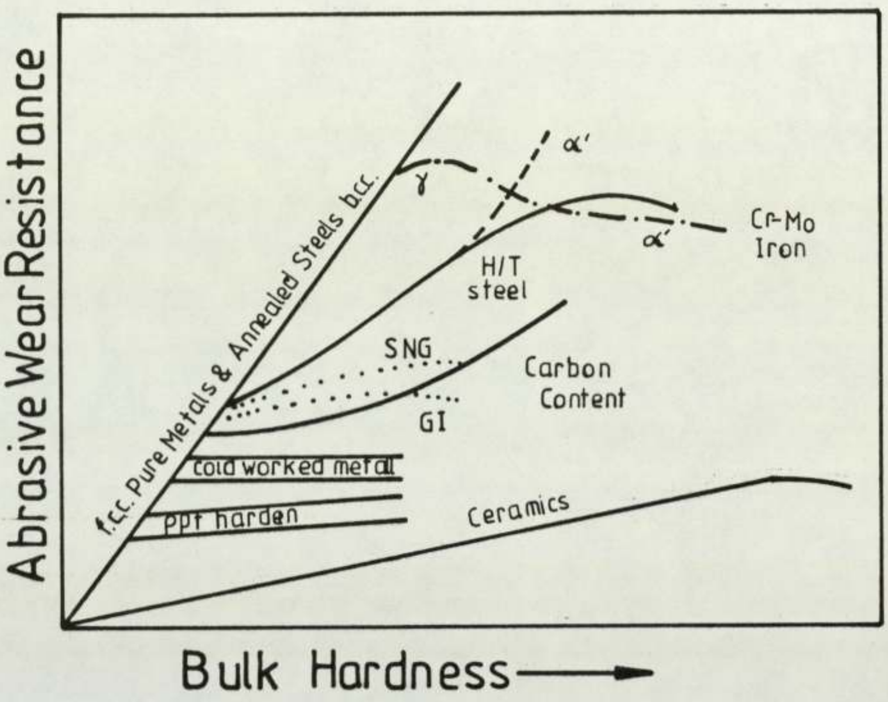

FIGURE 1.3.

Abrasive wear resistance of different materials as a function of bulk hardness (47) of similar hardness but different chemical compositions also exhibited differing abrasive wear resistance. The inference from these results being the inability of a single hardness parameter to accurately describe a general theory of wear. A more complicated model was required. It was believed that the effect of microstructure on the deformation and fracture behaviour was responsible for these observed deviations from a simple, linear relationship. Studies involving the effects of alloying additions on wear resistance have been difficult to interpret because of the range of parameters influenced by alloying elements. Under conditions of low wear severity the presence of metallic carbides such as VC and Mo_2C have been found to increase wear resistance. (See Table 1.1 for mineral and metallic hardness values.) More arduous wear conditions or when carbides have been associated with an inadequately tough matrix have resulted in high rates of spalling wear.

The retention of austenite may have either a favourable or deleterious effect on wear resistance. While austenite surrounding martensite laths has shown a beneficial crack blunting effect the transformation of retained austenite to a brittle martensite has resulted in adverse wear resistance. It was interesting to note Miller's observation (10) that some retained austenite appeared to be required in order to optimise wear resistance.

In a review on abrasive wear of steel castings (48) it was reported that reduced grain size encouraged wear resistance while grain boundary segregation and precipitation resulted in accelerated wear.

The adhesive wear of steels has been reviewed by Miller (10) with particular reference to the work of Welsh (49) this included a discussion on mild oxidative wear and severe metallic wear together with white layer formation.

Mineral	Hardness			Metallic Material	Hardness	
	MOHS	KNOOP	Hv		KNOOP	Hv
Talc	1	20		Ferrite	235	70/200
Carbon, Bituminous Coal		35		Pearlite, Unalloyed		250/320
Gypsum	2	40	36	Pearlite, Alloyed		240/460
Calcite	3	130	140	Austenite, 12% Mn Steel	305	170/230
Fluorite	4	175	190	Austenite, 12% Mn Steel Work Hardened	645	
Apatite	5	335/435	540	Austenite, Low Alloy		250/350
Glass		455	500	Austenite, High Chromium Alloy		300/600
Felspar	6	550	600/750	Martensite, 0.3% Carbon	550	500
Magnetite		575		Martensite, 0.4% Carbon	710	650
Orthoclase	6	620		Martensite, 0.6% Carbon	800	800/1000
Flint		820	950	Cementite, Fe_3 C	1025	840/1100
Quartz, Silica	7	840	800/1280	M_3C Carbide in High Chromium Irons.		1060/1200
Topaz	8	1330	1300/1430	Chromium Carbide, $(Fe,Cr)_7$ C_3	1735	1200/1800
Garnet	7	1360	800/1000	Molybdenum Carbide, Mo_2C	1800	1500
Emery		1400		Tungsten Carbide, WC	1800/2080	2400
Corundum, Al_2O_3	9	2020	1800/2000	Vanadium Carbide, VC	2660	2800
Silicon Carbide, SiC		2585	2500/2600	Titanium Carbide, TiC	2470/2955	3200
Diamond	10	7575	8000/10000	Boron Carbide, B_4C	2800	3700

Table 1.1

(188, 189, 130.)

TYPICAL HARDNESS VALUES FOR MINERALS AND METALLIC MATERIALS.

This white layer has been observed to form after surface deformation and resulted from an adiabatic shear process. (50) The differences between the mild and severe wear regimes have been characterised by smooth surfaces with small oxide flake debris and rough surfaces with metallic debris respectively. When the steel was sufficiently hard the transition between these two regimes was suppressed. Failure to form a white layer resulted in an extension of the severe wear condition.

Hsu et al (51) have studied the wear of austenitic stainless steels. They found that the friction, wear and galling resistance depended on the austenite stability and the hardness of the martensite phase. As the stability of the austenite was reduced the tendency to form martensite increased and a corresponding increase in wear and galling was observed.

The forgoing discussion has reviewed certain metallurgical and structural changes which influenced wear resistance. Other processes have been used to increase the wear resistance of steels. These include hardfacing, surface bonding with carbide materials and thermochemical treatments. For a discussion on the surface incorporation of hard carbide materials see section 5.0 . Detailed reviews of the other two techniques are beyond the scope of this work but for discussions on hard facing see References (52, 53) and for thermo chemical treatment References (54, 55, 56, 57)

1.4.2 Austenitic Manganese Steel.

Due to its importance in the mining and quarrying industries autentitic manganese steel requires particular attention. This material has frequently been exhaulted as a wear resistant material but its principle attribute has been toughness and ability to resist severe impact. The original production of a 1 - 1.3% carbon, 11 - 14% manganese steel dates back to 1882 by Sir Robert A. Hadfield. A characteristic of this alloy was its high work hardening rate whilst retaining toughness.

Although used in low impact situations its work hardening ability was not developed and high wear rates results. The detailed effects of chemical composition on the wear resistance has been comprehensively reviewed elsewhere. (48, 51, 58 ,61) Tasker (58, 59) has reported that the two most important variables to be considered when discussing austenitic manganese steel as being carbon content and section size. It has been shown that for optimum wear resistance a maximum amount of carbon in solid solution was required. Larger section sizes promoted the precipitation of embrittling carbides. While recognising the requirement of silicon for deoxidation Tasker has suggested that even a 0.6% - 1.0% addition can adversely affect toughness. It is worth noting that an underlying theme of Tasker's work was the often inappropriate application of mechanical property data generated from 25 mm diameter bars. In general, the deleterious effects of high pouring temperatures resulted in the development of a coarse grained, segregated structure. The mechanical properties have been adversely affected by the use of incorrect heat treatment temperatures. Too low a temperature produced incomplete carbide dissolution, while insipient fusion was a problem associated with a high heat treatment temperature.

1.4.2.1 Work Hardening of Austenitic Manganese Steel.

A general paper concerned with the importance of work hardening in the design of wear resistant materials has recently been published. (60) In this work, Ball treated abrasive and erosive wear as the result of a series of impacts within a given stress range. By adopting this approach Ball was able to illustrate the advantage of materials exhibiting a high work hardening rate. De Gee (61) used an argument based on a work hardening exponent to explain the findings of Bhansali and Miller. (62) These workers found that f.c.c. metals exhibited higher resistance to low stress abrasion wear than either h.c.p. or b.c.c. metals.

$$\sigma t = C\ \varepsilon t^{n} \qquad - 1.6$$

where σt = true stress

C = constant

εt = true strain

n = work hardening exponent.

For f.c.c. metals n has been found to be typically 0.35 while for b.c.c. metals n was of the order of 0.1. Tasker (59) has reported that no strain induced martensite has been observed in work hardened regions. In addition this worker suggested dislocation interactions as being the most probable mechanism of strain hardening. Honeycombe (63) has proposed that both α' and ε martensite have been detected in manganese steel. The work hardening characteristic was most likely to be responsible for the abrasion and toughness properties. The two principle factors to have influenced work hardening have been stated as being the stacking fault energy and structural stability of the matrix. Additions of C, Cr, Mn, Co, Si and N all reduced stacking fault energy thereby encouraging the dissociation of dislocations.

1.4.3. Wear Resistance of Grey Cast Iron.

A comprehensive review of the wear resistance of cast iron has been published by Angus. (64) This work included discussion of abrasive wear, dry sliding wear and combined fretting and corrosion conditions. Angus noted that a surface of hardness Hs would be scratched by a point of hardness Hp if $Hp \geqslant 1.2\ Hs$. Furthermore, Tabor (65) and Richardson (66) were in agreement by stating that abrasive wear resistance became greater when the metal hardness exceeded abrasive hardness by 20%.

The use of grey cast iron for machine tool slides and for internal combustion engine components has been much publicised. The presence of graphite has frequently been used as an explanation of the successful use of this material under such abrasive conditions. However, as pointed out by Angus while this lubrication property may have an initial anti-siezing and scaring effect during 'running-in' the amount of surface graphite would be small and quickly exhausted. These voids would then act as oil reservoirs and collection sites for wear debris. According to early work by Lane (67) and Smith (68) under conditions of boundary lubrication a random distribution of graphite flakes provided superior wear resistance compared with fine, undercooled graphite. With regard to matrix microstructure it has been documented that a predominantly pearlitic structure provided greater wear resistance than predominantly ferritic structures. An interesting model of abrasion-corrosion conditions in an internal combustion engine has been suggested by Burwell. (6) A motor car engine was considered to have operated on a daily two cycle system i.e. from cold to hot to cold occurred each morning and evening. During cooling the condensation of carbonic acid on the cylinder bore formed abrasive corrosion products such as Fe_2O_3. Starting up removed these particles which then accelerated the abrasive wear of the bore.

Noutiyal et al (69) have used such factors as surface temperatures and peak combustion pressures to explain the observation that most wear occurred at the top dead centre position of an internal combustion engine.

1.4.4. Nodular Irons.

The initial production of an iron containing nodular graphite has been credited to Morrogh in 1946 using a cerium addition. (64) Current nodularising practice has been based on subsequent work at Inco using a magnesium base addition. Barton (64) has summarised the wear resistance of nodular irons. Under dry conditions wear increased directly with increased matrix ferrite content and conversely decreased with pearlitic matrix structures. There was little difference in the performance of as-cast and annealed pearlitic structures. It was reported that substantially pearlitic structures (containing up to 8% ferrite) had a greater wear resistance than grey irons. According to Murthey et al (70) under dry friction conditions spheroidal graphite iron was more wear resistant than either compacted graphite or grey iron. All three materials exhibited evidence of the delamination wear mechanism.

Much work has been published regarding high strength nodular irons, particularly those formed by austempering. Blackmore (71) has succinctly reviewed these irons and highlighted both the high alloying additions necessary to form an as-cast accicular structure and the sensitivity to section size. Hardened and tempered alloys have found service in applications requiring wear resistance, for example crankshafts and pump casings.

More recently studies involving the production of an austempered bainitic structure have been documented. Dodd and Gundlach (72) have reported the developments of this type of iron and have suggested three possible classes for these materials. The three categories were:

i) Irons produced using low austenitising temperature giving maximum strength, hardness and resistance to abrasion.

ii) Irons produced using a higher austenitising temperature giving maximum ductility and toughness.

iii) Austempered irons given a high temperature retemper to transform the stabilised austenite into ferrite and graphite.

When discussing the quench operation Dodd et al (72) made mention to a salt bath quench unit which used a 4% water addition.

Typical wear resistant applications for austempered bainitic nodular irons have included wheels for heavy duty transfer carts, camshafts and various forms of gears. This high wear resistance has been attributed to the austenite content of the irons. (73) Janowak and Gundlach (74) have suggested that the high thermal conductivity and low thermal expansion combined with structural stability make the third class of irons suitable for brake rotors.

While much work appears to have been carried out on the development and application of acicular bainitic irons little information is yet available on precise wear machanisms or characteristics.

1.4.5. Wear Resistance of Nickel Chromium White Irons.

The wear resistance of nickel-chromium martensitic white irons, more generally known by the Inco trade name Ni-Hard, has been reported as early as 1960 by Dixon (75) In this work Dixon compared the wear resistance of Ni-Hard and steel grinding balls. The superiority of the cast iron material was attributed to the presence of the very hard carbide phase, Hv 1100-1200. During service the carbides stood in relief thereby protecting the softer matrix and in addition a fragmented carbide layer was observed. This so called 'armouring' effect was thought to result from the carbide wear debris becoming embedded in the matrix. It was also believed that this armouring was responsible for the bright surface appearance of worn material. Surface hardness values of Hv 1500 were noted after service. Much of this work by Dixon was latter reiterated in an International Nickel brochure. (76) This publication also discussed the beneficial effect of chill casting which bought about a refinement in structure. This was also confirmed by Provios (77) Further investigations by Dixon concentrated on the effect of heat treatment on the impact fatigue life of grinding balls. (78) In this report Dixon referred to the 'conditioning' of the material by secondary carbide precipitation and subsequent martensitic transformation. The examination of worn surfaces provided evidence of cracks propagating through the carbide phase. It was an interesting observation by Dixon that in the as-cast condition carbide hardness was Hv 1150-1200 whereas after heat treatment at 450°C the hardness had decreased slightly to 1000 - 1100. A variety of heat treatments have been recommended for improving the impact fatigue life of Ni-Hard grinding balls. These were:

i) 275°C for 4 hours

ii) -78% for 4 hours
275°C for 4 hours; air cool

iii) 450°C for 4 hours
275°C for 4 hours; air cool

iv) 750°C for 4 hours
275°C for 4 hours; air cool

The sub-zero quench, (75), using alcohol and dry ice has been suggested as industrially practicable. (77) Provided that suitable heat treatments were carried out grinding balls up to 100 mm diameter are reported to be free of any susceptibility (79) to spall or break.

A more recent study of wear damage (80) using alumina and silica abrasive has ellucidated some aspects of the wear mechanisms. Generally, the microstructure (particularly the retained austenite) was found to influence both the low stress grinding wear and gouging wear of Ni-Hard materials. There were two distinct observations. If the abrasive was very hard (e.g. Al_2O_3) then both matrix and carbide underwent uniform attrition by micromachining. However, when the abrasive was of a hardness intermediate between that of matrix and carbide (e.g. silica) then only the matrix underwent micromachining. In this instance the carbides were left standing proud with the exposed edges being chipped away.

A number of factors influencing the wear resistance of Ni-Hard have been identified. (78) Underalloyed material having graphite present gave undesirable wear performance. If the graphite was predominant at the ball surface then 'cap failures' frequently occurred. Similar problems were encountered if heat treatment above 750°C was carried out in an oxidising atmosphere. This practice resulted in intergranular oxide penetration.

1.4.6 Wear Resistance of High Chromium Cast Iron.

High chromium cast iron has frequently been referred to as an abrasion resistant alloy. As an example of this property consider their use in the cement and power generation industries. Many U.K. cement plants are using high chromium iron wear parts which have been operating in excess of 100,000 hours. Similarly, in vertical spindle mills used in the power generation industries on going service performance of 41,000 hours producing 310,000 tonnes of coal ground have been recorded. (81)

This superior wear resistance has been attributed to the hardness of the chromium carbides (see Table 1.1), being greater than that of quartz. (82) The significance of the comparison being the abundance of quartz as a consituent of many minerals. In addition, Durman (83) has stated the importance of the matrix both in supporting the carbide phase and contributing to the overall material hardness. Clearly, both carbide and matrix constituents have been responsible for developing the wear resistant characteristic of these materials and their contributions must be given equal consideration.

1.4.6.1 Low Stress Abrasion.

Low stress abrasion conditions appear to have been the most frequently reported test condition. Zum Gahr (82) has observed that wear resistance of high chromium cast iron varied with the volume fraction of carbide, matrix structure and abrasive material. It was found that when using a garnet abrasive, which was softer than chromium carbide, wear loss decreased with an increasing volume fraction of carbide. Conversely when a hard silicon carbide abrasive was used increasing the volume fraction of carbides increased the wear loss. The explanation for this observation was that the harder silicon carbide particles were able to penetrate and crack the carbides thereby reducing wear resistance. A similar exercise by Fulcher et al (84) revealed that for hypereutectic alloys tested in a rubber wheel abrasion test using quartz and alumina abrasives the wear resistance increased with volume fraction of carbides. No cracking or spalling of chromium carbides was reported with the alumina abrasive which effectively cut both matrix and carbide phase. Animportant result from these studies (82) was the reiteration of the poor correlation between bulk hardness or matrix hardness with wear resistance. Generally it was found that the wear resistance of materials having a nominally martensitic structure could be increased by reducing the amount of retained austenite.

Watson et al (85) have reported that low stress abrasion resulted in the micromachining of the surface. This was apparent as wear grooves cutting through both matrix and carbide phase. No significant evidence of cracking fragmentation or preferential removal of soft matrix was observed for this type of wear regime. These workers analysed their results in terms of the hardness ratio of material phase/abrasive particle as proposed by Hurricks. (86) If the material hardness was H and the abrasive hardness Ha then relatively large increases in wear resistance have been reported when $^{H}/_{Ha} \geq$ 0.5 to 0.6. This was illustrated by considering two matrix structures, martensite and martensite + carbides together with two mineral hardnesses. See Figure1·4. For the 'soft' abrasive, Hv 1000, wear resistance clearly began to increase at about Hv 500 - 600. Whereas for a 'hard' abrasive, about Hv 2300, the appearance of carbides in the microstructure had a less pronounced effect on wear resistance. This was due to the value $^{H}/_{Ha}$ being below 0.6 for both martensitic and martensitic carbide structures for Ha = 2300. However, for Ha = 1000 the value $^{H}/_{Ha}$ for carbide was of the order of 1 thus providing increased wear resistance. The soft abrasive regime which began at $^{H}/_{Ha} \approx 0.5$ did not end until the value exceeded unity, the upper limit may be $^{H}/_{Ha} = 1.2$ as defined earlier. (64) Furthermore Hurricks stated that beyond this limit low abrasive mediums will then cause the surface to take on a smooth surface appearance. The criterion for the cessation of damage being the equality of yield strengths for both metal and abrasive. Using these concepts as the basis of their analysis, Watson et al (85) proposed a combined mechanism of ploughing and cutting depending on matrix type. It was suggested that for an austenitic matrix the grooves were produced by a process of ploughing whereas martensite underwent grooving by cutting. Regardless of matrix type the carbides were subjected to a cutting mechanism. A significant result of this work was the similarity in results produced by high and low stress grinding tests. It was concluded that for many practical purposes either a high or low stress test need be used to examine high chromium cast iron. In a study of abrasion resistance by Sare (87) it was shown that despite wide variations in bulk hardness the abrasion resistance ratio only varied slightly. This observation lead Sare to suggest that under conditions of low stress abrasion the most important parameter was the dispersion of hard carbides within the structure. It was reported that wear resistance of a soft matrix/hard particle

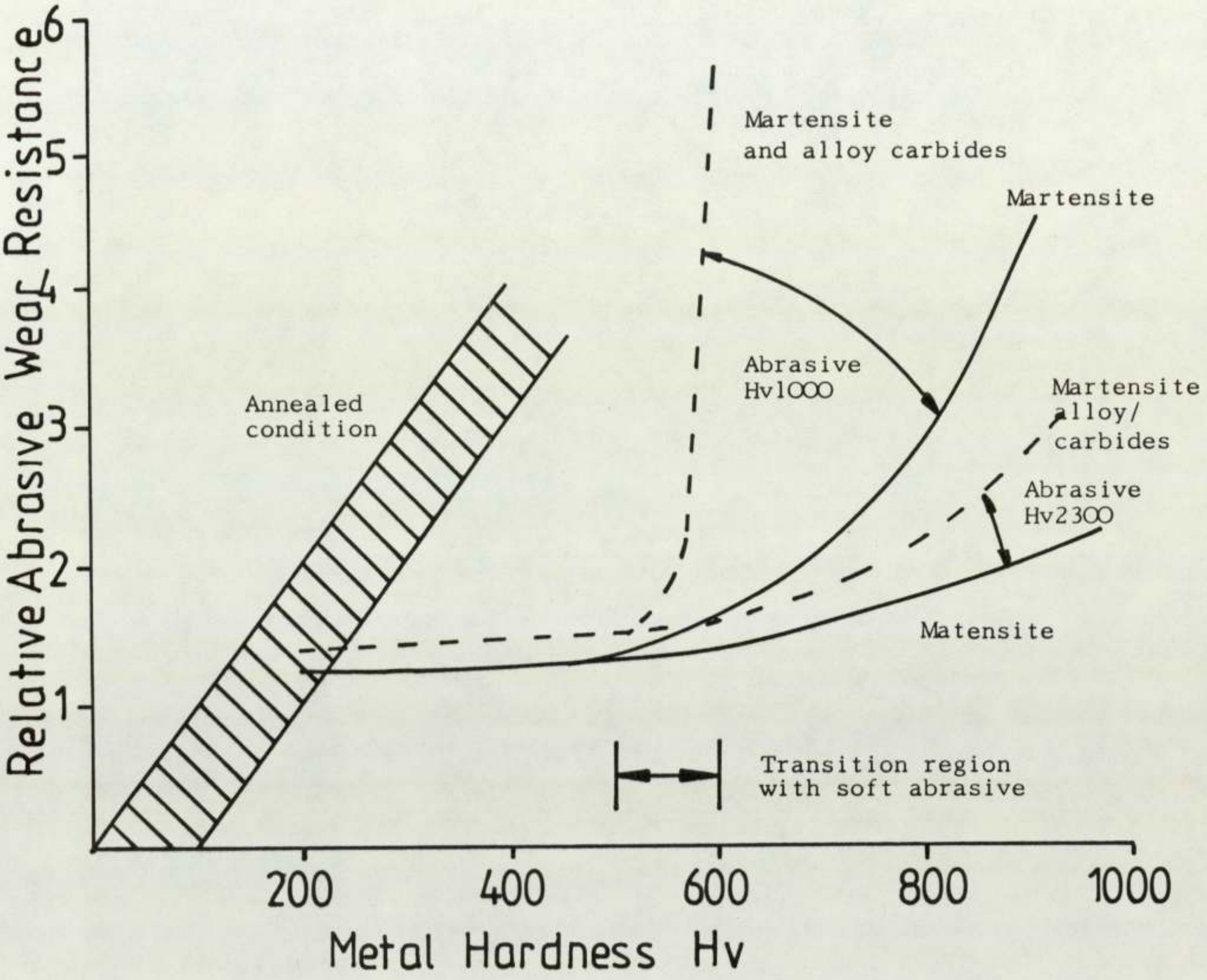

Figure 1.4

Effect of metal and abrasive hardness on the wear resistance of heat treated steels. (86)

composite was a balance between carbide and matrix removal. The overall wear rate being controlled by the slower of the two effects. The significant microstructural parameter, the mean free path between carbides or through the matrix was given by:

$$\lambda m = \frac{1 - Vfc}{N_L} = \frac{Vfm}{N_L} \qquad - 1.7$$

where λm = matrix mean free path

Vfc = volume fraction of carbide phase

Vfm = volume fraction of matrix phase

N_L = number of carbide particles per unit length.

The importance of this feature was verified by assessing the wear resistance of a chill cast material which exhibited a fine dispersion of chromium carbides. However, it must be remembered that a wear rate should apply to a system, in which case the ratio of mean free path/abrasive particle size should be important. If this ratio became large then particles of abrasive could preferentially wear the exposed softer matrix. A small ratio enabled the carbide phase to resist preferential matrix penetration.

In an interesting study by Prasad et al (88) the production of wear damage was observed in-situ by performing scratching tests with rounded quartz grains. These workers used three events to explain their results, that is, fracture at the edge of carbides left unsupported due to preferential matrix wear. Formation of larger pits by the fracture at edges of pre existing flaws in primary carbides. Finally, the grooving of carbides by wear debris formed by carbide fracture. Consideration of the first point leads to the formation of 'rounded' carbides protruding from the matrix. This work was later extended and quantified (89) to show that angular grains produced during wear were able to produce cracks in excess of the 1μm critical defect size for carbides. Once extended to about 4 μm in size the more common naturally occurring semi angular quartz particles were able to produce pits and ultimately carbide removal

1.4.6.2. Gouging Abrasion.

The variation in gouging abrasion resistance with carbon content has been shown graphically by Diesburg and Borik. (34) Figure1·5. As a general statement it would appear that increasing the hardness of a material increases the resistance to gouging abrasion.

It has been reported by Watson et al (85) that while the ranking of alloy white irons to gouging abrasion was similar to that produced under high stress conditions the mechanisms involved were different. During gouging abrasion there has been evidence of cracking and fragmentation of carbides, some of which may then become embedded in the softer matrix. Watson et al have suggested that as the role of the matrix was to support the carbides then the higher strength martensitic structure should have provided greater mechanical support than an austenitic matrix.

Two alternative explanations have been proposed to illucidate the mechanisms responsible for carbide cracking. These were the interaction of elastic stress waves at the carbide/matrix interface (24) and an elastic indentation mechanism. (85) Both mechanisms deserving equal consideration and discussion.

1.4.6.2.1 Stress Wave Interactions.

According to Sare (24) the impact conditions encountered by a swing hammer produced surface compressive stress waves which subsequently propagated into the subsurface regions at acoustic velocities. The behaviour of the stress waves after striking a carbide/matrix interface depended on the impedance of the two phases. The effects of an incident compressive stress wave propagating through a duplex α, β structure have been summarised

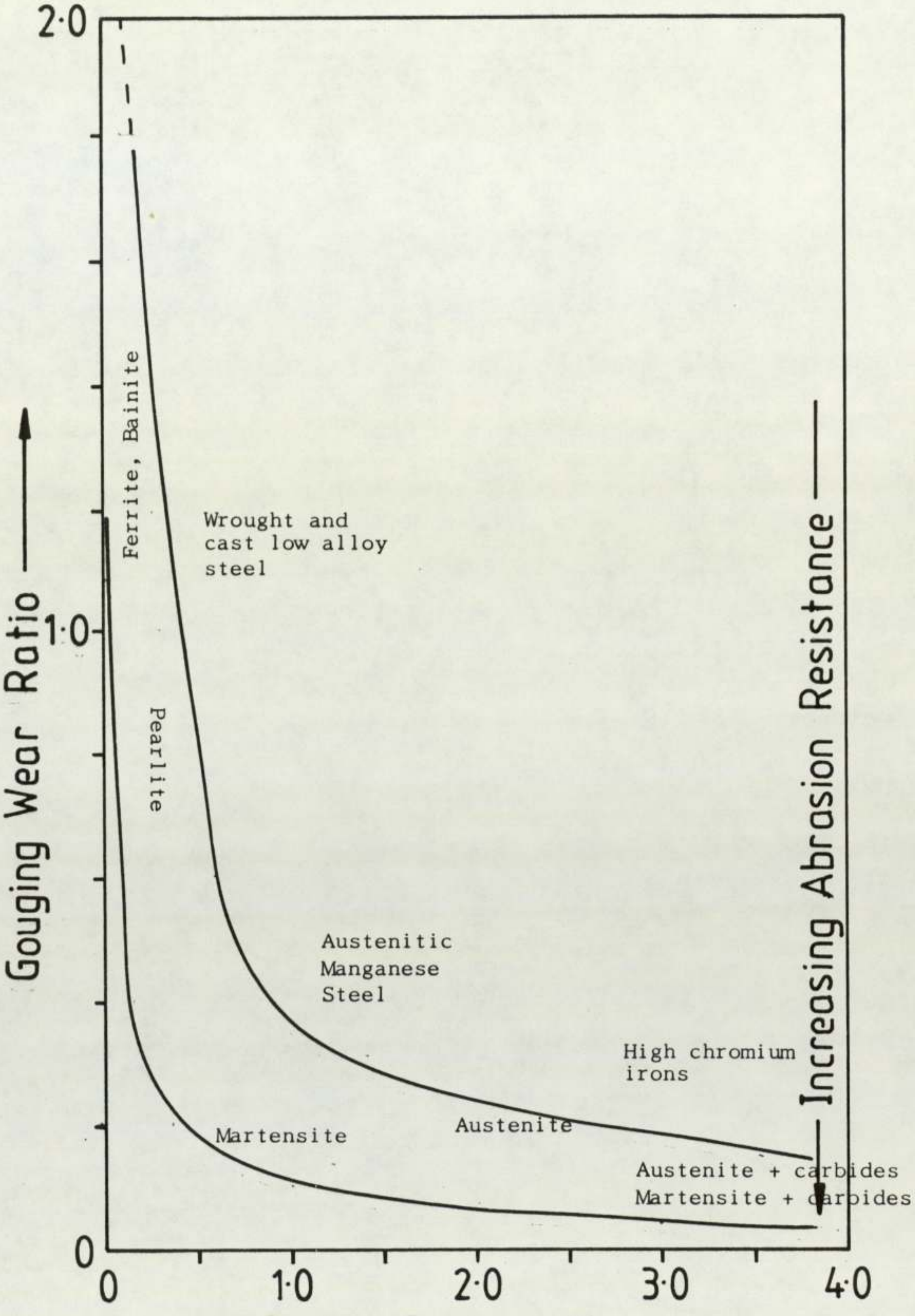

Figure 1.5

Variation of gouging wear ratios with carbon content for a range of ferrous alloys.

diagramatically in Figure 1.6 Fracture of the carbide (α) phase occurred when the reflected tensile stress wave exceeded the strength of that phase. A resultant series of parallel cracks formed which then facilitated material loss. Sare extended this explanation of reflected stress waves to account for the lack of cracks in some carbides due to a 'shielding' by the surrounding carbide phase.

The quantitative analysis for this model was as follows:

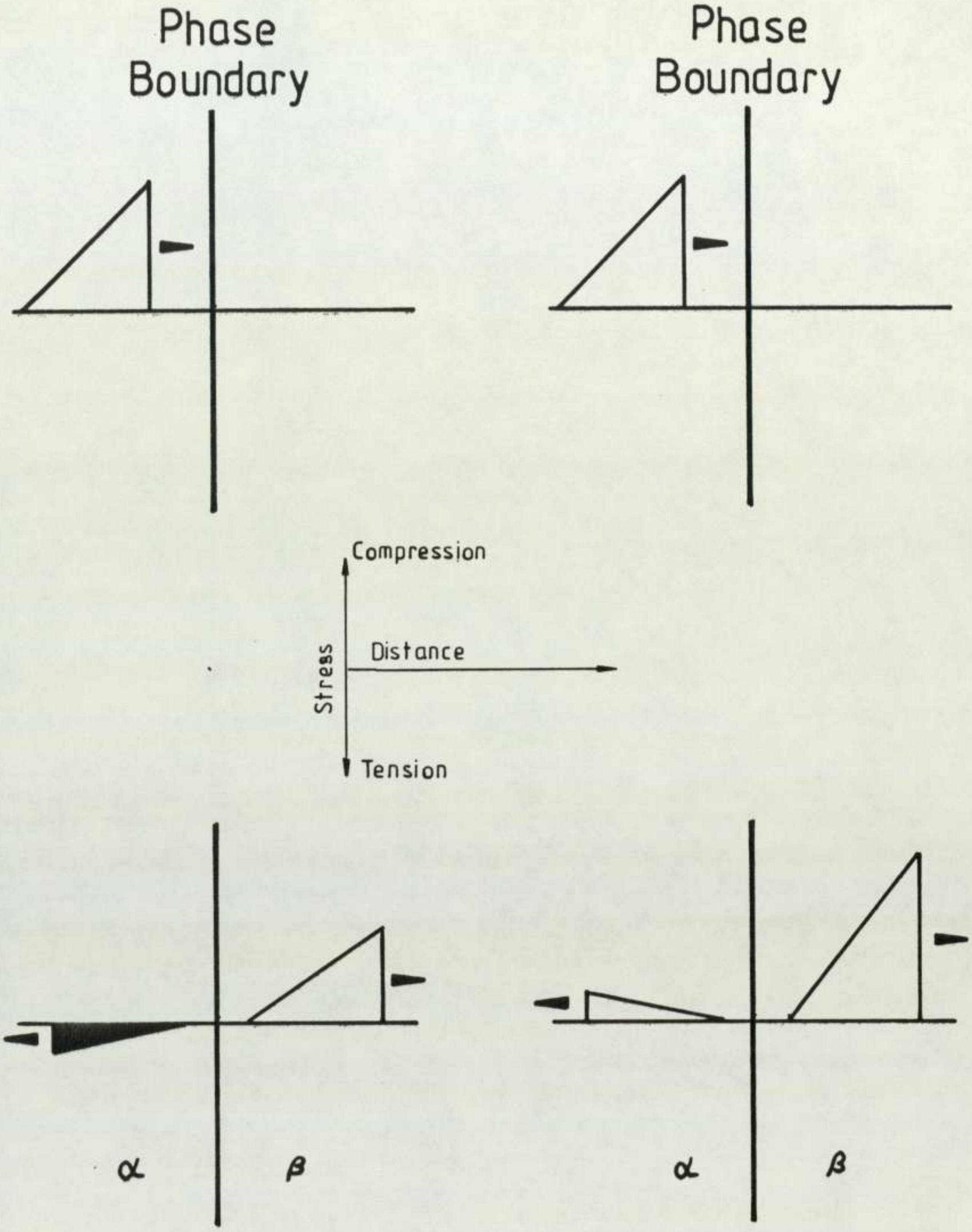

Figure 1.6

Schematic diagram illustrating behaviour of an incident prehensive stress wave (24)

The material impedance, I, was given by

$$I = \rho . C \qquad - 1.8$$

where ρ = density of phase

C = velocity of stress waves through phase

but $C = (E/\rho)^{1/2} \qquad - 1.9$

where E = Youngs Modulus

Then by substituting 1.9 into 1.8

$$I = (E\rho)^{1/2} \qquad - 1.10$$

Hence, characteristic impedance was given by

$$(E\rho)^{1/2}$$

Furthermore, the incident stress, σi, generated by the impact of the hammer and ore was

$$\sigma i = \rho_H V_H C_H$$

where ρ_H = density of hammer material

V_H = velocity of hammer tip

C_H = velocity of stress wave through hammer material.

By assuming that the incident stress wave propagated through phase β was reflected at a boundary with the α phase Sare was able to calculate the magnitude of the reflected stress, σr.

$$\sigma r = \sigma i \ \frac{\rho\alpha C\alpha - \rho\beta C\beta}{\rho\alpha C\alpha + \rho\beta C\beta} \qquad - 1.11$$

By the substitution of suitable values into these equations Sare showed that the reflected tensile stress wave was of the same order of magnitude as the tensile strength of the carbide.

1.4.6.2.2. Indentation Cracking.

The indentation cracking of brittle solids has been frequently reported, see for example the review by Lawn and Wilshaw. (90) The cases discussed have been for both sharp and blunt indenters, Figure1·7 (91) In each situation the indenter set up a contact stress field, the tensile component of which provided the driving force for the resulting fracture. The ensuing damage from the use of a sharp indenter has been interpreted by Evans et al (92) and Lawn et al (93) and the essential features identified. These may be illustrated with reference to Figure1·8. During stage 1, initial loading, the sharp indenter induced a zone of irreversible damage around the point of contact. The size of the zone was observed to increase with increased load. At some critical indenter load a crack suddenly initiated below the contact point, at the region of highest stress concentration. This crack has been termed the median vent and characterised stage 2 or critical zone formation. Throughout the third stage of stable crack growth, increased loads resulted in further stable extension of the median vent. The initial unloading caused the median vent to close. Residual stress cracking (stage 5) produced by the relaxation of deformed material within the contact zone prior to removal of the indenter superimposed a high residual tensile stress on the applied field. This caused the appearance of sideways extending cracks or lateral vents. The final stage in the sequence of events was the complete unloading of the material (6) Lateral vents continued to extend and cause chipping. Beginning the cycle again caused the median vent to re-open and simultaneiously close the lateral vent.

Indentation using a blunt indenter initially produced highly tensile stresses in a shallow, sub-surface skin outside the elastic contact circle which eventually nucleated a crack. This dominant flaw circumvented the contact circle and formed a shallow, surface ring crack. Once beyond

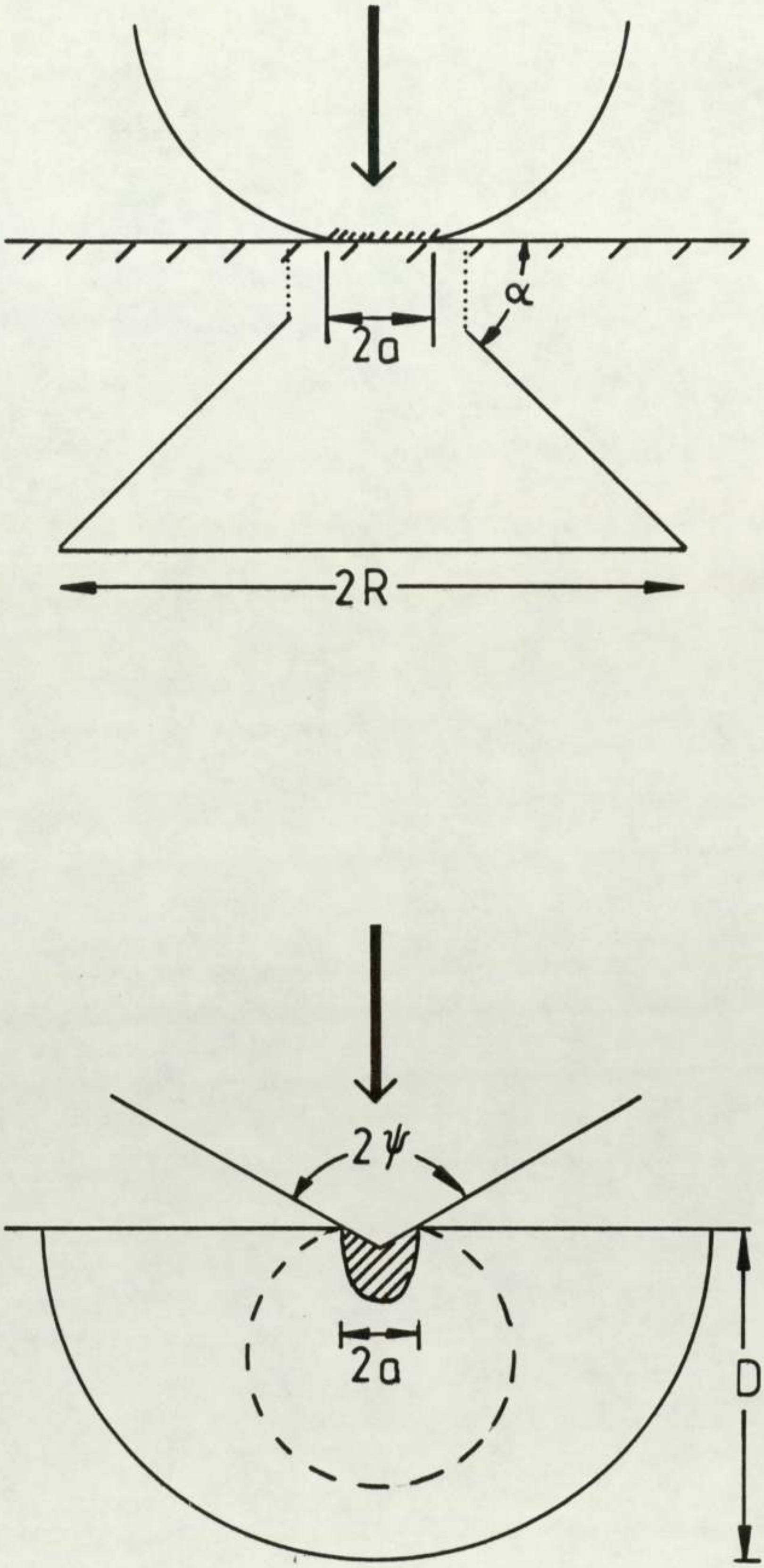

(b)

Figure 1.7

Basic identation fracture systems (91)

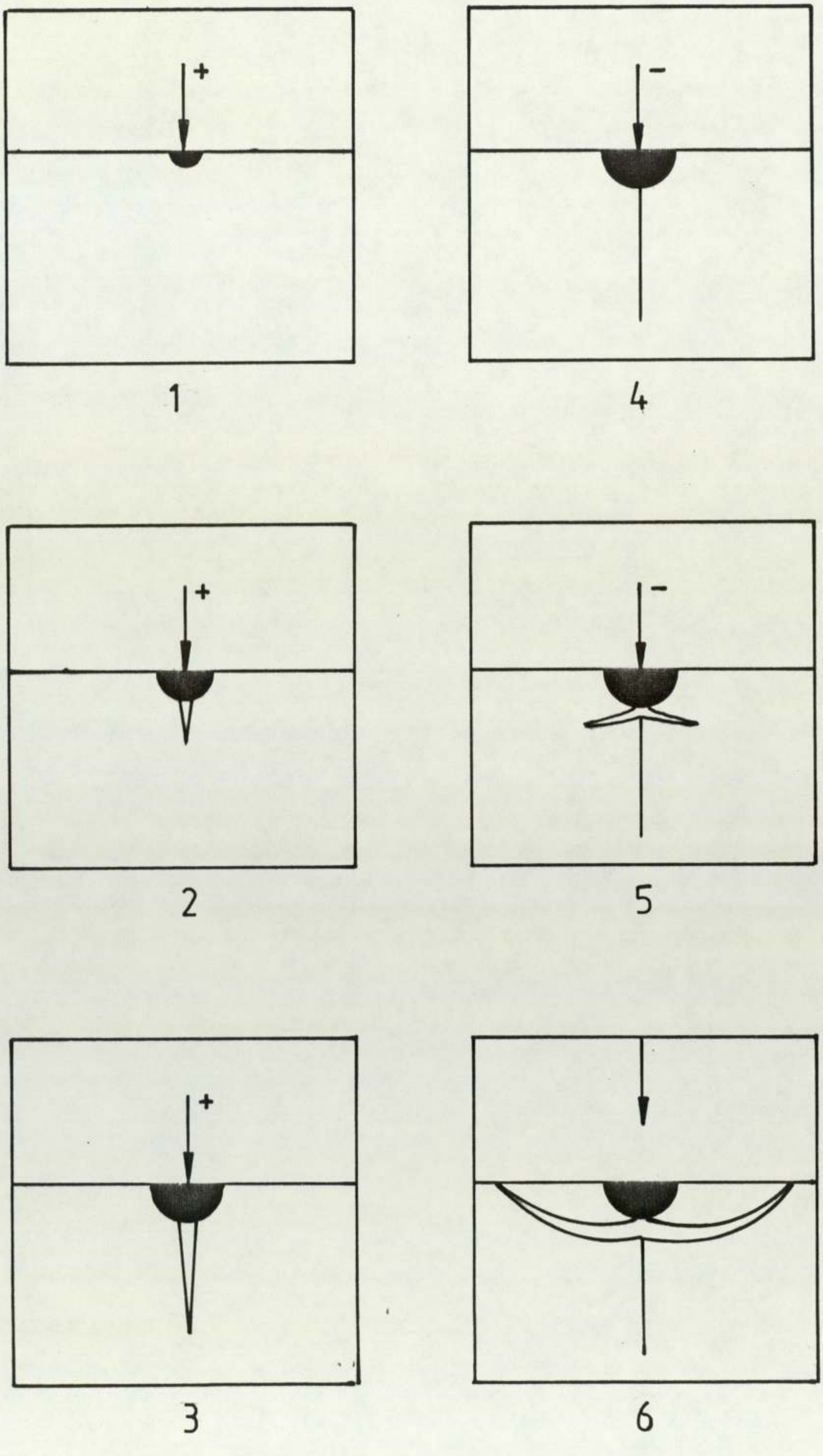

Figure 1.8.

Schematic of vent crack formation under point indentation.

a critical formation depth the surface ring propagated into a Hertzian cone. Unloading tended to close the cone crack.

These identation techniques have been recently developed by Lamy (94) who has related a concept of brittle scratch susceptibility to wear resistance.

1.4.6.3. High Stress Abrasion.

As stated earlier, high stress abrasion conditions have been reported for such practices as ball and rod milling. Bereza (95) has documented the use of high chromium cast iron grinding media as being economically viable only when grinding material of less than Mohs hardness 6. The reason given was that as mineral hardness increased the superiority of the alloy iron over forged steel diminished until eventually the economics of the process excluded the selection of an alloy iron. This review by Bereza summarised the interplay between eutectic carbide matrix, and mineral by stating that regardless of the carbide hardness they may be removed from a soft matrix by hard, angular abrasives. Hence, the poor wear resistance exhibited by relatively soft pearlitic material. This was confirmed by the work of Gundlach. (96)

The wear resistance of a series of high chromium irons has been investigated by Pearce. (97) This work revealed considerable cracking of carbides beneath a worn surface resulting from deformation in the wear direction.It was significant to observe that with the notable exception of a 30% chromium iron the martensitic structures were generally superior to austenitic material. The reason for this anomalous behaviour of the 30% chromium material was explained by the presence of $M_{23}C_6$ type carbides in the heat treated alloy.

When abrasives were harder than the eutectic carbides a high degree of strain hardening (or strain induced transformation) of an austenite matrix has been observed. (98) Thereby a work hardened layer was produced. By implication this suggested that the use of a bulk hardness value was inappropriate as an assessment of wear resistance.

Although no explanation was given by Gundlach (96) he stated that for austenitic structures additions of copper, nickel and manganese had a deleterious effect on wear resistance. Conversely, molybdenum and silicon additions improved performance with maximum wear resistance being achieved with a single addition of 2.9% molybdenum. Diesburg and Borik have also highlighted the increased wear resistance of an austenitic alloy containing about 2% molybdenum. These workers attributed the improved performance to an increase in matrix hardness. It was further suggested, again without explanation, that even in the heat treated martensitic condition a 2% molybdenum addition improved wear resistance.

One further problem encountered in certain high stress environments has been that of corrosion, as for example in wet ball milling. The use of a chromium addition to resist corrosion has been well reported and similar considerations apply in this application. It has been found (99) that during wet grinding the most important single factor in determining wear resistance was the matrix chromium content, it was the amount of chromium in solid solution in the matrix which was important, 13% being suggested as the minimum matrix content to resist corrosion. When the matrix content fell below about 13% wear was accelerated due to the corrosion of the matrix, all other variables being of secondary importance.

2.0 FRACTURE MECHANICS.

2.1 Introduction.

The analysis of fracture behaviour and its quantitative measurement have been the subjects of much published work. Traditionally, due to the lack of understanding in this field design engineers have applied safety factors of between 2 and 5 to their calculations in order to prevent catastrophic failure. Even so, disasters have occurred. (100, 101, 102) Fracture mechanics has quantified the inter-relationship between material toughness, stress level and defect size. That is, the stress field ahead of a sharp crack can be characterised in terms of a stress intensity factor, K, related to both defect size and nominal stress level.

2.2 Energy Balance Approach.

Griffith (103) carried out the first analysis of fracture based on energy considerations. It was assumed that for an ideally brittle material fracture occurred when the elastic energy supplied at a crack tip during an increase in crack length was equal to or greater than the energy present during crack extension. Consider an infinite plate having unit thickness and containing a through thickness crack of length 2a. If a uniform tensile stress, σ, was applied at infinity then the total potential energy of the system, U, may be given by

$$U = Uo - U_{\alpha} + U_{\gamma} \qquad -2.1$$

where Uo = elastic energy of uncracked plate

$U\gamma$ = decrease in elastic energy caused by introduction of a crack

U_{γ} = increase in elastic surface energy caused by the formation of crack surfaces.

By using a stress analysis developed by Inglis (104) Griffith showed that:

$$U\alpha = \frac{\sigma^2 a^2}{E} \qquad - 2.2$$

where σ = uniform tensile stress

a = half crack length

E = elastic modulus.

and $U\alpha\gamma = 2\ (2\ a\gamma e)$ - 2.3

where γe = elastic surface energy

Hence, the total energy of the system

U, may be written

$$U = Uo - \pi\frac{\sigma^2 a^2}{E} + 4\ a\gamma\ e \qquad - 2.4$$

At equilibrium for crack extension,

$^{du}/_{da} = 0$ therefore

$$\sigma\sqrt{a} = \left(\frac{2\ \gamma\ e\ E}{\pi}\right)^{1/2} \qquad - 2.5$$

As γe and E are material properties it may be appreciated that in brittle materials crack extension takes place when the product (σ^2 a) reaches a critical value.

Equation (2.5) may be re-arranged to give:

$$\frac{\pi\ \sigma^2 a}{E} = 2\ \gamma\ e \qquad - 2.6$$

The left hand side of the equation has been termed the energy release rate, G, while the right hand side represented the materials resistance to crack extension, R. Irwin (105) and Orowan (106) proposed that the Griffith's model could be modified and applied to metals which exhibited plastic deformation. This modification related the materials resistance to crack extension to the sum of the elastic surface energy, γe, and the plastic strain work, γp resulting from crack extension. Hence equation 2.6 became:

$$\frac{\pi \sigma^2 a}{E} = 2 (\gamma e + \gamma p) \quad - 2.7$$

But since ($\pi \sigma^2 a/E$) has been termed G, the energy release rate and $K_I = \sigma \sqrt{\pi a}$ for a through thickness crack of length 2a then:

$$\frac{\pi\sigma^2 a}{E} = G = \frac{K_I^2}{E} (1 - \nu^2) \quad - 2.8$$

This relates energy release rate G, to K_I for plane strain conditions.

2.3 Linear Elastic Fracture Mechanics (L.E.F.M.)

In addition to specifying a stress intensity factor, K, the opening mode of the crack surfaces are also important and must be stated in any definition. Three opening modes have been identified (107) and denoted as I, II and III hence K_I, these modes are illustrated in Figure 2.1. The value of the stress intensity factor reaches a critical value, Kc, at the crack tip when unstable fast fracture occurs. Furthermore, Kc is known to be dependant on specimen thickness, as shown in Figure 2.2 which illustrates a limiting value of the Kc which under plane strain conditions becomes K_{IC}. This diagram also shows the character of the fracture face. In thin section material crack tip stresses are in the sheet plane, through thickness stresses being negligible or zero. The tension stress in the yield zone is the same as the uniaxial yield stress and fracture occurs by shearing at 45° to the tensile stress axis. In thick sheets constraint stresses are produced in the width and thickness directions resulting from material remote from the crack tip resisting the Poisson contractions near to the crack. The result of these triaxial conditions is a considerable difference between the plastic zone size around the crack tip depending on whether conditions are predominantly plane stress or plane strain. (Figure 2.3) The size of the plastic zones may be given by:

$$ry \text{ (plane strain)} = \frac{1}{6\pi} \left(\frac{K_{IC}}{\sigma ys}\right)^2 \qquad - 2.9$$

and

$$ry \text{ (plane stress)} = \frac{1}{2\pi} \left(\frac{K_{IC}}{\sigma ys}\right)^2 \qquad - 2.10$$

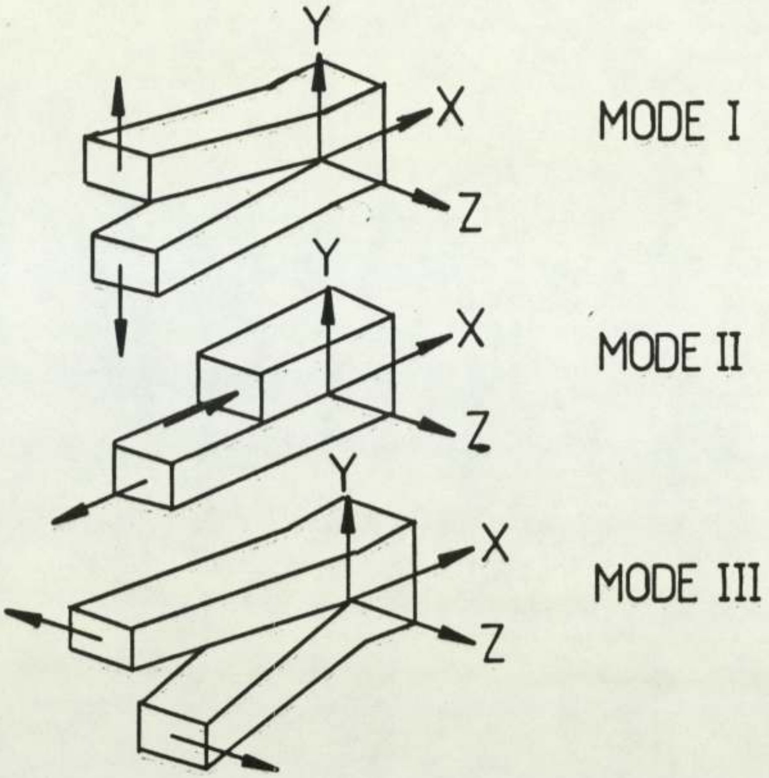

Fig. 2.1: Crack opening displacement modes

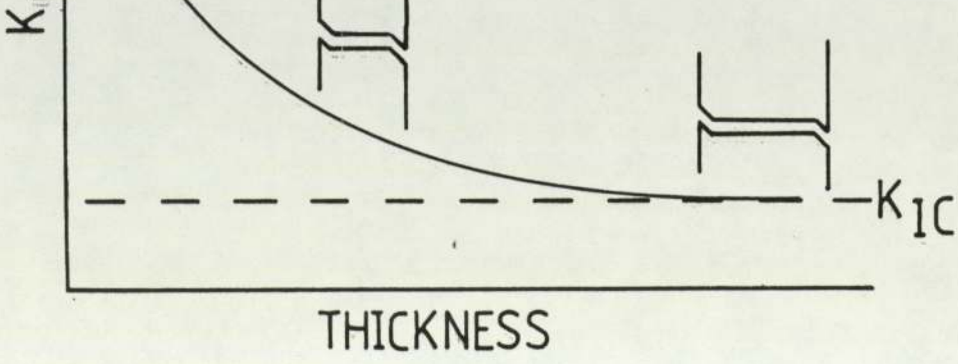

Fig. 2.2: Variation of K_C with specimen thickness

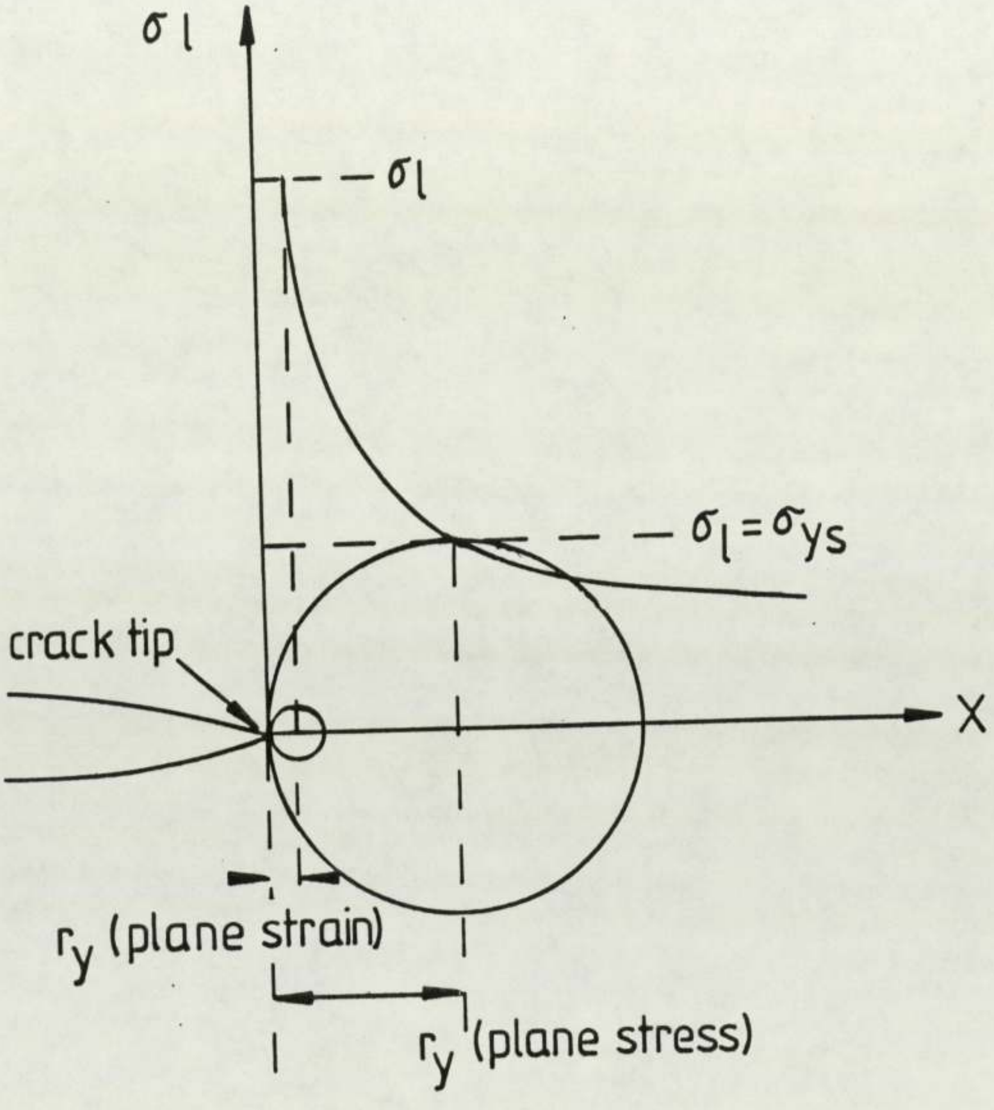

Figure 2.3.

Plastic zone size ahead of crack tip.

The lack of constraint stresses at free surfaces enables plane stress conditions to operate with the attendant 45° shearing. As the plate thickness increases so does the ratio of plane strain/plane stress fracture area, i.e. the plane stress region remains constant. As the plane strain fracture requires less energy than the plane stress area the Kc value decreases with sample thickness. Although plane strain fractures will always contain shear lips these may be ignormed if less than 10% of the total thickness. (108) To maintain plane strain conditions during a test to determine K_{IC} there is a specimen size constraint such that:

$$B > 2.5 \left[\frac{K_{IC}}{\sigma ys}\right]^2 \qquad - 2.11$$

when B = specimen thickness.

2.3.1 Assessment of Defect Size.

It is a feature of the fracture mechanics approach that permits defect analysis by manipulation of stress intensity factor equations. For an infinite plate containing a through crack and subjected to a uniform tensile stress σ, then the critical defect size a_c has been given by:

$$a_c = \frac{K_{IC}^2}{\pi \sigma_w^2} \qquad - 2.12$$

This simple elastic condition must be further modified for other conditions involving some plastic yielding at crack tips and various defect types.

A plastic zone correction factor estimated from

$$ry = \frac{1}{2\pi} \left(\frac{K_{IC}}{\sigma ys}\right)^2 \qquad - 2.13$$

increases the effective length of the crack by an amount equal to the plastic zone radius, ry, under plane stress conditions. This situation reduces the critical defect size by about 12%, similarly a plastic zone correction factor for plane strain conditions reduce a_c by about 3%.

2.3.1.1 Embedded Defects.

For a totally embedded defect under plane strain conditions, a_c has been given by:

$$a_c = \frac{K_{IC}^2}{\sigma w^2 \pi} \left[\Phi^2 - \frac{\sigma w^2}{4(2)^{1/2} \sigma ys^2} \right] \quad -2.14$$

The value of factor Φ varies with the ratio of minor to major axes (a/b) for the crack.

Typically these values may be:

a/b	0.0	0.2	0.4	0.6	0.8	1.0
Φ	1	1.05	1.15	1.28	1.42	$\pi/2$

2.3.1.2 Surface Defects.

In addition to allowing for the plastic zone correction factor a surface defect also experiences a free front face effect. Due to increased elastic opening of the defect (at a given value of σw) the stress intensity at the crack tip becomes increased.

The critical defect size being given by:

$$a_c = \frac{K_{IC}^{2}}{\pi \sigma_{w}^{2}} \left[\frac{\Phi^{2} - 0.212\left(\sigma_w / \sigma_{ys}\right)^{2}}{1.2} \right] \qquad - 2.15$$

2.3.1.3 Irregular Defects.

While the previous paragraphs have quantified a_c for specific, idealised conditions many defects are of highly irregular shapes. Barnby (109) has suggested that for a dog bone shaped defect K_{IC} values should be calculated for a number of positions based on inscribed ellipses. However, when the irregular shape could be fully enveloped by an ellipse of critical defect size then its precise shape became irrelevant. When groups of defects are to be considered then the stress concentrations resulting from each individual defect become additive in the region between the defects. The coalescence conditions have been summarised diagramatically (Figure 2.4) This analysis was for defects on the same plane, vertical separations of the same order as the horizontal separations would increase the diameter at which coalescence occurred by about 30%.

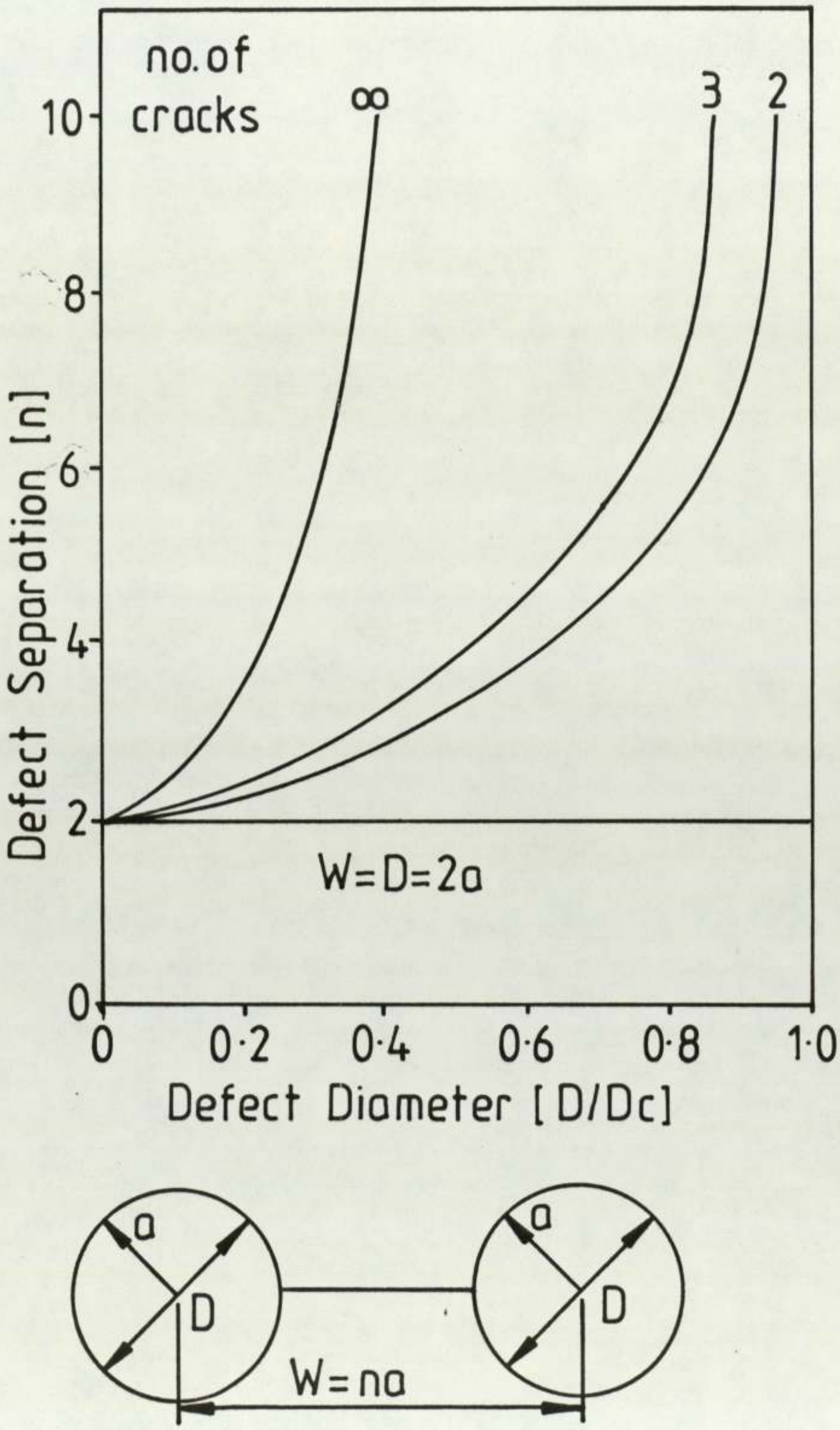

Figure 2.4

Coalescence conditions for various groups of circular embedded cracks.

2.4 Elastic-Plastic Fracture Mechanics.

The use of an elastic-plastic analysis to fracture criteria has become necessary for conditions where an L.E.F.M. approach may be invalid. For example, service conditions for low strength structural steel such as bridges require section sizes less than those specified for the mainteanance of plane strain conditions, hence, fracture toughness data generated from specimens having section sizes of design interest would be invalid because of the development of a large plastic zone. Alternatively, the use of specimens to ensure L.E.F.M. conditions would not be representative of the material in service and would require substantial test equipment.

In an attempt to overcome this problem a number of analytical techniques have been used to extend linear elastic fracture mechanics into the elastic-plastic regime. The most widely reported techniques being:

i) Crack opening displacement (C.O.D.)

ii) J - integral

iii) R-curve analysis.

2.4.1 Crack Opening Displacement (C.O.D.)

It was proposed by Wells (110) that the failure behaviour in the vicinity of a crack tip could be characterised by the opening of the notch faces figure 2.5 illustrates this point. Using Dugdales' strip yield model (III) the C.O.D. has been related to the applied stress and crack length such that the displacement at the original crack tip, , can be given by:

$$\delta = \frac{\pi \sigma^2 a}{E \sigma ys} \qquad - 2.16$$

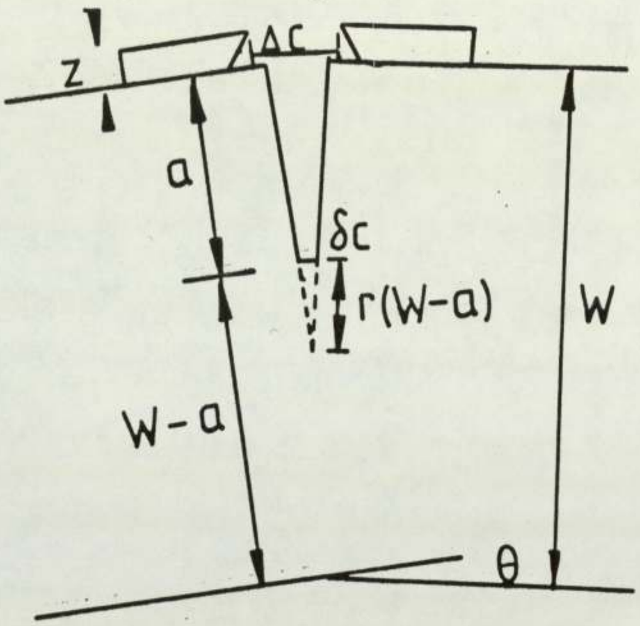

Figure 2.5.

C.O.D. specimen.

since for a through thickness crack of length 2a

$$K_I = \sigma\sqrt{\pi a} \qquad - 2.17$$

and hence $$K_I^{2} = \sigma^{2} \pi a \qquad - 2.18$$

by combining equations 2.18 and 2.16

$$K_I^{2} = E\ \sigma ys\ \ \delta^{w} \qquad - 2.19$$

and as $$E = \frac{\sigma ys}{\varepsilon ys} \qquad - 2.20$$

then by substituting equation 2.20 in 2.19

$$\frac{(K_I)^{2}}{(\sigma ys)} = \frac{\delta}{\varepsilon ys} \qquad - 2.21$$

or when K_I reaches a critical value K_{IC} and δ reaches δc

$$\frac{\delta c}{\varepsilon ys} = \frac{(K_{IC})^{2}}{(\sigma ys)} \qquad - 2.22$$

As $(K_{IC}/\sigma ys)^{2}$ has been related to the critical crack size in a particular structure so $(\delta^{c} / \varepsilon ys)$ maintains that relationship. By assuming that deformation occurs by a hinge mechanism rotating about a centre (w - a)/3 below the crack tip as shown in Figure 2.5 the δc can be obtained from:

$$\delta c = \frac{(w - a)\,\Delta C}{w + 2a + 3Z} \qquad - 2.23$$

It has been emphasised that due to the large scatter in experimental results (particularly in tests on welds) the lower bound values should be used for design purposes. However, as δc values are influenced by test temperature, specimen thickness and loading rate their interpretation and application must be done with the same care as C.V.N. or K_{IC} results.

2.4.2 J. Integral.

The J integral approach was developed by Rice (112) in 1968. This concept proposed that the stress-strain field at a crack tip could be characterised by an integration path sufficiently far from the crack tip to be substituted for a path close to the crack tip. By this method even though considerable yielding may have taken place at the crack tip its behaviour may be inferred by analysing a remote region. Hence, linear elastic concepts have been extended into the elastic-plastic region Figure 2.6 illustrates the schematic model. Under linear elastic conditions the J integral has been reported as being identical to the energy release rate per unit crack extension, G.

$$J_{IC} = G_{IC} = K_{IC}^2 \frac{(1 - \nu^2)}{E} \quad - 2.24$$

The energy line integral, J has been shown to be path independant and for elastic or elastic - plastic conditions may be given by:

$$J = \int_R Wdy - T \left({}^{\partial u}/_{\partial x} \right) ds \quad - 2.25$$

where: R = path surrounding a crack tip

W = strain energy density

given by $\int_0^\varepsilon \sigma \, d \varepsilon$

T = traction vector

U = displacement vector

S = arc length along R.

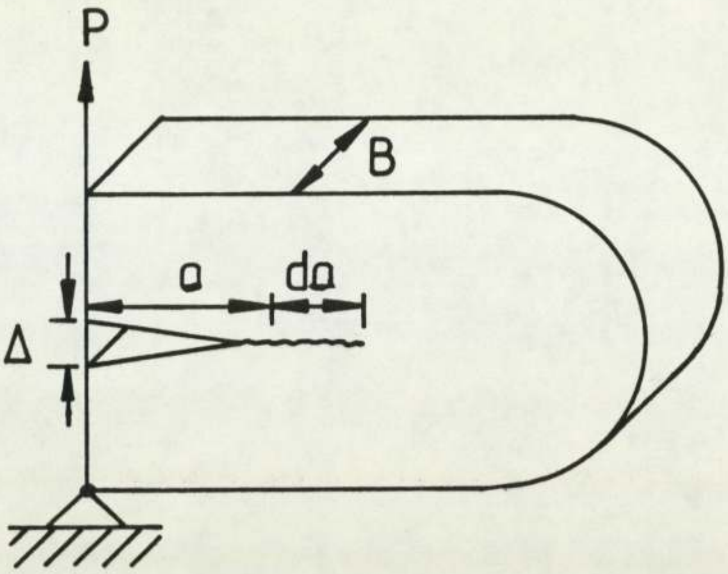

Figure 2.6

Schematic J - Integral test.

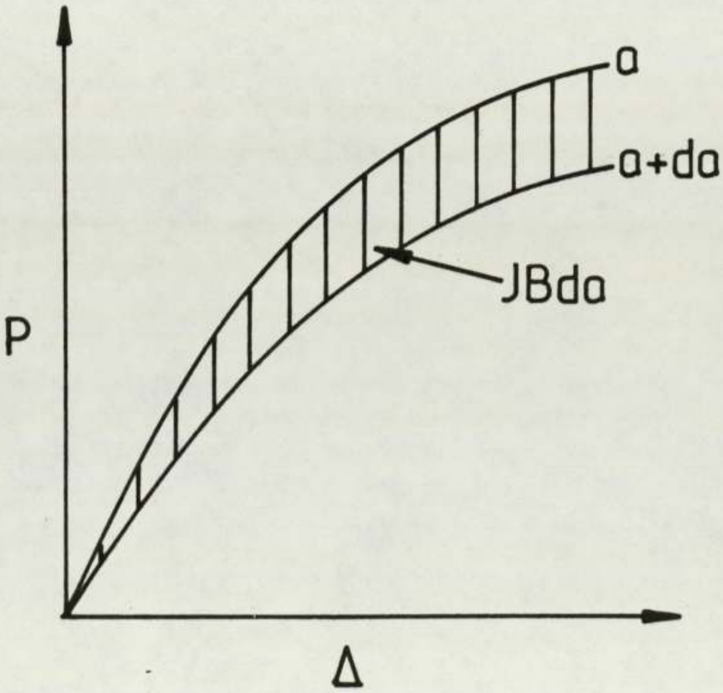

Figure 2.7

Interpretation of J - integral.

J may be considered as the difference in potential energy between two identically loaded bodies having neighbouring crack sizes.

$$J = \frac{1}{B} \frac{U}{a} \qquad - 2.16$$

From Figure 2.7 the shaded area being $dU = JBda$.

A tentative JIc test procedure and data analysis technique was suggested in 1973 by Landes et al (113) and is currently specified by A.S.T.M. E813-81 (114)

2.4.3. R - Curve Analysis.

R - curves characterise the resistance to fracture of materials during slow stable crack extension. An R (or resistance) curve is a graph illustrating the crack growth resistance in a material as a function of crack extension and is shown diagramatically in Figure 2.8. This analysis quantifies fracture toughness under plane stress conditions rather than plane strain i.e. negligible through thickness constraint and large scale crack tip plasticity. In Figure 2.8 the solid line represents the increase in crack growth resistance (K_R) with both increasing load and crack length for two initially different cracks. Where $K_R = K_C$ at $a_o = a_1$ and a_2 the two tangent points represent the critical plane stress intensity factor, K_c, for the particular crack length. While a JIc value denotes a single point on a curve the actual plot of an R-curve characterises the change in J with changes in crack length. The R-curve is the most general respresentation of plane-stress behaviour and depends only on temperature, strain rate and sample size.

The experimental determination of an R-curve has been detailed by A.S.T.M. E 561 - 81 (115). According to Novak (116) R - curves may be produced by using either 'load control' or 'displacement control' techniques. However, the load control procedure may only be used up to the K_c value, where unstable fracture occurred, while displacement control may be used to produce the complete R-curve. Heyer et al (117, 118) have developed the displacement control technique and reported on the equivalence of the two experimental procedures. Initial application of R - curve analysis was limited to high strength steel and aluminium alloys where L.E.F.M. principles directly applied. Non L.E.F.M. conditions such as experienced when testing low strength high toughness alloys has been more complex. The elastic - plastic analysis required for this operation has been termed the crack-opening-stretch (C.O.S.) method and its application has been documented by McCabe et al (119).

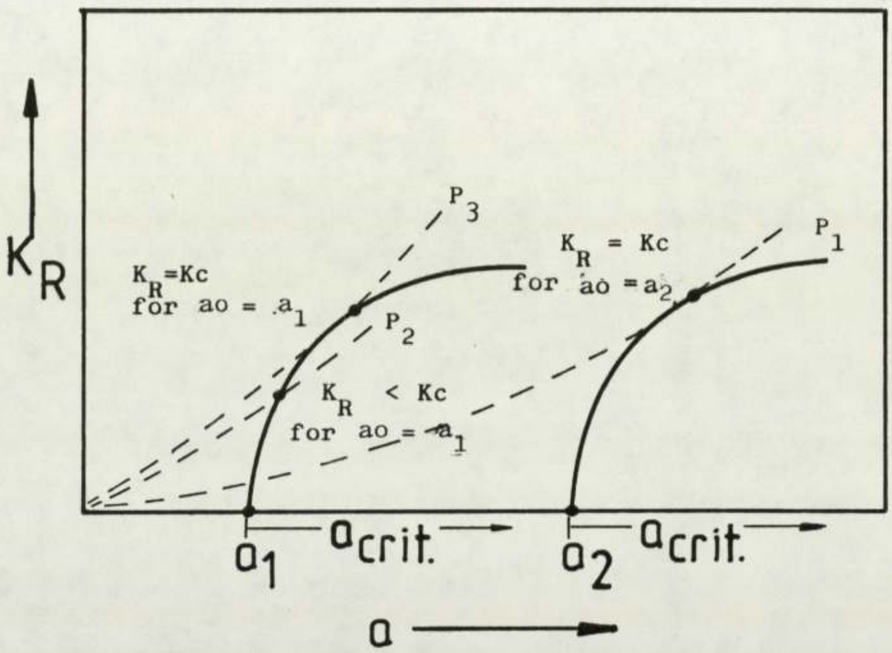

Figure 2.8

Basic principle of R - curves for use in determining Kc under different conditions of crack length.

2.5 Chevron Notched Specimens.

The widespread application and adoption of fracture toughness criteria in design and quality control has been retarded by the need for relatively complex and expensive speciments. In an attempt to overcome these problems extensive work has been carried out to develop a more simple and less expensive fracture toughness test. In this respect the analysis and use of chevron notched specimens has received much attention.

The two characteristic features of these specimens have been reported (120) as being:

i) A very high stress intensity concentration at the tip of the chevron notch.
ii) the stress intensity factor passes through a minimum value as the advancing crack grows.

As a direct result of these features a crack may be initiated at a low load therefore eliminating the need for expensive and time consuming fatigue precracking. Furthermore, as a graph of stress intensity against crack length exhibits a minimum value the fracture toughness may be calculated from the maximum test load. It has become generally accepted that the fracture toughness value generated from a chevron notched specimen is generally denoted K_{ICV}.

Due to the obvious advantages of such a specimen configuration considerable interest has been generated and their adoption for standardisation is currently being reviewed by A.S.T.M.

2.5.1 Historical Development of Chevron Notched Specimens.

The initial study of a chevron notch specimen was made in 1964 by Nakayama (121, 122) using an assymetrically notched bend specimen, Figure 2.9 The fracture energy of polycrystalline refractory materials was estimated from the area under the load - time record.

Tattersall and Tappin (123) extended this idea of Nakayama and produced a chevron V notched bend specimen. Figure 2.9b. By dividing the area under the load - displacement record by the area of the fracture surface it was possible to measure the work of fracture for ceramics and metals.

In 1972 Pook (124) suggested the use of a chevron notched bend bar as a possible simple fracture toughness test for quality control purposes. It was reported that by using suitably profiled side grooves the K_I against crack length characteristic may be modified to give a minimum at $a/w \approx 0.5$ where 'a' was the crack length and 'w' the specimen width. Additionally the initial K_I should be about twice the minimum value. It was expected that such a specimen should omit the fatigue precracking stage and allow a reasonable estimate of K_{IC} from the maximum test load value. Pook further reported that the presence of side grooves increased the stress intensity factor by about $(B/b)^{1/2}$ where b was the distance between side grooves and 'B' was specimen diameter.

Pooks' engineering approach was replaced by a more rigerous analysis in 1975 by Bluhm (125). The specimen was treated as a series of slices and the beam bending and beam shear effects on compliance were considered, interslice shear interactions being neglected. While this analysis only concerned mode I opening it was suggested that other modes would be reflected in the experimentally determined shear correction factor, k.

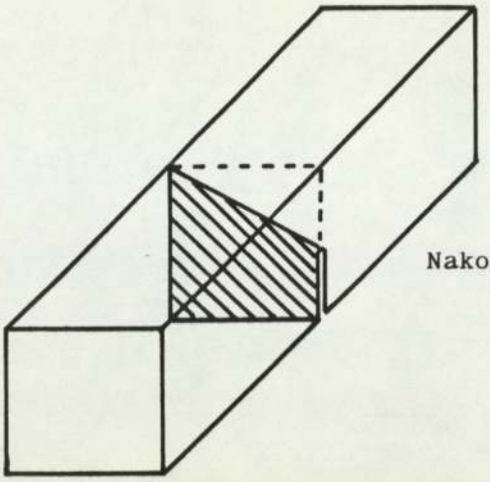

Nakoyama (1964)
(a)

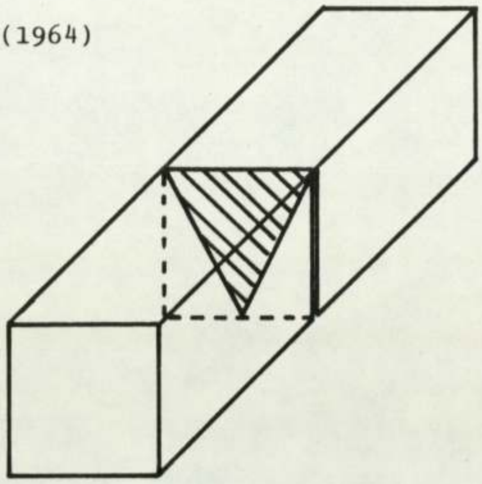

Tattersall
and
Tappin
(1966)
(b)

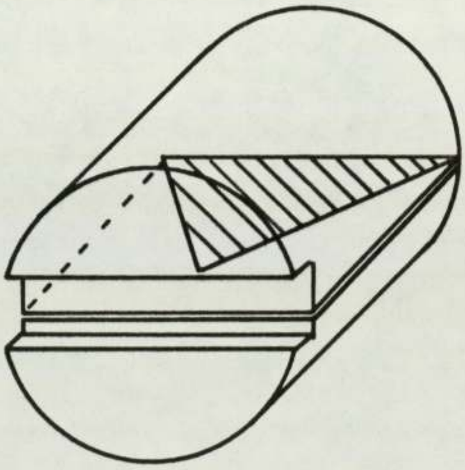

Short rod
Barker
(1977)
(c)

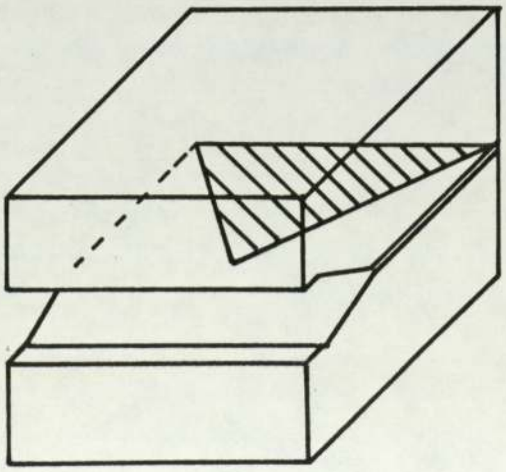

Short bar
Barker
(1979)
(d)

Figure 2.9

Chevron notched specimen configurations.

Although Bluhm concluded that the analysis appeared to be capable of predicting the compliance value of the Tattersall and Tappin specimen to within 3% it was Munz et al (126) who calculated this value for various specimens.

All of the foregoing investigations had concentrated on chevron notched bend specimens but in 1977 Barker (127) published a paper detailing the use of a short rod (SR) specimen. This geometry is illustrated in Figure 2.9 C and was proposed for simplified plane strain fracture toughness measurements. Barkers' work had been stimulated by the need for a rapid, inexpensive fracture toughness test for use on rock samples taken during mineral and oil exploration. As these samples were generally produced in the form of cylindrical rods this initial SR geometry was understandable. By 1979 a rectangular section specimen, the short bar (SB) had been presented (128), Figure 2.9 d. Numerous papers have been subsequently published covering aspects of compliance, size effects and validity.

2.5.2. The Short Rod/Short Bar Specimen.

The geometry of Barkers short rod/and bar specimens has been illustrated in Figure 2.9 c,d.

These consisted of specimen blanks into which the grip grooves and chevron V notches have been cut. It has been stated by Barker (129) that provided the specified specimen geometries and tolerances were adhered to then the compliance values of both samples will be equal. Having developed these specimen geometries Barker subsequently introduced a testing system specifically for short bars and rods. (129)

2.5.2.1 Theoretical Analysis of the Short Rod and Bar Specimen.

The analysis suggested by Barker (130) for the determination of K_{IC} from short bar specimens under L.E.F.M. conditions began by examining energy considerations such that.

$$\Delta W = G_{IC} \quad b \quad \Delta a \qquad - \ 2.27$$

Where ΔW was the irrecoverable work done on a specimen during a test, b was the average crack front width, Δa a small advance in the steady state crack length, G_{IC} has been defined as the crack extension force. From Figure 2.10 a the irrecoverable work ΔW done in advancing a crack an additional distance Δa was the area of the shaded region given by:

$$\Delta W = 1/2 \quad \overline{F} \quad \Delta X \qquad - \ 2.28$$

$\overline{F}$ was the average load between points A and B. ΔX was the distance between the release paths at the average load $\overline{F}$. Between A and B the incremental changes in elastic compliance, Δc, may be given by:

$$\Delta C = \frac{\Delta X}{\overline{F}} \qquad - \ 2.29$$

combining equation 2.28 with 2.29 to eliminate ΔX produced

$$\Delta W = 1/2 \quad \overline{F}^{2} \quad \Delta C \qquad - \ 2.30$$

Substituting for ΔW in equation 2.27 and taking the limit as ΔC and Δa approach 0 then

$$G_{IC} = \frac{F^{2}}{2b} \quad \frac{(dc)}{(da)} \qquad - \ 2.31$$

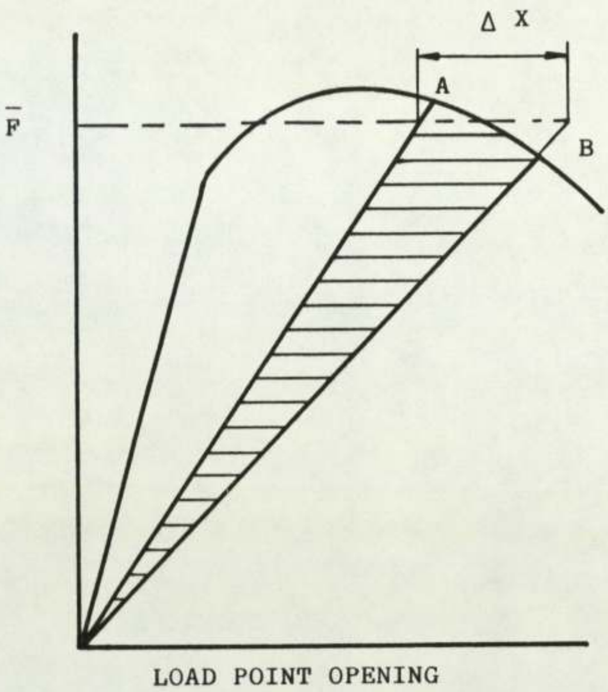

(a) Elastic

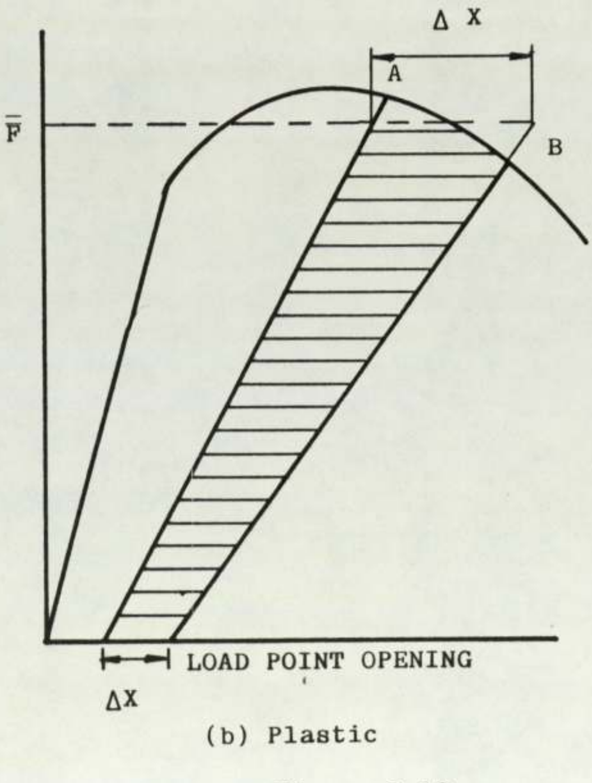

(b) Plastic

Figure 2.10

Schematic short rod/bar specimen behaviour.

from

$$G_{IC} = K_{IC} \frac{(1 - \nu^2)}{E} \qquad - 2.32$$

Equation 2.31 became

$$K_{IC} = \frac{F}{B^{3/2} (1 - \nu^2)^{1/2}} \quad f \quad ({}^{a}/_{b}) \qquad - 2.33$$

The factor $f\ (a/_{b})$ was given by:

$$f\ (a/_{b}) = \left[\frac{B\ d\ (CEB)}{2\ b\ d\ (a/_{B})} \right]^{1/2} \qquad - 2.34$$

Barker has stated that as this function was a dimensionless quantity it was therefore independent of specimen material. Under L.E.F.M. conditions the peak load was encountered at a constant position of (a_c /B) and hence the value of $f\ (a/_{B})$ at the maximum load Fc was a constant denoted by Barker as A. Hence,

$$K_{IC} = A \frac{Fc}{B^{3/2} (1 - \nu^2)^{1/2}} \qquad - 2.35$$

Barker subsequently replaced $(1 - \nu^2)^{1/2}$ by unity thus reducing equation 2.35 to

$$K_{IC} = A \frac{Fc}{B^{3/2}} \qquad - 2.36$$

In Barkers original work (127) A was estimated by comparing the published K_{IC} value for 2014 - T651 aluminium with the measured K_{ICSR}. This work produced an initial estimate of A = 20.8 ± 1.4, further exercises have attempted more detailed analytical procedures to evaluate A.

During non L.E.F.M. conditions the plastic deformation around the crack tip resulted in the unloading relaxation line being offset from zero, see Figure 2.10 b. Increased loading to a point B produced additional plastic deformation which on unloading accentuated the offset displacement. As in the L.E.F.M. analysis, the irrecoverable work may be given by the shaded area of Figure 2.10 b. By approximating this shape to a trapezoid

$$\Delta W = 1/2\ (1 + P)\ \bar{F}\ \ \Delta X \qquad - 2.37$$

P being defined as:

$$P = \frac{\Delta Xo}{\Delta X} \qquad - 2.38$$

This value P has now been referred to as a plasticity term. At extremes when P = 0 no additional plastic deformation was encountered and when P = 1 no further crack extension had occurred and ΔX would be due entirely to plastic deformation.

The change in compliance, ΔC, between the two relaxation paths was

$$\Delta C = (1 - P)\ \frac{\Delta X}{\bar{F}} \qquad - 2.39$$

Again, eliminating ΔX gave

$$W = 1/2\ (1 + {}^{P}/_{1 - P})\ \ \bar{F}^{2}\ \ \Delta C \quad - 2.40$$

and equating to G_{IC} produced.

$$G_{IC} = \frac{(1 + P)}{(1 - P)}\ \frac{\bar{F}}{2b}\ \frac{(dc)}{(da)} \qquad - 2.41$$

This equation was of the same form as equation 2.31 except for the additional $(1 + {}^{P}/_{1 - P})$ term and hence K_{IC} may be given by:

$$K_{IC} = \left(\frac{1 + P}{1 - P} \right)^{1/2} K\,a \qquad - 2.42$$

where K_Q was the L.E.F.M. K_{IC} value. Barker further simplified equation 2.42 by replacing $(1 + {}^{P}/_{1 - P})^{1/2}$ by $(1 + P)$, hence for non L.E.F.M. conditions.

$$K_{IC} = (1 + P)\, K_Q \qquad - 2.43$$

Ryder et al (131) have proposed an analytical procedure for obtaining the stress intensity co-efficients from experimental compliance results, such that:

$$CEB = \exp. \left(\exp \left(F \left({}^{a}/_{w} \right) \right) \right) - 2.7188 \qquad -2.44$$

2.5.2.1.1 Compliance Studies of Short Bar Specimens.

Munz et al (126) suggested the use of Bluhms (125) slice model for an analytical evaluation of the compliance of the short rod specimen. From Figure 2.11 the specimen was divided into a number of slices of thickness ΔZ and the total compliance was expressed by the summation of the reciprocals of compliance of all the slices. Thus:

$$\frac{1}{C_T} = \frac{[{}^{a}/_{W} - {}^{ao}/_{W}]}{[{}^{a1}/_{W} - {}^{a0}/_{W}]} \frac{1}{C(\alpha)} + \frac{k}{({}^{a_1}/_{W} - {}^{a0}/_{W}} \int_{({}^{a_1}/_{W})}^{({}^{a_1}/_{W})} \frac{1}{C\,\xi} \, \partial \xi \qquad - 2.45$$

where C_T was the total compliance of the short bar specimen.

$C(\alpha)$ was the compliance of a straight through crack specimen of thickness B and crack length ratio $\alpha = ({}^{a}/_{W})$. $C(\xi)$ was the compliance of a straight through crack specimen of thickness B and crack length ratio $= ({}^{x}/_{W})$. According to Bluhm, the interlamellar shear stress effectively increased the slice thickness. Quantitatively, this same effect has been achieved by increasing the slice thickness by an amount ΔZ^1 greater than the actual thickness.

$$\Delta Z^1 = k \, \Delta Z \qquad - 2.46$$

and for the short bar specimen k has been given by (132)

$$k = -1.38 \, ({}^{a0}/_{W}) + 2.71 \qquad - 2.47$$

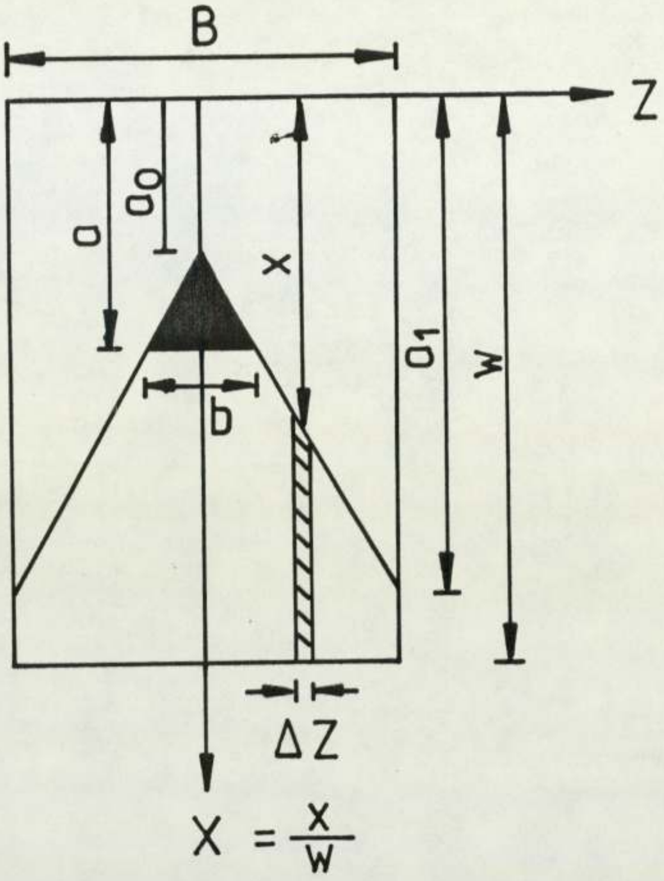

Figure 2.11

Fracture plane of a short-bar specimen using Bluhm's notation.

2.5.2.1.2 Stress Intensity Co-efficients from Compliance Studies.

By considering the geometric relation between crack front width, specimen width and change in compliance with crack length, the stress intensity factor K_{IC} for the short bar specimen has been presented as:

$$K_{IC} = \frac{P}{W^{1/2}} \left[1/2 \; \frac{[\, {a_1}/_{w} - {a0}/_{w} \,]}{[\, {a}/_{w} - {a0}/_{w} \,]} \; \frac{d\,(\,CEB)}{d\,({a}/_{w})} \right]^{1/2} \qquad - 2.48$$

or

$$K_{IC} = \frac{P\ Y^*}{BW^{1/2}} \qquad - 2.49$$

where

$$Y^* = \left[1/2 \; \frac{[\, {a_1}/_{w} - {a0}/_{w} \,]}{[\, {a}/_{w} - {a0}/_{w} \,]} \; \frac{d\ (CEB)}{d\ ({a}/_{w})} \right]^{1/2} \qquad - 2.50$$

The minimum values of the function given by equation 2.50, denoted by Ym*, corresponded to the maximum test load, Pmax. While most workers have presented their results in terms of Ym* Barker generally presented data in terms of a normalised factor A. Bubsey et al (133) related Ym* to A by:

$$Ym^* = A \sqrt{\left(\frac{w}{B}\right)} \qquad - 2.51$$

The differences in presenting data combined with the use of non standardidised specimen geometries has resulted in some disparity in published work. Newman (134) has reported Ym* values ranging from 25.1 to 32.7. It has been reported (130) that the value Y* (or A) is independant of specimen material.

2.5.2.2. Limitations of the Short Bar Specimen.

In Barkers' original works there was no limitation imposed on the plasticity value 'p'. Subsequent publications (135) suggested a limiting validity criteria to be $p \leq 0.2$.

Barker (136) has also put forward several constraints for the chevron notch tip configurations if plane strain conditions are to be maintained, see Figure 2.12. The scaled slot thickness τ/B must be $\leq 0.03B$. If $0.02 \leq \tau/B \leq 0.03$ the slot bottoms must be pointed with an included angle $\leq 60^\circ$. (2.12 a) When $0.01 \leq \tau/B \leq 0.02$ the slot bottoms may be either pointed or radiused as in 2.12b for $0.00 \leq \tau/B \leq 0.01$ any tip profile is considered acceptable (2.12C)

It has been reported that the use of chevron notched specimens for the testing of brittle materials, i.e. those exhibiting a 'flat' crack growth resistance curve is well justified. (135) Figure 2.13 (a) illustrates the ideal condition for fracture of a brittle material. As previously stated due to the high stress intensity at the notch tip cracks are initiated at low loads. As the load is increased to Pl the crack advances to point A i.e. where the stress intensity factor equals K_{IC}. Further increases in load are necessary to extend the crack to points B and C.At the maximum load, Pmax, a point of tangency is obtained between the crack growth curve and the minimum value of the stress intensity against crack length curve. However, as many engineering materials under non plane strain conditions exhibit a rising crack growth resistance curve the validity of using such an analysis is less certain. Figure 2.13 (b) illustrates a possible 'rising' crack

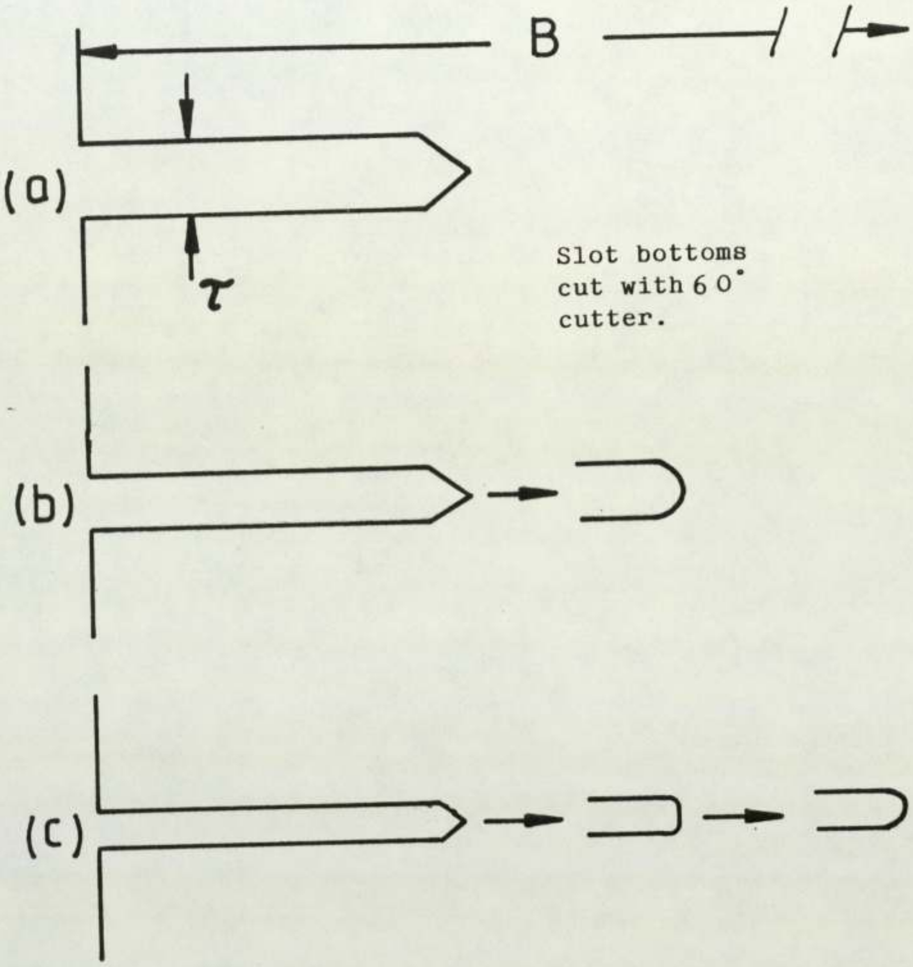

Slot bottoms cut with 60° cutter.

Figure 2.12

Chevron notch tip profile.

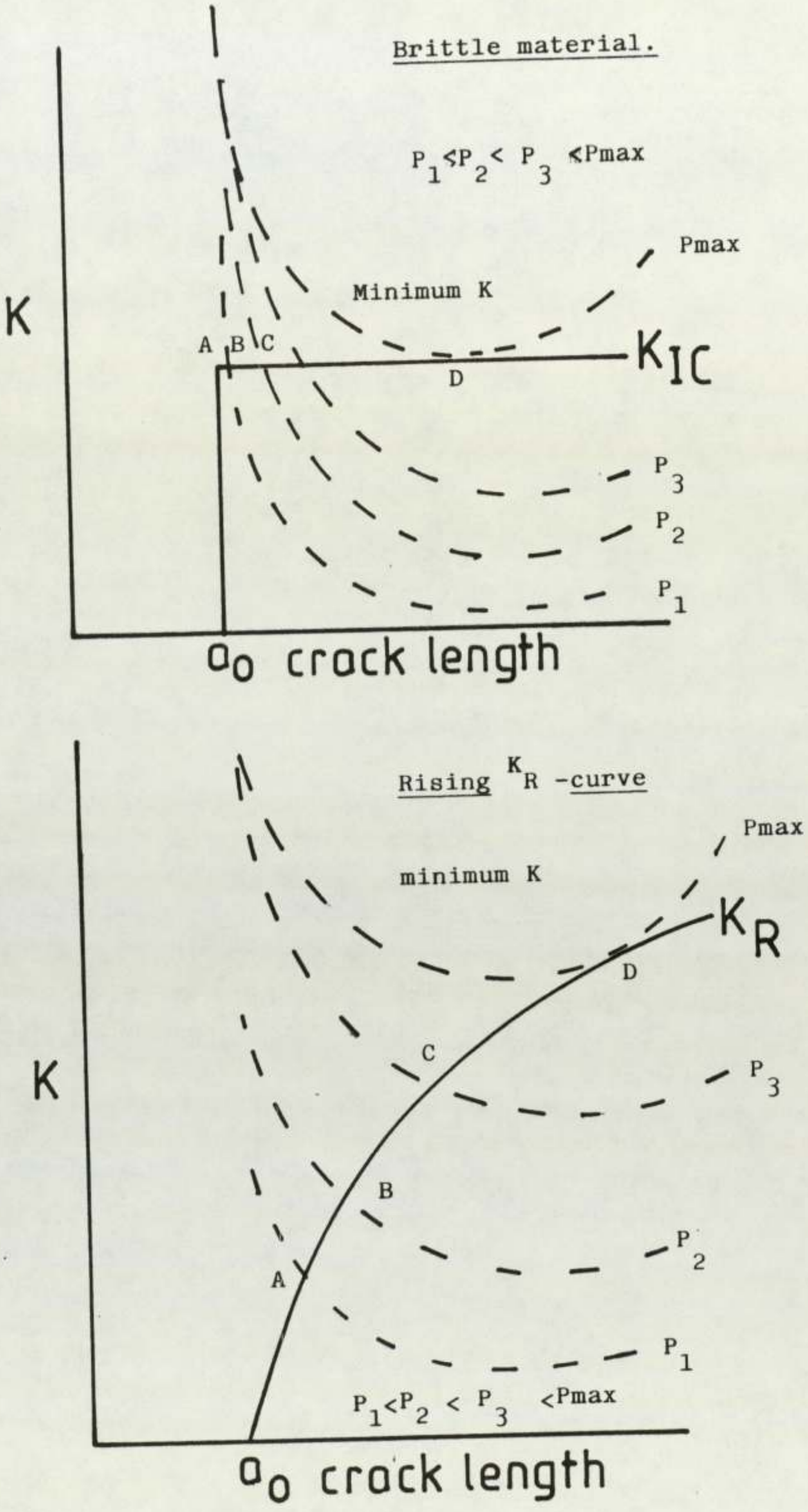

Figure 2.13

Fracture of material using a chevron notched specimen.

growth resistance curve. As the load is increased the crack extends stably until the maximum load is reached. The point of instability, D, does not correspond to the minimum K value and consequently the maximum load and minimum normalised K value cannot be used to measure K_{IC}. Furthermore, if the specimen width was smaller than the case illustrated then the point of instability would occur lower down the KR curve. Conversely, a larger specimen would exhibit unstable crack growth at a higher KR value. This characteristic introduces a specimen size effect. Barker (136) has suggested a specimen size criterion of

$$B \leq 1.25 \frac{(K_{ICSR})^2}{(\sigma \, ys)} \qquad - 2.52$$

Several authors have published results concerning specimen size effects (134, 137) but the most authoritative findings should be produced by an ASTM task group.

2.6 Fracture Toughness of Flake Graphite Irons.

A general summary of fracture toughness values, together with other engineering data, has been published which shows that K_{IC} increases with grade from 12 $MNm^{-3/2}$ to 24 $MNm^{-3/2}$ (138). It has been reported (139) that the first measurements of the fracture toughness of flake graphite irons were made by Glover and Pollard. (140, 141) This work investigated graphite size and varying matrix structures ranging from fully ferritic to fully pearlitic. It was found that the fracture toughness varied only slightly with graphite size but was significantly altered by matrix structure. As the matrix ferrite content increased, causing a decrease in hardness, the fracture toughness increased slightly to a maximum of about 20 $MNm^{-3/2}$ at 150 H_B When the hardness was reduced below 150 H_B the fracture toughness was significantly lowered to 12 $MNm^{-3/2}$ at 100 H_B this trend is illustrated in Figure 2.14. Other workers (142) reviewed the exercise by Glover and Pollard (140, 141) and demonstrated the variation of fracture toughness with matrix structure, see Figure 2.15. In the low ferrite materials the ferrite was always associated with the graphite flake and crack propatation, after failure of the graphite, crack extension was into the ferrite. The fracture mode was transgranular and exhibited brittle fracture river patterns. In mixed ferrite/pearlite matrix structures cleavage fracture of the ferrite propagated into the pearlite. If the pearlite was associated with the graphite then crack propagation was across the pearlite lamellae, dimples, indicate of plastic deformation being observed. When the graphite-pearlite interface exhibited decohesion then the crack was contained within the graphite. It was interesting to observe that these workers found that fatigue precracking was unnecessary as similar results could be produced using machined notches.

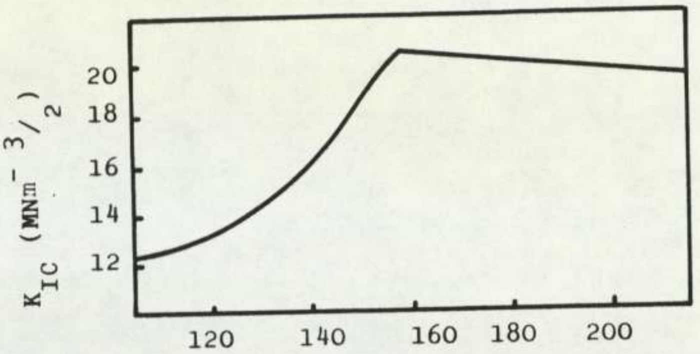

Hardness Hv
Variation of Fracture Toughness
with Hardness.

Figure 2.14

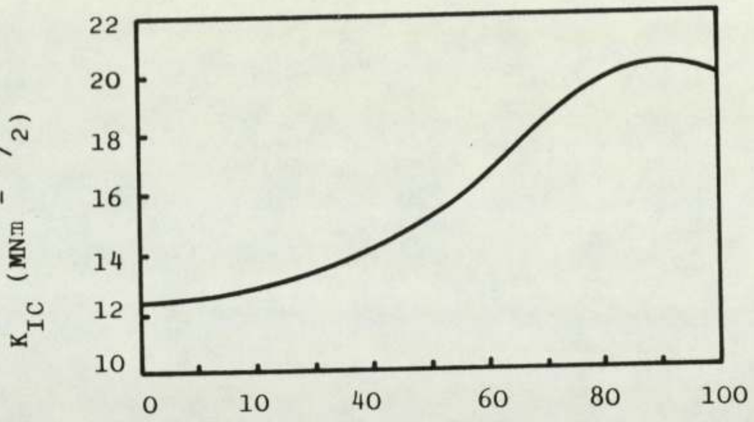

% Pearlite
Dependence of Fracture Toughness on
Amount of Pearlite in Matrix.

Figure 2.15

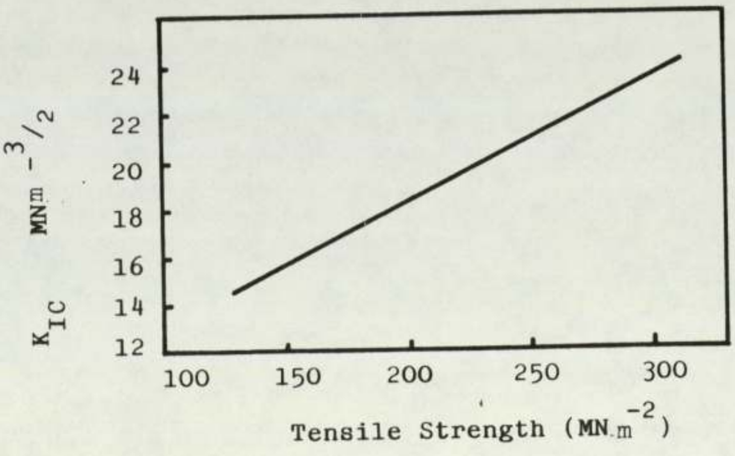

Relationship Between Fracture Toughness
and Tensile Strength for Flake Graphite
Cast Iron.

Figure 2.16

Baker (143) has also investigated the effect of varying structures, and hence tensile strengths, on the fracture toughness of irons of a given chemical composition. This relationship has been illustrated in Figure 2.16. It was reported by Baker that differences in fracture toughness of up to 25% could be produced by using single etched notch bend specimens rather than compact tension specimens. This apparent anomaly was attributed to the elastic modulus being higher in compression than tension.

Gruter (144, 145, 146) has measured the fracture toughness of a series of four as-cast flake graphite irons of various carbon equivalent and predominently pearlitic structures. A fifth iron was tested in the as-cast condition and after various heat treatments. It was found that the fracture toughness of the as-cast irons increased with tensile strength and with decreasing carbon equivalent. None of the heat-treated irons exhibited fracture toughness values comparable with those obtained in the as-cast condition. The minimum measured K_{IC} value being 11.53 $MNm^{-3/2}$ for an as-hardened martensitic iron.

Gilbert (147) has considered critical defect sizes for the general engineering grades of flake graphite irons using the equation:

$$Ac = \frac{1}{\pi} \frac{(K_{IC})^2}{\sigma \, Max} \qquad - 2.53$$

Where Ac was the critical crack length at the maximum design stress level, σ Max. A typical K_{IC} value of 20 $MNm^{-3/2}$ was assumed and the design stress was (0.25 x tensile strength) where the tensile strength varied between 220 and 300 MNm^{-2}.

The results of this analysis showed that the critical defect sizes were between 22.6 mm and 42.1 mm. From this it was concluded that as the critical defect size was very large, fracture toughness data had little relevance in the normal design of grey iron castings which could be safely based on established procedures.

A model for the fracture behaviour of pearlitic grey irons has been suggested by Verma and Berry (148) using the Hornbogen - Motz concept. (142) This proposed that under a tensile load the graphite flakes acted as cavities and carried no load. Furthermore, the stress intensity $K_{Ieff.}$ was not determined by the external stress σ, but by a higher effective stress $\sigma_{eff} = \sigma + \Delta\sigma$, where $\Delta\sigma$ was produced by the intrinsic microcracks. These authors indicated that the eutectic cell size was probably the most important parameter controlling the fracture behaviour of pearlitic grey irons. At a constant value of carbon equivalent the fracture toughness was found to decrease as section size increased.

2.7 Fracture Toughness of Nodular Graphite irons.

Bradley (149) has recently suggested that for the first 30 years of its commercial life nodular iron has been relegated to low toughness applications. This limitation was attributed to the relatively poor Charpy impact values obtained for nodular iron, typically 20J, compared with 84-112J for cast steels. Furthermore a lack of casting expertise sometimes produced disasterous service experiences due to the production of poor quality iron. The advent of fracture mechanics has assisted the more accurate characterisation of the toughness of nodular cast iron.

The earliest work on the fracture toughness measurements of nodular iron was carried out in America (150, 151, 152) and Britain (153, 154, 155) during the early/mid 1970's. Much of this early work was concerned with establishing test validity and investigating upper and lower shelf fracture modes. It was apparent from these authors that only high strength nodular irons produced valid, room temperature K_{IC} values. The irons contained predominantly pearlitic or martensitic matrix structures, ferritic structures required low temperature testing to obtain valid results. Many studies have now used J - integral or COD techniques to obtain fracture toughness results.

The large difference in Charpy toughness results between nodular iron and steel has not generally been confirmed by fracture toughness. This has been attributed (156) to the loss of constraint and general yielding of cast steel Charpy test pieces while nodular iron experienced crack extension while fully constrained. Hence, the toughness of steel was overestimated. Converseley fatigue pre-cracked steel and nodular iron specimens both experienced crack extension without any loss of constraint.

An analysis of critical defect sizes for a ferritic nodular iron, assuming upper shelf behaviour, has been stated as 13.5 cm at a design stress of 2/3 yield strength. Even at design stresses approaching the yield strength a critical defect size of 4.0 cm has been noted. (149) This worker concluded that nodular iron was very flaw tolerant.

It has been reported (157) that in ferritic nodular irons crack inition occurred in areas of high nodule count by a linking up of these nodules. Crack growth exhibited a similar mode causing cracks to follow a path connecting the maximum number of nodules. However, it has been stated elsewhere that fracture toughness was not influenced by increased numbers of nodules. (158) It has been considered (149) that as the ductile fracture process by void coalescence was initiated at the nodule/ferrite interface the maximum toughness should be obtained with well spheroidised evenly distributed nodules. In ferritic iron additions of silicon considerably reduce the fracture toughness. (159)

Recently there has been renewed interest in high strength nodular irons produced by solution treatment and subsequent austempering.(71, 72) Blackmore (160) has demonstrated that the fracture toughness of austempered nodular irons to be approximately twice that of normalised, pearlitic nodular iron, 84 - 95 $MNm^{-3/2}$ and 39 - 47 $MNm^{-3/2}$ respectively. In this work it was observed that increased silicon levels increased the fracture toughness of both pearlitic and bainitic irons. In pearlitic structures increased silicon additions promoted ferrite encapsulating the graphite nodules in a bullseye form. Fracture toughness being increased due to the ferrite retarding the progressive crack growth from nodule to nodule. In bainitic irons silicon additions favour the retention of austenite. It is known that in steels high levels of retained austenite increased fracture toughness (161) and a similar effect was thought to have occurred in the bainitic iron. Furthermore, large plastic strains ahead of a growing fatigue crack have caused the retained austenite to transform to martensite. The accompanying volume expansion resulted in plastically induced crack closure. This improved both the fatigue crack growth rate and the fracture toughness.

2.8 Fracture Toughness of Nickel-Chromium Martensitic White Irons.

The fracture toughness testing of white iron, particularly the higher alloyed nickel-chromium martensitic and high chromium irons has been restricted due to the difficulties of sample production. Diesburg (162) has shown that K_{IC} values may be obtained using compact specimens these samples being produced by grinding, electro discharge machining and finally fatigue precracking. This work revealed the K_{IC} of a tempered eutectic martensitic iron (9% chromium - 6% nickel) to be 25.5 $MNm^{-3/2}$ Diesburg and Borik (34) reiterated these results. The initial work was concerned with establishing techniques and engineering data, studies of metallurgical variables were developed later, however the emphasis appears to have been on high chromium irons not martensitic irons. Sare (87) has measured the fracture toughness of both a 2% chromium - 4% nickel iron and a 10% chromium - 6% nickel eutectic iron in various matrix conditions. It was evident that the highest K_{IC} values were obtained in the as-cast condition, 25.6 $MNm^{-3/2}$ and 30.6 $MN_m^{-3/2}$ respectively compared with 19.1 $MN_m^{-3/2}$ and 26.2 $MN_m^{-3/2}$ in the fully heat treated condition. This difference was generally attributed to the greater crack blunting effect of austenite relative to martensite. Blackmore (163) has quoted a published range of K_{IC} values of nickel-chromium irons as 19 $MN_m^{-3/2}$ - 31 $MNm^{-3/2}$, this range presumably being the experimental data of Sare. (87) Blackmores' own work yielded mean K_{IC} values for a 5% nickel - 9% chromium iron of 30.6 $MN\,m^{-3/2}$ and 28.7 $MN\,m^{-3/2}$ for SEN and CT specimens respectively. Table 2.1 summarises the fracture toughness values of nickel-chromium white cast irons.

Alloy	Condition	K_{IC} (MNm$^{-3/2}$)	Ref
6 NI - 9 Cr	2 hrs at 210°C	25.5	34
4 Ni - 2 Cr	As cast	24.2	34
4 NI - 2 Cr	As cast	25.6	87
	4 hrs at 275° C: AC	26.2	87
	4 hrs at 450°: AC:) 4 hrs at 275°C: AC)	19.1	87
6 Ni - 10 Cr	As cast	30.6	87
	4 hrs at 800°C: AC	26.6	87
	4 hrs at 800°C: AC:) 4 hrs at 275°C: AC)	26.2	87
5 NI - 9 CR	2 hrs 800°C: AC:) 10 hrs at 275°C: AC)	30.6 *	163
	2 hrs 800°C: AC:) 10 hrs at 275°C; AC)	28.7 +	163

* SEN specimens

\+ CT specimens

Table 2.1

Summary of K_{IC} values for Nickel - Chromium white irons.

2.9 Fracture Toughness of High Chromium Cast Iron.

Most of the published work involved with the fracture toughness of white iron appears to be principly concerned with high chromium cast iron. Much of the K_{IC} data generation being carried out by Climax Molybdenum personnel, particularly Diesburg. As these alloys exhibit a duplex microstructure the fracture modes have been observed to vary with changes in microstructural parameters. These will now be discussed:

2.9.1. The Matrix Phase.

The transformations which the matrix may undergo have been presented in section 4.6.2.1, but to summarise, may consist of austenite or some decomposition product of austenite such as pearlite or martensite. Service conditions being concerned with only two matrix structures, that is austenite and martensite, soft pearlitic structures exhibit poor wear characteristics.

2.9.1.1. Austenitic Matrix Structures.

It is generally agreed in the literature that predominantly austenitic matrix structures exhibit higher toughness values than martensitic ones (see for example 87 and 139). This fact being attributed to crack blunting effect of austenite as discussed with regard to martensitic nickel-chromium irons (section 2.8). Zum Gahr and Scholz (164) have reported that for austenitic material fracture toughness increased with increasing bulk hardness, see Figure 2.17 however, no explanation of this observation was offered. Diesburg and Borik (34) have found that the K_{IC} of predominently austenitic material decreased when patches of precipitated secondary carbides were present.

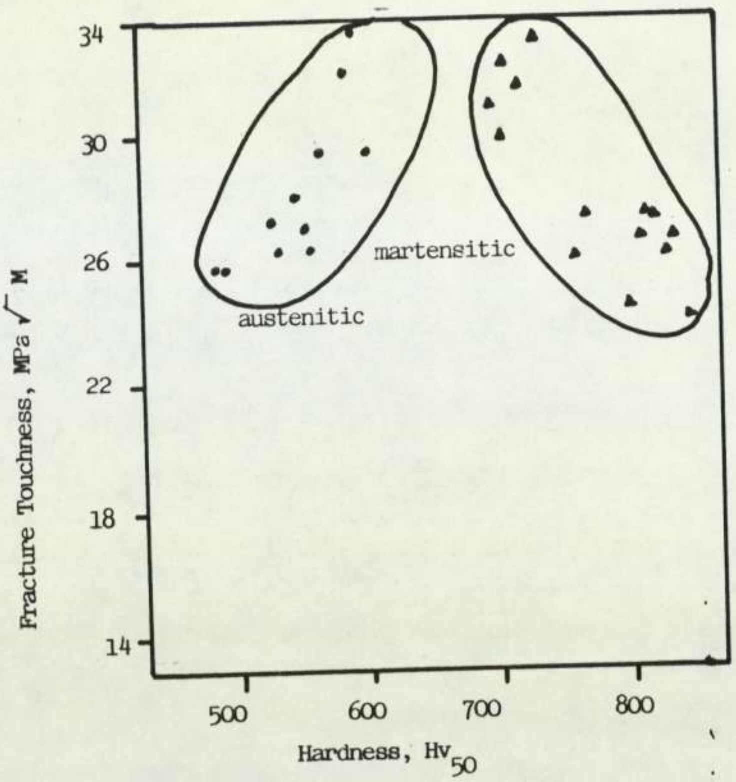

Figure 2.17

Relationship Between Fracture Toughness and Hardness

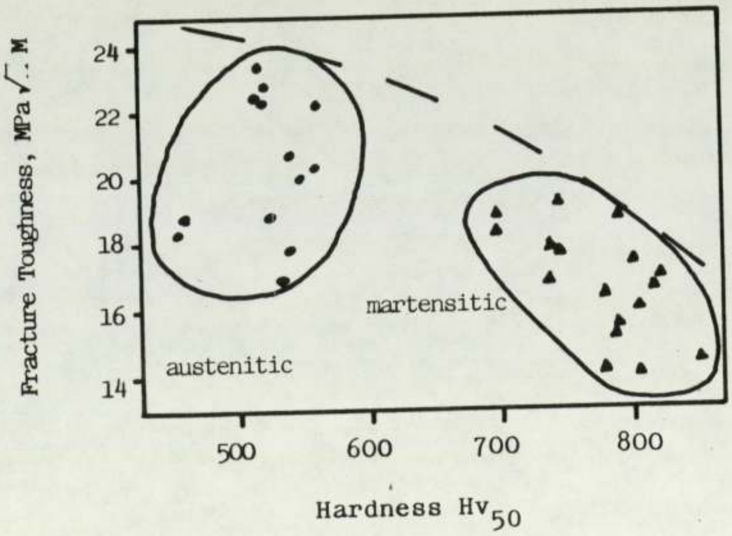

Figure 2.18

Fracture Toughness Against Hardness For A Carbon, Chromium, Molybdenum, Copper Alloy.

Fracture surfaces of these alloys have been observed to be dominated by cleavage cracking of eutectic carbides and preferential orientation of the crack path through eutectic carbides. Fracture of the matrix was reported to have been in a ductile manner although the failure mechanism was controlled by the attainment of a critical fracture stress (σF^*) of the alloys. (165) The fracture toughness was found to increase as the mean matrix ligament length increased i.e. the interparticle spacing increased. The fracture of the austenite has been described as ductile tearing.

2.9.1.2. Martensitic Matrix Structures.

The fracture toughness of martensitic high chromium cast iron has generally been reported as being lower than austenitic structures. Furthermore, Zum Gahr and Doane (169) have observed that increasing the bulk hardness of martensitic structures reduces the fracture toughness, see Figure 2.18. The literature is unanimous in emphasising the importance of the secondary chromium carbide precipitate in influencing the fracture behaviour of this material. Durman (166) has documented a constant level of toughness regardless of carbon content and volume fraction of eutectic carbide. In this work the dimple rupture feature size for all materials examined was found to be similar, approximate spacings being 0.8 - 1.0 μM. Furthermore, by using Krafts' equation (167) to predict a theoretical tensile instability size based on experimentally determined values of K_{IC}, E and N, values of 0.5 - 0.8 μM were predicted. These values correlated well with the observed characteristic microstructural feature dimension of secondary carbide spacing, 0.7 - 1.0 μM. It was concluded that uniformity of the secondary carbide distribution was responsible for the constant level of toughness in martensitic material. Biner (165) also studied the relationship between K_{IC} and secondary carbide distribution. It was argued that void formation

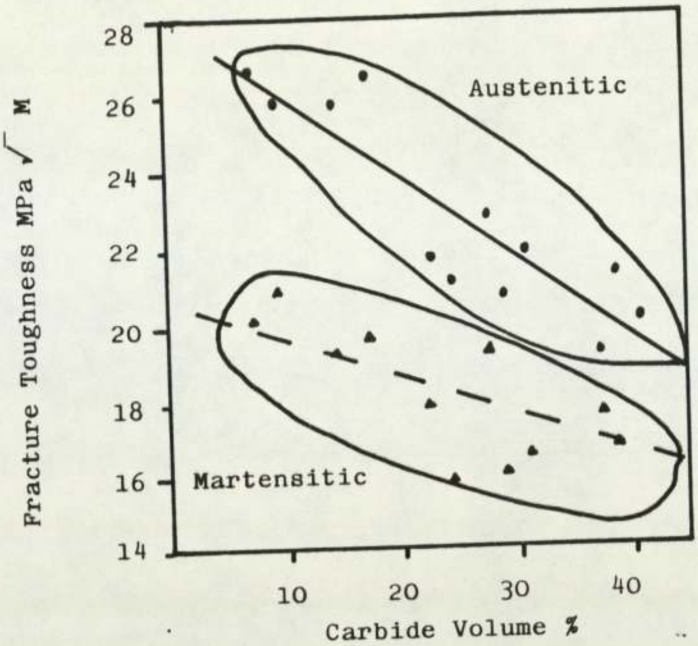

Figure 2.19

Fracture Toughness For Austenitic And Martensitic Matrix Irons as a Function of Carbide Volume.

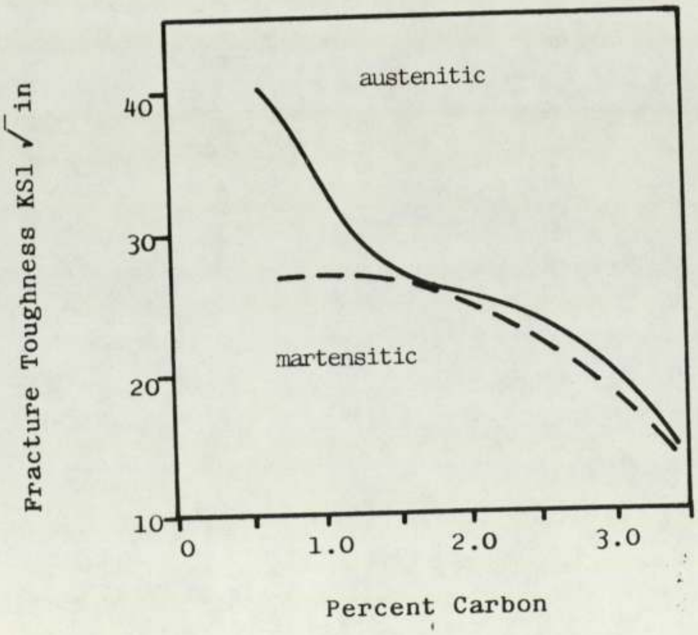

Figure 2.20

Fracture Toughness of As-Cast And Hardneed Material.

could be achieved at low levels of applied stress and the final stress controlled failure occurred just after void initiation producing a direct void sheet formation.

2.9.2. Eutectic Carbide Phase.

The eutectic carbide phase may be influenced by chemical composition, (thereby altering the volume fraction of carbide present) and high temperature modification. Both of these parameters may have significant effects on toughness.

2.9.2.1. Carbide Volume Fraction.

The volume fraction (V_f) of eutectic carbides may be estimated from the empirical relationship given by Maratray (168)

$$\% k = 12.33 (\%C) + 0.55 (\%Cr) - 15.2 \qquad - 2.53$$

This relationship may be used to produce the approximate carbide content for the range of carbon and chromium levels indicated on the austenite liquidus surface of the Fe-Cr-C system (see section 4.4)

Zum Gahr and Doane (169) have measured the K_{Id} values for a number of chromium irons with V_f ranging between 7% and 45%, these results are illustrated in Figure 2.19. It is clear that toughness decreased with increasing volume fraction of carbides for both martensitic and austenitic structures. A subsequent report by Zum Gahr and Scholz (164) also showed the same trend between K_{IC} and V_f for a similar range of alloys. Durman (166) investigated the effect of carbon content on K_{IC} and produced the graph illustrated in Figure 2.20. The austenitic material revealed the marked dependence of K_{IC} on carbon level up to 1.4% carbon (at which point the carbide formed a continuous phase.) A less pronounced dependence was then observed until at higher carbon levels when the material became hypereutectic. The heat treatment martensitic material was relatively insensitive to carbon content again until the hypereutectic structure was obtained.

2.9.2.2. Eutectic Carbide Morphology.

The usual, commercially practised thermal processing of high chromium cast iron does not have any significant effect on the morphology of the eutectic arbide. However some work has been carried out which investigated higher temperature, spheroidising heat treatments.

The first study was by Durman (166) who treated alloys at 1150°C and reported maximum K_{IC} of approximately 45 $MNm^{-3/2}$ after an 8 hour treatment time. This compared with a K_{IC} of 27 $MNm^{-3/2}$ in the as cast condition. Later work by Diesburg and Borik, (34) carried out at 1150°C, confirmed Durman's findings and also revealed that finer, chill cast structures spheroidised more easily than coarse, sand cast ones. Biner (165) studied the effects of chemical additions and treatment time on the 1180°C spheroidising process of a 15% chromium iron. Using additions of molybdenum, tungsten, vanadium and manganese at levels up to 6% it was found that molybdenum and tungsten both accelerated the spheroidising treatment. However, in order to obtain a similar degree of transformation approximately 2.5 times as much tungsten than molybdenum must be used. Vanadium and manganese did not produce any significant spheroidising effect. When using the molybdenum addition a definate peak in K_{IC} (Figure 2.21) was observed after an 8 hour treatment time.

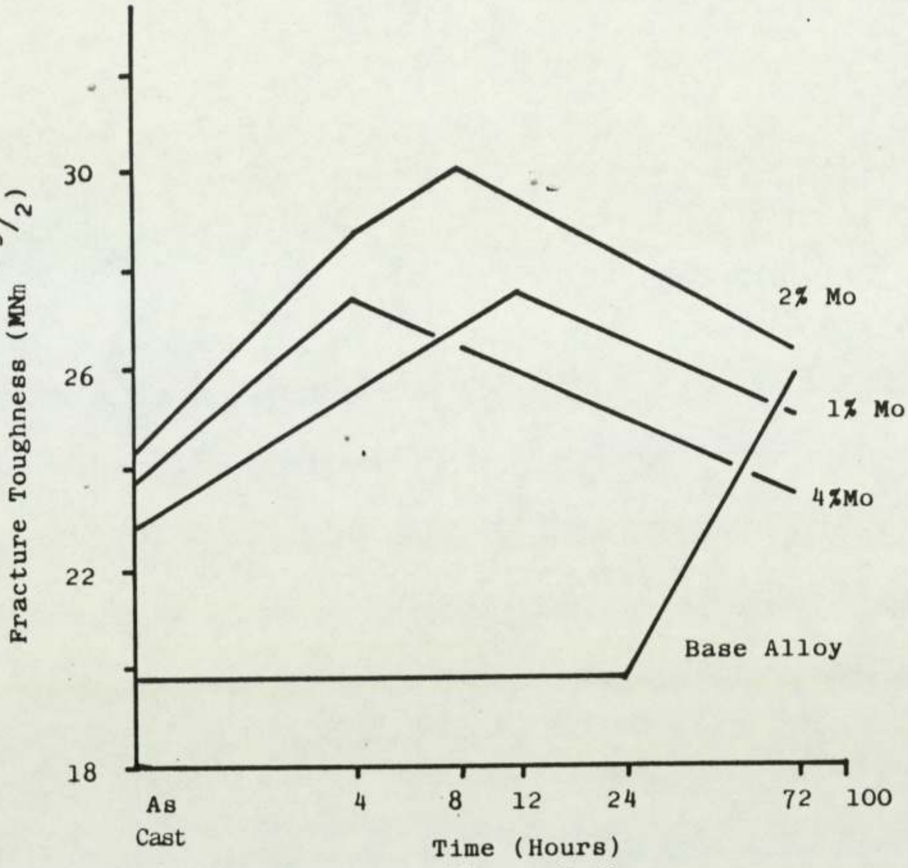

Figure 2.21

Fracture Toughness Variation of Molybdenum Containing Alloys with Holding Periods at 1180°C

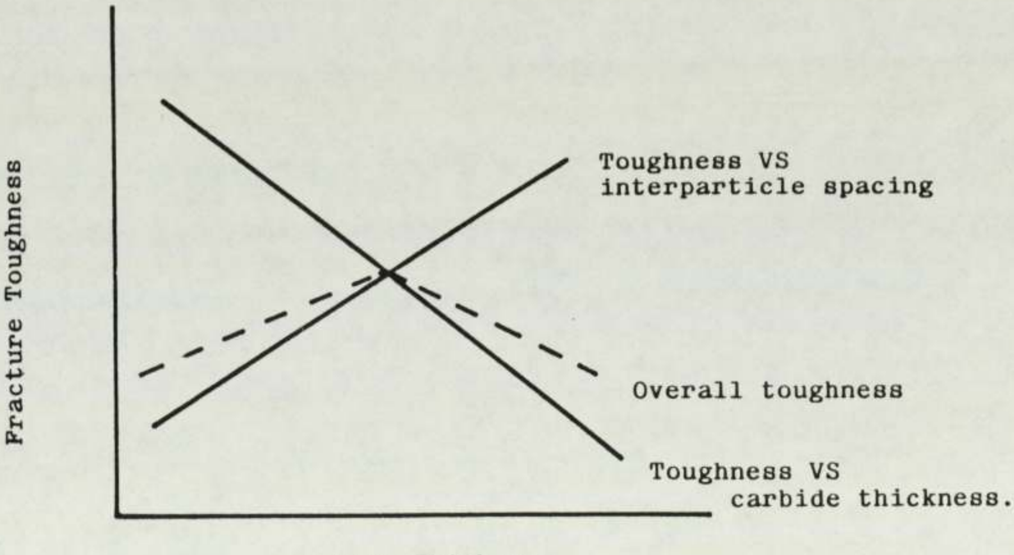

Figure 2.22

Schematic Representation of Role of Eutectic Carbide Morphology On The Fracture Toughness of High Chromium Cast Irons.

This peak in properties was attributed to the product of two competing fracture processes, namely:

i. Eutectic carbides fracture at relatively low stress levels. An increase in the size of the nucleated micro-crack which consequently lowers the stress level necessary for crack propagation.

ii. An increase in the interparticle spacing between eutectic carbides caused an elevation of the stress level necessary to propagate the crack between two eutectic carbides. This is due to a decrease in triaxiality and also due to an increase in the ligament length.

In summary, toughness increases with increasing interparticle spacing and decreases with increasing carbide size. This may be illustrated schematically as in Figure 2.22.

Katavic (170) has reported the rounding of carbides at 1175°C and an associated improvement in fracture toughness. In a paper principly concerned with microstructural examination of wear resistant cast irons Powell (171) has documented that high temperature annealing did not produce any modification of the eutectic carbide morphology.

The refinement of eutectic carbide morphology by hot working and the subsequent improvement in toughness has been noted by Durman. (166) Following a 50% deformation at 1150°C the K_{IC} of specimens having the notch orientated in the transverse (deformed) direction was up to 30% greater than specimens from the longitudinal direction.

It was obvious from the literature that many workers have been investigating techniques from improving the toughness of high chromium irons. The success of such an exercise would extend the alloy product range and permit the development of new markets.

2.10 Fracture Toughness Principles Applied to Castings.

The use of fracture toughness principles in high technology areas or in macro-engineering projects has been recognised and is practised. The application of fracture mechanics by the ferrous casting industry has been somewhat more restricted.

During the mid/late 1970's S.C.R.A.T.A. were involved with an R. & D. activity investigating the fracture toughness values of specific cast steels. Much of this data was summarised and presented with an overview of fracture principles by Selby in 1980 (172). In this paper Selby highlighted the use of fracture mechanics in ascertaining an N.D.T. standard for the inspection of the Beaubourg Centre in Paris and in predicting crack behaviour in a C.E.G.B. power station turbine. It was recommended that fracture mechanics could be used in making quantative fitness for purpose judgements. Jackson and Wright (173) discussed the use of fracture mechanics in design and flaw acceptance and proposed the adoption of more critical design polices. The authors state that 'the essence of a fracture toughness approach is to quantify an acceptable degree of unsoundness in a steel casting for a given application and not to attempt to agree on what constitutes complete soundness'.

From about 1980 onwards B.C.I.R.A. have published work on fracture toughness and recently a Broadsheet discussing its relevance to cast iron design stress has been issued.(174) It is stated that in flake graphite irons fracture toughness tests would be of no practical use since the flakes act as multiple cracks producing brittle fracture in a tensile test. Fracture mechanics is reported as being most applicable to high strength pearlitic, bainitic or hardened and tempered nodular irons, high strength compacted graphite irons and white irons. This report also suggests the use of fracture mechanics to specify inspection criteria for safety critical components.

It appears from the literature that the ferrous casting industry views fracture mechanics as a tool for estimating tolerable defect sizes and hence for specifying N.D.T. procedures.

3.0. Relationship Between Fracture Toughness and Abrasion Resistance.

Literature concerned with the inter-relationship between these two properties frequently describes the optimisation of fracture toughness and abrasion resistance. This suggests an inverse relationship between the properties.

Hornbogen (175) has studied the role of fracture toughness in the wear of metals and proposed a model to explain increasing relative wear rates with decreasing toughness of metallic materials. This author stated that two types of observation were not consistent with Archards equation (section 1.2.1 equation 1.1) that is:

i. A possible abrupt change in wear rate if pressure or sliding velocity changed. For example the breaking or formation of an oxide layer as a function of pressure and temperature.

ii. Wear rates may increase (and not decrease as predicted by equation 1.1) with increasing hardness. This is particularly relevant if the velocity or impingement angle of particles is increased or if material processing has produced a low fracture toughness.

From this second observation that for high wear rates fracture toughness may have an effect provided the initial impetus for Hornbogen's study. The proposal was based on a comparison of the strain which occurred during asperity interactions with the critical strain to initiate crack growth. If the applied strain was smaller than the critical strain then the wear rate was independent of toughness and Archards law was observed. Applied strains larger than the critical strain of the material produced or increased probability of crack growth and therefore of a higher wear rate. Figure 3.1 illustrates some of these conditions. If the plastic strain produced during asperity interaction is given by ε deff and ε ceff is the

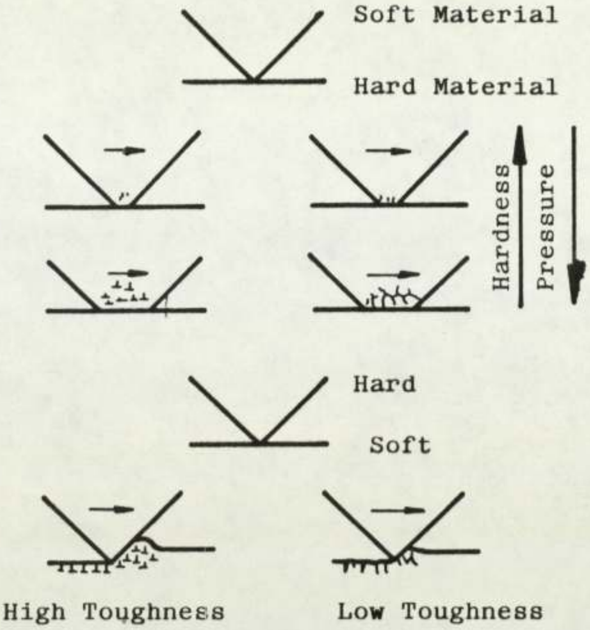

Figure 3.1

Schematic Representation of Asperity Deformation.

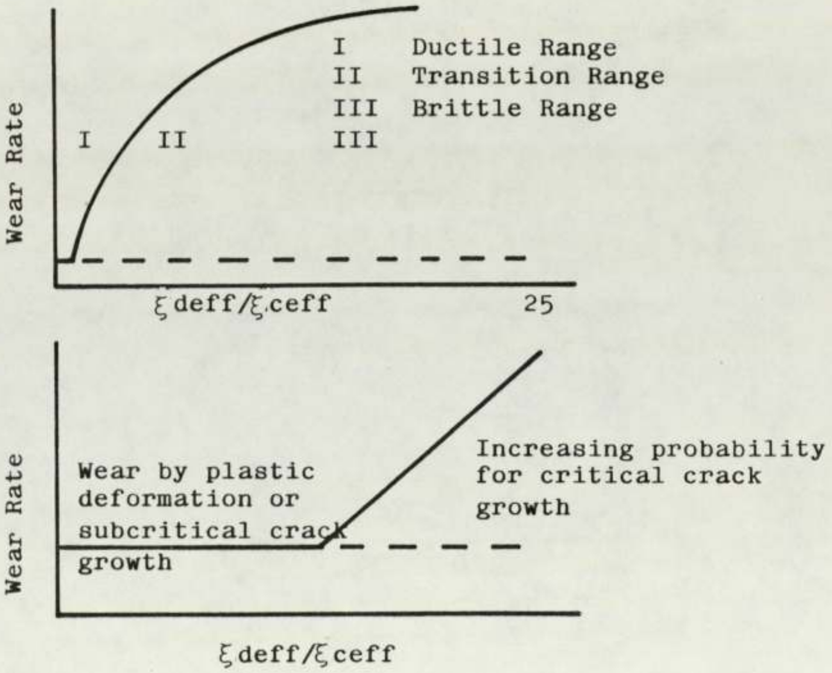

Figure 3.2

Schematic Representation of Range Modes with Different Wear Behaviour, For Constant Hardness And Presure.

critical strain at which cracks start to propagate then for conditions where ε deff $>\varepsilon$ ceff the wear rate has been described by:

$$W = k\,\frac{P}{H} = \frac{ko,\ \varepsilon deff\ \ P}{\varepsilon ceff\ \ H} = ko\ \frac{\alpha}{\beta}\,\frac{P^{1/2\;2}\ M\ \ E\,\sigma\,y\,P}{H^{1/2}K_{IC}^{\ 2}\ \ H} \qquad - 3.1$$

where W = wear rate.

k = wear co-efficient in range II

P = applied pressure

H = indentation hardness

ko= wear co-efficient range I

α = empirical factor

M = number of asperities in contact

E = elastic modulus

β = empirical factor.

For highly brittle materials Hornbogen expressed the intuitive relationship:

$$W = ko\left(1 + \ Ln\,\frac{\varepsilon\, deff}{\varepsilon\, ceff}\right)\frac{P}{H} \qquad - 3.2$$

A schematic illustration showing 3 identifiable wear regions has been presented in Figure 3.2. In range I Archards law is obeyed and toughness is not important. For very brittle conditions range III is approached in which Archards law will again be satisfied, however the wear rate will be higher than in range I. In the transition range II wear rate becomes a complicated function of mechanical properties. It was proposed that in range II the wear behaviour was determined by crack growth, it was expected that subcritical crack growth e.g. fatigue, thermal fatigue and stress corrosion cracking would be operative in range I.

Zum Gahr (176) has also studied the relationship between abrasive wear rate and fracture toughness. Figure 3.3 illustrates these findings. It was suggested that at low values of fracture toughness cracks can form and easily propagate if the wear severity is adequate and low wear resistance will be observed. As the fracture toughness is increased more plastic deformation occurs and larger stresses are required for crack nucleation and coalescence, hence wear resistance is increased. With further increases in fracture toughness there is an associated decrease in yield strength and hardness and large surface deformations produce different wear debris formation mechanisms and wear resistance decreases. Hence, for a given wear severity an optimum fracture toughness exists where wear resistance has a maximum value. Any increase in wear severity generally reduces wear resistance and moves the optimum toughness to higher levels.

The findings of both Hornbogen and Zum Gahr are similar in that three stages have been identified. However, Hornbogen was not discussing any specific systems but developing an idealised model. Zum Gahr based his concept on the results of pin on disk tests using silica sand as the abrasive and tool steels and grey irons as test specimens.

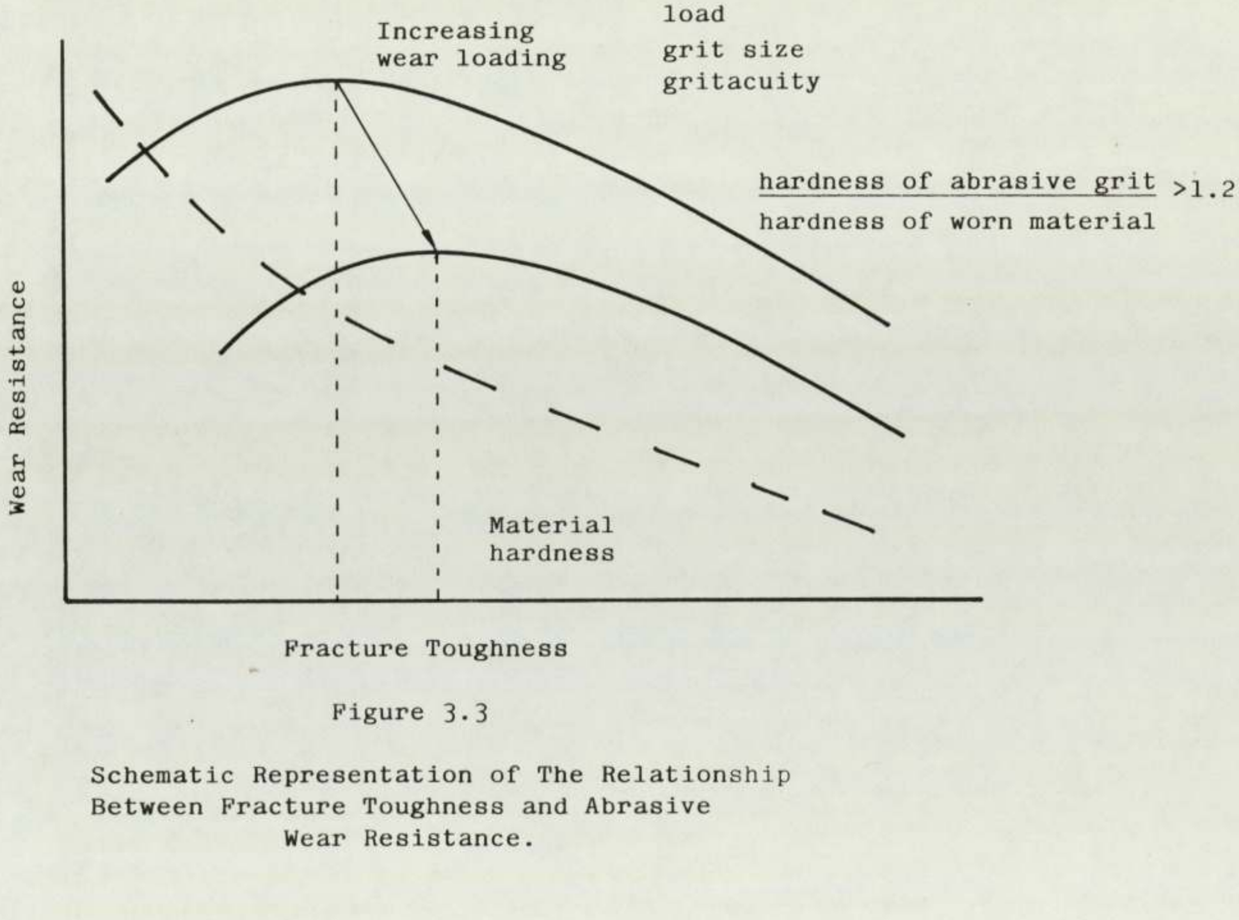

Figure 3.3

Schematic Representation of The Relationship Between Fracture Toughness and Abrasive Wear Resistance.

The role of fracture toughness in wear and grinding has been discussed by Atkins. (177) It was suggested that:

$$\frac{V}{L} \; \alpha f \left(\frac{1}{A} \right) = f \left(\sigma y \sqrt{h} / K_{IC} \; \xi \right) \qquad - 3.3$$

where V/L = volume wear rate per unit
sliding distance.
A = non dimensional parameter
σy = yield stress
h = characteristic length related to crack length
K_{IC} = fracture toughness
ξ = geometric term related to flow field.

The model by Hornbogen was reported to be similar to $1/A^2$.

Barwell (178) discusses the presence of dislocations observed by Andarelli (179) in a friction experiment and cited the work of Rosenfield (180) who applied an elastic-plastic model to represent the wear process. Barwell stated that 'the application of the science of fracture mechanics to wear studies may illuminate the process of particle formation' but does later conceed that 'there is still a great deal of mystery surrounding the process of wear'.

3.1. Optimising the Fracture Toughness and Wear Resistance of High Chromium Cast Irons.

Several authors have commented on optimising fracture toughness and wear resistance of high chromium cast irons. Diesburg and Borik (34) have produced a table listing a number of variables and their effect on abrasion resistance as determined by a high stress pin test and fracture toughness. see Table 3.1. It is interesting to note from this work that globularising (spheroidising) the eutectic carbides of both as-cast and heat-treated structures resulted in a large increase in fracture toughness. These results are contrary to the work of Durman (166) and Biner (165) who reported a constant level of toughness in heat-treated material regardless of spheriodising treatment. The discussion by these authors (34) was based on the selection of alloy composition and thermal processing to give a high value of fracture toughness without any sacrifice in abrasion resistance. It was stated that the best toughness combined with good resistance to high stress and gouging abrasion was observed with manganese steel. However, it was thought that the low yield strength of this material was a limitation. Cast and wrought steels exhibiting martensitic structures were also thought to provide a combination of good strength, toughness and abrasion resistance. It was reported that for these alloys the adjustment of carbon content could modify the mechanical properties such that the relative importance of toughness and abrason resistance could be accommodated.

For white cast irons it was considered necessary to avoid the formation of upper transformation products both in the as-cast and heat-treated condition if optimum properties were to be developed. An 18% chromium-molybdenum iron was suggested as offering excellent fracture toughness values regardless of condition although it was emphasised that the hardness and compressive strength were significantly higher in the martensitic condition.

Increasing Amount of Variable.	Pin Test Abrasion Resistance		Plane Strain Fracture Toughness	
	As-Cast	Heat-Treated	As-Cast	Heat-Treated
Carbon	Large Increase	Large Increase	Large Decrease	Large Decrease
Silicon	No Effect	Small Decrease	Large Increase	No Effect
Molybdenum	Small Increase	Small Increase	No Effect	No Effect
Eutectic Carbide Refinement	Large Decrease	Large Decrease	Large Increase	Large Increase
Eutectic Carbide Globularization	No Effect	No Effect	Large Increase	Large Increase
Secondary Carbide Precipitation	Small Increase	No Effect	Large Decrease	Large Decrease
Retained Austenite	NA*	No Effect	NA	Large Increase
Presence of 0 to 10% Martensite	No Effect	NA	No Effect	NA
Presence of 0 to 10% Pearlite	Small Decrease	ND*	Small Increase	ND
Presence of 0 to 30% Ferrite-Carbide Aggregate	ND	Large Decrease	ND	Large Increase
Tempering at 410 F (210C)	ND	Large Increase	ND	Large Increase
Tempering at 600 or 800 F (315 or 425 C)	ND	No Effect	ND	Large Decrease

* NA = not applicable.

* ND - Not determined.

Table 3.1.

Effect of Variables on the Abrasion Resistance
and Fracture Toughness of High Chromium Irons.

Using a low stress abrasion test Sare (87) was able to demonstrate that as-cast austenitic matrix white cast irons had a marginally better combination of abrasion resistance and fracture toughness properties than heat-treated martensitic matrix material. Most significantly Sare observed that there need not be a 'trade off' of one property against another, this is illstrated in Figure 3.4.

Zum Gahr and Doane (169) have related results from a rubber wheel abrasion test to fracture toughness and eutectic carbide volume as shown in Figure 3.5. The optimum combinations of these properties lie on the surface of the three-dimensional representation, the shape of the surface depending on the wear system used. At a constant volume fraction of eutectic carbides a maximum occurred in the relationship between abrasive wear rate and fracture toughness, at higher or lower values of fracture toughness the abrasion resistance decreased.

All workers appear to agree that results from laboratory wear tests on high chromium white irons show that reasonably consistent wear rates may be produced with material of varying fracture toughness. This would seem to suggest that these experiements have operated under the conditions identified by Hornbogen (175) as region I and not the intermediate transition region.

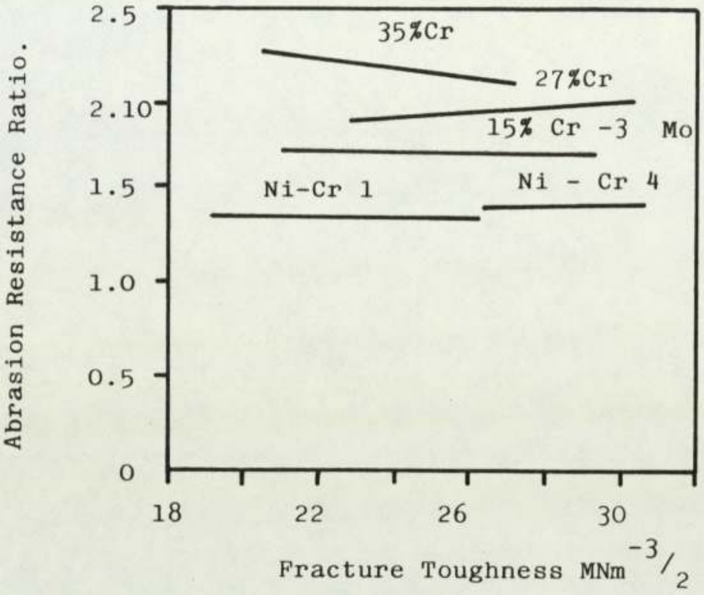

Figure 3.4

Abrasion-Resistance Ratio Against
Plane-Strain Fracture Toughness

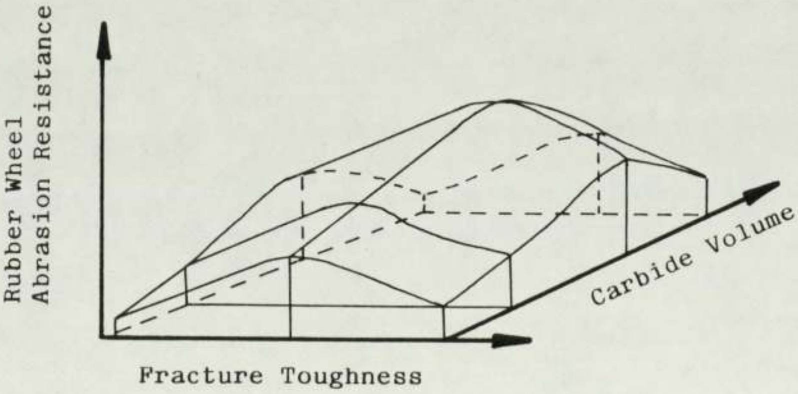

Figure 3.5

Schematic Relationship Between Abrasion Resistance,
Fracture Toughness And Carbide Volume For White Irons.

4.0 High Chromium Cast Iron.

4.1. Classification of Cast Irons.

The wide group of materials known collectively as cast irons have been broadly classified by Scholes (181) into three main groups:

1. Grey cast irons,
2. Nodular (or spheriodal graphite) cast irons,
3. Highly alloyed cast irons.

The first group of irons account for about 85% of the total U.K. iron production and are used in many general engineering applications. These materials exhibit microstructures containing flake graphite, pearlite and ferrite constituents (64) and are typically H_B 130 - 300 in hardness with tensile strengths of 150 MNm^{-2} - 400 MNm^{-2}. Flake graphite irons have moderate tensile, fatigue and wear properties but are relatively cheap and easy to produce.

Nodular iron is produced by the ladle treatment of the molten metal with a magnesium/cerium addition. On solidification the free graphite being present as nodules or spheroids rather than flakes. (64) Compared with the flake irons this grade of material has generally higher tensile and elongation properties and exhibits greater resistance to fatigue and repeated impacts during operating conditions. Typical applications of nodular irons include crackshafts and vehicle suspension and steering components. This class of irons has also been regarded as including the malleable cast irons produced by the graphitization of the cementite constituent of white iron during a high temperature treatment at 950 - 1000°C.

The final group of alloy cast irons has been further subdivided by Scholes (Figure 41) following a similar classification of special cast irons (Figure 42) by Barton. (182) These materials have been designed to operate under extreme conditions of either abrasion, corrosion or temperature. The abrasion resistant high chromium range of materials thus belong to the graphite free class of alloy or special cast irons.

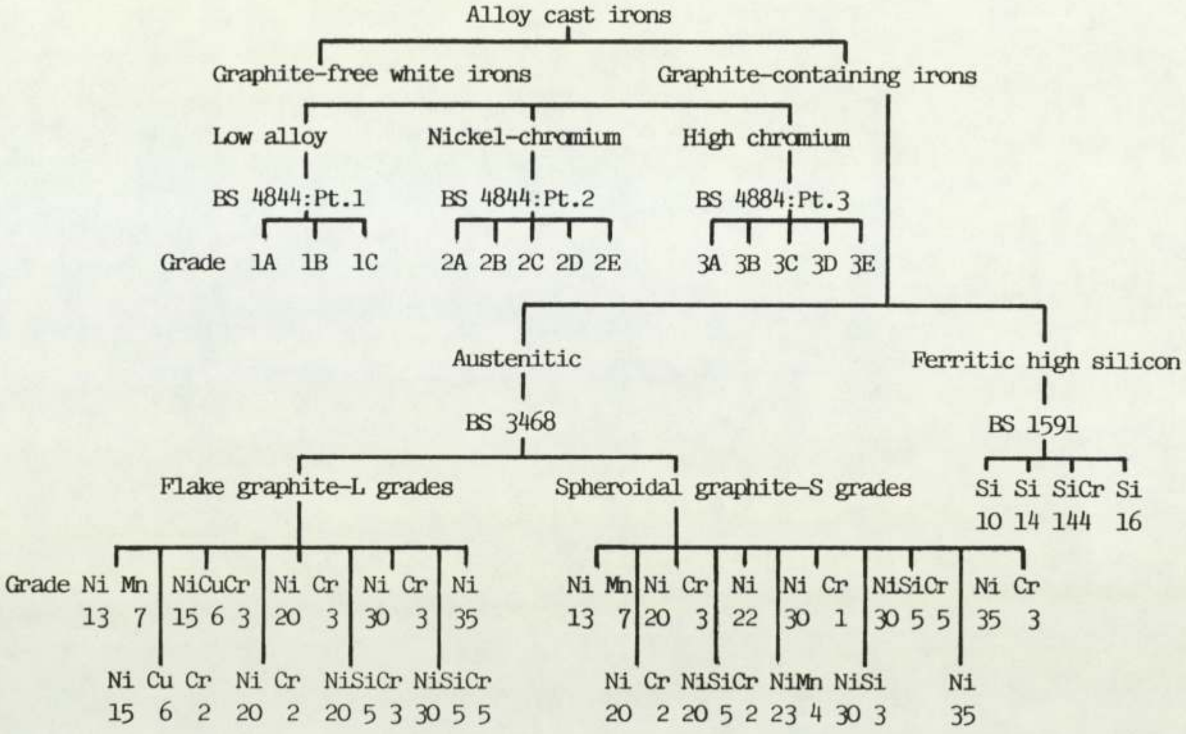

Figure 4.1

Classification of alloy cast irons.

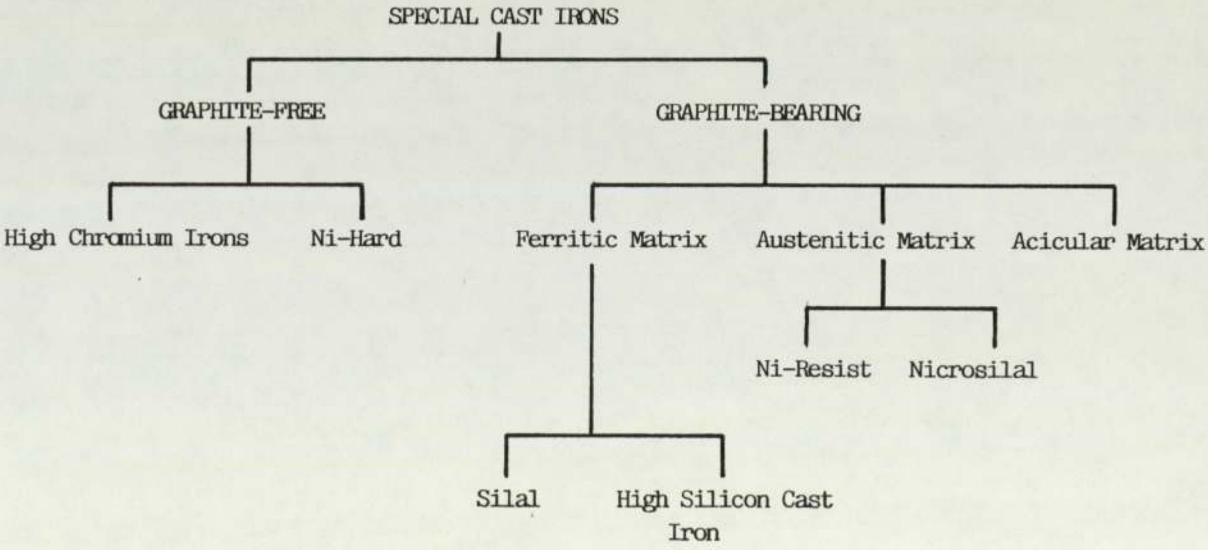

Figure 4.2

Classification of special cast irons.

4.2. Historical Development of High Chromium White Cast Irons.

It has been reported (183) that over one hundred years ago the white iron material intended for use in the malleabalizing process was used in the as cast condition to produce wear resistant castings. Subsequent development of this material resulted in the production of a lower silicon, higher carbon white iron specifically for use as a wear resistant alloy.

The microstructure of a typical white iron consists of pearlite islands surrounded by a cementite (Fe_3C) network (Plate 4.1.) Although the macrohardness of this material would be of the order of Hv 400 (181) its toughness is relatively low, about 22.0 $MNm^{-3/2}$ (184.) This inherent brittleness has been attributed to the continuous nature of cementite which permits the uninterrupted propagation of a crack (183). A slight improvement in toughness may be achieved by reducing the phosphorus content to below 0.1% maximum. While the use of unalloyed white irons remain confined to selected low impact applications its success is due to ease of production and low cost compared with the alternative higher alloyed irons.

The production of the first high chromium white cast iron has been credited (185, 186) to Becket of the Electro-Metallurgical Company, New York who was working on alloy substitution in high carbon tool steels. Recognising the good wear resistance and future potential of the high chromium material the American company took out a patent in 1917 for a 27% chromium, 2.75% carbon cast iron for use as grinding media and ball mill linings.(187) High chromium irons have an austenite (or some transformation product of austenite) matrix and a discontinuous chromium carbide ($(Fe, Cr)_7C_3$) network (Plate 4.2.) It is reported that the replacement of the iron carbide by chromium carbide has a twofold effect on the material properties.

Plate 4.1

Typical microstructure of a low alloy white iron X 300.

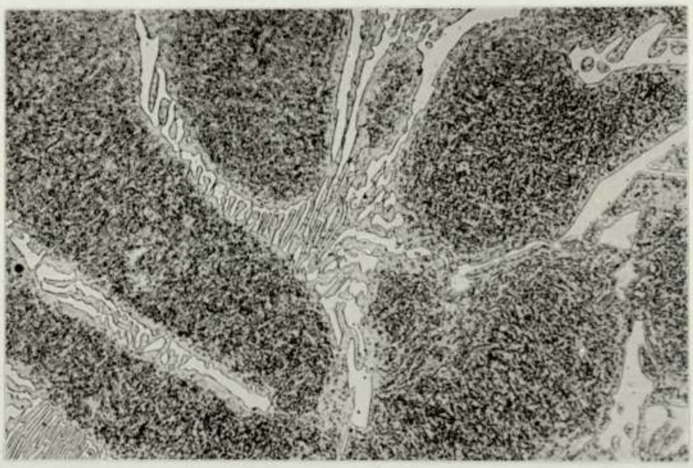

Plate 4.2

Typical microstructure of a high chromium cast iron X 300.

Plate 4.3

Typical microstructure of a nickel chromium martensitic white iron X 300

Firstly, the M_7C_3 carbide is significantly harder than the M_3C (Table 1.1) thus improving wear performance. Secondly the morphology of the carbide changes from a continuous to a discontinuous nature, thus increasing toughness due to the formation of a less direct fracture path. (183, 185.) According to Durman (183) and Dodd (186) the continued improvement of high chromium alloys were delayed because of the development in the 1920's. of a nickel, chromium martensitic white iron. This material (now known by its trade name of Ni-Hard II) could be produced in a cupola unlike the high chromium irons which required expensive and at that time uncommon electric melting units.

The original martensitic white irons contained about 4.0% nickel and 2.0% chromium and exhibited an as cast microstructure of a mixed austenite, martensite matrix and a continuous cementite network (Plate 4.3.) It is well documented (190) that heat treatment, either at 275°C for 16 hours or 475°C for 4 hours transforms the austenite matrix to bainite or martensite respectively. In the heat treated condition Ni-Hard II has found many applications in the crushing and grinding industry (191, 192) but its use has remained restricted due to its general low level of toughness (87).

In the U.S.A. during the 1930's work was carried out on the addition of molybdenum to high chromium irons. This alloying addition helped to overcome a major problem of low hardenability displayed by the earlier 27% chromium materials and is reputed to have lead to the development of the 15% chromium, 3.0% carbon, 3.0% molybdenum iron. An alloy still recognised for its high wear resistance. (188, 193)

Perhaps due to the renewed interest in high chromium irons a eutectic martensitic iron was produced during the 1950's and commercially exploited in the 1960's as Ni-Hard IV. This material contained about 6.0% nickel and 8.0% chromium which produced a discontinuous form of carbide and thereby increasing the material toughness. Ni-Hard IV appears to have had only a limited success as a wear and impact resistant alloy. This could possibly be due to the high cost of the nickel addition and its limited performance compared with the developing high chromium irons.

During the 1960's in the U.K. and in Europe further advances in high chromium iron technology were made and alloy ranges were begining to be formulated. By the mid 1970's American, A.S.T.M. and British, B.S.I. standards had been produced (194, 195) which encompassed several grades of low alloy, martensitic and high chromium white irons (Table 4.1 and Table 4.2)

Part 1: Unalloyed and low alloy grades

Grade	Chemical composition %				
	C	Si	Mn	Cr max	P max
1A	2.4-3.4	0.5-1.5	0.2-0.8	2.0	0.15
1B	2.4-3.4	0.5-1.5	0.2-0.8	2.0	0.5
1C	2.4-3.0	0.5-1.5	0.2-0.8	2.0	0.15

Part 2: Nickel-chromium grades

Grade	Chemical composition %							
	C	Si	Mn	Ni	Cr	Mo max	P max	S max
2A	2.7-3.2	0.3-0.8	0.2-0.8	3.0-5.5	1.5-2.5	0.5	0.3	0.15
2B	3.2-3.6	0.3-0.8	0.2-0.8	3.0-5.5	1.5-2.5	0.5	0.3	0.15
2C	2.4 -2.8	1.5 -2.2	0.2-0.8	4.0-6.0	8.0-10.0	0.5	0.3	0.15
2D	2.8-3.2	1.5-2.2	0.2-0.8	4.0-6.0	8.0-10.0	0.5	0.3	0.15
2E	3.2-3.6	1.5-2.2	0.2-0.8	4.0-6.0	8.0-10.0	0.5	0.3	0.15

Part 3: High chromium grades.

Grade	Chemical composition %							
	C	Simax	Mn	Cr	Mo	Ni	Cu	P max
3A	2.4-3.0	1.0	0.5-1.5	14-17	0-2.5	0-1.0	0-1.2	0.1
3B	3.0-3.6	1.0	0.5-1.5	14-17	1-3.0	0-1.0	0-1.2	0.1
3C	2.2-3.0	1.0	0.5-1.5	17-22	0-3.0	0-1.5	0-1.2	0.1
3D	2.4-2.8	1.0	0.5-1.5	22-28	0-1.5	0-1.0	0-1.2	0.1
3E	2.8-3.2	1.0	0.5-1.5	22-28	0-1.5	0-1.0	0-1.2	0.1

Table 4.1 (194)

Chemical Composition of Abrasion Resistant Cast Irons. BS 4844.

			Chemical Composition (weight %)								
Class	Type	Designation	C	Si	S	P	Mn	Ni	Cr	Cu	Mo
I	A	Ni-Cr-HC	3.0-3.6	0.8max	0.15max	0.30max	1.3max	3.3-5.0	1.4-4.0	-	1.0max
I	B	Ni-Cr-LC	2.5-3.0	0.8max	0.15max	0.30max	1.3max	3.3-5.0	1.4-4.0	-	1.0max
I	C	Ni-Cr-GB	2.9-3.7	0.8max	0.15max	0.30max	1.3max	2.7-4.0	1.1-1.5	-	1.0max
I	D	Ni-HiCr	2.5-3.6	1.0-2.2	0.15max	0.10max	1.3max	5.0-7.0	7.0-11.0	-	1.0max
II	A	12% Cr	2.4-2.8	1.0max	0.06max	0.10max	0.5-1.5	0.5max	11.0-14.0	1.2max	0.5-1.0
II	B	15% Cr-Mo-LC	2.4-2.8	1.0max	0.06max	0.10max	0.5-1.5	0.5max	14.0-18.0	1.2max	1.0-3.0
II	C	15% Cr-Mo-HC	2.8-3.6	1.0max	0.06max	0.10max	0.5-1.5	0.5max	14.0-18.0	1.2max	2.3-3.5
II	D	20% Cr-Mo-LC	2.0-2.6	1.0max	0.06max	0.10max	0.5-1.5	1.5max	18.0-23.0	1.2max	1.5max
II	E	20% Cr-Mo-HC	2.6-3.2	1.0max	0.06max	0.10max	0.5-1.5	1.5max	18.0-23.0	1.2max	1.0-2.0
III	A	25% Cr	2.3-3.0	1.0max	0.06max	0.10max	0.5-1.5	1.5max	23.0-28.0	1.2max	1.5max

Table 4.2

CHEMICAL COMPOSITION FOR ABRASION RESISTANT CAST IRONS A.S.T.M. A532 - 80.

4.3. Additions of Chromium to Cast Iron.

It has been reported that chromium is probably the most widely used alloying element in cast iron and may be present in amounts ranging from 0.2% to inexcess of 30%. (196)

Small additions of chromium, 0.03% - 0.4%, in grey iron promotes both the formation of pearlite within the matrix and the formation of cementite. Due to the increase in pearlite content a harder, stronger iron may be obtained. Residual chromium levels in ductile iron should be below 0.04% for as cast ferritic structures and 0.10% for pearlitic structures (197) If the chromium content of grey iron is increased to about 1% the resistance to growth, resulting from the breakdown of pearlite, will be increased within the 450°C - 650°C temperature range (64). Depending on section thickness between 1% and 3% chromium will produce a white cast iron suitable for certain low impact abrasion resistant applications (198)

When chromium is used in conjunction with nickel additions the abrasion resistant series of martensitic cast irons are formed (see section 4.2) These materials contain approximately 4.0% nickel and 2.0% chromium or 5.0% nickel and 9.0% chromium depending on specification range.

As the chromium content exceeds about 10% (199) the cementite, Fe_3C, phase predominant in the low alloy and martensitic materials is replaced by the harder, discontinuous chromium carbide, $(Fe, Cr)_7C_3$. According to Barton (196) the higher chromium containing irons may be divided into three groups:

i) 15.0% -17.0% chromium for heat and wear resistance.

ii) 26.0% - 28.0% chromium for abrasion resistance.

iii) 30.0% - 35.0% chromium for heat and corrosion resistance.

This classification now appears to oversimplify the chromium ranges currently employed for abrasion resistant materials. However, it does illustrate the abrasion, heat and corrosion resistant properties of high chromium white cast irons.

4.4. The Iron-Chromium-Carbon System.

Early investigations of the iron-chromium-carbon system have been reported by Murakami et al, (200) Westgren et al., (201) Tofaute et al, (202) and discussed by Kinzel and Crafts. (203) Inconsistencies between the findings of Bungardt et al (204) and Griffing et al (205) prompted Jackson (206) to reinvestigate the austenite liquidus surface. Using high purity electrolytic chromium and vacuum refined iron Jackson (206) combined his results with those of numerous previous workers for example (205, 207) to establish a revised austenite liquidus surface. The three dimensional space model of the ternary system is illustrated in Figure 4.3. Figure 4.4 shows the plan of the invariant planes. The constitutional diagram consists of five primary liquidus surfaces, illustrated in Figure 4.5, that is, austenite, ferrite, $(Cr, Fe)_{23}C_6$, $(Cr, Fe)_7C_3$ and $(Fe, Cr)_3C$ The following ternary peritectic reactions have been reported:

$$L + Cr_{23}C_6 \rightarrow \alpha + Cr_7C_3 \text{ at } 1449^\circ C$$

$$L + \alpha \rightarrow \gamma + Cr_7C_3 \text{ at } 1292^\circ C$$

$$L + Cr_7C_3 \rightarrow \gamma + Fe_3C \text{ at } 1184^\circ C$$

together with a ternary peritectoid.

$$\alpha + Cr_7C_3 \rightarrow \alpha + Fe_3C \text{ at } 975^\circ C$$

Woodyatt and Krauss (208) published their finding of the Fe-Cr-C system at 870°C and concluded that the only carbides present are M_3C, M_7C_3 and $M_{23}C_6$.

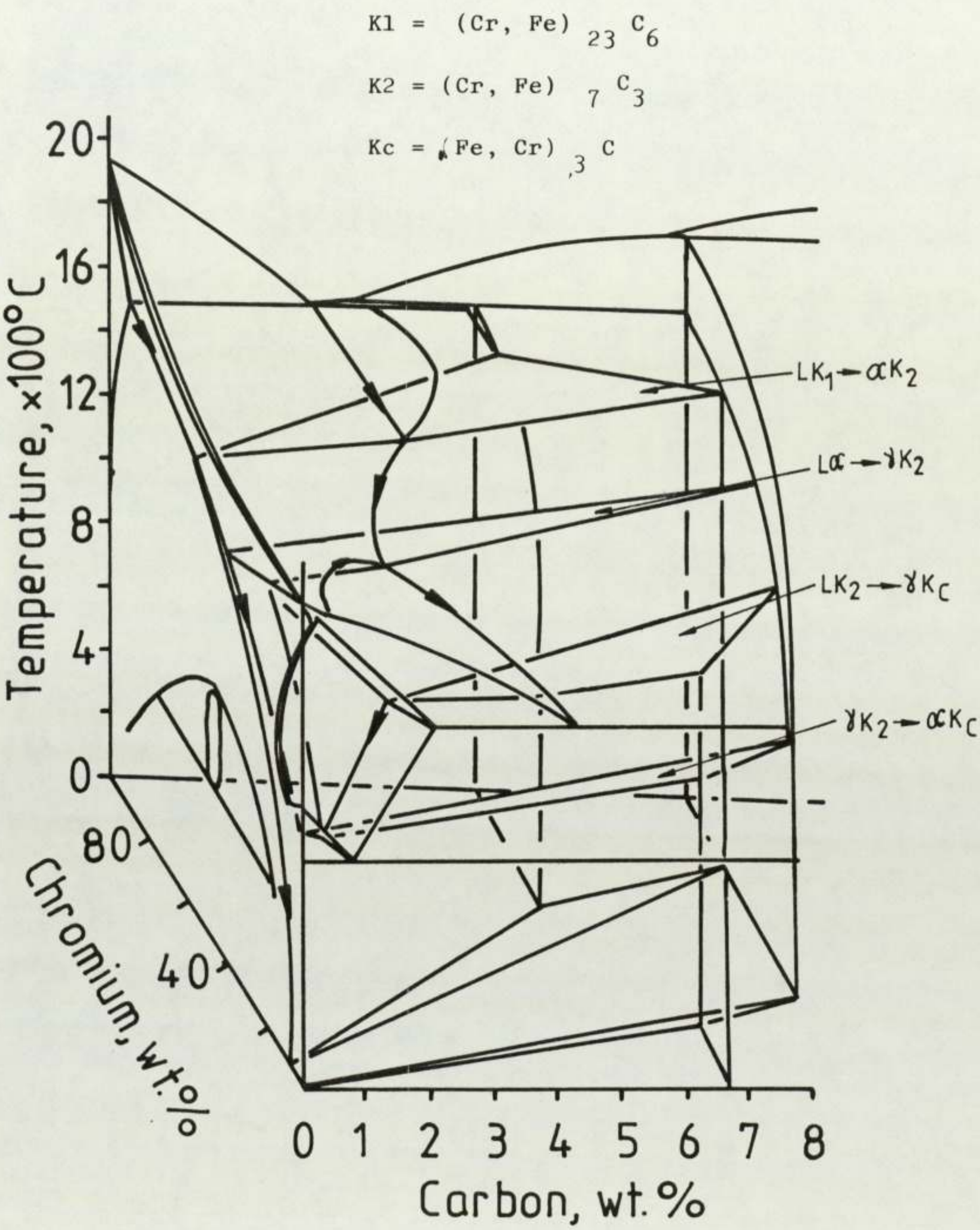

Figure 4.3

Three Dimensional Space Model of the Ternary

Fe - Cr - C System.

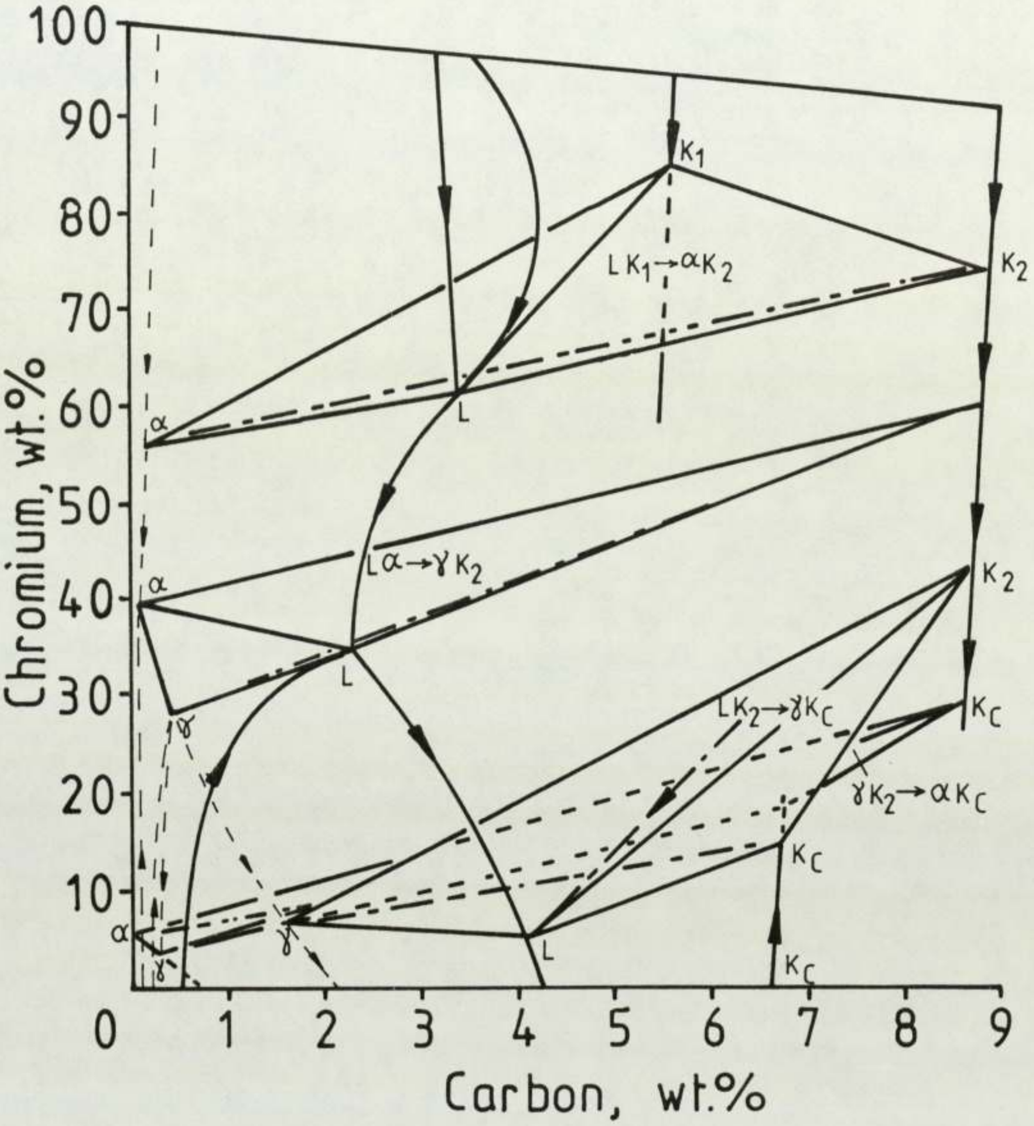

Figure 4.4

Plan of Invariant Planes of The

Fe - Cr - C System.

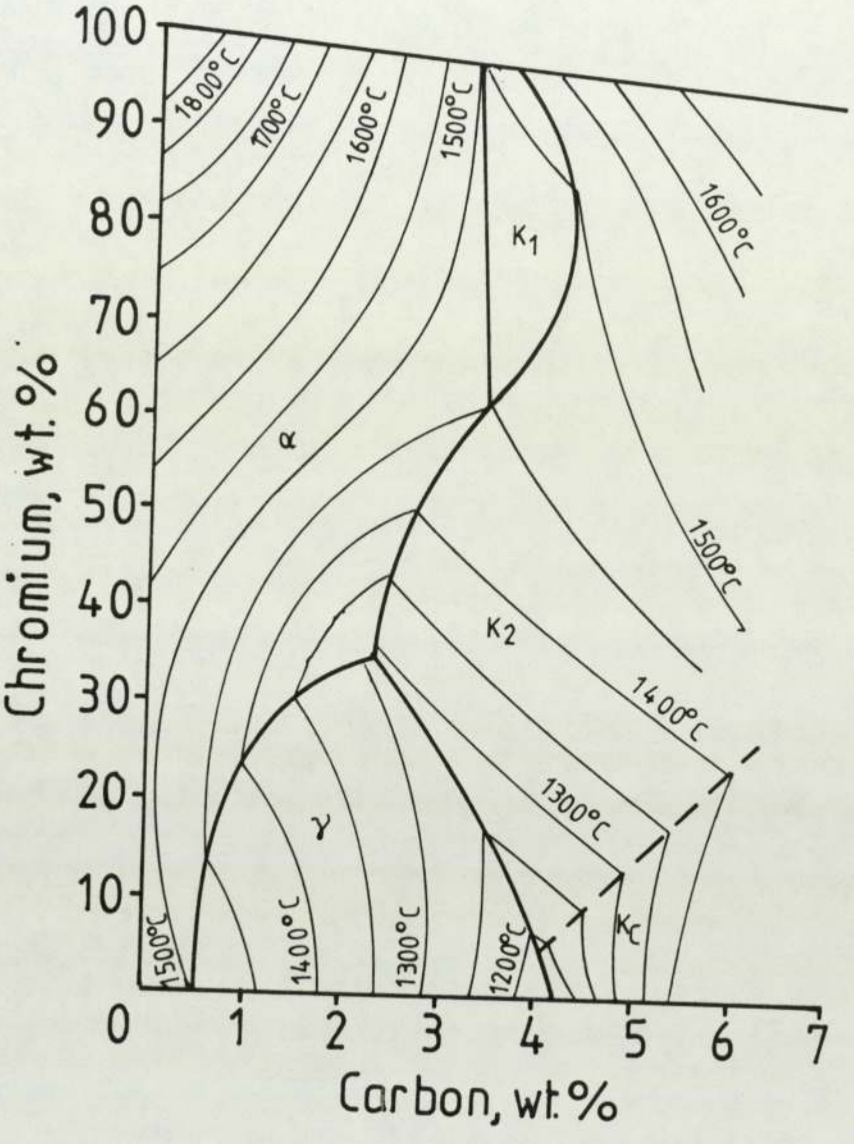

Figure 4.5

Primary Liquidus Surfaces of

The Fe - Cr - C System.

The computer calculated isothermal sections of the Fe-Cr-C system between 873°C and 1373°C (209) are in general agreement with those published by Jackson.

4.5. The Solidification of High Chromium Iron.

The materials under consideration may be of either a hypoeutectic, eutectic or hypereutectic composition. Most of the industrially important alloys have a chromium and carbon content which lies within the austenite liquidus field, see Figure 4.5. Consequently, these materials solidify with a primary austenite phase and a eutectic of chromium carbide and austenite . The distance between the primary and secondary branches of the dendrites has been found to depend on both the chemical composition and cooling rate. (210) While the primary dendrite branch spacing is reported to decrease with the inverse of the square root of the cooling rate a similar function involving a cube root holds for secondary branch spacings. Furthermore the size of the dendrites also decrease as the volume fraction of the eutectic increases (211) It has been documented that increased cooling rates favour the primary precipitation of austenite. (212) After the solidification of the primary phase the eutectic structure is developed. If the primary phase occupies a high volume fraction then the carbide phase of the eutectic tends to form as a continuous network. Maratray has indicated that when the carbide content is between 20% and 30% the eutectic contains lamellae radiating from centres located in interdendritic spaces (168) As the eutectic composition was approached the austenite no longer interfered with the growth of the eutectic which then became completely lameller. When the eutectic composition was exceeded and hypereutectic alloys produced the structure contained characteristic primary chromium carbides. These carbides were of a hexagonal shape and frequently faulted. (40) Powell (185) citing the classification of eutectics by Hunt and Jackson (213) disputed the lamellar term used by Maratray (168). Hunt and Jackson classified eutectic solidification as lamellar being nonfaceted - nonfaceted and not faceted - nonfaceted or faceted-faceted growth regimes. In text by Chadwick (214) the white iron eutectic has been reported as being of a faceted-nonfaceted nature and therefore not within the lameller classification. However, Chadwick does note that 'white irons are more akin to metal-metal eutectics than metal-non metal'.

The segregation of alloying elements during solidification has been investigated by Dupin et al. (215) These workers produced concentration profiles for a number of elements across primary austenite dendrites. Figure 4.6 and 4.7. In addition, the relative difference in carbon distribution between primary and eutectic austenite has been illustrated. Figure 4.8 Due to the significant influence of carbon on the Ms temperature this diagram assists with the explanation of how as cast material may exhibit a transformation of austenite to martensite in areas adjacent to the carbide phase. The observation that this transformation occurs more readily in eutectic austenite rather than dendritic austenite is also consistent with the relative carbon levels of Figure 4.8. The solidification segregation of molybdenum which enriches the liquid remaining in interdendritic spaces is reputed to promote the precipitation of molybdenum rich carbides. (216) In alloys having a chromium/carbon ratio of 5 a very fine Mo_2C carbide has been identified while in material having a chromium/carbon ratio of 10 a fish bone like M_6C carbide has been noted.

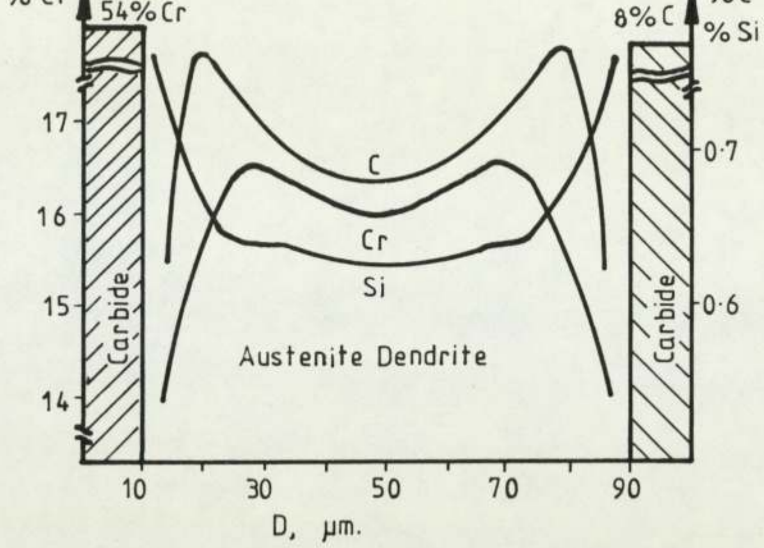

Figure 4.6

Carbon, Chromium and Silicon distribution profile in an austenite dendrite.

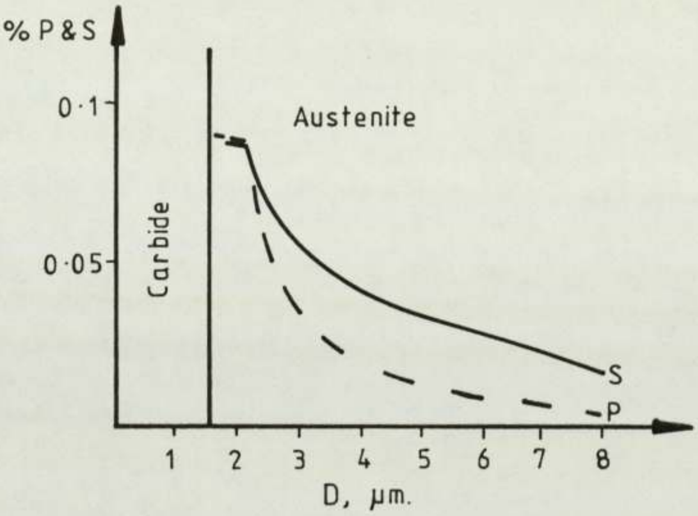

Figure 4.7

Sulphur and phosphorus distribution profile in an austenite dendrite.

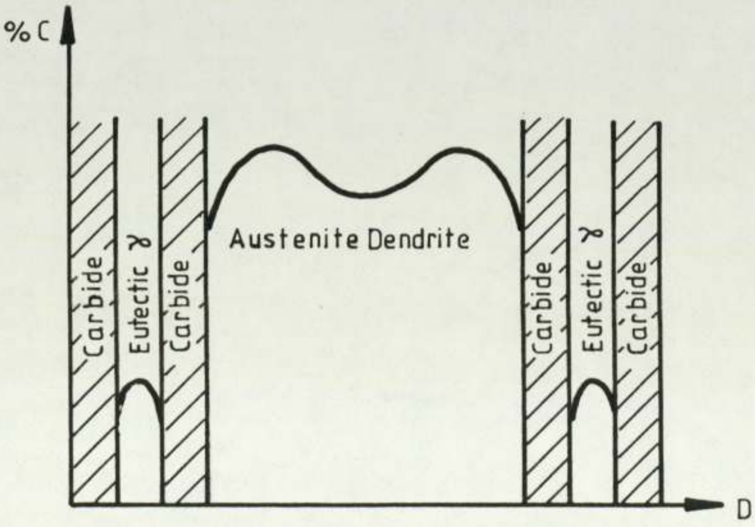

Figure 4.8

Distribution diagram for carbon in proeutectic or eutectic austenite.

4.6. The Matrix Phase.

The matrix of high chromium cast irons may be austenite or some transformation product of austenite. In the as cast condition an austenitic structure may be retained to room temperature in materials of a high Cr/C ratio while less highly alloyed irons will undergo a pearlitic transformation during mould cooling. The principle heat treatment processes are concerned with the production of either a softened, machinable matrix structure or a destabilised martensitic structure. This section will review these solid state transformations.

4.6.1 The As Cast Matrix.

Even in slowly cooled, thick section castings the pearlite reaction may be suppressed by correct alloying additions and a metastable austenitic structure retained to room temperature. (40) In this austenitic condition the material would be essentially non magnetic and exhibit a hardness of about Hv 500. If subjected to service conditions involving repeated impacts a self replacing, work hardened surface layer of about Hv 1000 may be developed. (40, 217)

In less highly alloyed material a pearlitic transformation at about 750°C may occur. While this granular pearlite product has been reported as undesirable due to its poor wear resistance, (40) (Hv 350) it is this matrix structure which confers the greatest degree of machinability.

4.6.2 The Heat Treated Matrix.

The matrix heat treatment processes have clearly defined purposes:

i) transformation of an as-cast austenitic structure into a soft, machinable ferrite and carbide aggregate.

ii) the production of a martensitic structure resulting from the destablising effect of secondary carbide precipitations.

iii) the sub critical transformation of retained austenite and tempering of martensite.

Heat treatments therefore consist of annealing, hardening and tempering processes.

4.6.2.1 Transformation Mechanisms of the Austenite Matrix.

Much of the work on transformation mechanisms of the austenite matrix can be attributed to Maratray. (218, 219) It is reported that austenite is stable at both high and low temperatures but decomposition may occur at an intermediate temperature.

4.6.2.1.1 Isothermal Decomposition of Austenite.

This has been reported as occuring within two temperature ranges, above 975°C ± 25°C and at about 675°C ± 25°C. According to Maratray (218) at temperatures above 975°C secondary carbide precipitation may occur by two possible mechanisms:

i) Above A_3

$\gamma \rightarrow \gamma$ + secondary carbide

ii) Below A_3

$\gamma \rightarrow \alpha + \gamma$ + secondary carbide.

Since secondary carbide precipitation is reported as depleting the matrix of chromium and carbon there is a resultant influence on the transformation characteristics of the austenite. It has been recorded that secondary carbide precipitation enables a bainitic transformation in some alloys, permits a martensitic transformation and retards pearlite formation.

4.6.2.1.2 Precipitation of Secondary Carbides.

Maratray has shown that precipitation above the A_3 resulted in only M_7C_3 type carbides being formed but at temperatures below A_3 both M_7C_3 and $M_{23}C_6$ carbides are reported. However, due to the presence of the eutectic M_7C_3 it was not possible to conclude whether both carbides had been formed within the lower temperature range.

The time required for the complete precipitation reaction to occur can be up to six hours. Carbon, chromium and molybdenum do not affect the kinetics of the reaction but increasing the chromium/carbon ratio will result in the precipitation range being extended to higher temperatures. The initial precipitation occurs around the matrix/eutectic carbide interface where it is fine and dense and progresses into the austenite along three preferred crystallographic planes.

This precipitation reaction is generally referred to as the destabilising treatment, or sometimes as conditioning.

4.6.2.1.3 The Pearlite Transformation.

It has been documented that in addition to being inhibited by secondary carbide precipitation the pearlite transformation may be retarded by increasing the chromium/carbon ratio. Both of these processes involve an increase in the incubation period for the pearlite transformation and thereby increase the hardenability of the alloy.

A typical annealing process suitable for the subsequent machining of a 15% chromium, 3% carbon alloy has been stated. (220)

Soak 970°C for 1 hour minimum

Furnace cool to 820°C

Cool at a rate not exceeding 40°C/hour
down to 590°C

Air cool to ambient.

Approximate hardness Hv 350 - 400

More recent work by Maratray (210) has shown that the amount of pearlite transformation (P%), at a given temperature, obeys the general form of the Johnson-Mehl relationship (221)

$$P\% = 1 - \exp\left[-(kt)^{n}\right] \qquad - 4.1$$

where K involves nucleation and growth rates

t = time

and n is an exponent related to nucleation mechanism. However, Maratray has not commented on the value of the exponent n, (given as between 1 and 4 by Christian (222) or on the individual nucleation and growth rates. It is the view of at least one author (223) that since similar values of n may be exhibited by different nucleation mechanisms reaction kinetics have played only a small role in understanding processes. The determination of separate nucleation and growth rates being of more significance.

4.6.2.1.4 The Bainite Transformation.

Work by Maratray (218) has shown that a bainitic transformation was only possible in destabilised alloys with chromium/carbon ratios of less than about 5. Furthermore, since the formation of bainite tended to stabilise untransformed austenite it was not possible to obtain more than 50% bainite. During continuous cooling the bainite transformation was still further restricted by the rapidity of pearlite formation.

4.6.2.1.5 The Martensite Transformation.

This is probably the most industrially important transformation which occurs within this range of materials.

Again Maratray (218) has reported that it was impossible to produce martensite without prior precipitation of secondary carbides. The temperature at which precipitation occurred determined the Ms temperature and both the quantity and hardness of martensite. If destabilisation was carried out at lower temperatures than the Ms temperature was observed to rise due to increased matrix impoverishment of carbon and chromium. The quantity of secondary carbides had no effect on the Ms temperature but was directly related to the amount of martensite which subsequently formed. Maratray has suggested that in view of the apparently minor effect of the quantity of martensite on the as quenched hardness some other hardening mechanisms may be operating.

Fredrikssen and Remaeus (212) have put forward the following techniques for obtaining peak as quenched hardness.

i) austenitise at a high temperature after quenching to room temperature cool in liquid nitrogen to below Mf temperature.

ii) reduce the chromium content of the alloy (i.e. reduce the chromium/carbon ratio) thus producing a higher carbon content in solution with austenite and a correspondingly higher carbon martensite.

Point ii) has also been highlighted by other workers. (188)

4.6.2.1.6 The Transformation of Retained Austenite.

It has been widely reported that a fundamental problem associated with the heat treatment of high chromium irons was the incomplete transformation of austenite to martensite. The resulting matrix structure thus contained a proportion of retained, or residual, austenite. Furthermore, it has been a common belief that any component used in this condition would exhibit spalling, premature wear or possibly catastrophic failure due to the stresses impossed by the mechanically induced transformation of austenite. In fact, a patent specification limited the amount of retained austenite to a maximum of 3%. (224) Considerable effort has been directed towards the measurement of retained austenite levels and to sub critical and subzero treatments to affect its elimination.

4.6.2.1.6.1 Measurement of Retained Austenite.

In an attempt to measure retained austenite in textured alloys using an X-ray diffractometer technique Miller (225) proposed that in addition to rotating the specimen it should also be tilted to an angle of ± 56°. This extra plane of movement would increase the number of crystallites within the specimen conforming to the Bragg condition. Kim (226) constructed a similar rotating and tilting specimen holder and subsequently reported a technique for the measurement of retained austenite in white cast irons. For several years this technique was considered satisfactory until work by Fillit et al (227) who made further refinements to the system.

While the laboratory X-ray measurements appear to be fully developed this was not of an immediate use to the cast iron producer who required a simple but reliable inspection tool for the assessment of austenite in production material. La Count investigated the use of portable magnetic thickness gauges in assessing the austenite content of known standard materials.(228)

From this work developed a usable method and calibration to permit the on site assessment of retained austenite using a portable magnetic instrument.

4.6.2.1.6.2 Transformation of Austenite by Sub-Critical Treatments.

The effect of sub-critical isothermal tempering treatments within the range 500-650°C has been studied by Maratray. Within this temperature range both as-cast austenite and retained austenite may be transformed. When the amount of austenite was of the order of 60-70% the transformation products consisted of pearlite and a ferrite/$M_{23}C_6$ aggregate. However, when lower levels of austenite were involved only the ferrite /M_7C_3 aggregate was reported. Since the tempering process precipitated carbides from the austenite the Ms temperature was found to increase with holding time. The effect of a cryogenic treatment on the transformation of austenite appears to be of limited applicability. Maratray has reported that subzero quenching, down to - 196°C has only been effective if more than 50% retained austenite was initially present at room temperature.(210) The treatment was found to be most effective if the initial room temperature structure contained between 70-90% austenite although final austenite levels of 25% were also recorded. (229)

Parks (230) has studied the isothermal transformation behaviour of subcritically heat treated chromium-molybdenum irons. From this work he concluded that when as cast austenitic/martensitic structures have been heat treated at 500°C an increase in hardness results from the precipitation of alloy carbides and the formation of further martensite. Parks has suggested the use of such sub-critical treatments as a technique for reducing production costs by the elimination of the high temperature destabilising treatment.

4.6.2.1.6.3 The Mechanically Induced Transformation of Austenite.

The change in chemical free energy with temperature for the austenite to martensite transformation can be represented schematically. see Figure 4.9 The temperature corresponds to the condition of thermodynamic equilibrium. The martensite start (Ms) temperature is the temperature at which the martensite reaction occurs on cooling. The total free energy change at temperature Ms may be given by:

$$\Delta G^{\gamma \to \alpha^1} = \Delta G_c^{\gamma + \alpha^1} + \Delta G_{nc}^{\gamma \to \alpha^1} \qquad - 4.2$$

where $\Delta G^c \; {}^{\gamma \to \alpha^1}$ is a chemical free energy contribution

and $G_{NC} \; {}^{\gamma \to \alpha^1}$ is the non chemical free energy charge

i.e. strain energy component.

At some temperature, T_1 intermediate between Ms andTo an additional mechanical driving force, U, where U is given by

$$U = \Delta G_{Ms}^{\gamma \to \alpha^1} - \Delta G_{T_1}^{\gamma \to \alpha^1} \qquad - 4.3$$

will initiate the martensite reaction. The reaction occurs when the total charge in free energy is equal to

$$\Delta G_{Ms}^{\gamma \to \alpha^1}$$

and U is the critical mechanical driving force necessary for the stress induced martensite transformation at T_1. It therefore follows from Figure 4.9 that as the change in chemical free energy decreases linearly with temperature between Ms andTo then the critical applied stress necessary for transformation must increase with increasing temperature. However, it has been observed (231, 232) that the linear increase of applied stress with temperature has a limited range, see Figure 4.10 denoted by $\overset{\sigma}{\mathrm{Ms}}$. Above $\overset{\sigma}{\mathrm{Ms}}$ plastic deformation of the austenite prior to transformation occurs. At some temperature, T_2, above $\overset{\sigma}{\mathrm{Ms}}$ the austenite is plastically

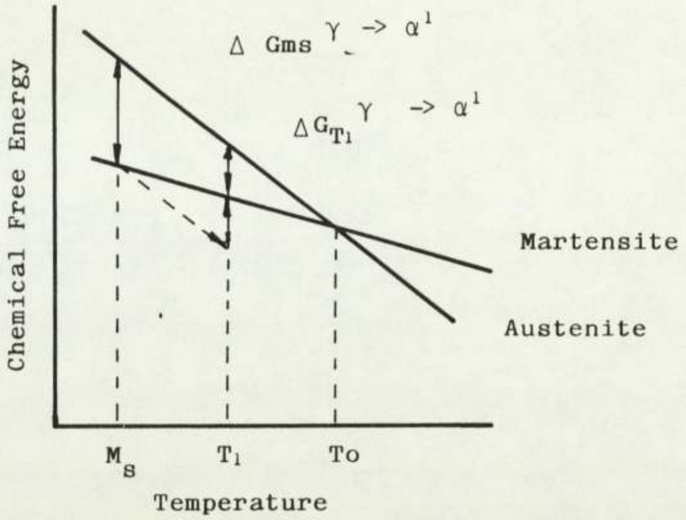

Figure 4.9

Schematic Diagram Showing The Free Energy Change For A Martensitic Transformation.

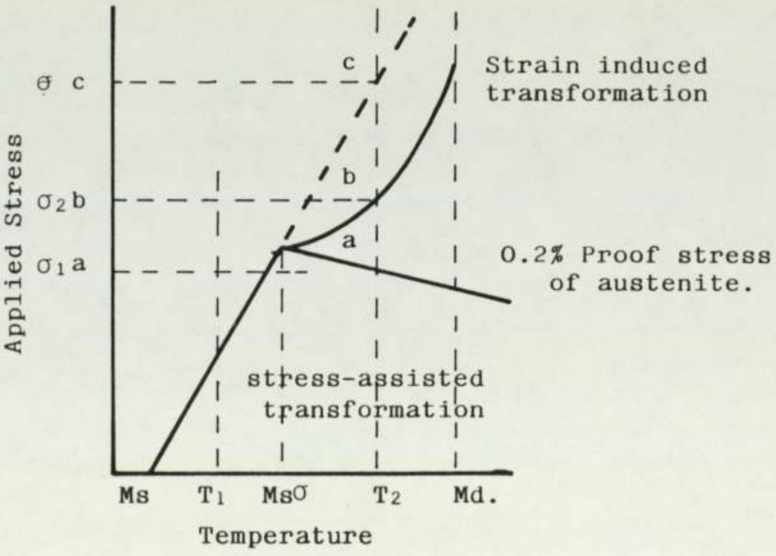

Figure 4.10

Schematic Stress-Temperature Diagram For The Formation of Martensite.

deferred at a stress of $\sigma 2$ and strain hardened up to $\sigma 3$ at which point the martensite transformation occurs. This stress level, $\sigma 3$, is significantly lower than the stress obtained by extrapalation of the linear region of Figure 4.10. The difference in stress levels ($\sigma 4 - \sigma 3$) is the critical applied stress for martensite formation due to the plastic deformation of austenite. Above the Md temperature the chemical driving force for martensite transformation becomes negligible and nucleation cannot be mechanically induced.

It has been proposed (233) that during plastic deformation of the austenite concentrated stress levels (at grain boundaries) locally raise the applied stress to the level suggested by extrapalation of the stress assisted regime. Alternatively, an hypothosis for the strain induced nucleation of martensite has been suggested.(231, 234)

4.7. The Chromium Carbide Phase.

The chromium carbides present in high chromium cast irons exhibit a very high hardness (see Table 1.1) and are of prime importance when considering the wear resistance of these materials.

Maratray (168) has proposed an empirical relationship which allows the estimation of the volume fraction of eutectic carbides within the microstructure

$$\%K = 12.33\ (\%C) + 0.55\ (\%Cr) - 15.2 \quad - 4.4$$

It is evident that for most commercially produced alloys the percentage of carbides will be within the range 12-30%.

Three carbides have been identified which dominated the binary Cr - C equilibrium system namely,

$Cr_{23}C_6$, Cr_7C_3 and Cr_3C_2.

The crystal structure of these carbides has been recorded (235)

$Cr_{23}C_6$	Complex f.c.c., 116 atoms/unit cell a = 1.0655 nm
Cr_7C_3	Hexagonal, 80 atoms/unit cell a = 1.401 nm; C = 0.4525 AM
Cr_3C_2	Orthorhombic 20 atoms/unit cell a = 1.147 nm; b = 0.5545 AM, C = 0.2830 AM.

In the presence of iron, as an impurity or in a ternary system where iron may substitute for chromium a complex carbide can be formed these are generally denoted $M_{23}C_6$ etc.

It has been postulated (235) that the super cooling effect known for the binary C - Cr system may also be found in the ternary Fe - Cr - C system. This would account for the presence of M_7C_3 and $M_{23}C_6$ in the alloys while homogenised material contained only $M_{23}C_6$

It had been generally accepted that the morphology of the eutectic carbide could not be modified by a chemical addition or inoculant, however, a recent Patent Application (236) would appear to invalidate this idea.

The globularising or spheroidising of the eutectic carbide was first reported by Durman (166) who also recorded an associated improvement in fracture toughness and 50% dissolution of eutectic carbide. This increase in fracture toughness exhibited by spheroidised carbide structures has also been highlighted by Diesburg and Borik. (34) Maratray (210) has suggested the use of a high temperature treatment to improve the toughness of hypereutectic alloys containing large, faulted primary carbides. A more thorough study of the spheroidising effect has been made by Biner (165) who also isolated molybdenum and tungsten additions as having a catalytic effect on the process. The use of a spheroidising treatment at 1175°C to improve the dynamic fracture toughness of chromium-molybdenum irons has been presented by Katavic.(170)
It was apparent from the literature that while the improvement in toughness resulting from high temperature spheroidising of the eutectic carbides has been well documented for laboratory scale tests its industrial application and commercialisation were unexplored.

4.8. The Effect of Alloying Elements.

While the carbon and chromium content are prime factors in influencing the microstructure and properties of chromium irons the effects of other alloying elements must not be neglected. It is apparent from the literature that most alloying elements are used to modify the stability of the matrix, they are not generally used to change the morphology of the eutectic carbides.

4.8.1 Molybdenum.

It is obvious from the literature that molybdenum is an important alloying element and has a significant effect on the hardenability of high chromium cast irons. Maratray (168) has quantified this effect and produced an expression relating the maximum air hardening section size to chromium, carbon and molybdenum content.

$$\log \left[\begin{array}{l}\text{Maximum diameter} \\ \text{(mm) for air} \\ \text{hardening}\end{array}\right] = 0.32 + 0.158 \frac{Cr}{C} + 0.385\ Mo \qquad - 4.5$$

Furthermore, multiple linear regression analysis of experimental data (218) has been used to produce regression equations for the pearlite incubation period under both isothermal and continuous cooling conditions. These are:

$$\log \text{Pearlite time (sec)} = 2.61 - 0.51C + 0.05\ Cr + 0.37\ Mo \qquad - 4.6$$

for isothermal transformations and

$$\log \text{Pearlite time (sec)} = 2.90 - 0.51C + 0.05\ Cr + 0.38\ Mo \qquad - 4.7$$

for continuous cooling transformations. The relationships were obtained from material within the range 1.95% - 4.31% carbon, 10.8% - 25.8% chromium and 0.2% - 0-3.8% molybdenum. Other relationships have been produced for more limited alloy ranges. (237, 238). Molybdenum increases hardenability by retarding the pearlite transformation. Generally, any improvement in properties or performance resulting from additions of molybdenum can be attributed to the hardenability effect and the production of a fully martensitic matrix which can support the hard eutectic carbides. (239)

According to Maratray (210) molybdenum also increases the subcritical heat treatment range. That is, for a specific 17% chromium molybdenum free alloy 1000 minutes at 496°C causes the Ms temp to rise from 4°C to 20°C. So far the review has been concerned with the effect of molybdenum forming a solid solution with the austenitic matrix. Molybdenum does in fact partition between the matrix, the M_7C_3 carbides and Mo_2C carbides. Maratray (218) has produced the following empirical relationships for this partitioning effect. If % ΔMo is the amount of molybdenum in the form of Mo_2C and %Mo is the total molybdenum content of the alloy then:

$$\% \Delta Mo = 0.53 \ (\%Mo) - 0.05 \qquad - 4.8$$

Also if the amount of molybdenum in the matrix is $\%Mo_m$ then:

$$\% \ Mo_m = 0.23 \ (\%Mo) - 0.029 \qquad - 4.9$$

The remaining molybdenum partitioning to the M_7C_3 carbides. However, the amount of scatter in these results leads Maratray to suggest the following as a first approximation. For every 1% Molybdenum addition about 0.5% forms Mo_2C, 0.25% forms a solid solution in the matrix and 0.25% partitions into the M_7C_3 carbides. In contrast to this work by Maratray, Typpsin et at (240) has reported that in chromium-molybdenum irons most of the molybdenum is combined with the M_7C_3 carbides and has little effect on hardenability.

Biner (165) has determined that molybdenum additions assist the high temperature spheriodization of eutectic carbides and produce resultant improvements in fracture toughness.

4.8.2. Manganese.

Although both the American A.S.T.M. A.532-80 standard (195) and B.S. 4844 part 3 (194) allow 0.5% – 1.5% Manganese in all grades of high chromium irons the German DIN 1695 standard (241) restricts the addition to 0.5%-1.0 in all but one alloy grade. Manganese is used to increase material hardenability but it is reported to be much less effective in suppressing pearlite than either nickel or copper. It does however exhibit a marked tendency to promote the retention of austenite. (188) Furthermore, if for economic reasons high levels of manganese are used to increase hardenability the effect on austenite retention is unpredictable due to its sensitivity to minor process parameters. In addition because manganese suppresses the Ms temperature it is possible that the risk of cracking castings will be increased. Cias (237) reinforces the effect of manganese on the Ms temperature and adds that the effect of molybdenum was found to be synergistically amplified by manganese additions.

While for the heat treated irons the manganese content is generally limited to about 0.8%, Dodd and Parks (242) recommend an alloy with 1.2% - 1.5% manganese for a pearlite free as-cast austenite matrix structure in thick section castings. These same workers report that at the suggested manganese levels severe acid refractory erosion can occur, particularly in electric induction furnaces. This may be overcome by limiting the melt out manganese content to 1.0% and using a ladle addition for the remainder.

4.8.3 Nickel and Copper.

These two alloying elements are frequently used together to increase hardenability. Unfortunately both nickel and copper exhibit a strong tendency to stabilise austenite. It has been reported (188) that since these elements are completely soluble in the matrix the austenite stability can only be reduced by excessive heat treatment times. For example, in a nickel and copper free chromium-molybdenum iron destabilization is complete after about one hour. With additions of 0.5% to 1.0% nickel or copper a six hour destabilization process is necessary. As a result of these problems associated with the use of nickel and copper additions Fairhurst and Rohrig (188) recommend their cautious use, amounts of 0.5% generally being sufficient for an increase in hardenability.

Dodd and Gouin (239) report that a 15% chromium material alloyed with 2% molybdenum and 1% copper has a hardenability exceeding that of a 3% molybdenum addition only. This work also suggests that an alloy specification suitable for heavy section castings would include 15% to 20% chromium with 2% molybdenum and 1% copper. The effect of amplifying the role of molybdenum with nickel or copper has also been reported by Cias (237)

4.8.4 Vanadium.

Additions of vanadium to cast iron have been studied for many years. In 1960 Barton (196) reported the powerful carbide stabilizing effect of vanadium and its tendency to form massive carbides probably of the V_4C_3 type.

Parent and Magerie (243) investigated the effect of a 6% vanadium addition on the mechanical properties of a base 15% chromium iron. It was concluded that the influence of vanadium would be improved if it could be associated with a higher hardness matrix. Further work comparing the abrasion resistance of a 4.5% chromium, 4% vanadium iron with a 15% chromium, 3% molybdenum iron and a 15% chromium, vanadium material has been carried out. (244) These workers reported that in a 15% chromium alloy a 5% vanadium addition must be made to significantly improve wear resistance. However, as these tests were performed using as-cast material the results should be viewed with caution, the 15% chromium iron being intended for use in the heat treated condition.

A more thorough investigation into the effect of vanadium in cast iron has been carried out by Dawson. (245) This work reiterated the need for a minimum 5% vanadium addition and also recorded as-cast hardness values of vanadium alloy material comparable with standard hardened 15% chromium irons. It has been suggested that when 5% vanadium is present the austenitic matrix becomes destabilized by the precipitation of secondary carbides (possibly secondary vanadium carbides) during the initial cooling cycle. Thus, a martensitic matrix can be obtained in the as-cast condition, retained austenite being transformed by tempering at 450°C. If a 5% vanadium addition is made to a 25-30% chromium alloy then a relatively soft ferritic matrix is produced having low wear resistance and poor high temperature oxidation resistance. Some workers (246) suggest that founding problems such as poor feeding characteristics may be associated with the production of high chromium irons alloyed with 5% vanadium.

4.8.5. Boron.

The addition of boron to high chromium cast irons is the subject of an international application under the Patent Co-operation Treaty (P.C.T.) (236) It is claimed that a boron addition of 0.001% to 4.0% increases the entropy of the iron and produces considerably smaller eutectic carbides of an almost spherical shape. The resultant mechanical properties of a 27.2% chromium, 2.04% carbon material alloyed with 0.17% boron are tensile strength of 830 MPa and 3% elongation. Due to the reported benificial effects of the boron addition to high chromium irons such material may be used in more arduous high wear and stress operations than boron free irons.

4.8.6. Other alloying elements.

The silicon content must be carefully controlled because of its ability to promote pearlitic microstructures. Dodd and Parks (242) illustrate this tendency by quoting an example of inadequate abrasion resistance resulting from a high silicon content. Barton (196) reports the additional facts that silicon increases the oxidation resistance but reduces the resilience to thermal shock. Other workers (242)give a silicon range of 0.3% to 0.8%, the lower value resulting from the now little practised deoxidation procedure. If the silicon content falls below about 0.4% a particularly viscous slag may form.

The use of aluminium as a deoxidation agent is also no longer practised. Russian investigators (246) report that aluminium additions of 0.05% to 0.1% alter the inclusions from type II sulphides to type III inclusions. This modification results in a corresponding increase in mechanical properties. If 0.1% aluminium is exceeded the mechanical properties deteriorate due to the production of a spinel and contamination by Al_2O_3.

Unspecified amounts of aluminium are reported to decrease hardenability.

Titanium has a grain refining effect which also produces an improvement in mechanical properties of 20-30% with a 0.2-0.3% addition (246) It is recorded that titanium, like aluminium, can also promote pearlitic structures and cause feeding problems. Biner (165) investigated the high temperature spheriodizing effect of titanium on the eutectic carbides.

While the literature contains no reference to the benificial effects of rare earth inoculants producing a spheroidized carbide structure it is reported (246) that cerium additions spheroidize non-metallic inclusions.

4.9 The Production of High Chromium Cast Irons.

4.9.1 Charge Material.

The raw material constituting the furnace charge usually comprise of refined pig iron, steel, ferro additions and foundry returns. The actual quantities of these materials should be calculated and weighed prior to charging into the furnace

The use of pig iron is principally to supply the total carbon content of the charge although some contribution to the manganese and silicon levels may occur. It is important to calculate the phosphorus and sulphur pick up from the pig iron as it is possible to exceed the compositional limits (0.05%) of these elements by incorrect selection of pig iron.

The most commonly used ferro additions include high and low carbon-ferro chromium, ferro silicon, ferro manganese and ferro molybdenum. The two grades of ferro chromium nominally contain 4.5% carbon, 66.0% chromium and 0.05% carbon, 70.0% chromium respectively. On a cost basis the cheaper high carbon grade is preferable, in some circumstances, for example the production of a high chromium, low carbon material, the lower carbon grade of ferro chromium must be used. As ferro chromium may also contain about 1.5% silicon this addition should be accounted for when producing furnace charges. The remaining ferro additions contain about 70.0% of the addition element by weight (ferro manganese also contains about 6.0% carbon) and they are a relatively simple and efficient method of making alloy additions.

The foundry returns may be either reject castings or running and feeding systems but in each case correct alloy identification is necessary to facilitate the production of an accurate furnace charge.

The steel addition is primarily required to provide the balance of the iron for the charge material and thus a low carbon steel containing negligible alloying elements would be considered ideal. The steel should be clean and free from any surface coatings.

The complete charge should be free of non metallic contaminents and must be as dry as possible before charging into the furnace.

4.9.2. Melting.

High chromium irons are usually melted in either electric arc or induction units. It has been reported that cupola melting is not possible due to problems with high carbon pick up and in attaining sufficient temperature. (182) Acid refractory linings may be used for both furnace and ladle operations despite their greater erosion than basic linings. (199) It is usual to employ a single slag melting practice with no refining stage, the raw material being 'dead melted'.

4.9.3. Foundry Techniques.

High chromium irons can be satisfactorily used to produce castings by most of the conventional moulding processes other than die casting which suffers from excessive die erosion. (199) It has been suggested (247) that for light castings green sand moulds are adequate but volatile matter should be maintained at less than 1%. Larger castings being successfully produced in air set resin or silicate sand moulds.

Current production procedures use shell mould plants for castings requiring a good surface finish and dimensional accuracy together with urea formaldehyde and furfuryl alcohol systems for larger floor or semi-mechanised track production routes. Pattern equipment may be of either the loose wood, split pattern or metal type but in all cases the contraction allowance should be of the order of 18 - 20 mm per metre. (242) The design of the running and feeding system is very important. In addition to obtaining sound castings with the maximum possible yield it is necessary to incorporate some feeding device to trap oxide-dross. The use of exo-insultating sleeves to maintain fluid risers which assists feeding is frequently practiced as is the addition of an exothermic powder to the top of the riser. Ingates should be positioned so that they are not located on the wear face of a casting this is to avoid possible shrinkage causing premature wear during service. Furthermore, for the same reason, castings should not be positioned in moulds such that the wear face is at the top of the cope mould. While sound castings may require the use of large ingates these areas must be removed during subsequent processing. In addition to being difficult to separate the feeding system from the casting, possibly causing a 'broken-in' area, the remainder of the ingate must be removed from the casting by grinding. To avoid the problem of ingates 'breaking-in' it is possible to remove the section with a soft grade slitting wheel. (239) Grinding large areas of castings is liable to cause localised cracking or heat checking if carried out to excess. Therefore, it is advantageous to use a sand core, situated within the mould, to produce a notch in the ingate to assist with its removal. This technique minimises the force required to separate the casting from the feeding system and reduces the amount of material for subsequent removal.

4.9.4. Casting.

The molten metal may be superheated to about 1650°C within the furnace but before pouring the chemical analysis is checked by rapid spectrographic techniques. At this stage any necessary changes in composition can be achieved easily either by dilution or addition of elements. After removing the slag from the surface of the metal while still in the furnace the metal is poured into pre-heated ladles. Pouring temperatures should be about 1550°C, if too low the casting may miss run but if too high problems with shrinkage and burned sand may occur. Further removal of slag may take place before commencing to fill the mould cavity which should be carried out quickly and without interruption.

Although deoxidation has been recommended (248) by the ladle addition of 1 kg/tonne calcium silicon and 0.75 kg/tonne aluminium this practice is now considered to be unnecessary (242)

The castings should remain in the moulds until cold unless some alternative method of controlled cooling is available. This avoids the production of a highly stressed or cracked casting and permits diffusion controlled transformations to occur.

After removal from the mould the casting should be shot blasted to remove excess sand and then the feeding system is removed. Any necessary grinding to clean the casting of parting line flash or fins from around cored holes should be carried out at this stage.

4.9.5. Heat Treatment.

Although this topic is covered in detail elsewhere some of the more practical aspects will be delt with here.

The stages of heat treatment, annealing, hardening and tempering can be carried out in either gas or electric fueled continuous or batch furnaces. In all cases castings should not be exposed to excessive temperature gradients and the initial heating rate should be limited to about 100°C per hour up to 750°C. Above 750°C when the stresses are able to plastically redistribute themselves the heating rate may be increased to 200/250°C per hour. These rates apply to relatively simple section castings, more complex designs may be limited to an initial heating rate of about 30°C per hour. (239)

The time/temperature relationship for the heat treatment cycles is to a large extent intuitive but related to section size, initial microstructure, historic performance and commercial circumstances. The rate of quenching from the hardening temperature is generally dictated by alloy composition. Low hardenability low chromium/carbon ratio material requires oil (or polymer) quenching to avoid pearlite formation. High chromium/carbon ratio material having a higher hardenability may be forced air cooled. Tempering is usually carried out as soon as possible after hardening so that problems arising from the transformation of retained austenite can be minimised.

4.9.6. Machining.

Most commercial machining operations carried out on high chromium cast irons are limited to grinding processes. This is because of the presence of hard chromium carbides, (see Table 1.1.), martensite and possibly retained austenite within the microstructure. Grinding should be carried out using a soft grade of wheel and limiting the depth of cut, copius amounts of cutting fluid may also be advantageous. Recently the development of cubic boron nitride tool material has greatly improved the turning operations carried out on martensitic white irons. (249) Progress with the turning of high chromium irons is encouraging. For example, considering the machining of coal pulverizer tracks measuring 2.50 M diameter and produced in a hypoeutectic 20% chromium iron. Conventional grinding techniques require about 80 hours of machine time compared with 30 hours for the machining of similar castings using cubic boron nitride cutting tools. Typical machining conditions using a 12.5 mm diameter tool are 45 - 62 M/minute feed rates and cuts of 4 mm depth. While it is apparent that considerable time savings can be made by using machine tooling techniques the tips are relatively expensive, about £140 each. Additionally to prevent tip breakage during interrupted cutting the machine must be rigid and free from vibration.

Fully annealed 25% chromium iron having a hardness of Hv 350 can be turned and bored to produce internal thread forms using conventional high speed steel tools. (250) This operation requires condsiderable operator skill and a controlled, protracted annealing process.

Electro discharge machining (E.D.M.) is capable of successfully cutting high chromium iron. Due to the relatively slow cutting rate and size limitations the commercial adaption of the E.D.M. process for anything other than specialised orders is unlikely.

4.10 Applications of High Chromium Cast Irons.

It is apparent from the literature that two, quite seperate areas of utilization of cast high chromium irons exist, namely, material processing and rolling mill rolls.

The use of abrasion resistant high chromium irons in material processing has been comprehensively reviewed by Durman (183) and Fairhurst and Rohrig (251) who identify three principle areas that is, ball milling, crushing and grinding and abrasive slurry pump components.

4.10.1 Ball Milling.

Ball or tube mills such as those used in the cement grinding industry require a number of wear and impact resistant components.
Figure 4.11 The interior of the mill shell is protected by individual bolt on lining plates each weighing about 20 kg. In addition to protecting the inside surface of the mill these plates assist with the grinding processes. The mill may be divided into compartments by chromium iron diaphragm plates which act as large sieves to grade the charge.

The mill charge consists of the raw material to be ground and a specific addition of sized grinding balls ranging from about 100 mm to 20 mm in diameter. A typical ball mill would measure about 2.2 M in diameter, 12 M long and a throughput of 16-22 tonnes per hour. Media wear rates for both the first and second chambers are about 25g/tonne and liners would carry a 30,000 hour and 60,000 hour guarantee respectively.

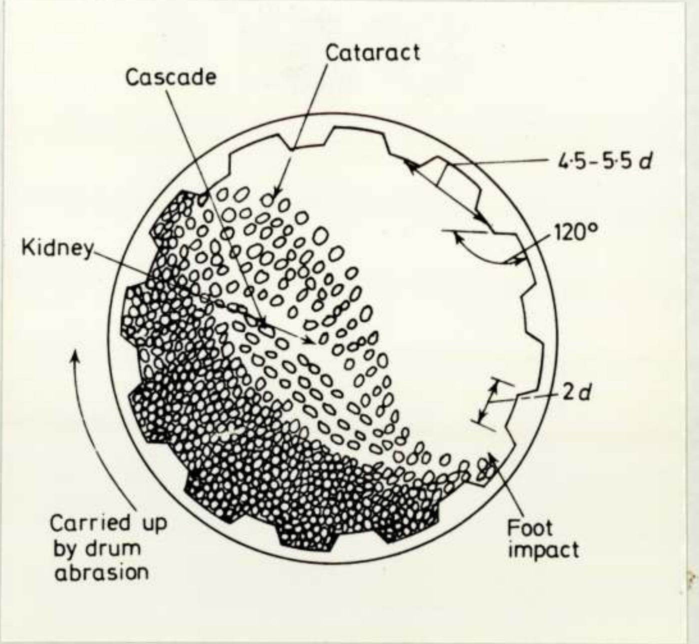

Figure 4.11

Schematic diagram of ball milling action.

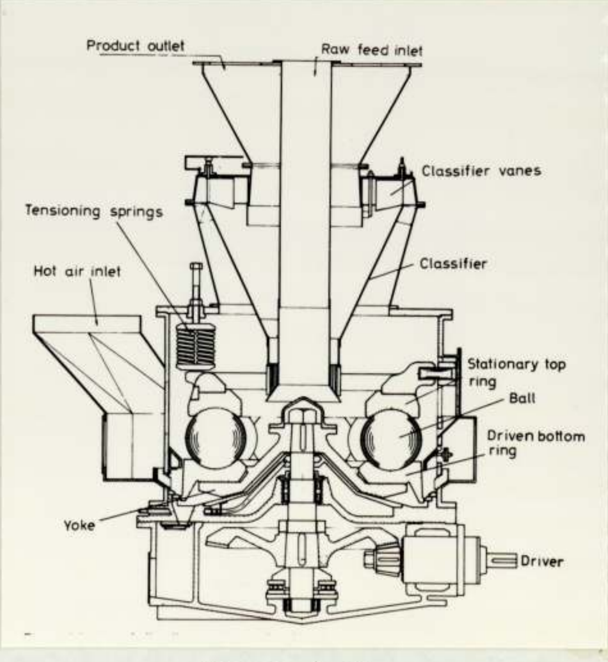

Figure 4.12

Schematic diagram of ring ball mill.

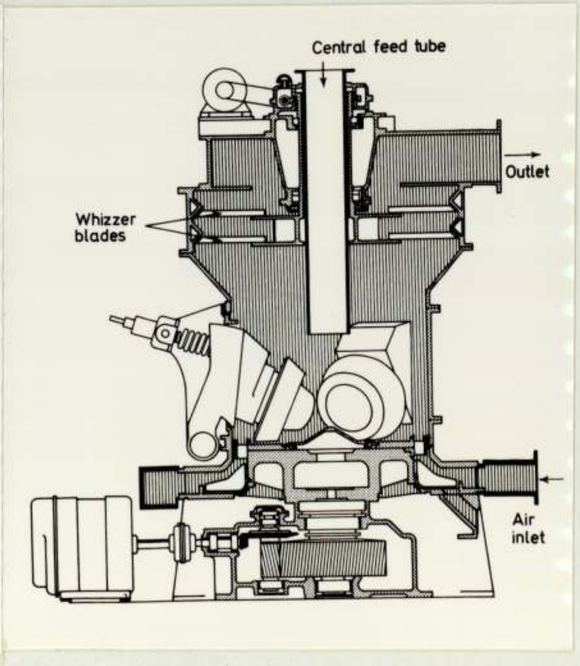

Figure 4.13

Schematic diagram of a three roller ring mill.

4.10.2 Ring Ball Mills.

As an alternative to the ball milling process material may also undergo a size reduction from about 1 cm down to 100 μ m in ring roll or ring ball mills. The wear elements of these types of machines essentially consist of a number of balls or rolls pressing on to a ring. The load may be applied mechanically or by gravitational forces and either the rolls/balls and or the ring may be driven. This produces a rolling action which brings about the size reduction. Typical examples of these machines are illustrated schematically in Figures 4.12 and 4.13.

Ring ball and ring roll grinding machines are frequently used for the pulverization of coal for use in electricity generating plant (252) and to fuel rotary cement clinker mills. (253) It is reported that the use of pulverized coal for heating is more efficient than the burning of coal lumps on a grate. (254)

4.10.3 Abrasive Slurry pumps

Transporting abrasive slurries is a necessary process in many mining operations. These slurries may contain abrasive particles ranging in size from 5 m up to approximately 300 mm and with slurry densities of 60% by weight of solids. (255) The centrifugal pumps consist of three main components, an outer shell, a rotating impeller and two outer liners. In addition to resisting abrasive wear slurry pumps must exhibit a degree of corrosion resistance and sufficient structural integrity to withstand surges of pressure within the system.

4.10.4 Rolling Mill Rolls.

It has been reported (256) that high chromium cast iron rolls are now established in the finishing stands of European hot strip mills. In addition, high chromium-molybdenum rolls up to 1.4 M in diameter are also being used as work rolls in plate mills and smaller rolls are being evaluated for the hot rolling of copper alloys.

The rolls are produced either by the duplex or certrifugal casting process and may have either a pearlitic or martensitic matrix structure.

It is claimed that high chromium iron rolls may produce a greater tonnage of steel than the older chill type rolls. This improvement is principally due to the development of a much finer fire cracking pattern consisting of shallow, narrow cracks which produces a corresponding reduction in the severity of surface damage to the steel strip.

4.10.5 Rotary Impact Hammer Machines.

In this class of crusher the comminution is by impact and not compression. Figures 4.14 and 4.15 illustrate these types of machines and the mechanisms involved during the crushing process. The principle difference between these two types of machines is the method of locating the hammers on the rotor. The pivoted hammers, sometimes known as swing hammers, have a limited degree of movement and are able to accommodate oversize or extraneous feed material. The machines which utilize rigidly mounted hammers or blow bars tend to be somewhat larger than the swing hammer variety, exhibiting higher throughputs (e.g. up to 1000 tonnes per hour) and larger feed sizes(500 kg compared with 15 kg).

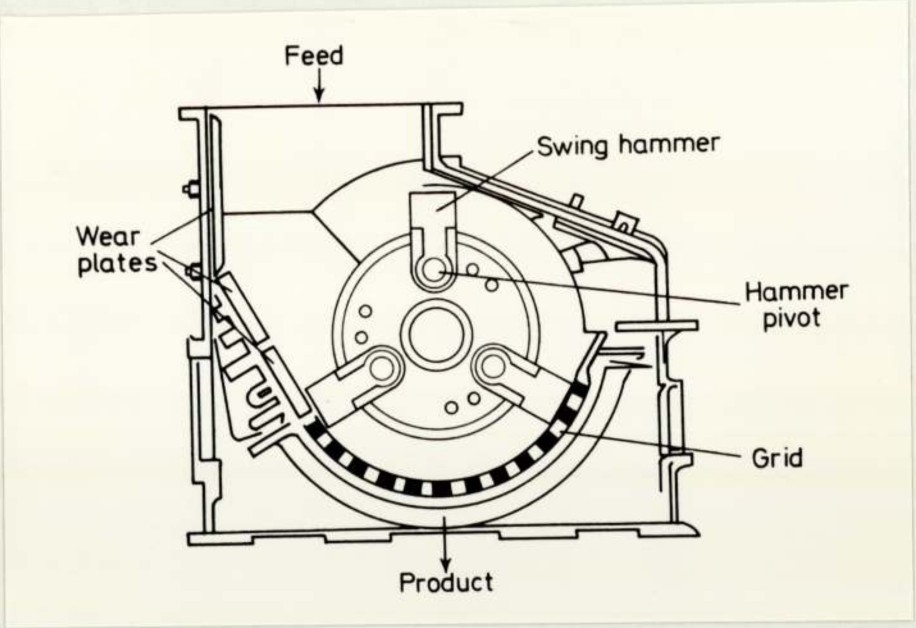

Figure 4.14

Schematic diagram of a swing hammer mill.

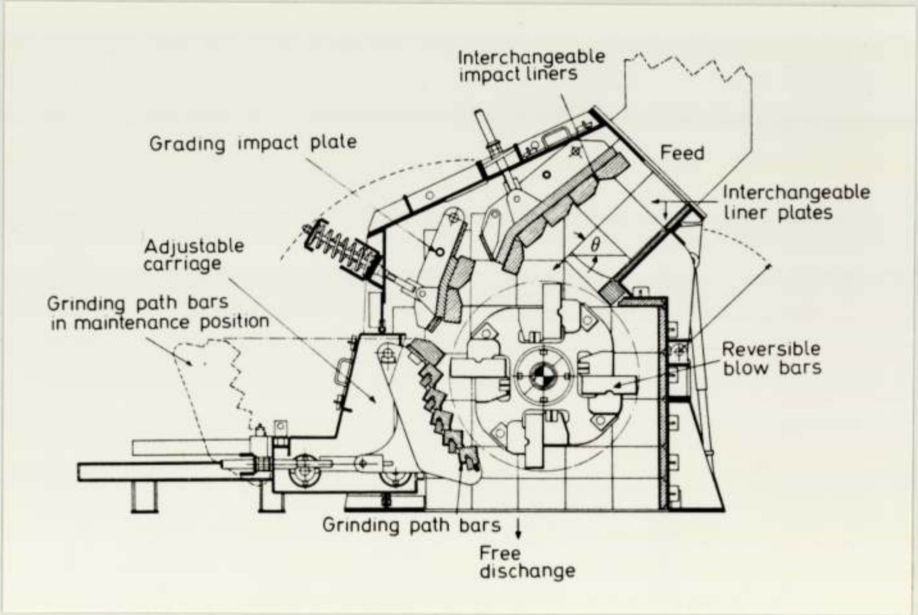

Figure 4.15

Schematic diagram of a rotary impact crusher.

The crushing action is initially by the transfer of kinetic energy from the rotating hammer (400 - 2000 r.p.m.) to the free falling feed material, this may cause an immediate shattering of the particles. The secondary grinding action occurs by the accelerated particles impinging against the impact or breaker plates. In many cases the exit from the mill is covered by a classification screen. Thus, particles too large to pass through the screen may undergo attrition or be recycled around the mill for further breakage. To allow for wear of the hammers it is usually possible to adjust the position of the impact plates so that a constant gap between the hammers and plates is maintained. Furthermore, in the more simple mill design it is possible to turn a worn hammer around so that a new leading edge becomes exposed.

There are a number of advantages claimed for rotary impact mills compared with other crushing machines. (257) these are:

i) A higher proportion of in grade product is achieved because of the classifying action.

ii. The even balance of the rotor does not demand heavy, expensive foundations.

iii. The enclosed construction simplifies dust extraction and water cooling systems.

iv. As breakage tends to be along grain boundaries some separation of minerals with mixed composition is possible.

v) Suitable for weathered materials having soft surfaces but retaining ahard core.

vi) Very large reduction ratio (40:1)

While disadvantages are:

i) Machines may act as fans and entrap material in resulting air flow.

ii) In some small machines the control of product size may be difficult due to the lack of adjustment.

An important difference between material crushed by impact rather than pressure should be emphasized. (258) Material which has undergone comminution by pressure retains a high level of residual stress whereas impacted material exhibit negligible residual stress.

As residual stresses can cause subsequent cracking of the material they should be avoided if a dimensionally stable product is required.

A development of the impact crusher uses a conventional rotor and impact bars which rotate within a revolving cylindrical grate. (259) The grate acts as both a grading screen and a breaking surface. The advantages of this system include the rapid removal of fines, on almost linear particle size distribution and economic superiority compared with conventional models.

4.10.5.1 Hammer Mill Design Considerations.

Probably the most obvious parameters when considering the operation of a mill are rotor speed together with the number and geometry of the hammers. It is reported that an increase in rotor speed increases both the kinetic energy of the rotor (257) and the selection function. (That is, the number of particles broken per revolution.) In addition, the faster the rotor the smaller the product size for a given material. Harder minerals generally require faster rotor speeds than soft minerals if a similar product is to be produced.

As the number of hammers increase the selection function increases but there is no significant change in the size distribution of the product. The spacing between the hammers should be such that the rotor is balanced and no material should be able to penetrate more than a few millimetres into the mill before being impacted. In order to minimize the effect of the impacts on the rotor speed the moment of inertia should be as high as possible.

5.0 Alternative Impact and Wear Resistant Materials.

High chromium irons are in many instances in direct competition with the time proven nickel chromium martensitic white irons. This is an inevitable consequence of the development of an alloy system. However, the generally superior mechanical properties of the high chromium alloy has allowed new applications to be explored, for example impact crusher hammers. A number of other alternative materials are also in competition with high chromium iron, this is particularly evident in the more arduous applications. Dodd (260) has said 'Engineers are still seeking the abrasion resistant alloy which ideally would have the toughness of manganese steel and the abrasion resistance of high chromium-molybdenum alloy iron'. In an attempt to satisfy this requirement of combined properties a composite approach has been adopted. The term composite may be interpreted in several different ways. Kemp (261) discusses the use of a laminated material comprising a wear resistant chromium iron surface backed by a mild steel plate, the banding being achieved by vacuum brazing. This same idea has also been reiterated more recently by Davies and Wilding. (262) A similar concept of lamination involving a rubber bond between the iron and steel materials has also been reported. (263) The composite component may be likened to hard faced weld deposits, (a further competing material (264)) although the thickness of the alloy cast iron may be several times the thickness of the steel substrate. Typically the mild steel would be 5 mm thick and the cast iron 22 mm thick. This composite technique provides support to the cast iron thereby preventing catastrophic failure and provides an easy, convenient method of locating and fixing a component.

A variation on the composite theme involves the use of steel mesh or bars networked throughout the casting similar to the reinforcing rods in concrete. (260, 263) Again, this system only prevents total collapse of the component in the event of premature failure.

The final composite approach has been used on impact hammers (260) in which a steel shank has been fabricated on to a high chromium iron head.

Probably the most conventional of the competitive materials are the manganese steels. Developed by Hadfield in 1882 these alloys are extensively used in applications requiring low abrasion but high impact resistance. Under these conditions the material may work harden from Hv 200/250 up to Hv 400/450. It has been reported that one severe limitation of this material is its comparatively low tensile strength of 618/1004 Nmm^{-2} (265) which may cause problems with 'spreading'. This results in a shape distortion of the casting and can make replacement difficult.

A cast material comprising of a wear face of tungsten carbide particles held together by a nodular cast iron has also been reported. (266) This may be of two forms. If resistance to abrasion is the major problem and only minimal impacts are expected then a cast in carbide clad material has been suggested as suitable. This consists of a wear face of tungsten carbide tiles backed by the nodular iron. If impact conditions are envisaged the alternative cast in carbide composite may be more suited than the former. In this case the wear face (and to a depth of about half of the casting section) is occupied by tungsten carbide granuals between 1 and 5 mm in size. These are held together and supported by a nodular cast iron. A similar type of material has been reported as being used by the C.E.G.B. on exhaust fans transferring pulverised coal from the pulverising mills to the burners. In this case each fan blade has been covered with tungsten carbide tiles located in position by a brazed bond. It is recorded that this technique has extended blade life from 500 hours to between 4000 and 5000 hours. (267)

One specific example of the use of a dissimilar material competing with wear resistant iron is the use of rubber mill linings. The wear characteristics of rubber liners are reported (268) to be significantly different from those of steel or iron, failure to recognise this fact can lead to eroneous comparisons. Rubber liners do not undergo the normal mill corrosion but may suffer degredation if operating temperatures in excess of 80°C are reached or if oil concentrations greater than 0.5 Kg/tonne are present. Unlike ferrous liners the abrase wear of rubber is almost independant of mineral hardness (Figure 5.1) In general, the harder the material feed to the mill the more economical rubber liners become, rubber cannot compete with a cheap steel liner for the grinding of soft material. Furthermore, when the media charge exceeds about 90 mm steel liners become more competitive than rubber. This is because of a more pronounced increase in wear rates of rubber as the size of the mill charge is increased. (Figure 5.2) Correctly designed rubber liners should give at least equivalent capacities and grinding efficiency as other types of liners and should also improve lining economy except for large primary ball mills.

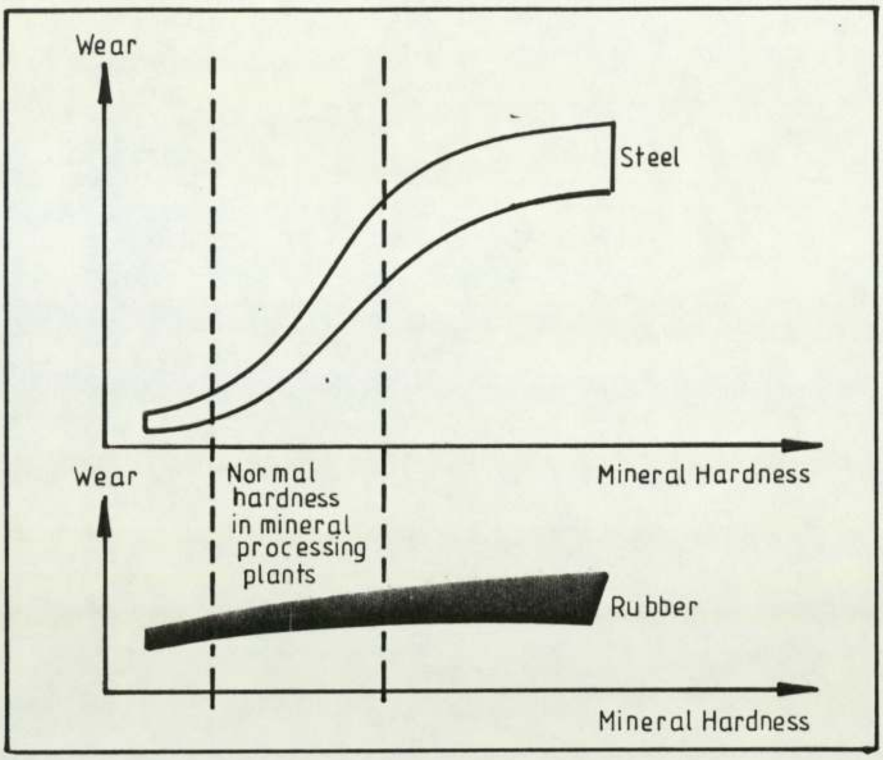

Figure 5.1

Comparative wear for rubber and steel in relation to mineral hardness.

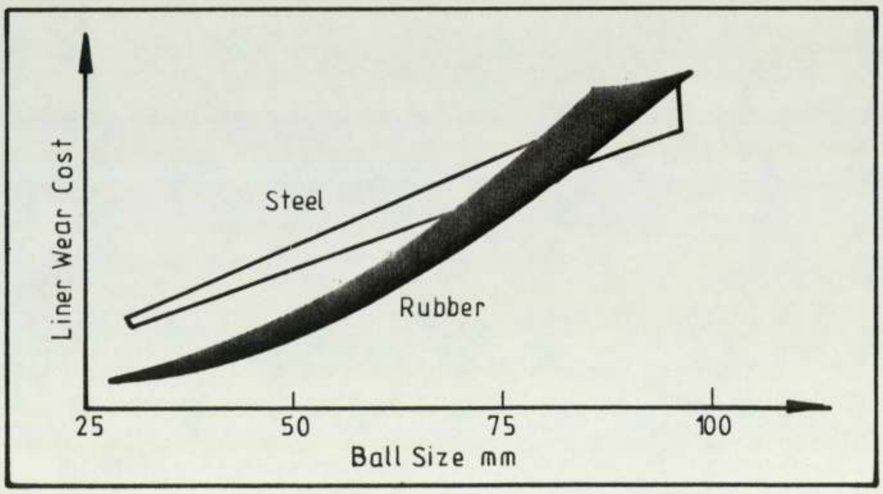

Figure 5.2

Ball size versus Liner wear costs for steel and rubber liners.

6.0 Experimental Procedure.

The procedure involved the evaluation of a set (20 off) of trial cement clinker crusher hammers. The specially processed castings were examined both before installation and following 16 months service. For comparison purposes a casting having the same chemistry was conventionally processed and examined. The conventional material was not subject to the service environment as similar material was known to be unsuitable and failed prematurely after less than 4 hours exposure. The use of short bar fracture toughness specimens permitted the characterisation of toughness at several specific component locations. Studies of the worn surfaces enabled the micromechanisms of wear, operating in the studied system, to be elucidated.

6.1 Production of Trial Samples.

6.1.1. Casting

The trial clinker crusher hammers, as illustrated in Figure 6.1, were produced by Bradley and Foster Ltd. Darlaston. Green sand moulds were made using a loose wood pattern and incorporated a 31 mm diameter sand core to produce the pivot hole. In each mould a running and feeding system ensured an adequate supply of hot, clean metal to the mould cavity.

Two, 250 kg. raw material charges comprising pig iron, steel and ferro alloys were melted in a 500 kg capacity high frequency induction unit. Before pouring the metal a chill cast coin sample was spectrographically analysed and any necessary chemical adjustment made. No deoxidation procedure was carried out and the metal was cast at a temperature of 1440°C. The castings were allowed to mould cool to ambient temperature before being shot blast cleaned and dressed. At this stage all castings were visually inspected for evidence of casting defects, particularly

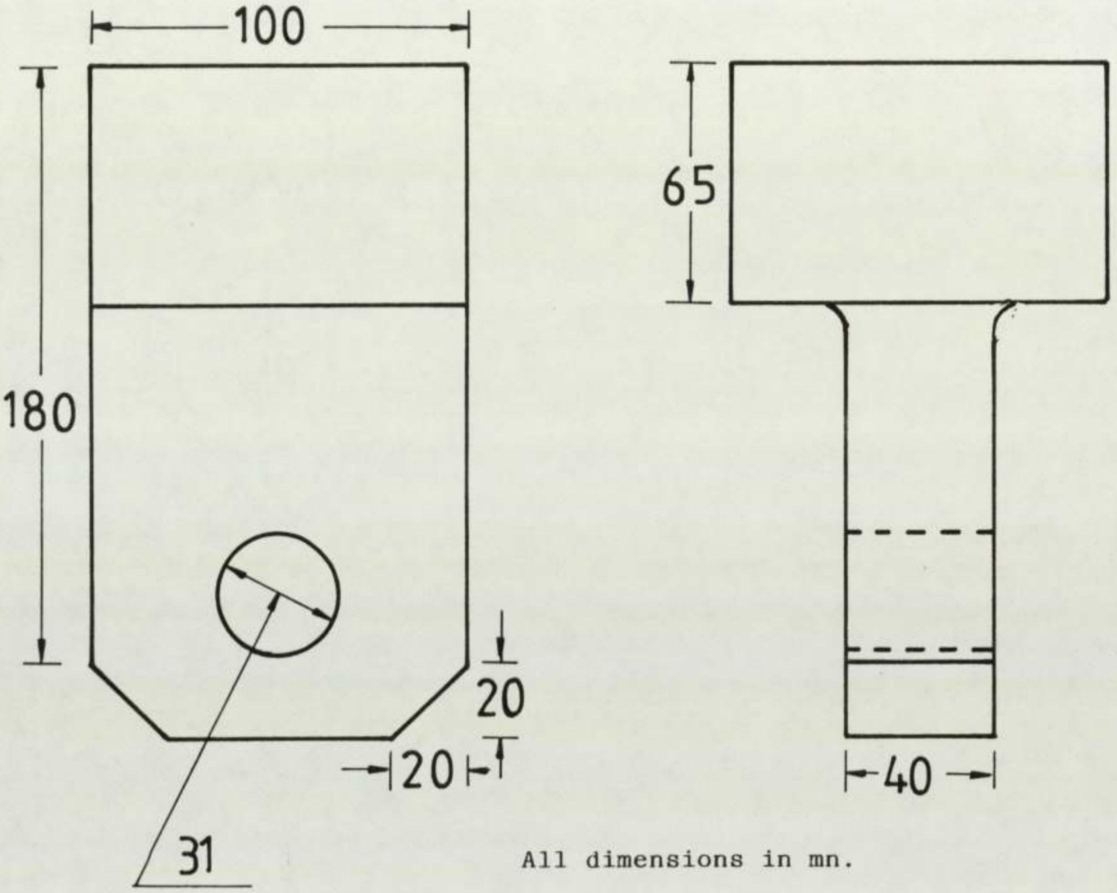

All dimensions in mn.

Figure 6.1.

Trial clinker crusher hammer.

cracks. The castings were again shot blast cleaned prior to despatch for vacuum heat treatment.

6.1.2 Heat treatment.

6.1.2.1 High Temperature Heat Treatment.

Twenty three castings were subjected to the specialised vacuum treatment cycle which was carried out using an Ipsen VTC 524R pressure quench vacuum furance. The castings were arranged on the furnace tray as a single layer with shank end uppermost. The load thermocouple being located in the pivot hole of a centrally positioned casting. The treatment schedule was as follows:

1. Heat from ambient to 750°C at a rate not greater than 150°C/hour.

ii. Heat from 750°C to 1180°C at a rate not greater than 250°C/hr.

iii. Hold at 1180°C for 8 hours

iv. Gas quench to ambient temperature.

The gas quench was carried out by backfilling the furnace chamber with nitrogen gas to a maximum pressure of 5 atmospheres an internally mounted circulating fan further assisted the quench process.

6.1.2.2. Conventional Heat Treatment.

One as cast hammer was conventionally hardened and tempered using an electric muffle furance. This heat treatment cycle consisted of:

i. Heating from ambient to 780°C and holding for four hours, followed by furnace cooling. (Anneal)

ii. Heating to 980°C and holding for two hours followed by a forced air quench (Destabilise and harden.)

iii. Heat to 275°C and hold for two hours followed by air cooling. (Temper)

6.1.2.3 Subcritical Heat Treatment Exercise.

Samples of material taken from an unused vacuum heat treated casting were used to investigate material response to sub-critical heat treatment. The treatments were carried out using a laboratory sized electric muffle furance at temperatures between 200°C and 700°C. The furnace was allowed to stabilise at temperature for 24 hours before commencing a treatment. All treatment times were for 24 hours as it was believed that this length of time would be sufficient to allow the completion of any transformation. One sample of vacuum treated material was cooled in liquid nitrogen. All samples were metallographically examined and hardness tested.

6.1.3 Inspection Procedures.

On return of the vacuum treated castings further visual and dye penetrant crack detection was carried out. An on site metallographic examination and dynamic hardness tests were used to assess the response of the material to the heat treatment cycle.

Twenty castings were despatched for use in a service trial, three were retained for investigation. The conventionally treated casting was also examined and used for comparison purposes.

6.2 Production of Short Bar Fracture Toughness Specimens.

The size and geometry of the short bar specimen is illustrated in Figure 6.2, their production from the trial castings involved several clearly defined stages.

i. Electrodischarge machining of specimen 'blanks' from casting.

ii. Surface grinding of 'blanks' to produce correct outer dimensions of specimens.

iii. E.D.M. of grip grooves.

iv. Electrodischarge machining of chevron notch.

Stage (i) utilised a wire slice attachment fitted to conventional E.D.M. equipment and a continuous copper wire electrode of 0.25 mm diameter. The specimen positions and orientations are illustrated in Figure 6.3. As it was only possible to make cuts in the vertical plane several operations were required before obtaining the specimen 'blanks'. Details of the sectioning procedure and electrical condition for the E.D.M. process have been reported elsewhere. (269)

The specimen blanks produced in stage (i) were about 1 mm oversize in all dimensions. Surface grinding was carried out to obtain correctly sized specimens having perpendicular and parallel faces.

The electro-discharge machining of the grip grooves involved the use of a single copper electrode. After each operation the 60° included angle of the electrode was reground using a specially produced jig.

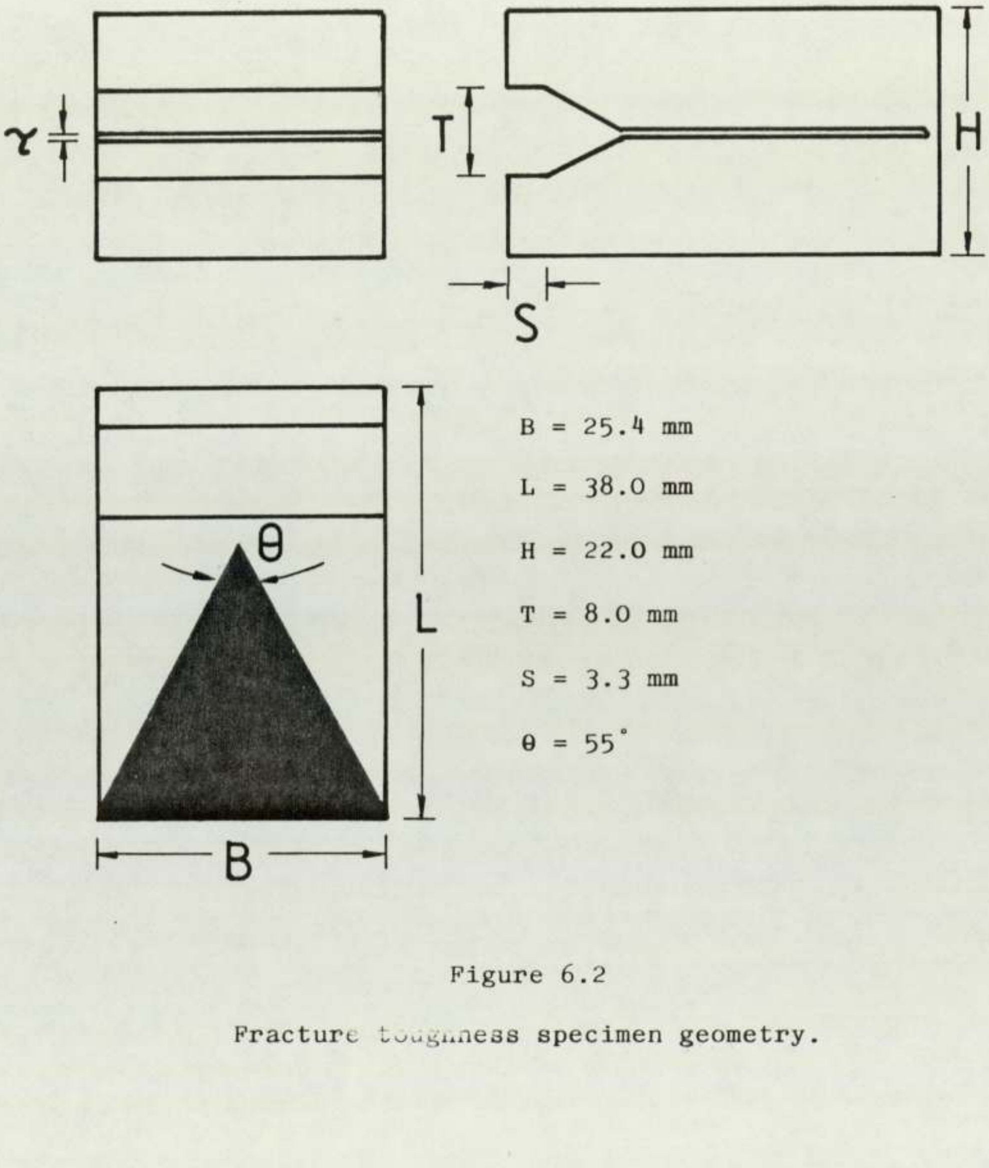

B = 25.4 mm

L = 38.0 mm

H = 22.0 mm

T = 8.0 mm

S = 3.3 mm

θ = 55°

Figure 6.2

Fracture toughness specimen geometry.

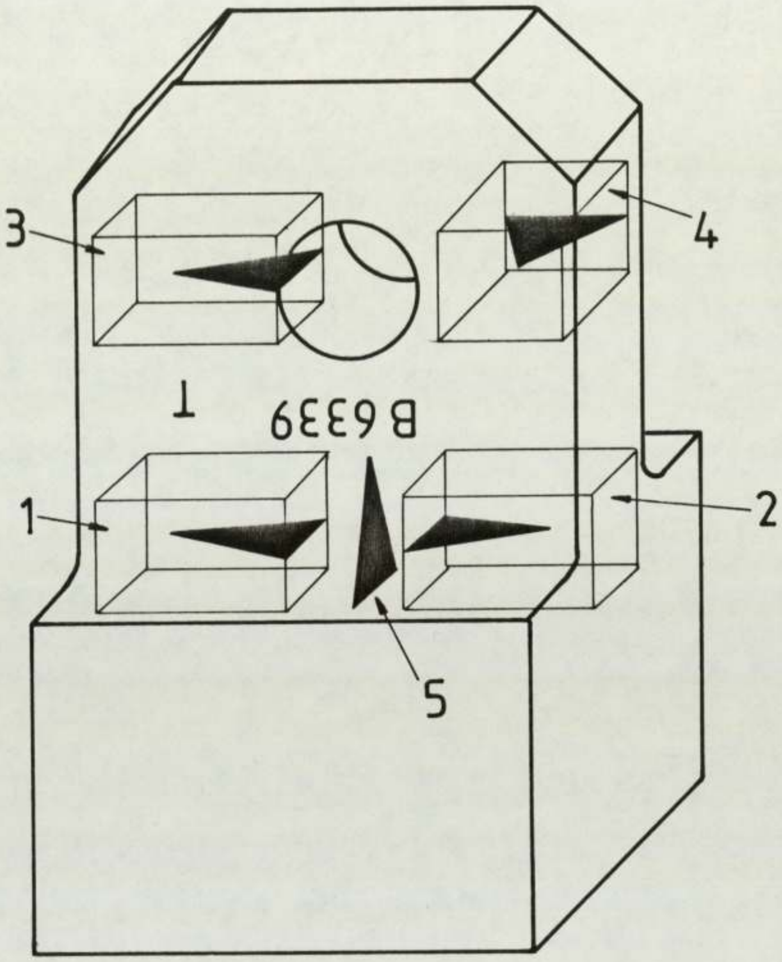

Figure 6.3

Fracture toughness specimen location.

The final stage of sample production was the production of the chevron notch. This was obtained by using a 0.2 mm diameter copper wire on the E.D.M. wire slice unit. A jig held the specimen such that a vertical movement of the horizontal wire produced the required inclined cut. Each specimen needed two cutting operations to form the chevron.

6.3 Fracture Toughness Testing.

The testing of the short bar fracture toughness specimens was carried out using a Fractometer II machine. This equipment has been especially produced for this test procedure and is illustrated in Plate 6.1. Before commencing each series of tests the machine was allowed to stabilise for about 1 hour and the recommended zeroing and calibration procedures were carried out. (135) Depending on specimen material and processing a maximum load setting of 8.088 KN or 20.2 KN was selected. The maximum jaw displacement was measured as being 10 mm and the typical loading rate was 0·1 mm/min. An integral X-Y recorder allowed the production of a load versus displacement trace for each specimen. During each test an unloading and reloading cycle was carried out just before and after the maximum load had been achieved. After each test had been completed the samples were fractured such that two halves were produced. These fracture surfaces were then protected for subsequent S.E.M. examination and a Nikon shadow graph used to determine the values of θ and Ao.

6.3.1 Examination of Fracture surfaces.

Specimens measuring approximately 1.0 cm x 1.0 cm x 0.5 cm. were cut from fractured halves of short bar samples using the E.D.M. technique. Following thorough ultrasonic cleaning and mounting on aluminium stubs all samples were viewed using a Cambridge 150 scanning electron microscope.

Plate 6.1

The Fractometer II

6.4 Compression Testing.

Due to the lack of success of other workers (165, 166) to obtain valid tensile data from standard samples produced from similar material no such attempt was made during this study. As an alternative exercise compression test specimens measuring approximately 5 mm diameter by 9 mm in length were produced by electro discharge machining of the fractured short bar specimens. These samples were tested in an Instron testing machine and the compressive strength was determined from the experimental data. During each test the specimens were located between plates produced in a hardened and tempered tool steel. This prevented any damage occurring to the test equipment and assisted with maintaining the specimen vertically. All tests were carried out at a crosshead speed of 0.5 mm/minutes.

6.5 Microstructural Examination.

6.5.1 Optical Metallographic Study.

Samples suitable for metallographic examination were cut using the E.D.M. technique from the fractured halves of the short bar samples. These samples were ground, polished to a 1μm finish and etched in Picral solution acidified with hydrochloric acid. In an attempt to differentiate between M_7C_3 and $M_{23}C_6$ type carbides selected samples were also etched in alkaline picrate. All samples were examined using a conventional optical microscope.

6.5.2 Quantitative Metallographic Study.

A quantitative metallographic study of the polished and etched samples was undertaken. Due to difficulties in obtaining sufficient phase contrast for image analysis procedures the samples were viewed at a nominal magnification of 600X on a Vickers projection microscope and a horizontal linear intercept technique was used. The magnification was periodically checked using an etched graticule and a total of 50 fields on two perpendicular planes were examined. This technique enabled the calculation of carbide volume fraction, mean interparticle size and mean interparticle spacing. The total number of intercepted particles per field was used as a measure of the degree of spheroidisation of the eutectic carbide.

6.5.3 Carbide Morphology Study.

Samples of a suitable size for examination in a Cambridge 150 S.E.M. were produced from fractured halves of selected short bar specimens. These samples measured approximately 0.7cm x 0.7cm x 0.7 cm and were ground and polished on one face to a 1μm finish. The remaining five faces were painted with a protective lacquer. The samples were then deep etched. (or matrix leeched) using a 1% solution of hydrochloric acid in water. This process, which required about 14 days, preferentially dissolved the matrix and permitted the examination of the carbide network. Daily cleaning and a thorough final cleaning using a caustic surface activant and ultrasonic bath was necessary to remove the adherent debris. Final soaking in methy-ethyle-ketone and rinsing in acetone removed the lacquer and assisted the drying of the matrix leached samples.

6.6 Hardness Testing.

The metallographic samples were also used for the hardness determinations. A minimum of ten Vickers hardness tests using a 30kg load were carried out on each sample. Microhardness tests were carried out on representative samples to determine matrix and carbide hardness. For these tests a Vickers microhardness machine was used with loads of 100g and 50g respectively, again a minimum of ten tests were performed on each sample.

The fracture toughness testing, metallography and hardness testing was also carried out on the conventionally hardened and tempered casting.

6.7 Examination of Worn Casting.

After about 16 months service a hammer casting was taken out of the mill and made available for examination, a replacement having been supplied. This sample was also sectioned in a similar manner to the previous castings and short bar fracture toughness tests, metallographic examinations and hardness evaluations were carried out. In addition, samples measuring about 1 cm x 1 cm x 0.5 cm were produced from areas of the casting which exhibited clearly different forms of wear. Initially, these samples were subjected to a minimum amount of ultrasonic cleaning before examination by S.E.M. of wear damage. Subsequent deep etching of these samples in dilute hydrochloric acid enabled the subsurface observation of eutectic carbide.

Metallographic samples perpendicular to the damaged surface were also prepared. The worn surface was protected by an electrodeposited nickel layer before mounting in thermo setting bakelite. Surface damage and subsurface effects were observed on polished and etched samples using an optical microscope. To investigate the depth of work hardening a larger specimen was produced having its polished face perpendicular to the damaged surface. This sample was macro etched using acidified Picral solution and allowed to oxidise slightly before viewing.

7.0 Service Trial.

The service trial was conducted at Blue Circle Industries, Weardale Works. The company is concerned with the production of cement by combining a secondary addition of clay or shade with limestone. The operation encompasses all material handling processes from the initial limestone quarrying to final ball milling of cement clinker and gypsum.

7.1 Description of Cement Production process.

Cement production may be either a wet or dry process depending upon the constituent raw materials. Clay and chalk require a wet process route because of the 20% moisture contained within chalk while shale and limestone are processed dry. As a result of the inefficiency of the wet process it is the dry route which is currently favoured.

During dry processing the crushed limestone and shale are ball milled and blended to form the raw meal. The raw meal is pre-heated to about 800°C before entering an oil, gas or coal fired rotary kiln. The temperature achieved in the kiln (1400°C) converts the meal into cement clinker which then exits the kiln as nodules. The hot nodules pass over a series of cooler grates before ball milling together with a gypsum addition. The final cement product is stored in silos and despatched either in bulk containers or bags.

7.2 Cement Chemistry.

Cement clinker contains four main compounds, namely:

$3CaOSiO_2$	denoted by C_3S
$2CaOSiO_2$	denoted by C_2S
$4CaOAl_2O_3Fe_2O_3$	denoted by C_4AF
$3CaOAl_2O_3$	denoted by C_3A

together with about 6% of, MgO, Na_2O K_2O and TiO_2. As the principle compounds have various hydration rates the cement properties can be modified by control of chemistry and the addition of gypsum (calcium sulphate.) Table 7.1 lists the key types of cements and their compositions.

Cement	C_3S	C_2S	C_4AF	C_3A	CaO	Others
Ordinary Portland (OP)	47	25	8	11	1.5	7.5
High Early Strength (RM)	52	21	9	9	2.0	7
Large Mass Work (LM)	16	61	6	9	0.8	7.2
Sulphate Resisting (SR)	49	24	17	2	1.9	6.1

Table 7.1

Typical Cement Chemistry.

Details of the various grades of cement together with specific properties and applications may be found elsewhere. (270)

7.3 Description of Swing Hammer Mill.

The Polysius mill consisted of a central rotor about 2.0 m long and 0.24 m diameter rotating at 420 r.p.m. 20 hammers were located around the rotor in 5 rows of 4 hammers. (see Plate 7.1) Each hammer was located in position by a 30 mm diameter by 215 mm long black bolt which passed through the central pivot hole. The hammer tip to tip diameter was 0.55 m. Although the amount of cement clinker which passed through.

Plate 7.1

Swing Hammer Mill Used for Service Trial.

mill was not measured the kiln capacity was 40 tonnes per hour, the mill therefore handled something less than this amount. The unit operated on a continuous basis with interruptions only for annual maintenance and any unscheduled shutdowns.

7.4 Description of Swing Hammers.

The hammer shape and dimensions are illustrated inFigures 6.1 and 6.3. The individual piece weight being about 10 kg. While the pivot hole allowed a 1 mm clearance for the locating bolt the tolerance in allignment between front and back face was only 0.5 mm this was to enable accurate positioning between the stirrup side plates which prevented lateral movement of the hammers during service.

The usual hammer materials were an austenitic manganese steel and a hardfaced steel, neither giving in excess of six months service.

8.0 Data Analysis.

8.1 Quantitative Metallographic Study.

The raw data generated from the linear horizontal intercept study was used to quantify four metallographic parameters:

i. Volume fraction of eutectic carbide.
ii. Mean interparticle spacing.
iii. Mean particle size.
iv. Eutectic carbide 'density'.

The volume fraction, V_f, was calculated using the relationship

$$V_f = \frac{Lc}{L} \qquad - 8.1$$

where Lc = total length of line intercepted by eutectic carbide particles.

L = total length of line

To determine the mean interparticle spacing, Lo, the relationship

$$Lo = [(1 - V_f)/Nc]\ L \qquad - 8.2$$

has been used, where

Nc = total number of intercepted carbide particles.

The mean carbide size, Co, was estimated from:

$$Co = [V_f/Nc]L \qquad - 8.3$$

8.2 Determination of Short Bar Fracture Toughness Values.

The fracture toughness values calculated during this investigation have been denoted by K_{ICSR}. This has been done to distinguish between plane strain fracture toughness values produced by carrying out ASTM E399-81, K_{IC} and the values produced using a chevron notched specimen.

A typical trace of load against mouth opening displacement has been shown in Figure 2.10. Using this illustration as an example the data analysis procedure suggested by Baker (135) has been followed.

i. The high and low points of the unloading, reload cycle were found. The high points (H) were taken as the points at which the grips started to move together. The low points (L) were the position on the reloading line at half the load of the high point. An ideal release line was drawn through both sets of points, H and L.

ii. An 'average load' line was drawn between the two ideal elastic release lines.

iii. The distance between the ideal release line at the average load level (ΔX) and the zero load level (ΔXo) was measured.

The plasticity value, p , was calculated from

$$p = \frac{\Delta Xo}{\Delta X} \qquad -8.4$$

The plasticity correction factor was given by

$$\left(\frac{1 + P}{1 - P} \right)^{1/2} \qquad - 8.5$$

Hence, K_{ICSB} was calculated from

$$K_{ICSB} = \frac{A\,F_{max}\,(1 + \sqrt{1 - P})^{1/2}}{B^{3/2}} \qquad - 8.6$$

8.3 Determination of compressive yield strength.

The compressive strength of the materials was calculated by dividing the maximum load before fracture by the initial cross-sectional area.

9.0 Results.

To assist with sample identification the following alpha - numeric identification system has been identified.

Code	casting chemistry/processing.
A.	unused trial hammer after specialised high temperature treatment.
B.	unused trial hammer after specialised high temperature treatment.
C.	unused trial hammer after specialised high temperature treatment.
D	casting and chemical composition as casting A, B and C but subjected to conventional hardening heat treatment.
E.	used trial hammer, chemistry and processing as castings A, B and C after 16 months service.
F.	conventional high chromium cast iron hammer, dimensionally as other castings but failed in service.

Specific specimen locations have been identified using the above code letter as a prefix to a number as indicated in Figure 6.3.

Table 9.1	Chemical composition of trial castings.
Table 9.2	Summary of hardness results.
Table 9.3	Summary of matrix and carbide microhardness results.
Table 9.4	Summary of hardness results from subcritical heat treatment specimens.

Weight %

Casting	C	Si	S	P	Mn	Ni	Cr	Cu	Sn	Mo
A	2.45	0.51	0.024	0.041	0.33	0.12	15.3	0.14	0.01	2.09
B	2.41	0.52	0.031	0.042	0.31	0.19	15.6	0.14	0.01	1.99
C	2.35	0.49	0.034	0.035	0.34	0.15	15.3	0.15	0.01	2.06
D	2.45	0.49	0.031	0.034	0.34	0.16	15.2	0.13	0.01	2.11
E	2.45	0.52	0.029	0.041	0.32	0.19	15.3	0.15	0.01	2.01
F	2.12	0.84	0.056	0.043	0.93	0.65	20.2	0.37	0.01	1.68

Table 9.1

Chemical composition of trial castings.

Sample location	Average Vickers Hardness (Hv_{30})					
	Casting					
	A	B	C	D	E	F
1	416 ± 11	417 ± 9	413 ± 9	803 ± 8	439 ± 6	737 ± 9
2	423 ± 8	410 ± 8	417 ± 6	812 ± 13	446 ± 5	740 ± 8
3	422 ± 6	407 ±10	415 ± 6	755 ± 10	440 ± 7	-
4	431 ± 6	409 ± 5	417 ± 7	768 ± 8	440 ± 8	-
5	445 ± 6	394 ± 9	426 ±10	789 ± 5	450 ± 7	741 ± 8

Table 9.2

Summary of hardness results.

Specimen	Average Vickers Micro Hardness.	
	Matrix ($Hv_{0.1}$)	Carbide ($Hv_{0.05}$)
A1	402 ± 15	1511 ± 159
A2	384 ± 12	1649 ± 160
A3	398 ± 14	1779 ± 127
A4	403 ± 11	1623 ± 144
A5	410 ± 20	1719 ± 140
B1	377 ± 13	1782 ± 180
B2	373 ± 18	1840 ± 98
B3	387 ± 10	1588 ± 138
B4	376 ± 19	1585 ± 117
B5	415 ± 16	1608 ± 158
C1	381 ± 5	1597 ± 83
C2	399 ± 11	1584 ± 56
C3	356 ± 18	1514 ± 39
C4	349 ± 12	1577 ± 71
C5	382 ± 8	1608 ± 104
D1	751 ± 18	1664 ± 74
D2	760 ± 21	1663 ± 163
D3	714 ± 13	1618 ± 115
D4	715 ± 22	1727 ± 133
D5	742 ± 17	1577 ± 101
E1	434 ± 14	1602 ± 176
E2	469 ± 17	1768 ± 177
E3	441 ± 16	1676 ± 128
E4	442 ± 15	1772 ± 102
E5	460 ± 20	1569 ± 138
F1	707± 14	1585 ± 73
F2	705 ± 11	1627 ± 76
F5	708 ± 11	1569 ± 168

Table 9.3

Summary of matrix and carbide microhardness results

Treatment temperature (°C)	Mean hardness (Hv_{30})
710	410 ± 7
652	459 ± 12
603	522 ± 12
550	446 ± 10
508	447 ± 7
404	436 ± 9
327	421 ± 10
211	425 ± 8

Table 9.4

Summary of hardness results from subcritical heat treatment specimens.

Distance below worn surface (mm)	Hardness Hv_5	Distance below worn surface (mm)	Hardness Hv_5	Distance below worn surface (mm)	Hardness Hv_5
0.525	666	5.775	633	11.025	501
1.050	655	6.300	623	11.550	540
1.575	644	6.825	623	12.075	557
2.100	623	7.350	593	12.600	532
2.625	603	7.875	603	13.125	575
3.150	655	8.400	593	13.650	584
3.675	603	8.925	566	14.175	566
4.200	644	9.450	566	15.175	524
4.725	633	9.975	524	16.175	540
5.250	666	10.500	516	17.175	494

Table 9.5

Hardness traverse across work hardened layer.

Sample	Density	Carbide Volume (% V_f)	Mean Carbide Size (µm)	Mean Inter carbide Spacing (µm)
A1	30.1 ± 6.2	20.4 ± 4.4	11.07 ± 1.85	44.84 ± 10.87
A2	44.8 ± 9.6	20.1 ± 3.2	7.45 ± 1.55	30.14 ± 6.56
A3	41.4 ± 6.7	19.7 ± 4.5	7.63 ± 1.12	32.59 ± 8.19
A4	48.6 ± 12.9	19.0 ± 2.8	6.62 ± 1.49	29.52 ± 10.28
A5	43.2 ± 11.1	18.3 ± 3.8	7.32 ± 1.79	35.22 ± 9.14
B1	30.0 ± 3.6	16.0 ± 2.1	8.67 ± 1.35	45.88 ± 5.91
B2	31.6 ± 5.8	15.3 ± 2.6	7.95 ± 1.48	45.24 ± 11.11
B3	43.5 ± 10.2	18.5 ± 3.4	7.04 ± 1.19	32.26 ± 9.29
B4	37.8 ± 10.9	14.5 ± 3.2	6.45 ± 1.55	40.13 ± 7.32
B5	23.4 ± 5.3	11.5 ± 4.5	7.86 ± 2.00	64.14 ± 15.53
C1	26.1 ± 8.8	13.7 ± 2.7	9.14 ± 2.80	59.52 ± 9.33
C2	28.7 ± 12.8	15.1 ± 5.0	9.39 ± 2.03	61.51 ± 12.45
C3	43.3 ± 13.9	15.9 ± 3.6	6.39 ± 2.08	36.11 ± 9.84
C4	39.7 ± 11.5	15.7 ± 3.7	6.57 ± 1.39	38.83 ± 6.79
C5	33.0 ± 5.8	16.9 ± 3.9	8.32 ± 1.48	42.09 ± 8.80
D1	40.3 ± 10.5	17.3 ± 5.6	7.32 ± 1.71	37.51 ± 9.84
D2	37.9 ± 9.7	20.5 ± 7.3	9.50 ± 1.92	43.12 ± 13.19
D3	43.3 ± 10.2	17.8 ± 3.3	7.38 ± 2.46	34.35 ± 8.43
D4	44.3 ± 9.6	18.4 ± 5.5	7.02 ± 1.37	32.75 ± 7.93
D5	38.7 ± 12.8	19.0 ± 5.1	8.64 ± 2.10	39.10 ± 11.76
E1	34.7 ± 12.6	15.9 ± 2.7	8.19 ± 1.82	44.58 ± 7.42
E2	34.4 ± 7.6	21.5 ± 4.5	10.81 ± 1.43	40.60 ± 9.97
E3	40.9 ± 7.2	17.6 ± 3.8	7.36 ± 1.46	35.23 ± 6.99
E4	38.1 ± 10.6	16.7 ± 4.5	7.69 ± 2.09	40.88 ± 4.81
E5	35.0 ± 12.3	18.8 ± 4.2	9.39 ± 1.50	45.41 ± 5.20
F1	48.5 ± 9.1	16.3 ± 2.0	5.54 ± 0.97	29.02 ± 6.41
F2	46.4 ± 13.7	17.3 ± 4.0	6.37 ± 1.27	31.38 ± 9.24
F5	40.5 ± 10.7	14.0 ± 5.6	5.50 ± 1.60	38.49 ± 7.50

Table 9.6

Quantitative Metallographic results.

Sample	Sample Dimensions				
	W (MM)	B (MM)	L (MM)	Ao (MM)	Θ (MM)
A1	22.10	25.43	38.10	13.56	56.05
A2	22.10	25.40	38.02	13.37	56.04
A3	22.10	25.46	37.97	13.26	56.02
A4	22.15	25.40	38.10	13.45	56.04
A5	22.07	25.37	38.10	13.38	55.47
B1	22.05	25.45	38.13	13.45	55.79
B2	22.00	25.45	38.02	13.36	55.35
B3	22.12	25.40	38.10	13.55	55.54
B4	22.02	25.43	38.13	13.46	55.82
B5	22.05	25.35	38.15	13.41	55.90
C1	22.10	25.30	38.10	13.80	56.05
C2	22.12	25.30	38.18	13.87	55.43
C3	22.12	25.40	38.10	13.47	55.41
C4	22.02	25.37	38.10	13.65	55.17
C5	22.07	25.35	37.77	13.29	55.22
D1	22.07	25.37	38.15	13.47	55.0
D2	22.12	25.35	38.20	13.55	55.5
D3	22.15	25.40	38.05	13.41	55.1
D4	22.02	25.43	38.10	13.56	55.7
D5	21.97	25.45	38.05	13.65	55.6
E1	21.97	25.43	38.13	13.56	55.5
E2	22.05	25.45	38.13	13.36	54.9
E3	22.10	25.40	38.13	13.36	54.8
E4	22.07	25.40	38.07	13.45	55.7
E5	22.20	25.40	38.05	13.65	55.6
F1	22.00	25.45	38.10	13.51	55.81
F2	22.15	25.35	38.18	13.53	55.58
F3	22.07	25.45	38.13	13.45	56.17

Table 9.7

Fracture Toughness Specimen Dimensions.

Sample	F max (KN)	F ave (KN)	P	1 + P	$\frac{[1 + P]^{\frac{1}{2}}}{[1 - P]}$
A1	6.640	6.195	0.22	1.22	1.25
A2	6.390	6.066	0.23	1.23	1.26
A3	7.158	6.794	0.17	1.17	1.19
A4	8.007	7.643	0.24	1.24	1.28
A5	7.037	6.673	0.22	1.22	1.25
B1	6.390	6.147	0.32	1.32	1.39
B2	7.117	6.996	0.38	1.38	1.49
B3	7.562	7.077	0.31	1.31	1.38
B4	7.360	7.117	0.33	1.33	1.41
B5	6.875	6.673	0.35	1.35	1.44
C1	6.390	6.106	0.18	1.18	1.20
C2	7.481	6.996	0.26	1.26	1.30
C3	7.785	7.026	0.30	1.30	1.36
C4	7.441	7.117	0.26	1.26	1.30
C5	6.632	5.985	0.28	1.28	1.33
D1	6.391	6.133	0.04	1.04	1.04
D2	6.180	6.084	0.06	1.06	1.06
D3	7.207	7.087	0.09	1.09	1.09
D4	5.783	5.662	0.04	1.04	1.04
D5	6.237	6.112	0.03	1.03	1.03
E1	8.007	7.608	0.26	1.26	1.31
E2	7.684	7.279	0.23	1.23	1.27
E3	8.208	7.808	0.14	1.14	1.15
E4	8.594	8.189	0.18	1.18	1.20
E5	7.537	6.834	0.33	1.33	1.41
F1	6.187	5.985	0.09	1.09	1.09
F2	6.228	6.026	0.06	1.06	1.06
F5	6.349	6.026	0.07	1.07	1.07

Table 9.8

Fracture toughness test data.

Sample	Fracture Toughness K_{ICSB} (MNm $^{-3/2}$)	
	Fmax (p=0)	Fmax. p= p^1
A1	33.0	41.2
A2	31.7	40.0
A3	35.6	42.3
A4	39.8	50.9
A5	35.0	43.7
B1	31.7	44.1
B2	35.4	52.7
B3	37.6	57.8
B4	36.6	51.6
B5	34.2	49.2
C1	31.7	38.1
C2	37.2	48.3
C3	38.7	
C4	37.0	48.1
C5	32.9	43.8
D1	31.7	33.0
D2	30.7	32.5
D3	35.8	39.0
D4	28.7	29.9
D5	31.0	31.9
E1	39.8	52.1
E2	38.2	48.5
E3	40.8	46.9
E4	42.7	51.2
E5	37.4	52.8
F1	30.7	33.5
F2	30.9	32.8
F3	31.5	33.7

Table 9.9

Fracture toughness (K_{ICSB}) values

Specimen	Compressive Strength (Nmm^{-2})	
		Average
A	2728	
	2574	2651 ± 77
D	3270	3332 ± 62
	3393	
E	2896	2887 ± 9
	2878	
F	5855	5876 ± 21
	5896	

Table 9.10

Compressive Strength Data.

10.0 Discussion of Results.

10.1 Metallography

10.1.1 As-Cast Microstructure.

The typical as-cast microstructure of the sand cast trial castings has been illustrated in Plate 10.1. The light etched chromium carbide phase was surrounded by an austenitic matrix containing some martensitic transformation products. The effect of the chromium/carbon ratio of the material, approximately 6.5, combined with the molybdenum addition has suppressed a pearlite transformation thereby retaining a metastable austenitic structure. The region of matrix adjacent to the eutectic carbide has undergone a martensitic transformation due to the localised elevation of the Ms temperature resulting from solute segregation.

10.1.2 Conventional Heat Treated Structure.

The microstructures obtained by carrying out the standard hardening process on the 15% chromium alloy, sample casting D, have been illustrated in Plates 10.2 - 10.6. These structures comprised of a light etching chromium carbide phase and a dark etched martensitic matrix containing secondary chromium carbides. During the holding period at 1000°C the secondary chromium carbides have been precipitated from the alloy rich austenitic solid solution thereby permitting the martensitic transformation to occur on subsequent air blasting to room temperature. The density of secondary carbide precipitation within the original primary austenite dendrites appears to have been greater at the centre of the dentrites, remote from the carbide phase. The finer matrix structure contained significantly less precipitate and therefore less transformation product. These observations are consistent with the reports by Maratray (218) and Dupin (215) who have noted the initiation of precipitation at dentrite centres and the segregation of carbon and chromium.

Plate 10.1

As-cast 15% chromium, 2% carbon, 2% molybdenum alloy.

All optical photomicrographs X 175 unless otherwise stated. Samples etched for 20 seconds in saturated Picral solution acidified with concentrated HCL.

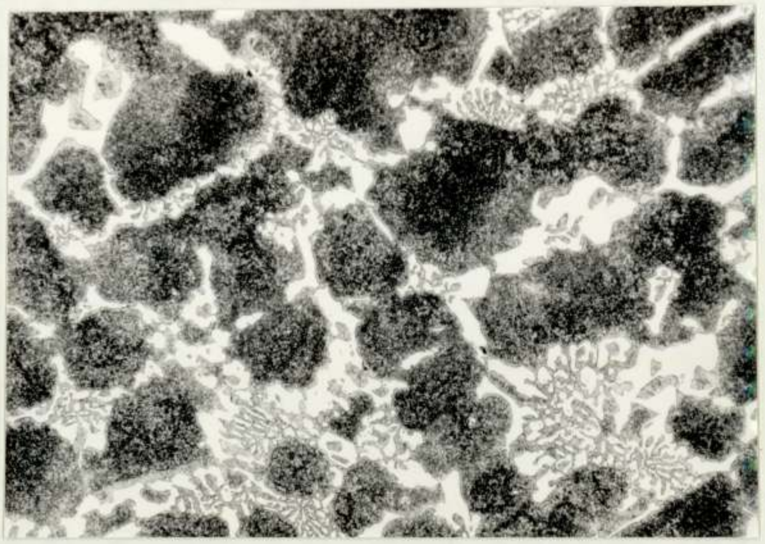

Plate 10.2

Conventionally hardened 15% chromium alloy, D.1

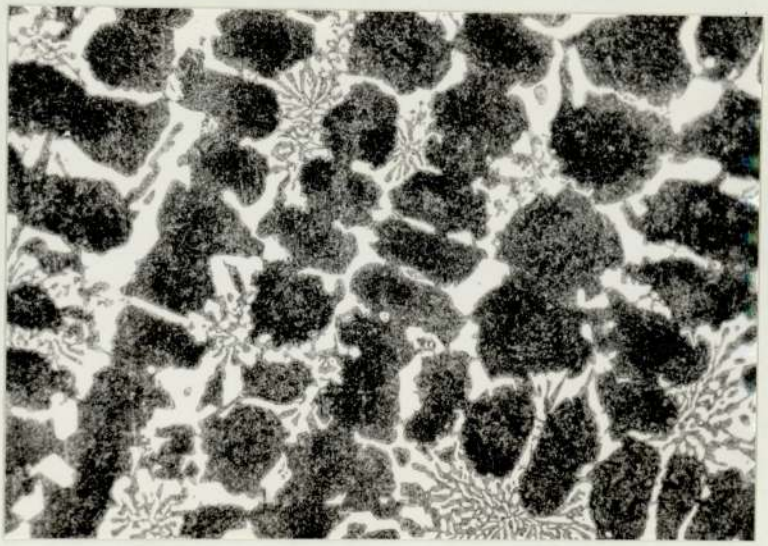

Plate 10.3

Conventionally hardened 15% chromium alloy, D.2.

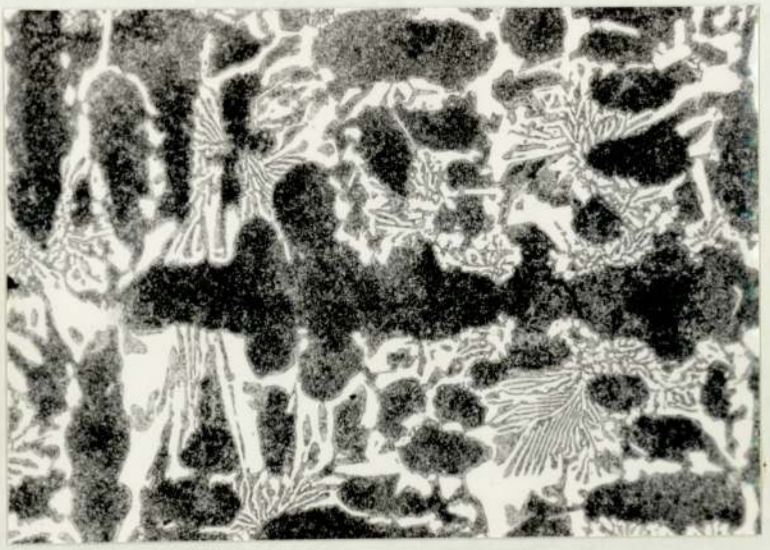

Plate 10.4

Conventionally hardened 15% chromium alloy, D.3

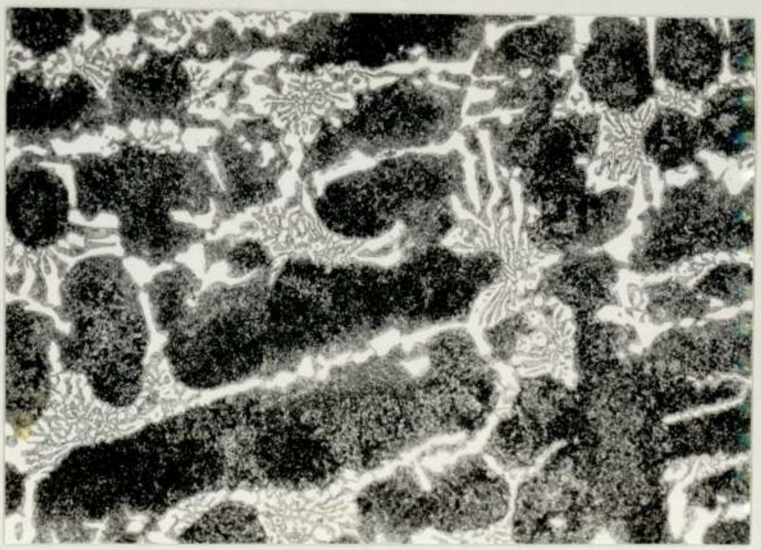

Plate 10.5

Conventionally hardened 15% chromium alloy. D.4

Plate 10.6

Conventionally hardened 15% chromium alloy, D.5

The microstructure of the failed 20% chromium material, casting F, has been shown in Plates 10.7 - 10.9. Again these structures consisted of a chromium carbide phase and a matrix consisting of martensite and secondary chromium carbides. The carbide precipitation has been less uniform than in casting D and some areas of matrix adjacent to the eutectic carbides were devoid of precipitates.

10.1.3 High Temperature Heat Treated Structures.

The metallographic structures of the three castings subjected to the 1180°C spheroidising treatment, (castings A, B and C) are shown in Plates 10.10 - 10.24. The matrix phase is essentially austenitic although some carbide precipitation is present towards the centre of the dentrites. There has been no detectable martensitic transformation. The chromium carbide appears to have become less continuous and less angular compared with Plates 10.2 - 10.6. The carbides precipitated during the destabilising treatment range of 950°C - 1050°C have coarsened and commenced to redissolve into the austenite. Quenching to ambient temperature has retained the metastable austenitic structure.

The microstructures of casting E after 16 months service are illustrated in Plates 10.25 - 10.29. As with the previous castings the structures consisted of a modified chromium carbide network and a metastable austenitic structure. There was no evidence of martensitic transformation products within the matrix.

All castings exhibited some microporosity and non metallic inclusions, although these features were not excessive and considered as normal for any commercially produced castings.

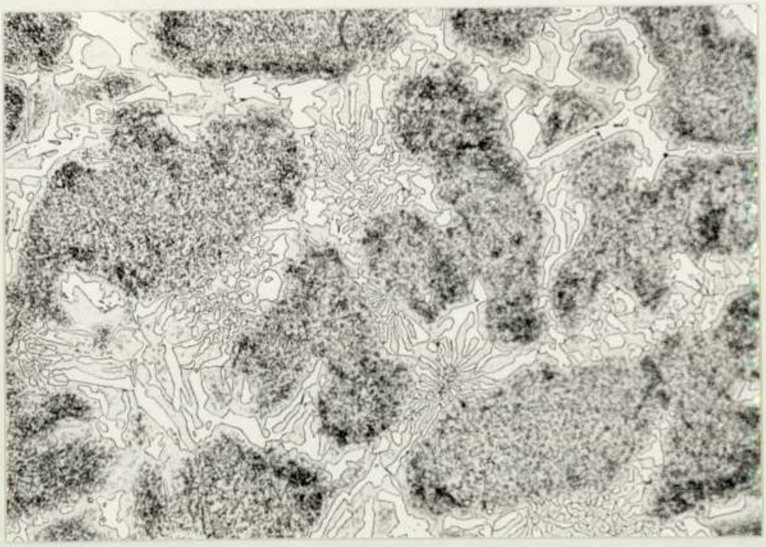

Plate 10.7

Conventionally hardened 20% chromium alloy, F.1

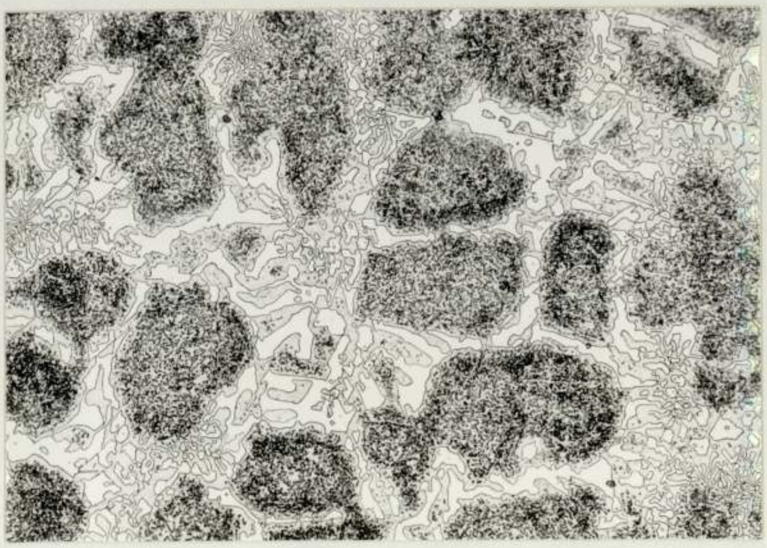

Plate 10.8

Conventionally hardened 20% chromium alloy, F.2

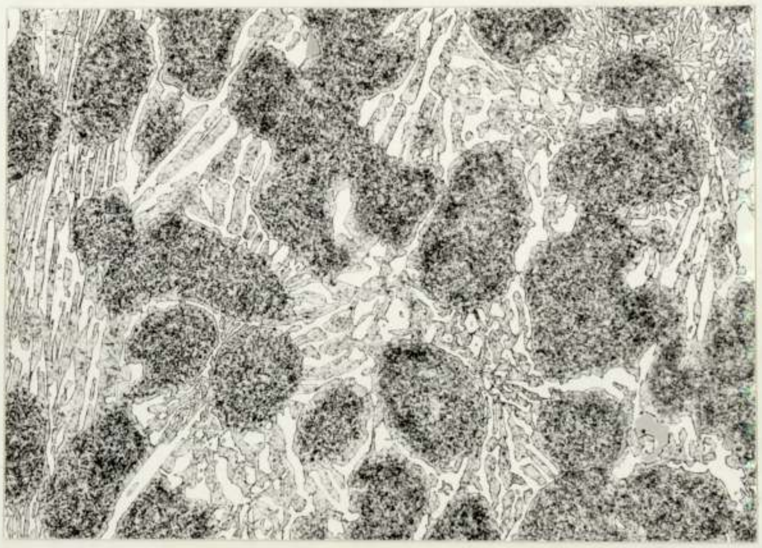

Plate 10.9

Conventionally hardened 20% chromium alloy, F.5

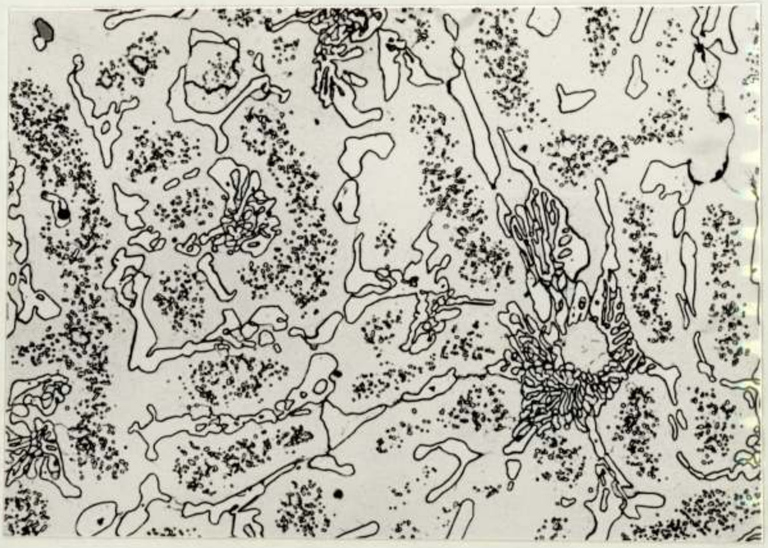

Plate 10.10

Vacuum processed 15% chromium alloy, A.1

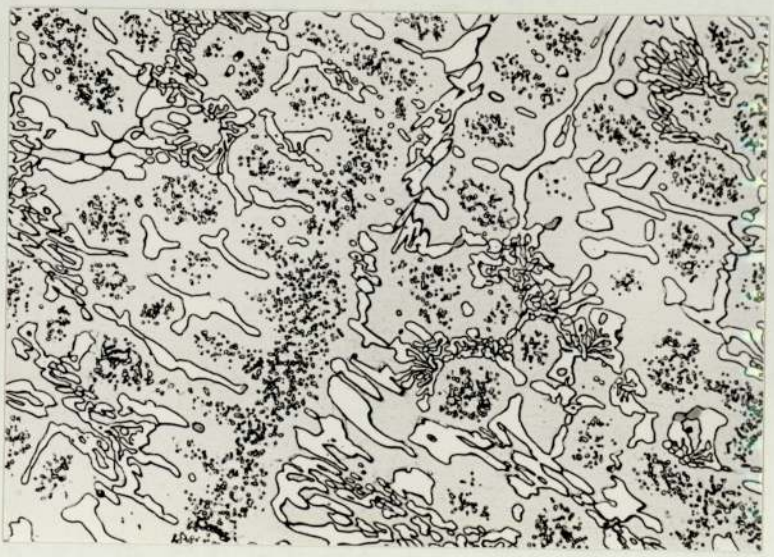

Plate 10.11

Vacuum processed 15% chromium alloy, A.2

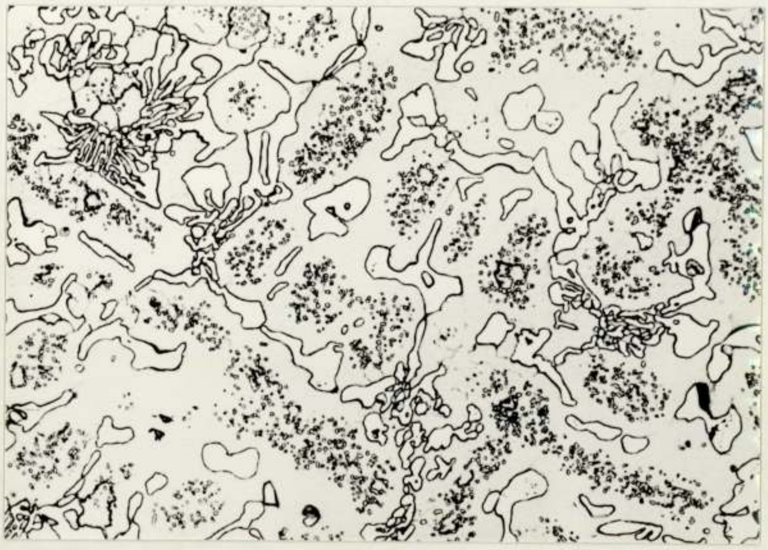

Plate 10.12

Vacuum processed 15% chromium alloy, A.3

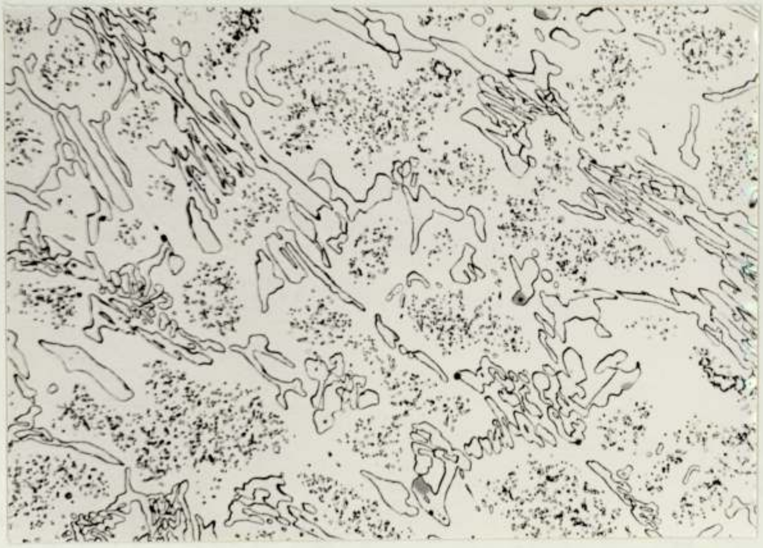

Plate 10.13

Vacuum processed 15% chromium alloy, A.4

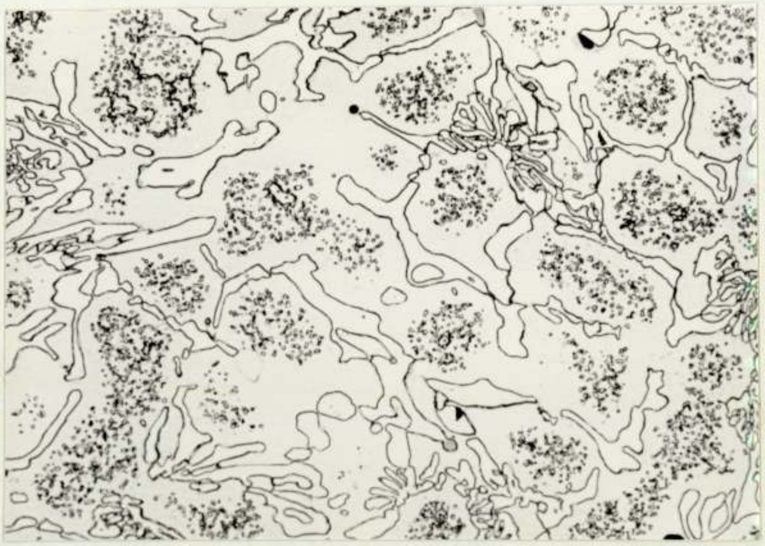

Plate 10.14
Vacuum processed 15% chromium alloy, A.5

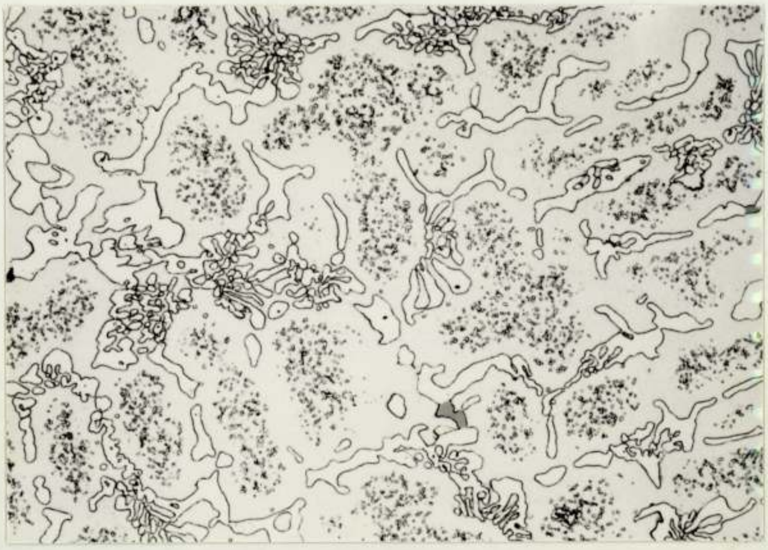

Plate 10.15

Vacuum processed 15% chromium alloy. B.1.

Plate 10.16

Vacuum processed 15% chromium alloy, B.2

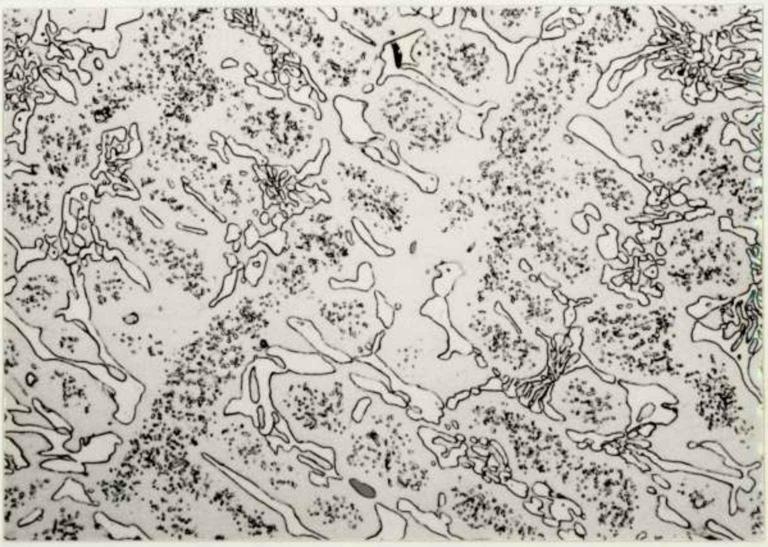

Plate 10.17

Vacuum processed 15% chromium alloy, B.3

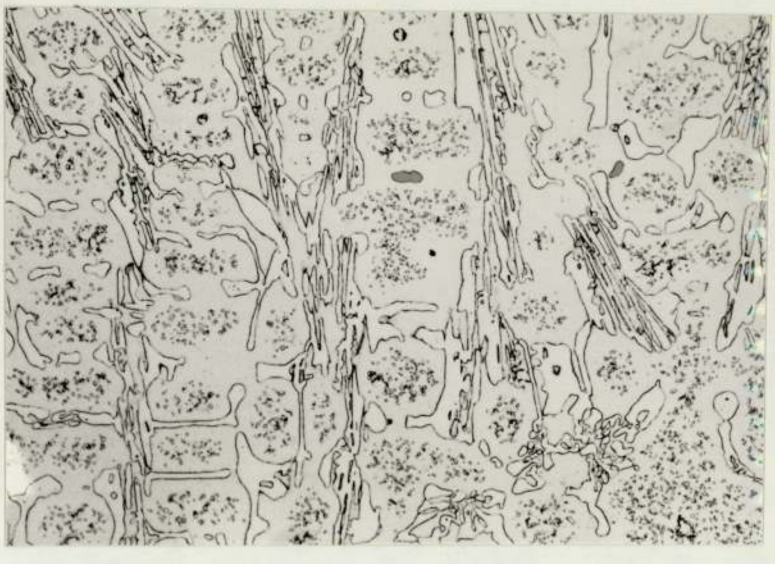

Plate 10.18

Vacuum processed 15% chromium alloy, B.4

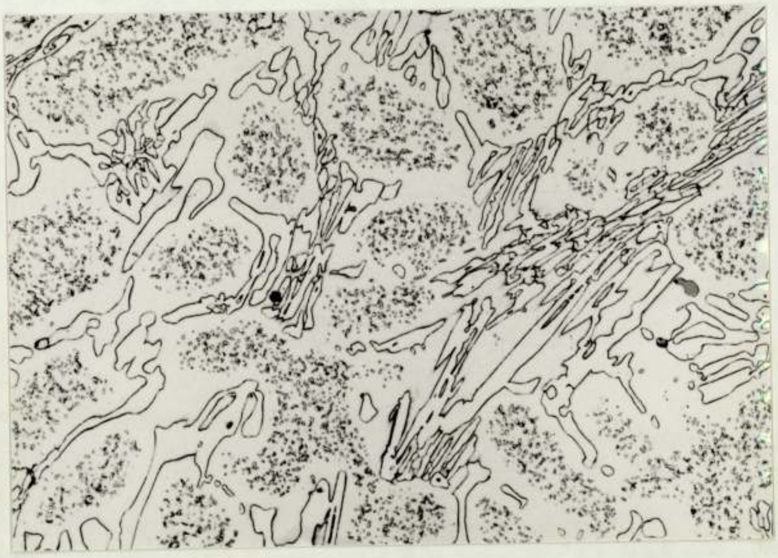

Plate 10.19

Vacuum processed 15% chromium alloy, B.5

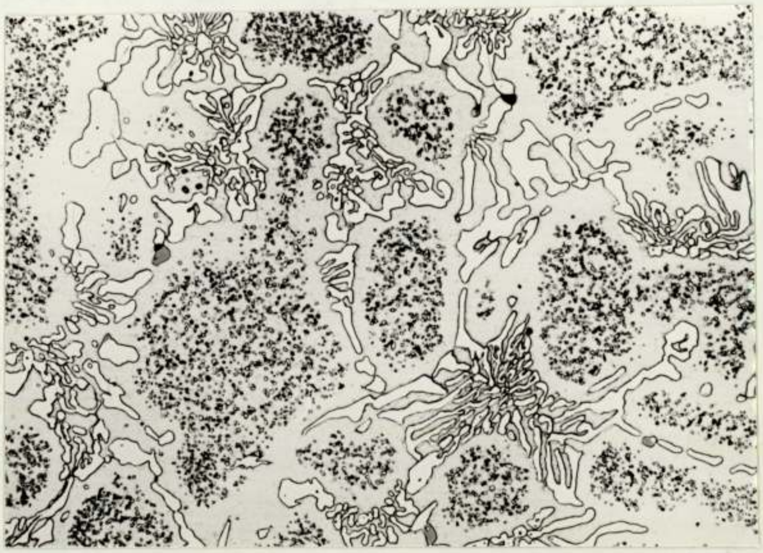

Plate 10.20

Vacuum processed 15% chromium alloy, C.1

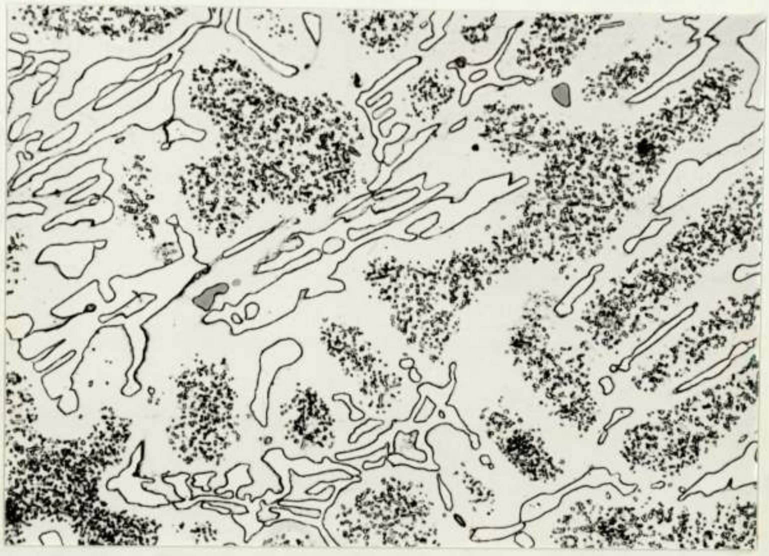

Plate 10.21

Vacuum processed 15% chromium alloy, C.2

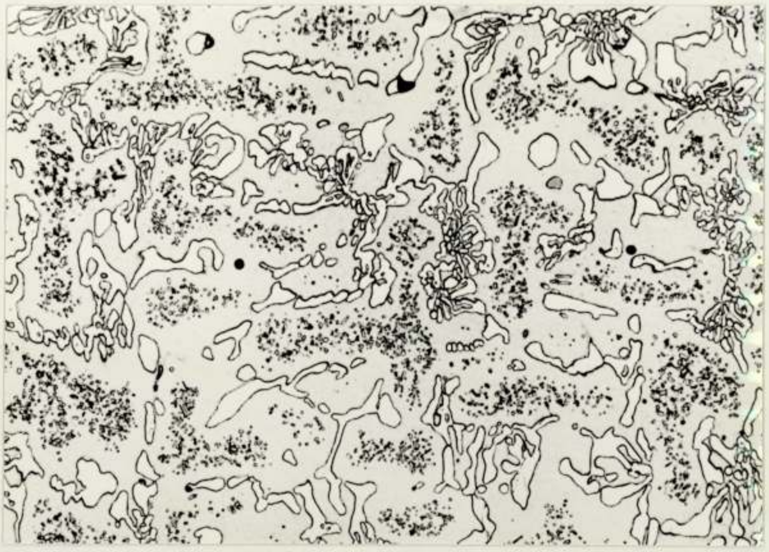

Plate 10.22

Vacuum processed 15% chromium alloy C.3

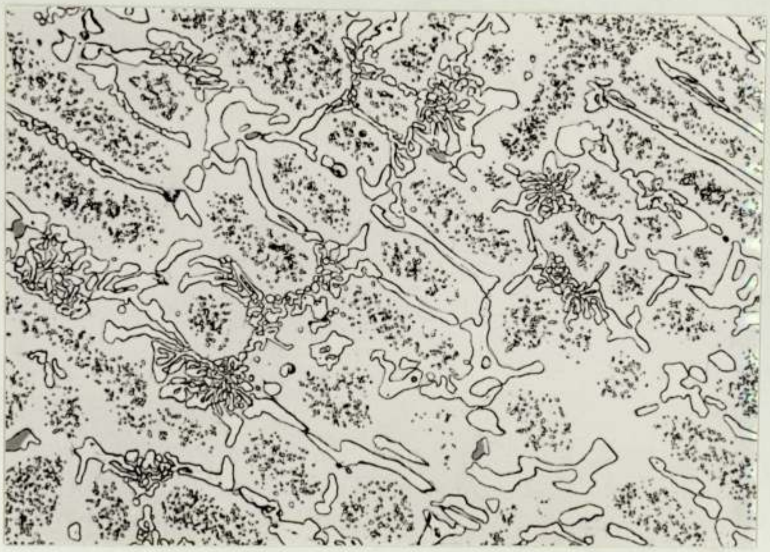

Plate 10.23

Vacuum processed 15% chromium alloy, C.4

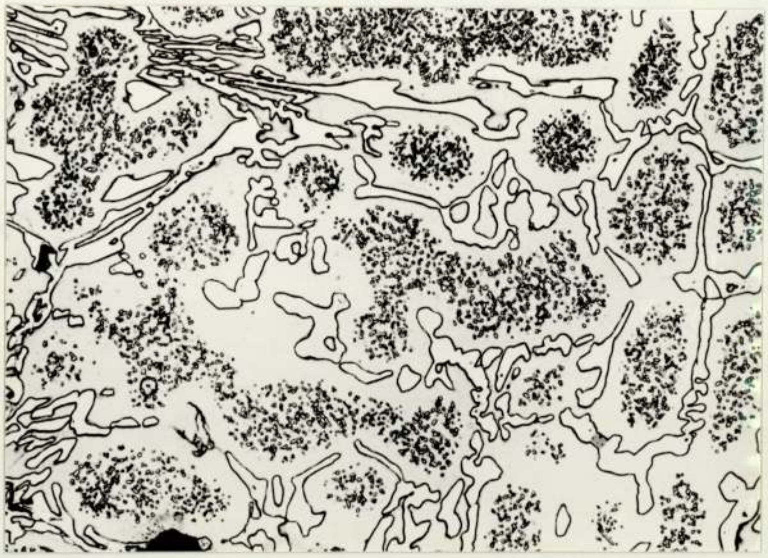

Plate 10.24

Vacuum processed 15% chromium alloy, C.5

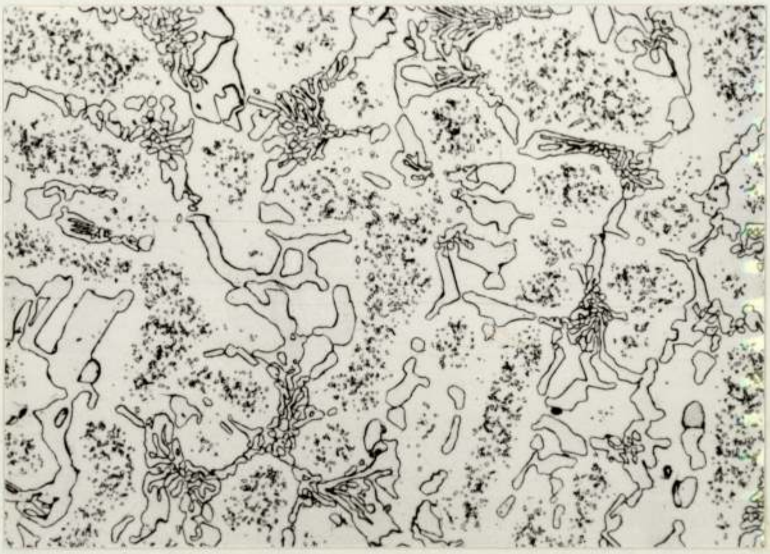

Plate 10.25

Vacuum processed 15% chromium alloy after
16 months service, E.1.

Plate 10.26

Vacuum processed 15% chromium alloy after
16 months service, E.2

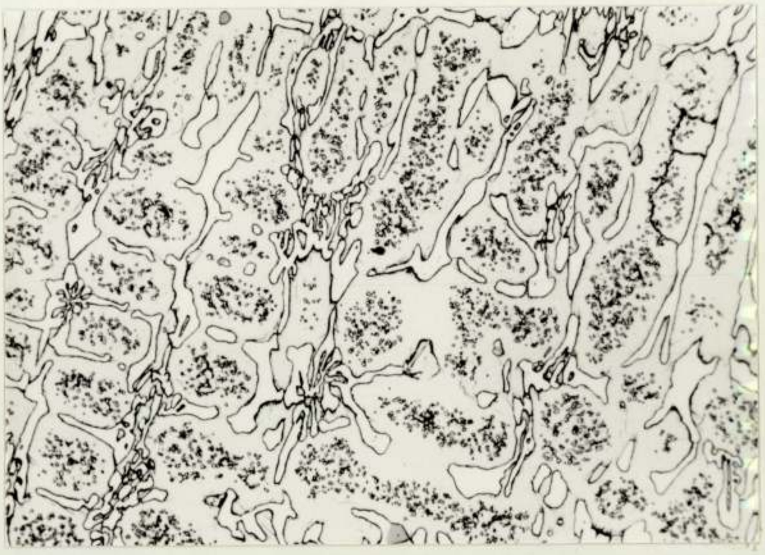

Plate 10.27

Vacuum processed 15% chromium alloy after
16 months service, E.3

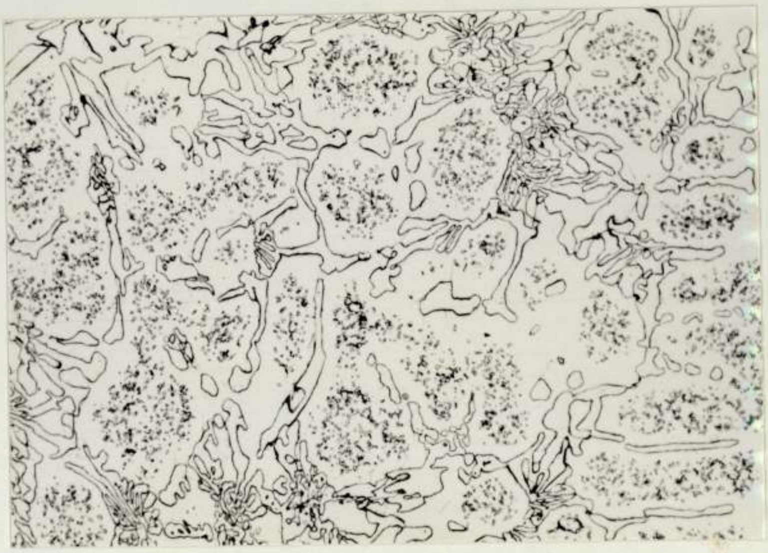

Plate 10.28

Vacuum process 15% chromium alloy after
16 months service, E.4

Plate 10.29

Vacuum processed 15% chromium alloy after
16 months service, E.5

10.1.4 Subcritical Heat Treated Structures.

The structures produced during the subcritical heat treatment exercise are shown in Plates 10.30 - 10.39. At treatment temperatures up to 508°C no transformations had taken place and the microstructures remained as standard high temperature structures comparable with Plates 10.10 - 10.24. The specimen processed at 550°C began to exhibit some transformation of the matrix in isolated areas adjacent to the eutectic carbides. The transformation was probably occurring in areas of localised low Cr/C ratio material which was more responsive to decomposition than the remaining austenite. A temperature of 603°C has resulted in a significant amount of transformation although some areas clearly remained unaffected by the thermal treatment. At 652°C the entire matrix appears to have transformed but there was some suggestion of a pearlitic transformation product at the centre of matrix dendrites. The secondary carbide precipitation observed on other specimens subjected to the high temperature treatment can still be observed. Processing at 710°C has homogenised the extent of the pearlitic transformation.

The microstructures obtained by quenching a sample of casting A directly into liquid nitrogen can be seen in Plates 10.38 and 10.39. The acicular products of a martensitic transformation were clearly evident and emphasised the fact that Plates 10.10 - 10.24 illustrated a metastable austenite constituent.

10.1.5 Carbide Morphology.

The matrix leeching exercise provided a technique which enabled the examination of the three dimensional carbide network. The carbide morphology of sample F, the failed, conventionally alloyed and processed 20% chromium alloy, can be seen in Plates 10.40 - 10.41. The carbides

Plate 10.30

Subcritically heat treated at 211°C for 24 hours.

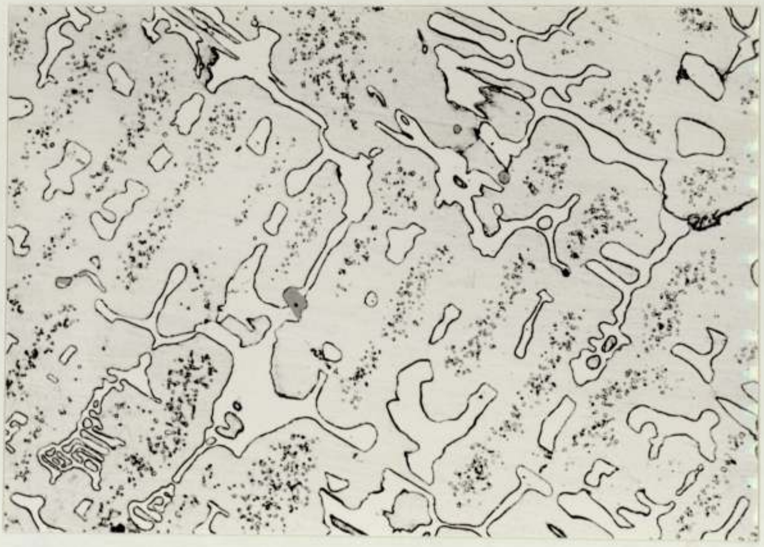

Plate 10.31

Subcritically heat treated at 327°C for 24 hours.

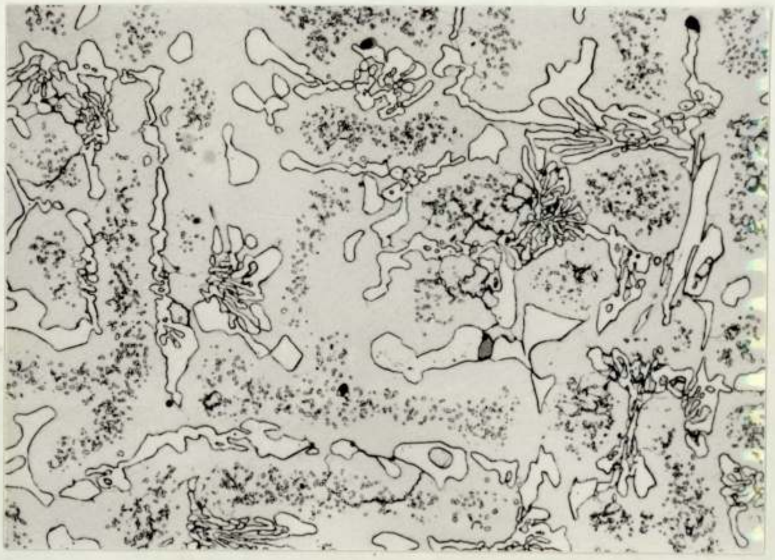

Plate 10.32

Subcritically heat treated at 404°C for 24 hours.

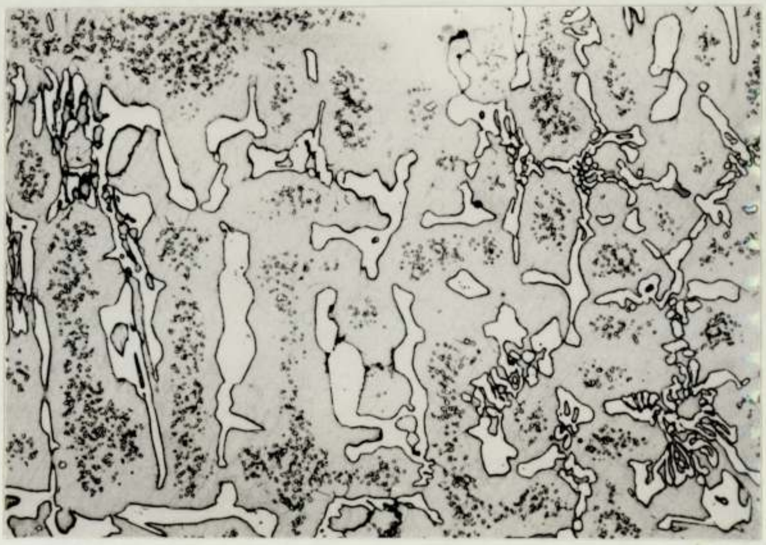

Plate 10.33

Subcritically heat treated at 508°C for 24 hours.

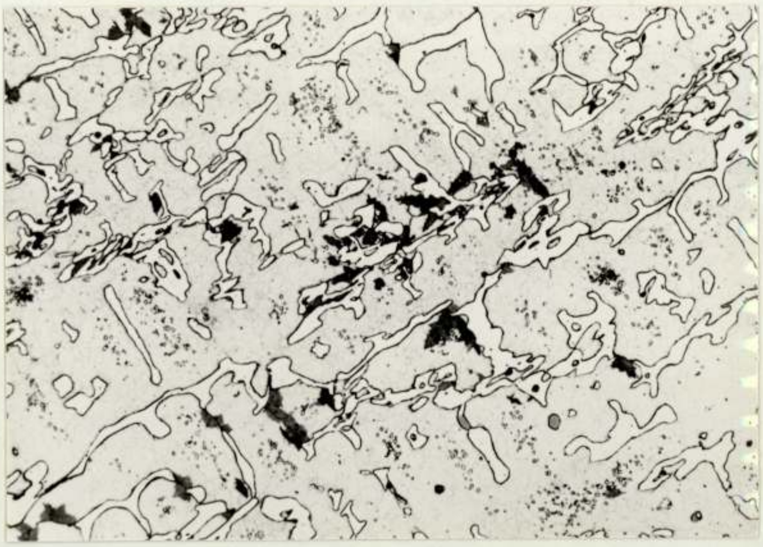

Plate 10.34

Subcritically heat treated at 550°C for 24 hours.

Plate 10.35

Subcritically heat treated at 603°C for 24 hours.

Plate 10.36

Subcritically heat treated at 652°C for 24 hours.

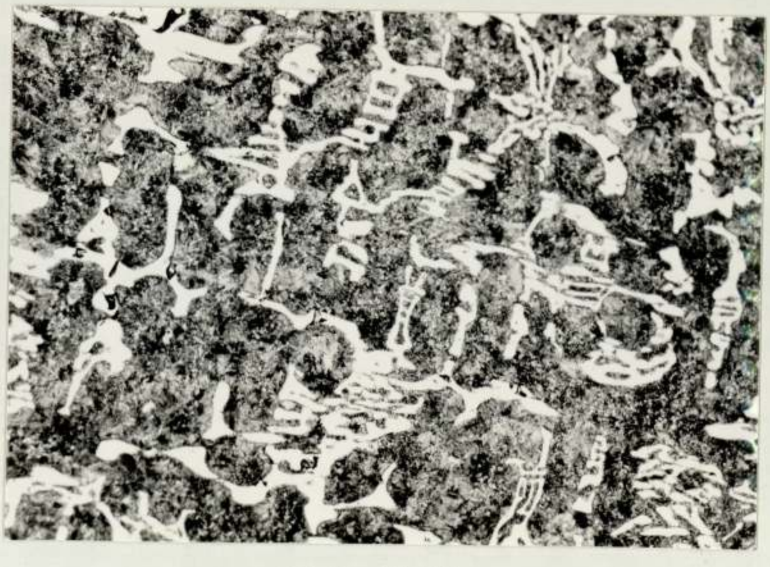

Plate 10.37

Subcritically heat treated at 710°C for 24 hours.

Plate 10.38

Subzero treated in liquid nitrogen.

Plate 10.39

Subzero treated in liquid nitrogen.

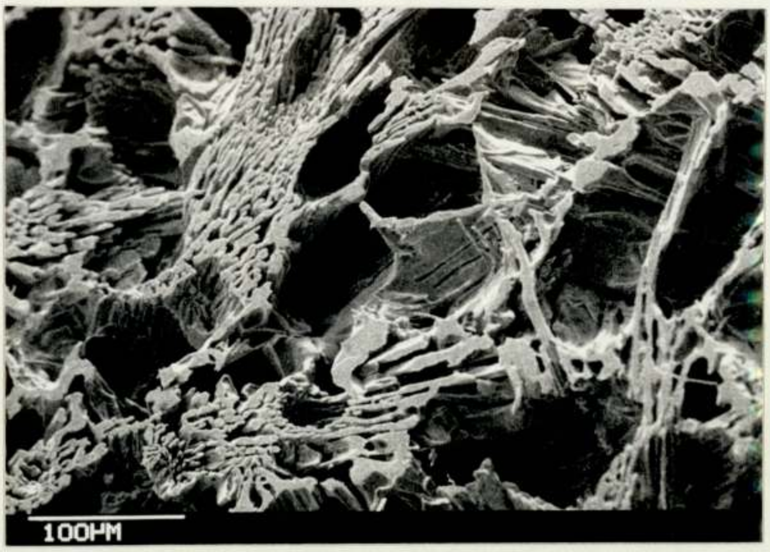

Plate 10.40

Eutectic carbide morphology in matrix leeched casting F.

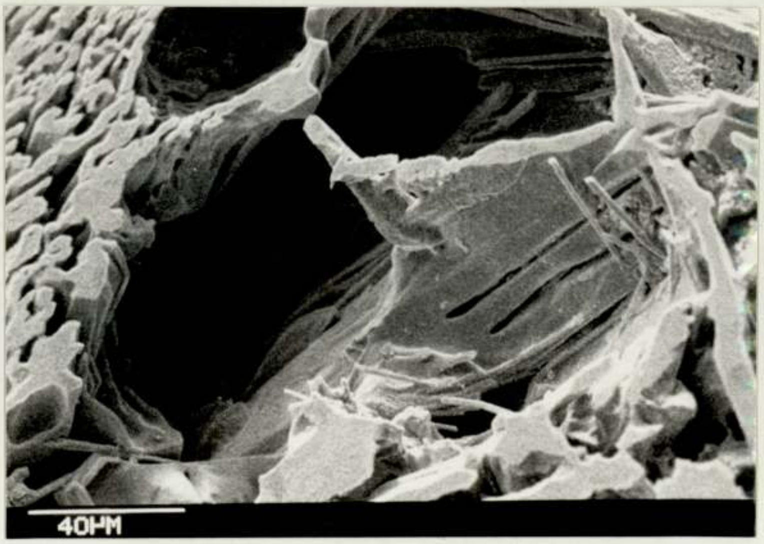

Plate 10.41

Eutectic carbide morphology in matrix leeched casting F.

clearly formed an interconnected network and comprised of individual rods and blades (i.e. multiple rods joined together.) (185) The carbides generally exhibited an angular appearance. A similar form of carbide was observed in casting D, Plates 10.42 - 10.43. Both of these specimens had received a conventional hardening treatment during which the eutectic carbide remained unaffected. The modification of the carbide morphology resulting from the high temperature treatment was apparent in Plates 10.44 - 10.45. There has been a significant loss of angularity as the carbide has adopted a more curved and reounded profile. The eutectic arbide clusters visible as radiating lamella in Plate 10.44 seem to have responded less than the larger interdendritic carbide to the modification treatment.

One further aspect of the matrix leeching exercise was evident from Plates 10.46 - 10.47. The specimen from casting C had received an incomplete leeching operation but as a result the morphology of the secondary carbides within the austenitic matrix became visible. It was clear that these carbides existed as rods approximately 1μm in diameter and in excess of 5μm in length. As with specimen C in Plates 10.44 - 10.45 the modification to the eutectic carbides was again apparent.

10.1.6 Differentially Etched Structures.

The use of a potassium permanganate/sodium hydroxide etchant was used in an attempt to differentiate between M_7C_3 carbides (unattacked) and $M_{23}C_6$ (coloured light brown/orange.) (271.) Plate 10.48 illustrates the etched structure of specimen F which revealed an etched outer carbide shell and an unetched inner core. This observation was consistent with the work of Pearce (272) who reported an insitu solid state transformation of the form $M_7C_3 \rightarrow M_{23}C_6$ in a 30% chromium iron.

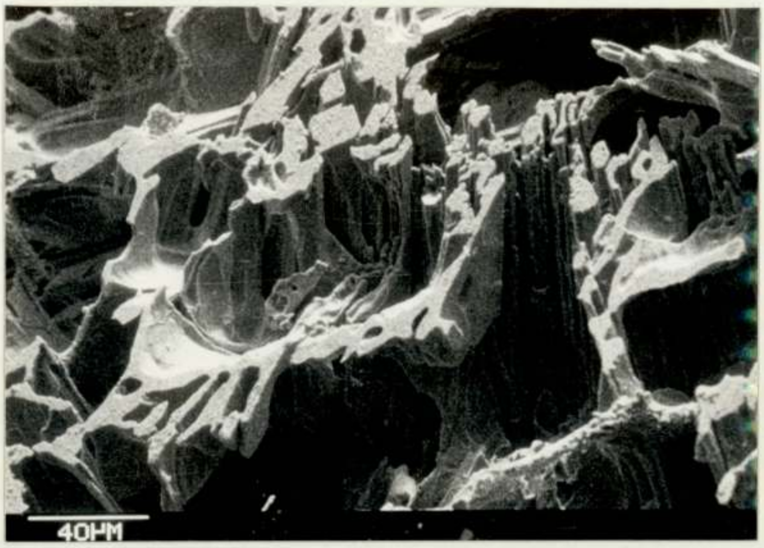

Plate 10.42

Eutectic carbide morphology in matrix leeched casting D.

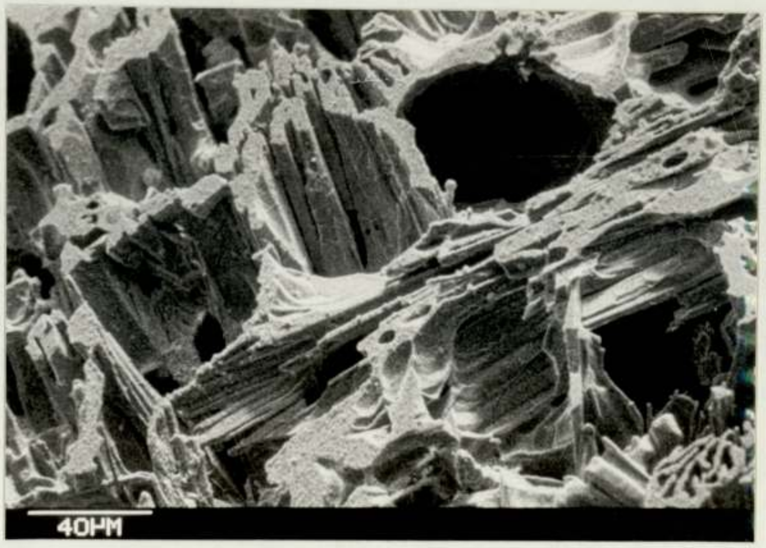

Plate 10.43

Eutectic carbide morphology in matrix leeched casting D.

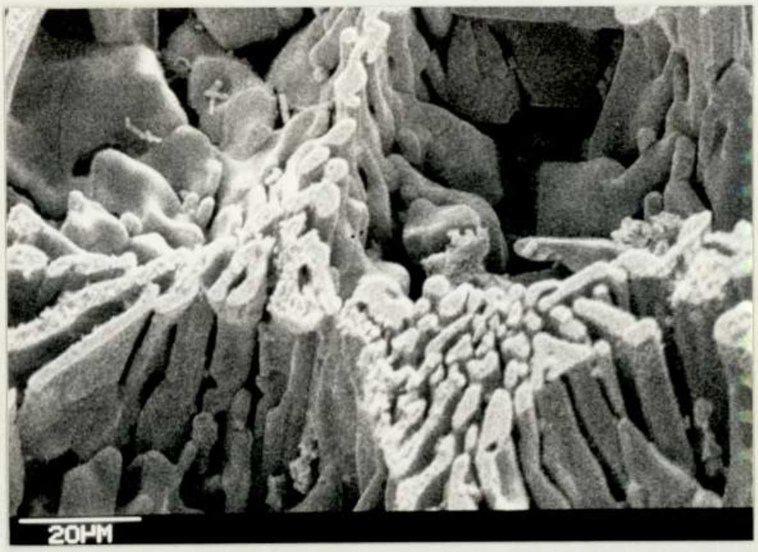

Plate 10.44

Eutectic carbide morphology in matrix leeched casting C.

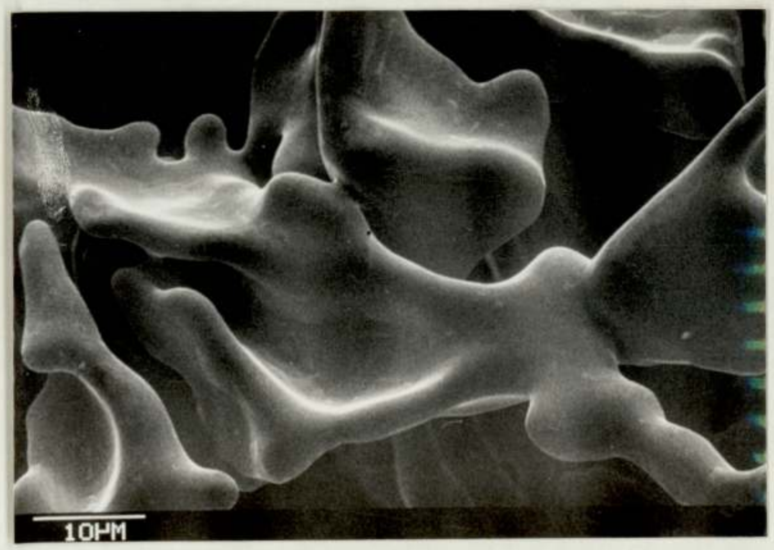

Plate 10.45

Eutectic carbide morphology in matrix leeched casting C.

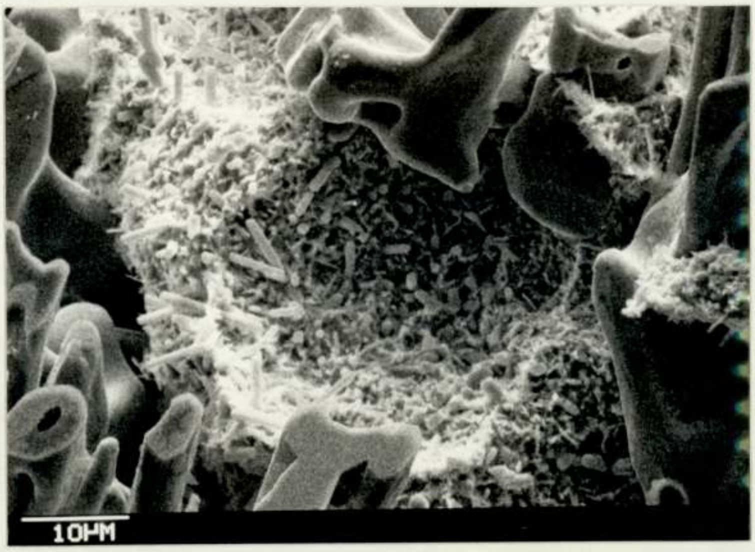

Plate 10.46

Incomplete matrix leeching in casting B.

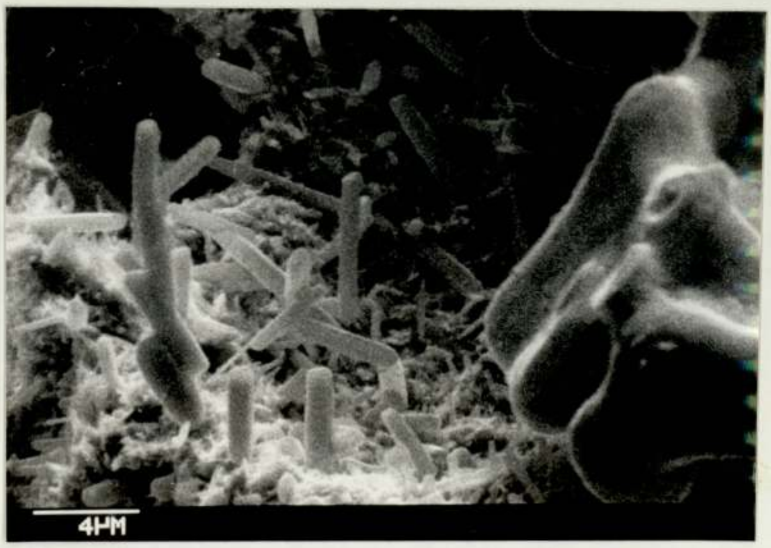

Plate 10.47

Incomplete matrix leeching in casting B.

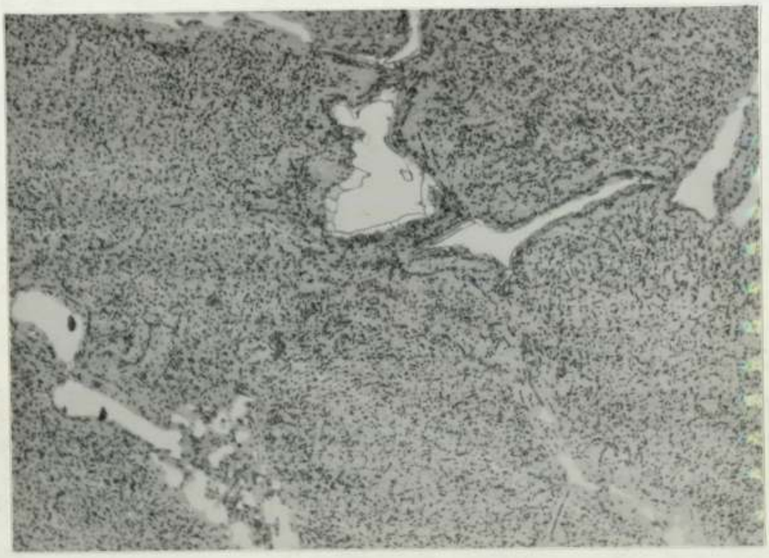

Plate 10.48

Differentially etched specimen F.

Plate 10.49

Differentially etched specimen C.

A similar etching technique applied to the high temperature, vacuum processed material has been illustrated in Plate 10.49. Again a duplex carbide can be identified but the transformation mechanism was clearly different to that observed in the conventional alloy. Figure 10.1 (a) and (b) illustrates these observations schematically. Transformation modeshave been suggested by Inoue et al (273) as being representative of the M_7C_3 - $M_{23}C_6$ and $M_{23}C_6$ - M_6C_3 reactions respectively. It was reported that in the reaction M_7C_3 - $M_{23}C_6$ the $M_{23}C_6$ - first nucleated over the entire matrix/M_7C_3 interface and growth proceeded towards the M_7C_3. Conversely, for $M_{23}C_6$ - M_6C the M_6C nucleated on the $M_{23}C_6$/ matrix interface and inside the $M_{23}C_6$. It was believed that the intercarbide nucleation may have been due to preferred precipitation on planes or faults existing in $M_{23}C_6$.

While the presence of an $M_{23}C_6$ - M_6C reaction in this study is inconsistent with the observed etch effects it is possible that the nucleation mechanism of the M_7C_3 - $M_{23}C_6$ reaction changed with temperature.

10.1.7 Quantitative Metallography.

The results of the qualitative metallographic exercise did not illustrate microstructural variation consistent with sample position. However, there was some indication that specimens produced from location 3 generally exhibited less variation than from any other specimen position. A feature evident from Figure 10.2(a)was the reduced carbide size of casting F (failed 20% chromium) compared with the other castings examined.

The relationship between intercarbide spacing and carbide size has been shown in Figure 10.2 (a).The straight line relationship between these two parameters is expected to be applicable for a constant volume fraction of carbide phase. This relationship also approximated for the results of Biner (165) who investigated materials of similar chemical composition

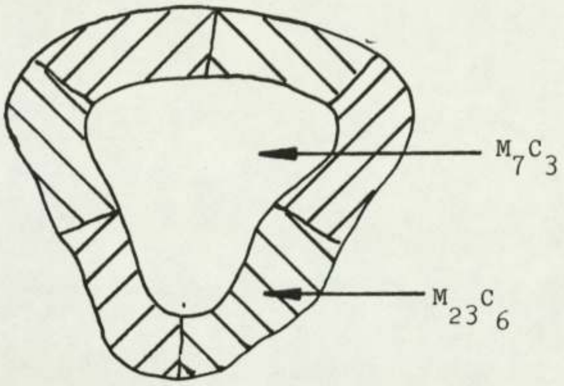

10.1 (a)

Schematic illustration of duplex carbide in sample F (conventional 20% chromium.)

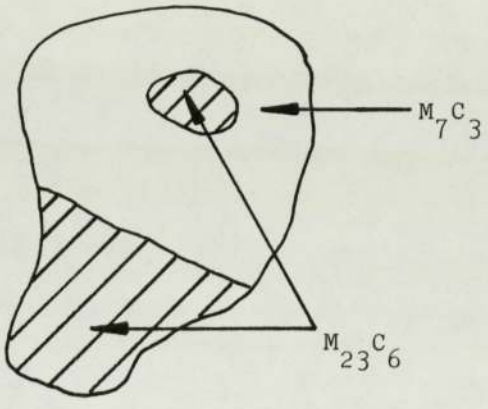

10.1 (b)

Schematic illustration of duplex carbide in sample C (high temperature processed 15% chromium.)

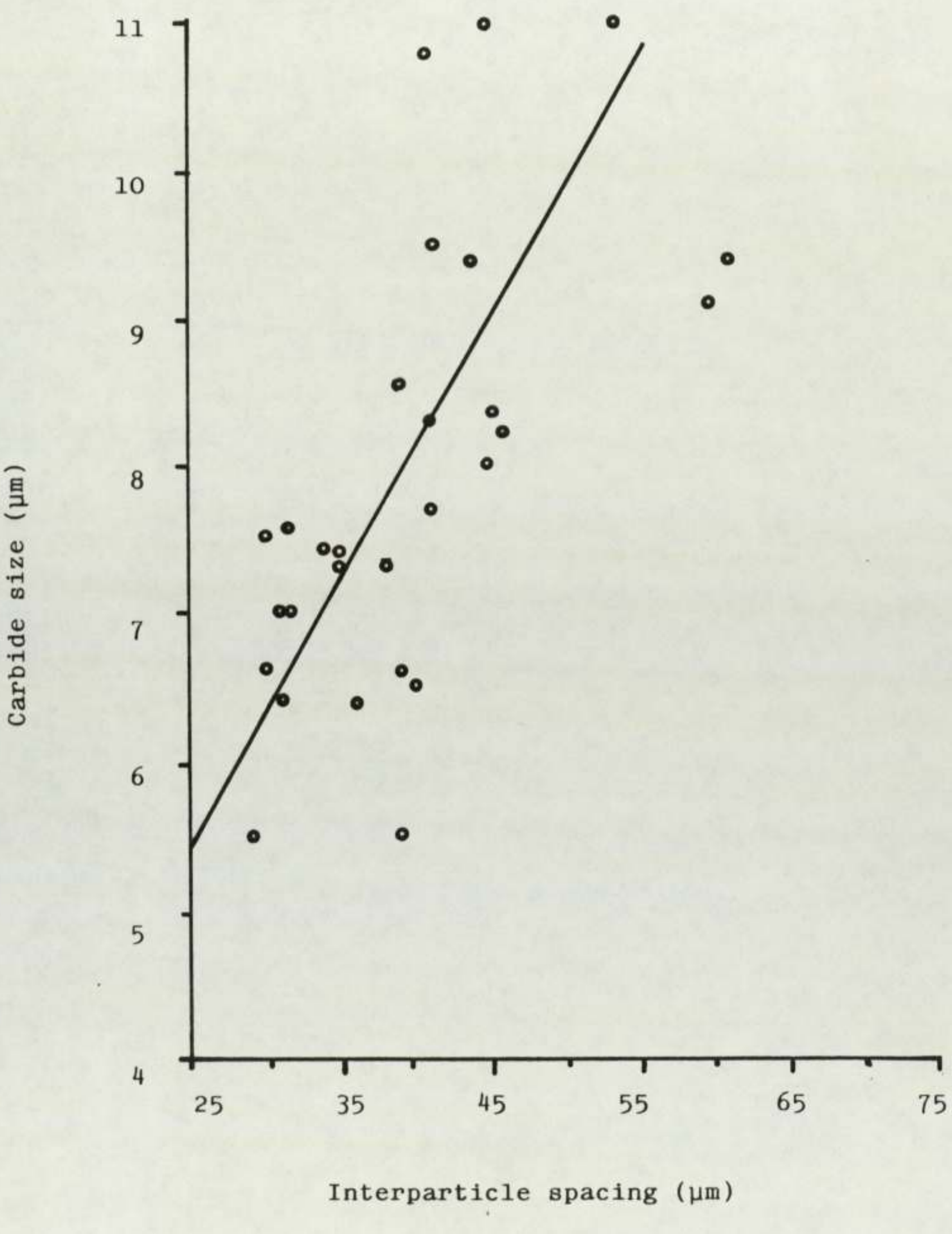

Figure 10.2 (a)

Relationship between carbide size and interparticle spacing.

but different section sizes. Hence, both matrix and carbide phase experienced a similar degree of structural refinement when cast in various section sizes.

The relationship between interparticle spacing and density has been shown in Figure 10.2 (b) the increase in interparticle spacing with decreasing density being consistent with reasoning.

10.2 Hardness.

10.2.1 Hardness of Castings.

The general level of hardness exhibited by the vacuum treated castings was typically within the range Hv30 400 - 450. The hardness of the conventionally treated martensitic material was significantly higher than this value being of the order of Hv30 730 - 740 and HV30 750 - 810 for castings F and D respectively. The hardness values obtained from the five locations identified in Figure 6.3 have been illustrated graphically in Figure 10.3 (a.), for clarity the individual hardness ranges have been omitted from this diagram but included in Figure 10.3 (b). The most apparent feature of the results for the three unused castings, A, B and C, was the wider variation in hardness at position 5, compared with other specimen locations, no specific trend in hardness was otherwise evident.

10.2.2 Microhardness of Matrix Phase.

The microhardness of the matrix, Table 9.3, reflected the variation in macrohardness discussed above. Whereas the difference between micro and macrohardness values for austenitic material varied between 6 and 68 the difference for the martensitic structure was 30 - 53. Thus suggesting that the martensitic matrix was more homogeneous than the austenitic matrix. This was confirmed by microstructural examination which revealed areas of hard secondary chromium carbides within the austenite.

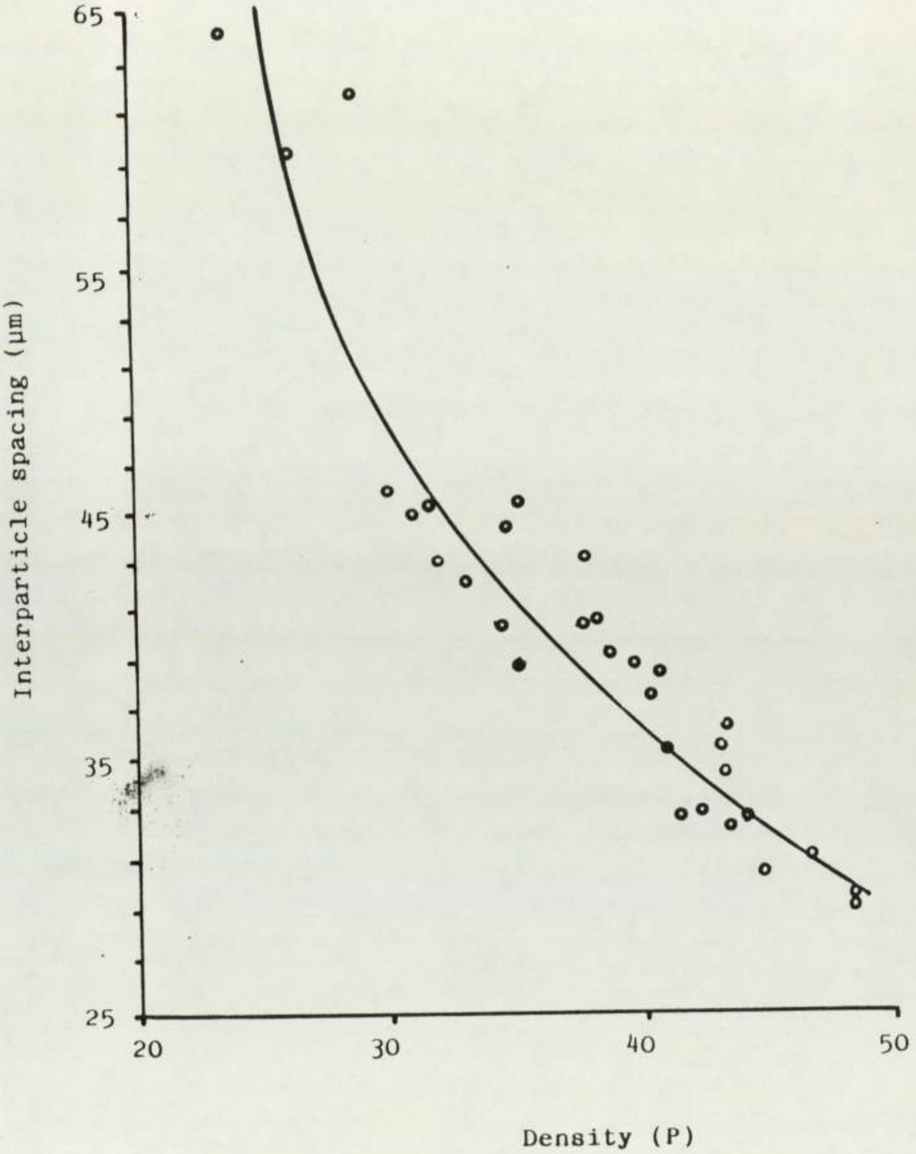

Figure 10.2(b)

Relationship between interparticle spacing and particle density.

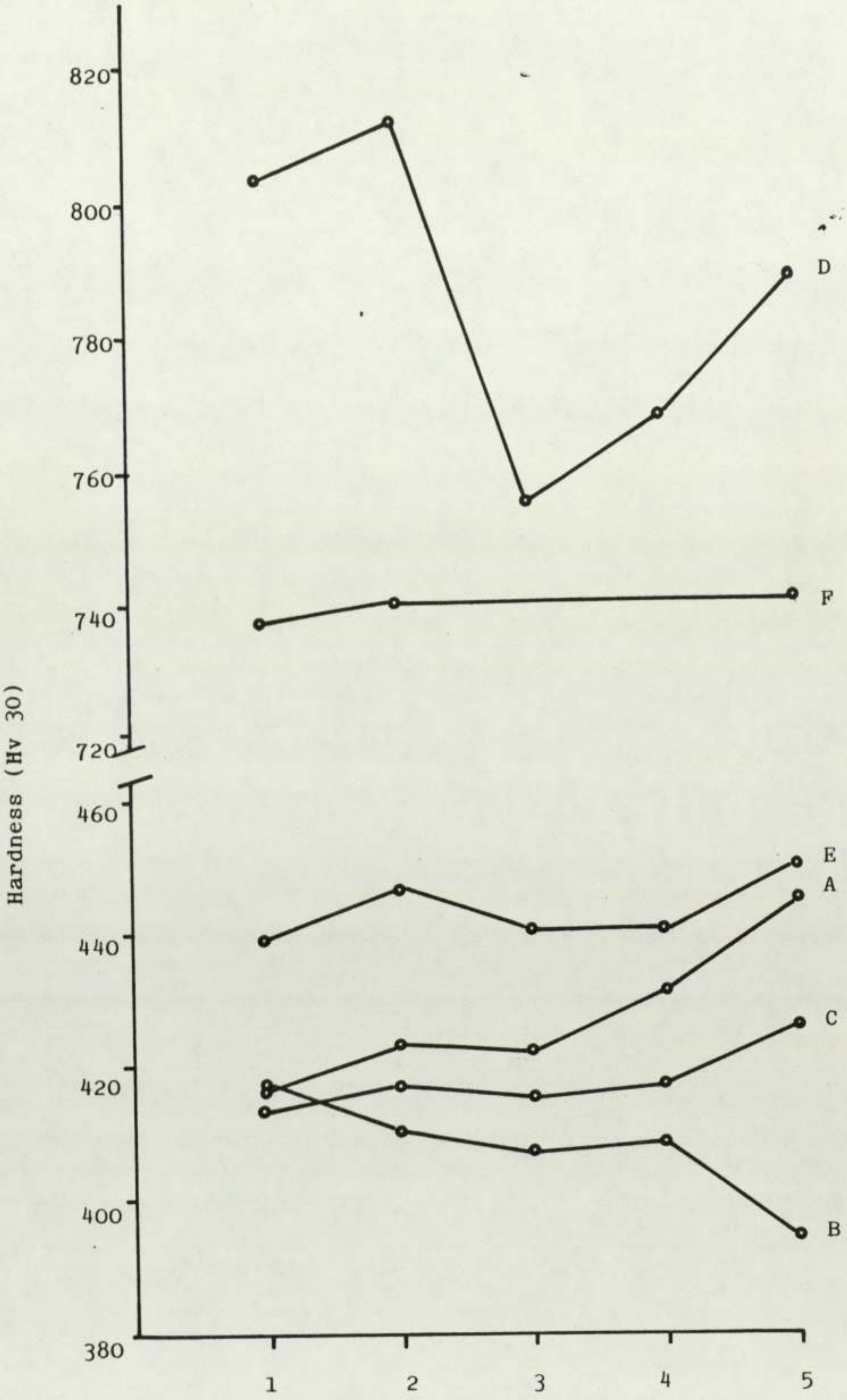

Figure 3 (a)

Hardness variation with sample position.

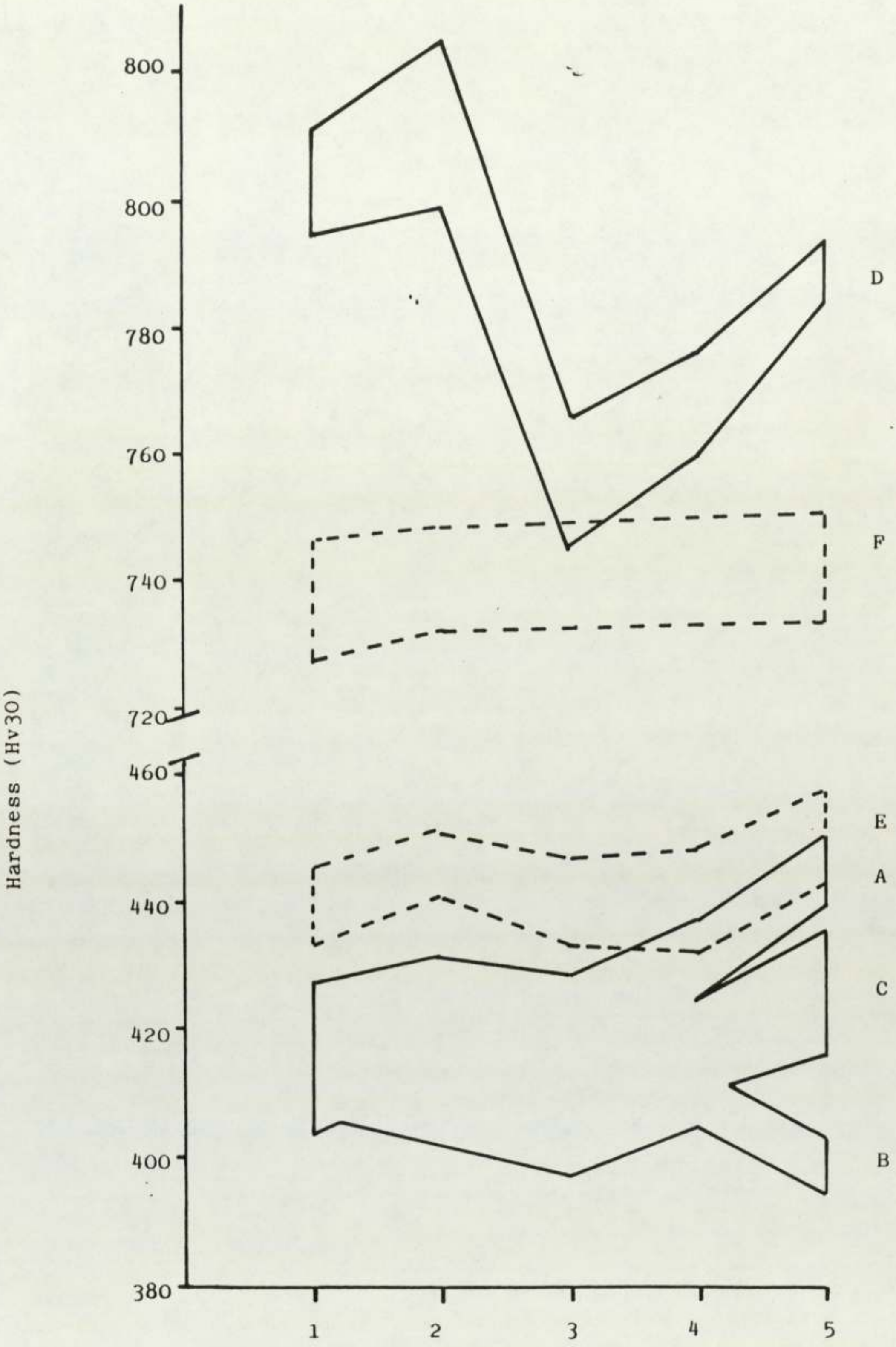

Figure 10.3 (b)

Hardness range against sample position.

10.2.3 Microhardness of eutectic carbides.

The average microhardness of the eutectic carbide was Hv1642 which was in agreement with other published works, see for example Table 1.1. No significant variation in carbide hardness was evident between the castings although subtle differences due perhaps to changes in carbide chemistry may have been masked by the inherent scatter of micro hardness results. (274) The high carbide hardness confirms one of the principle reasons for the abrasion resistance of high chromium cast irons.

10.2.4 Hardness Measurements of subcritical heat treated specimens.

The hardness of samples subjected to the subcritical heat treatment has been illustrated in Figure 10.4. The gradual increase in hardness up to treatment temperatures of 550°C reflected the decomposition of the relatively soft austenite to a harder transformation product, probably bainitic in nature. Similarly, the rapid increase in hardness that occurred between 550°C and 603°C can be explained by consideration of the extent of transformation within this temperature range. As the treatment temperature increased above 603°C there was a rapid decrease in material hardness, approximately Hv 10 per 10°C. The presence of an increasing amount of soft pearlitic transformation product could account for this reduction from peak hardness. A similar hardness trend has been reported by Parks (230) who investigated the subcritical transformation behaviour of a chromium iron. Parks suggested that if adequate mechanical properties could be achieved without the need for an expensive high temperature destabilising treatment then energy cost savings would result. Furthermore it was reported that less complex production techniques could be utilised for the production of large, intricate castings which may normally have shown a tendency to crack during the high temperature treatment.

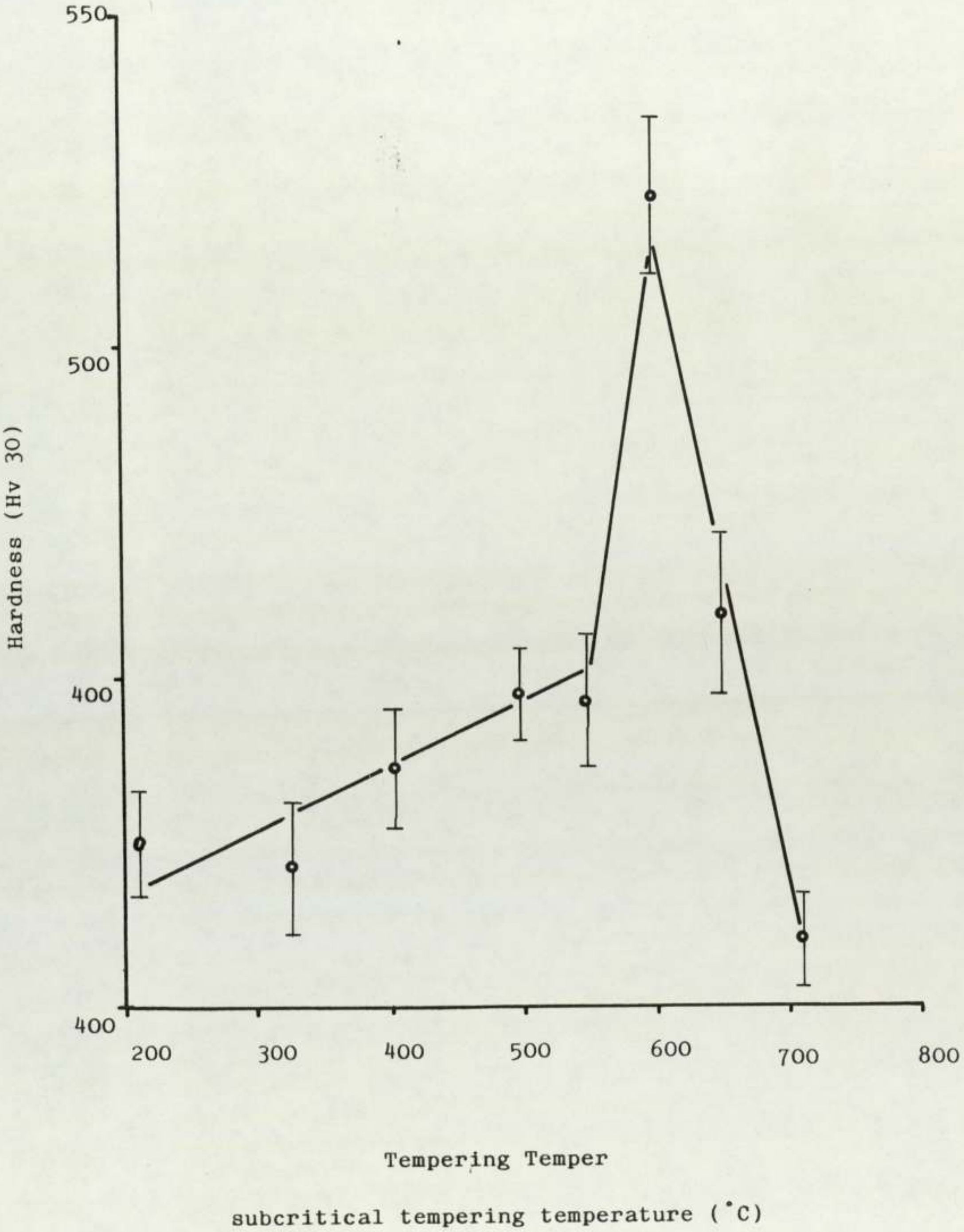

Figure 10.4
Variation in hardness with subcritical treatment temperature.

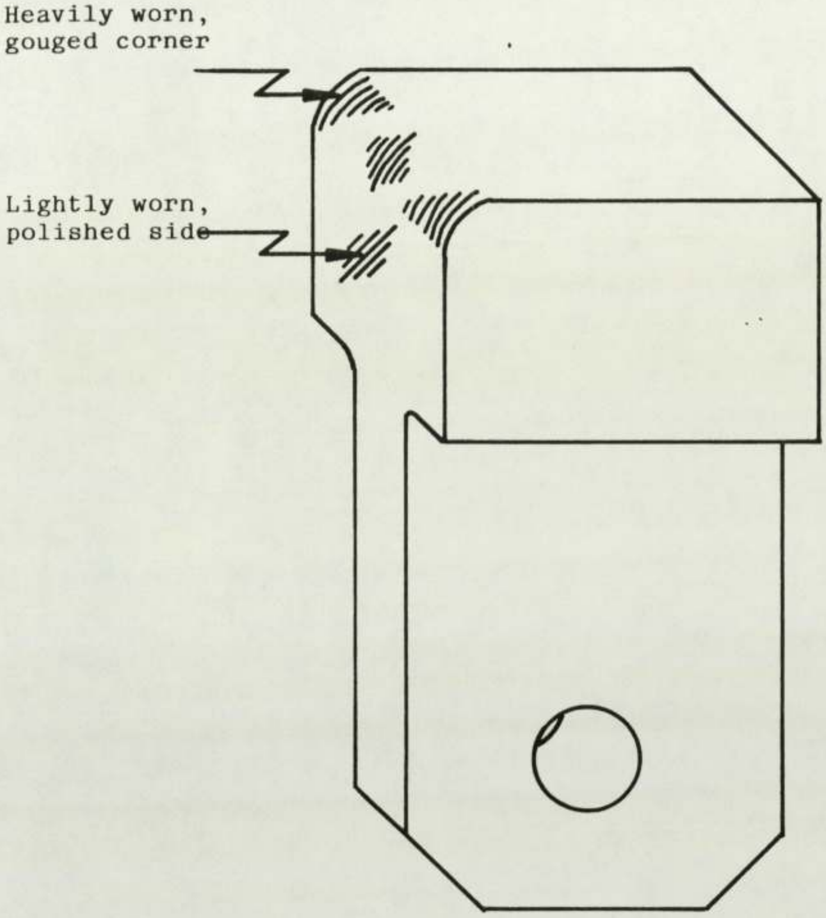

Figure 10.5

Schematic diagram showing worn surfaces on trial castings.

10.3 Compression Test Data.

The compressive strength results reported in Table 9.9 were generally in accordance with published data for similar alloys and thermal processing. (34, 275) Castings A, D and E were of the same nominal chemical composition and while the austenitic material of castings A and E exhibited the lowest of the measured values a martensitic structure (D) significantly increased the compressive strength values. Furthermore the martensitic 20% chromium alloy (F) exhibited an even higher compressive strength. The use of this 20% chromium, 2.0% carbon alloy in applications involving resistance to high compressive loads e.g. roller ball/ring mills is becoming an increasingly accepted practice. Compressive strength data generated by Biner (165) for a similarly specially treated 15% chromium alloy was of the order of 900 - 1000 N/mm^2 compared with approximately 2600 - 2900 N/mm^2 for this study. Although no other reported values for this specific combination of chemistry and thermal processing have been found,published works generally agree on austenitic high chromium irons having compressive strengths of typically 1900 - 2300 N/mm^2.(275)

10.4 Wear Trials.

10.4.1 Service Performance.

The trial castings were installed into the number 2 cement clinker hammer mill on the 20th April 1983. No breakage problems have been reported and maintenance inspections have suggested an expected service life approaching 10 years. After 16 months use a trial hammer casting was removed from the mill for inspection and examination.

10.4.1.1 Description of worn casting.

The general appearance of the worn casting can be seen in Plate 10.50 where for comparison it has been photographed with an unused hammer. It was clear that wear processes had been active on two principle areas of the castings, these have been identified in Figure 10.5 and illustrated in Plate 10.51. The lightly worn, polished face showed no evidence of directional wear grooves although some residual defects such as sand inclusions from the original cast surface were apparent. The heavily worn corner exhibited a series of parallel wear grooves consistent with the direction of rotation. The absence of wear on all other surfaces was evident from the clear definition of casting marks and the remnants of the ingate area, visible in Plate 10.51. The extent of the worn leading edge can be appreciated by examination of Plate 10.52 which illustrates the worn profile of the hammer head. It has been estimated that about 40g. of metal has been removed from this edge during the service period.

An important operating parameter which may adversly affect service life is the severity of wear around the pivot hole. However, in the returned casting minimal wear had taken place in this area. This point is emphasised

Plate 10.50

Trial hammer casting, unused and after 16 months service.

Plate 10.51

General view of worn areas of castings.

Plate 10.52

Profile view of worn edge.

Plate 10.53

Original E.D.M. electrode located in pivot hole of worn casting.

in plate 10.53 which shows the original E.D.M. electrode located in the pivot hole.

10.4.1.2 Analysis of the service tribosystem.

The wear regimes observed on the worn casting can be explained by considering the mechanism of the mill operation. The feed material entered the mill at a point where the impacting hammer was approximately horizontal, see Figure 10.6. This face, which achieved attrition of the cement clinker by impact forces, exhibited the lightly worn surface. Impact forces where nominally at 90° to the casting face and no cutting or ploughing of the material by the abrasive could be achieved. Movement of abrasive continued around the mill until the final stages of attrition were carried out by a high stress grinding or 'three body' process. This resulted in the preferential edge wear of the casting and the observed wear scares.

There were clearly two micromechanisms ofwear operating in this application thereby highlighting the problem of using a simple laboratory test to assess abrasion resistance.

10.4.2 Analysis of surface damage.

The analysis of the surface damage was carried out using both optical and S.E.M. techniques. For convenience this section will give a general indication of surface macro and microstructure followed by discussion on the two principle mechanisms of wear encountered during the service trial.

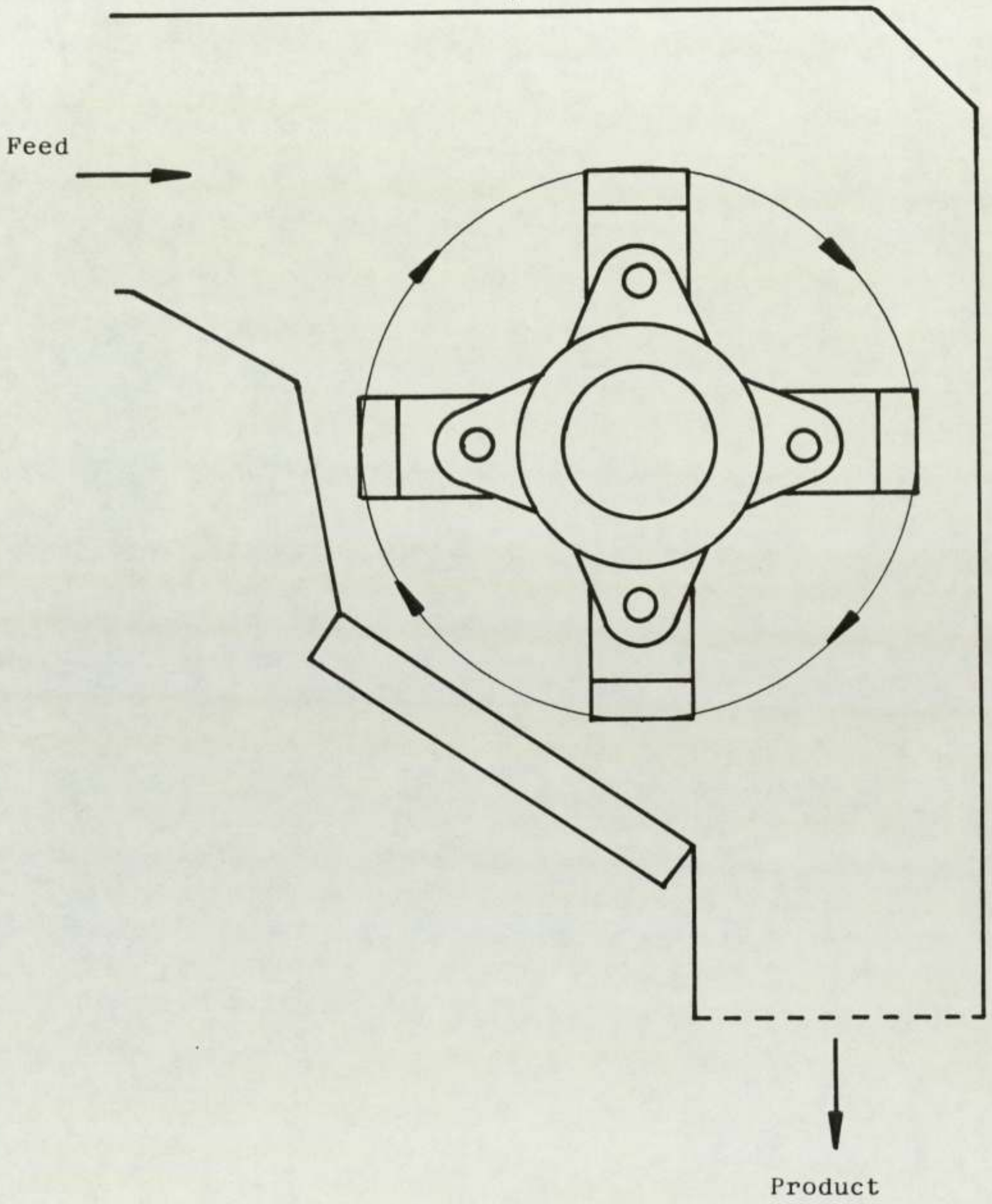

Figure 10.6

Schematic illustration of mill operation.

10.4.2.1 Microstructural transformation.

The macro etched structure of a transverse section through the heavily worn corner has been illustrated in Plate 10.54, the darker etched areas indicating the transformed region of the section. This transformation has penetrated to a maximum of approximately 20 mm and exhibited a gradual reduction in intensity rather than a distinct boundary. The extent of the transformation at areas other than the heavily worn corner was negligible.

The microstructure of the transformed region has been shown in Plate 10.55 and clearly exhibited an acicular martensitic product together with a higher temperature bainitic transformation product. Reference to Plates 10.25- 10.29 confirm that neither of these products were present in the fracture toughness specimens taken from locations 1 - 5. The presence of bainite was similar to that observed during the subcritical heat treatment exercise suggesting an operating temperature of approximately 550°C within this region of the casting. This is not unrealistic since the feed material would have retained some heat from its thermal processing and temperatures of up to 1000°C during punching operations have been reported. (276) It is likely that at the service temperatures indicated a strain induced martensitic reaction was operative.

A hardness traverse from the heavily worn corner towards the core material revealed a general decrease in hardness from Hv 665 to Hv 495 see Figure 10.7 The variation in hardness measurements reflected the inhomogeneous nature of the transformed microstructure which contained varying proportions of eutectic and secondary chromium carbides, austenite, martensite and bainite.

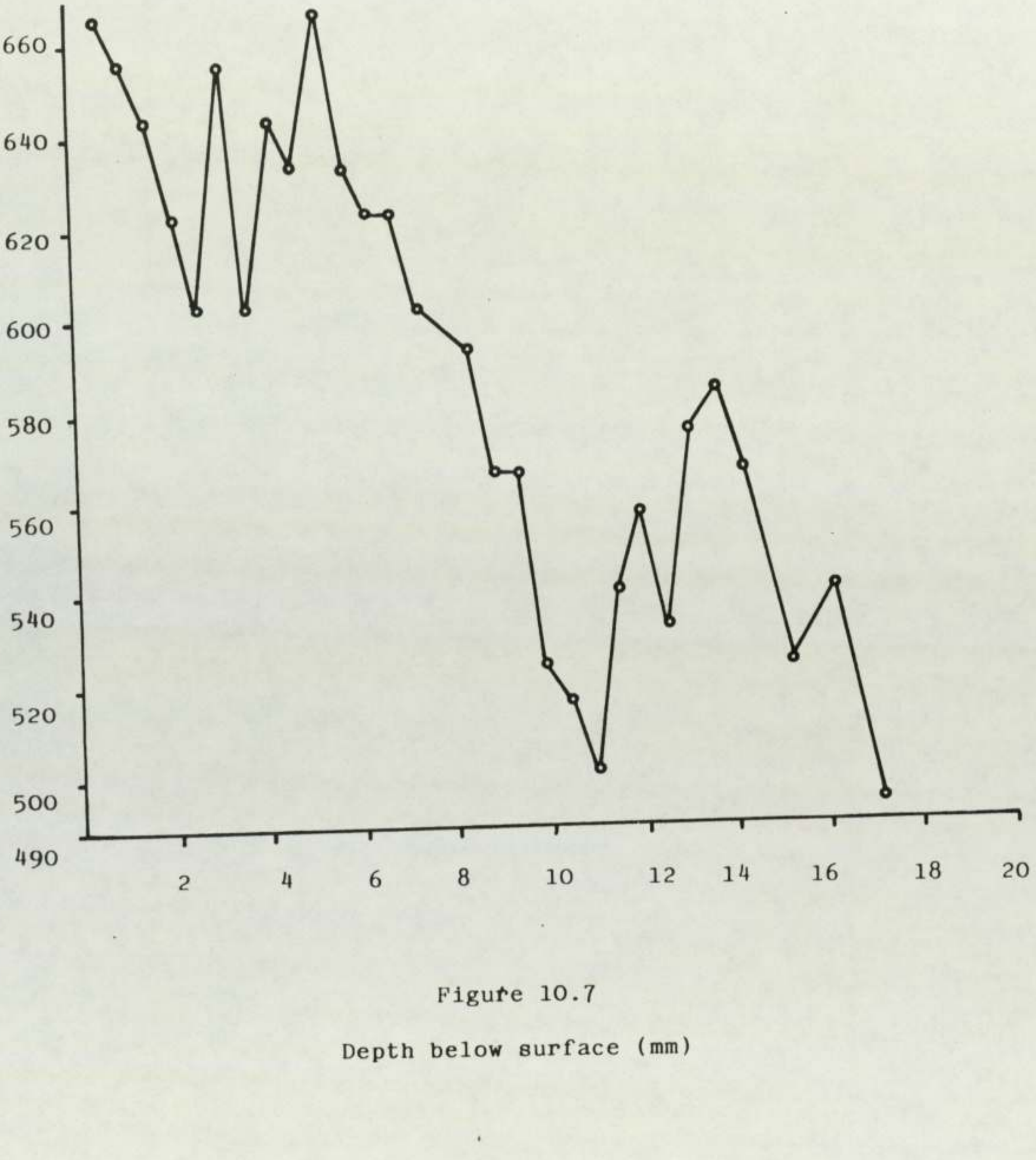

Figure 10.7

Depth below surface (mm)

Plate 10.54

Macrostructure of worn edge of casting.

Plate 10.55

Microstructure of work hardened region.

10.4.2.2. Surface Roughness Measurements.

Representative surface roughness traces obtained from both the smooth and heavily worn areas of the casting have been illustrated in Figure 10.8. Both examples exhibited traces consisting of small riples superimposed on a higher amplitude, lower frequency wave. Reference to the quantitative metallographic results (Table 9.6) and the S.E.M. of worn surfaces suggested that the small irregularities were due to microstructural features while macroscopic surface effects, particularly wear scares on the impact surface were responsible for the more obvious peak and valley troughs. Eutectic carbides above a preferentially worn matrix would cause the minor effect, this being more obvious in the lightly worn area where a greater height of unsupported carbide was possible due to the less severe impact conditions

The subjective visual classification of surfaces as rough and smooth must be questioned since the maximum amplitude of the worn surfaces was greatest for the surface referred to as being polished. The frequency of the wear scare not its amplitude may be the important parameter in decideing the texture of an abraded surface.

10.4.2.3 Structural Study of Lightly Worn Surface.

This exercise involved the optical examination of transverse sections through the worn casting and a S.E.M. study of the abraded surface.

10.4.2.3.1 Optical Study of Lightly Worn Surface.

Transverse sections through the worn section of the casting enabled an examination of both matrix and carbide phases at the surface and near surface regions.

C.L.A. = 4.00 μm

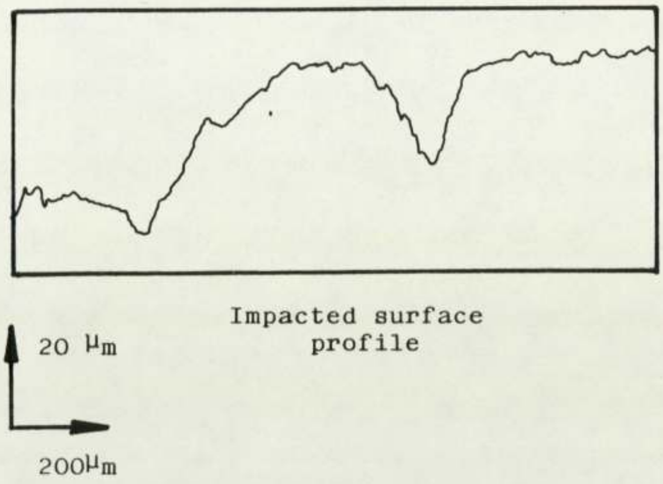

Impacted surface profile

C.L.A. = 4.9 μm

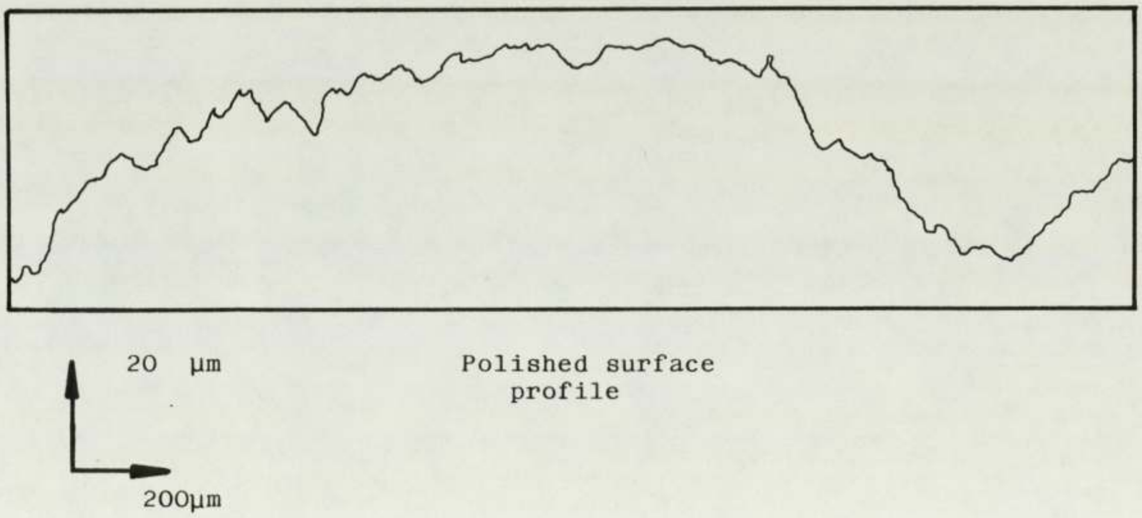

Polished surface profile

Figure 10.8

Surface roughness traces.

The matrix had transformed as indicated in section 10.4.2.1 and the inhomogeneous nature of the reaction can be appreciated from Plate 10.56. This may have resulted from inconsistent matrix chemistry due to solute denudation by secondary carbide precipitation. A similar effect may also be observed in Plate 10.57. More detailed examination of the worn surface, Plate 10.58, indicated the fracture of surface eutectic carbides to a depth of approximately 20μm. Although fractured these carbides had not been removed from the matrix and no decohesion at the interface between carbide and matrix was visible. The craters visible on the polished face of these carbides was believed to have resulted from metallographic preparation.

10.4.2.3.2 S.E.M. Study of Lightly Worn Surface.

At a relatively low magnification, approximately X150, the hypoeutectic, dendritic structure of a matrix phase surrounded by a eutectic was apparent, see Plate 10.59. The matrix had been preferentially abraded while the chromium carbides stood in relief. There was no evidence of directional wear scares resulting from the cutting or ploughing of mineral products through the surface layer.

Higher magnifications revealed additional information regarding the micromechanisms operating on the matrix and carbide. The eutectic carbides had undergone microfracture at the unsupported edge thereby accentuating the previously reported rounded morphology of the eutectic carbides, Plates 10.60 - 10.61. Microcracking of the carbide, evident in the transverse sections, was also identified during this S.E.M. exercise. Plate 10.61. Carbide removal occurred in a minority of situations when adjacent microcraks coalesced and an irregular pit was formed such as illustrated in Plate 10.62.

Plate 10.56

General microstructural features of lightly worn surface.

Plate 10.57

General microstructural features of lightly worn surface.

Plate 10.58

Details of microstructural damage on lightly worn surface.

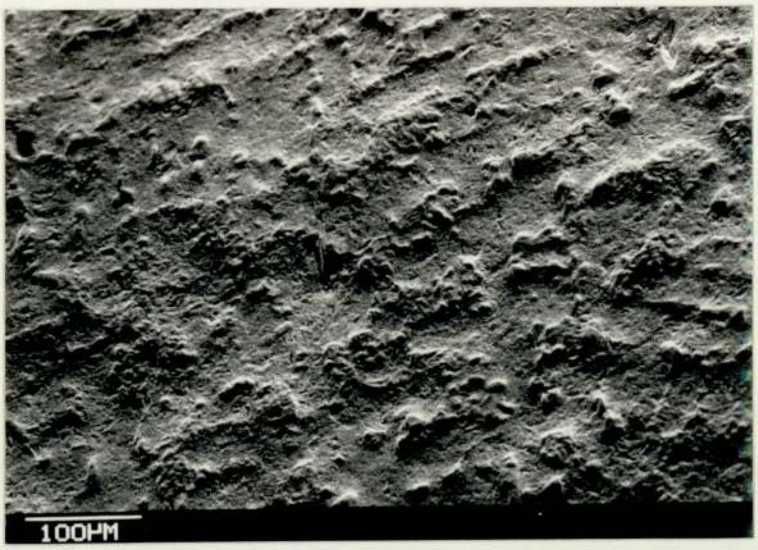

Plate 10.59

General view of lightly worn surface.

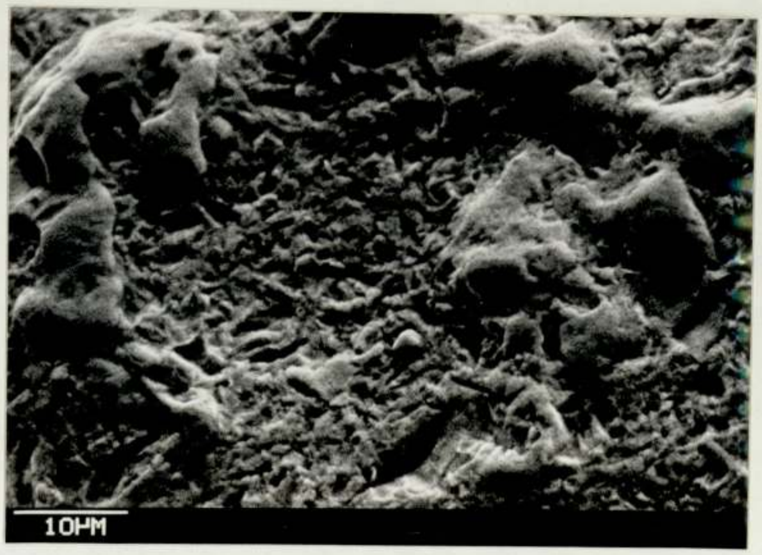

Plate 10.60

Microfracture of unsupported eutectic carbides.

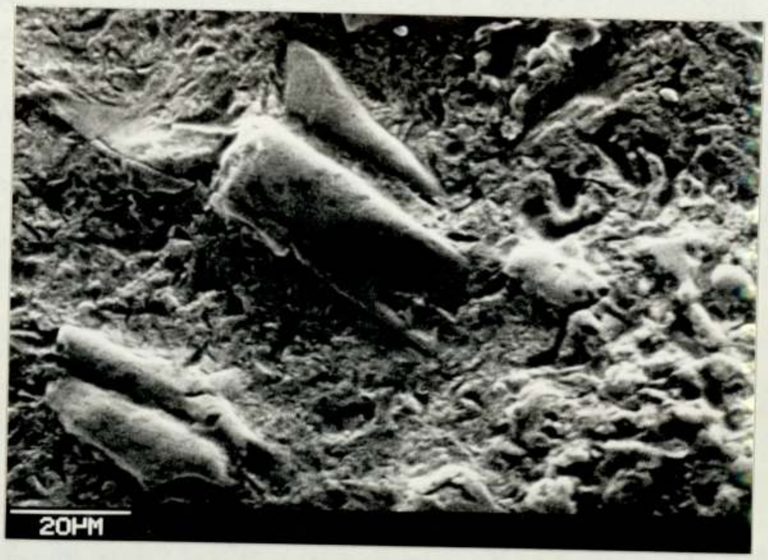

Plate 10.61

Microfracture and microcracking of eutectic carbides.

Plate 10.62

Carbide removal by pit formation.

The dimpled structure of the matrix was similar to that observed by Sare (24) who attributed the effect to the preferential removal of secondary carbides followed by plastic deformation of a weakened matrix. It is believed that while the secondary carbide removal mechanism undoubtably contributed to the general characteristics of this feature its occurrance was more widespread than the carbide precipitation. It is suggested that a further contribution to the effect is by micro gouging of the matrix resulting from the interactions with eutectic carbide wear debris or ground product.

The morphology of the eutectic carbides was again confirmed by the deep etching of the wear samples. Plates 10.63 - 10.64. These micrographs illustrated several important points, i.e. there was no distortion of carbide at the wear surface and there was only minimal evidence of subsurface cracking of carbide. However, any fractured carbides present may have been lost when the support of the matrix was removed.

10.4.2.3.3 Proposed Wear Mechanism in Lightly Worn Area.

It is considered that the lightly worn or polished area of the used swing hammer casting was the result of high surface compressive stresses combined with abrasive wear of the matrix surface. The surface stresses encountered during service were of a sufficient magnitude to cause fracture of the eutectic carbide and together with the effect of operating temperature a martensitic transformation of the austenite was possible. The carbides remained adhered to the matrix and although fractured were not preferentially removed. The hard carbide particle (Hv 1650) suffered microfracture on unsupported edges but generally appeared to resist the abrasive conditions. The matrix underwent some abrasive attack due to the loss of secondary chromium carbides and the microgouging by a combination of ground product and chromium carbide wear debris.

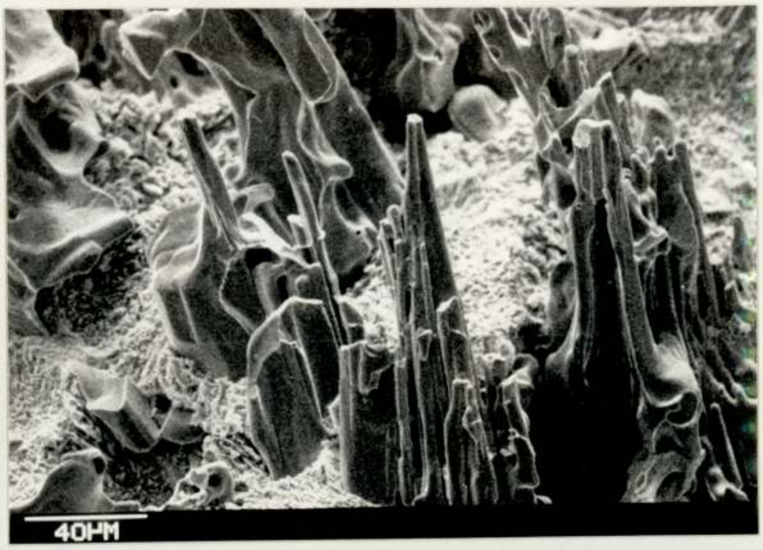

Plate 10.63

Eutectic carbide morphology at near surface location.

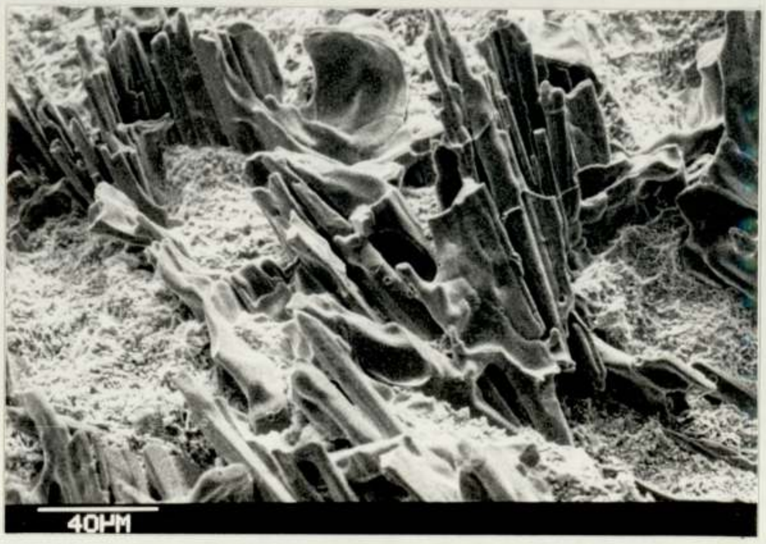

Plate 10.64

Micro cracks in eutectic carbide.

10.4.2.4 Structural Study of Heavily Worn Surface.

As with the examination of the lightly worn surface this investigation involved the optical examination of transverse sections through the worn casting together with a S.E.M. study of the worn surface.

10.4.2.4.1 Optical Study of Heavily Worn Surface.

The matrix within this section had again transformed and consisted of an inhomogeneous mixture of secondary and eutectic carbides, austenite, martensite and lower transformation products. There was no evidence to suggest that the transformation of the matrix was significantly more pronounced at locations close to the worn surface. Plates 10.65 and 10.66 illustrate this general structure. A more detailed examination of the surface layer and worn edge, as shown in Plate 10.67, revealed evidence of carbide fracture and matrix deformation to a depth of approximately 20μm. The presence of an unetched surface layer associated with the matrix was similar to the 'white layer' observed by Sare (24) on heat treated steel swing hammers. Sare suggested that under the operating conditions encountered the white layer formed as a consequence of intense plastic deformation and not as a result of surface reaustenitisation and quenching as proposed elsewhere (277). Sare's deformation hypothosis has been supported by Turley (278) while working on the white layer formed around reamed holes in high strength steel. It is considered reasonable to regard the matrix structure of a high chromium cast iron as being essentially steel like in character and hence involing Sare's mechanism for 'white layer' formation.

The eutectic carbides at the surface of this heavily worn section can be seen in Plates 10.65, 10.66 and in more detail in Plate 10.67. The carbide illustrated in Plates 10.65 and 10.66 where clearly on a similar

Plate 10.6 5

Transverse section through hevily worn surface

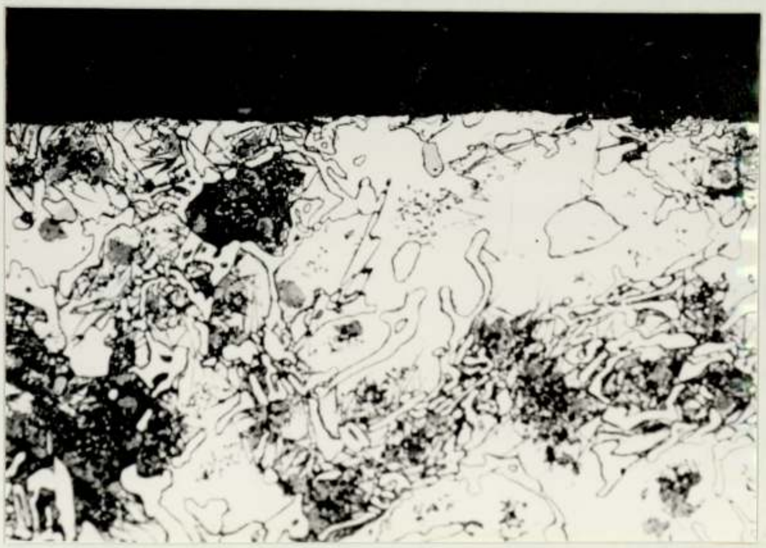

Plate 10.66

Transverse section through hevily worn surface

Plate 10.67

Details of structure at edge of heavily worn surface.

general level as the worn matrix or slightly elevated. The exception to this observation being small areas of the radial form ofeutectic which appear to have been preferentially removed, see Plate 10.66. There was no evidence of eutectic carbide deformation, however close examination of Plate 10.67 does reveal surface cracking of carbides. The fractures where parallel to the abraded surface and extended to a depth of approximately 20µm. The carbides had been retained within the matrix and no decohesion at the carbide/matrix interface was apparent.

The matrix structure close to the worn surface showed clear evidence of deformation of the acicular structure to a depth of approximately 20µm (similar to the depth of carbide cracking.)

10.4.2.4.2 S.E.M. Study of Heavily Worn Surface.

The general appearance of the heavily worn surface has been illustrated in Plate 10.68. Unlike the smooth polished surface, in this example definite parallel wear grooves cutting through both matrix and carbide were clearly apparent. When viewed at a higher magnification, Plate 10.69, wear scars could be identified running along the sides of the macroscopic grooves. There was some suggestion of the phase boundaries between the matrix and eutectic carbides being visible although this was clearer in Plate 10.70. The irregular microchipped surface appearance may have resulted from the removal of secondary carbides from the matrix or fragmenting of eutectic carbides. An example of a eutectic carbide exhibiting multiple microcracks has been illustrated in Plate 10.71. In addition to the microcracks which had generally extended to the edge of the carbide a number of smaller defects where also identified. Prasad et al (89) made similar observations when studying the hypereutectic carbide removal mechanism using a multipan scratch test made with a semi angular quartz particle. It was proposed that carbide removal was predominantly due to the extension of a pre-existing crack within a

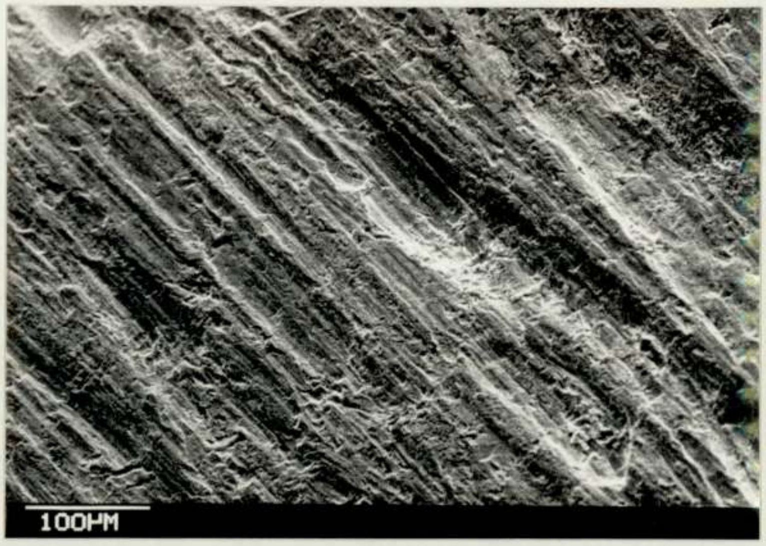

Plate 10.68

General appearance of heavily worn surface.

Plate 10.69

Wear scares across heavily worn surface.

Plate 10.70

Wear scares and irregular abraded appearance of heavily worn surface.

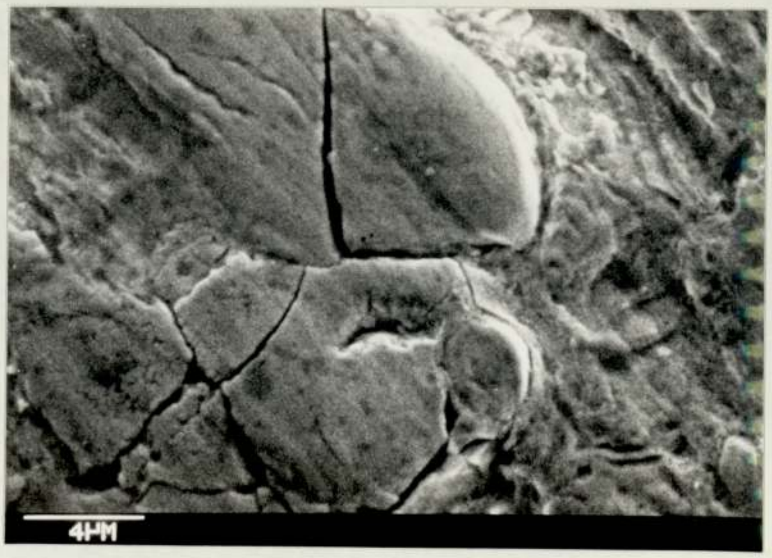

Plate 10.71

Microcracks and pit formation in eutectic carbide.

a carbide. As the crack developed a carbide chip was removed thereby forming a small pit which was subsequently enlarged. This progressive behaviour of the carbide removal was contrary to the catastrophic mechanism observed using a sharp broken quarz particle. It was also apparent from this current study that there was no observed decohesion of the matrix/ carbide identified in Plate 10.71 while undergoing considerable micro-fracture it had remained within the matrix. The ability of fractured carbides to be retained within the structure is considered to be a significant parameter in deciding the abrasion resistance of an alloy of this type.

Scanning electron micrographs after light etching of the worn surface to preferentially dissolve the matrix and hence permit the observation of eutectic arbide near to the surface have been illustrated in Plates 10.72 - 10.75. The modified morphology of the eutectic carbide was again visible (Plated 10.72 and 10.72) but no deformation of the carbide was descernable. Fracture faces of the carbide were identified as being brittle cleavage, showing evidence of fatigue striations. Other carbides revealed only minimal fracture areas possibly due to their random orientation and morphology enabling a thin section neck to be suitably located for fracture. Micro-cracks of the order of 15μm long and 1 m wide where apparent in these carbides, see Plate 10.74. Microfractured carbides similar to those illustrated in Plate 10.71 have also been identified during this exercise, Plate 10.75. In this example the carbide chip removed was not a superficial flake but exhibited a significant depth relative to the overall carbide dimensions. Carbide wear debris of approximately 2μm x 4μm x 4μm would be capable of producing some of the wear scares previously reported, see for example Plate 10.70. Furthermore, the acute angularity of these particles could effectively micromachine the surface material.

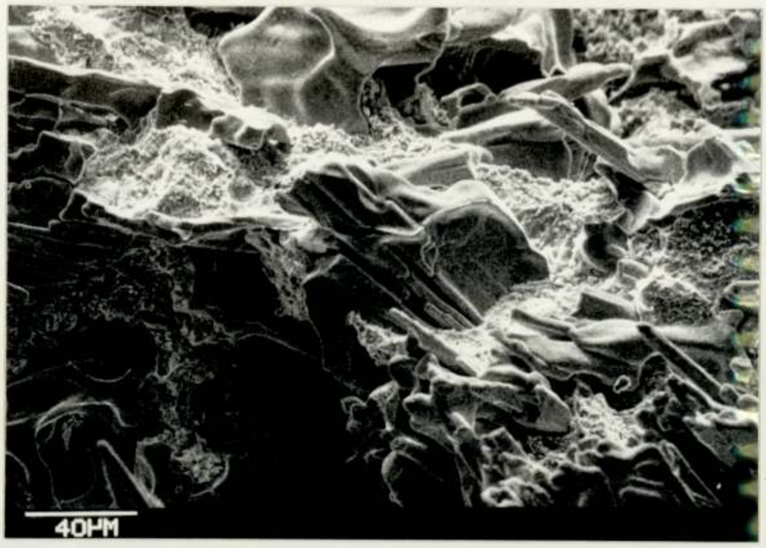

Plate 10.72

Carbide morphology following light etching of worn surface.

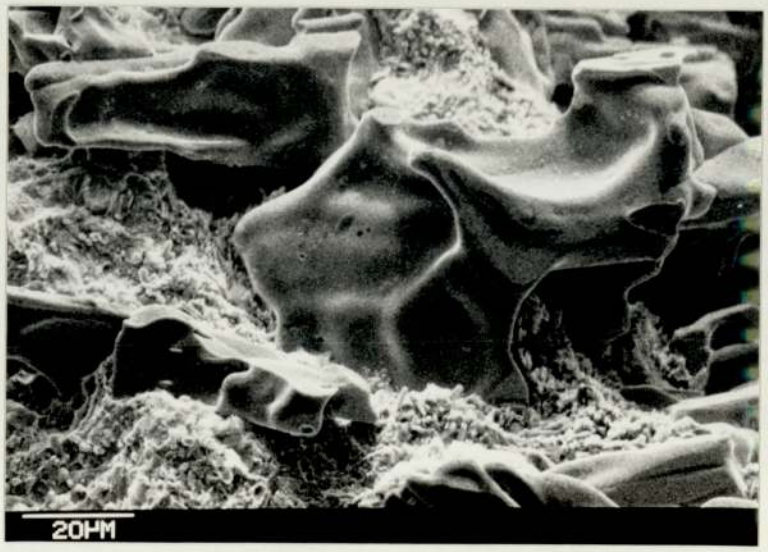

Plate 10.73

Carbide morphology following light etching of worn surface.

Plate 10.74

Cleavage fracture of carbides on worn surface.

Plate 10.75

Microcracked eutectic carbide.

10.4.2.4.3 Proposed Wear Mechanism In Heavily Worn Area.

It is considered that the heavily worn area of the used swing hammer was the result of high surface shear deformations and gouging encountered during service. This contributed to the formation of a 'white layer' associated with the matrix surface and the deformation of the martensitic structure. As a consequence of the shear deformation of the matrix the brittle eutectic carbides (K_{IC} approximately 3.0 $MNm^{-3/2}$) fractured parallel to the direction of deformation thereby accommodating the overall shape change. The appearance of the fractured carbides suggested that a fatigue mechanism was operative. Although the eutectic carbide generally remained adhered to the matrix even when fractured, some chromium carbide wear debris, probably in the form of acute, angular flakes could have contributed to the micromachining of the worn surface.

10.4.2.5 Elastic Stress Wave Interactions.

The analysis employed by Sare (24) may be applied to the castings used in the service trial of this work. The characteristic impedence, given by $(E\rho)^{1/2}$, can be calculated for the matrix, carbide phase and bulk material using typical published data

Phase	Elastic modulus E (GNm^{-2})	Ref	Density ρ(Kgm^{-3})	Ref
Matrix (austenite)	190	274	7930	274
carbide	296	24	6920	24
bulk material	186	274	7668	This work

Table 10.1

Typical material values used in impedence calculations.

Hence, the calculated impedence values are:

Phase	Impedence ($Kgm^{-2}S^{-1}$)
Matrix (γ)	3.862×10^7
Carbide	4.526×10^7
Bulk material	3.779×10^7

Table 10.2

Calculated Impedence Values.

The stress generated at the front face of the hammer, given by equation

$$\sigma i = \rho h \; Vh \; Ch$$

and approximating Ch to $(E/\rho)^{1/2}$ and $Vh = 12.5 \; ms^{-1}$. Then

$$\sigma i = 0.481 \; GNm^{-2}$$

The reflected stress wave, σr was given in equation 1.11 as:

$$\sigma r = \sigma i \left[\frac{\rho\gamma \; C\gamma \; - \; \rho k \; Ck}{\rho\gamma \; C\gamma \; + \; \rho^k \; Ck}\right]$$

this becomes 36.83 MNm^{-2}, representing 7.7% of the incident stress wave. Sare expressed the tensile strength of carbide to be approximately 300 MNm^{-2} and σr was calculated to be 130 MNm^{-2} this was considered by Sare to be sufficiently close to the carbide tensile strength to explain the observed carbide cracking. In this work a similar analysis has not suggested the occurrance of carbide cracking due to elastic stress wave interactions. This has been supported by direct observations of transverse sections through worn surfaces. While some near surface carbide cracking has been detected this feature did not extend to depths of the order of 70μm below worn surfaces as reported by Sare .(24) It is probable that the reason for this disparity is due to the hammer tip velocities used in each trial. This work has studied the castings used in a mill which developed tip velocities of 12.5 M/sec whereas Sare reported findings related to velocities of 60 M/sec. If the data given in Table 10.2 is used to generate a graph of reflected stress wave intensity versus hammer tip velocity the relationship illustrated in Figure 10.9 is produced. It is clear from this graph that using the data in Table 10.1 combined with Sare's assumptions then carbide cracking should only be evident at hammer tip velocities in excess of approximately 44 M/sec.

The occurrance of this form of microstructural degredation would be expected to exhibit an adverse effect on abrasion resistance.

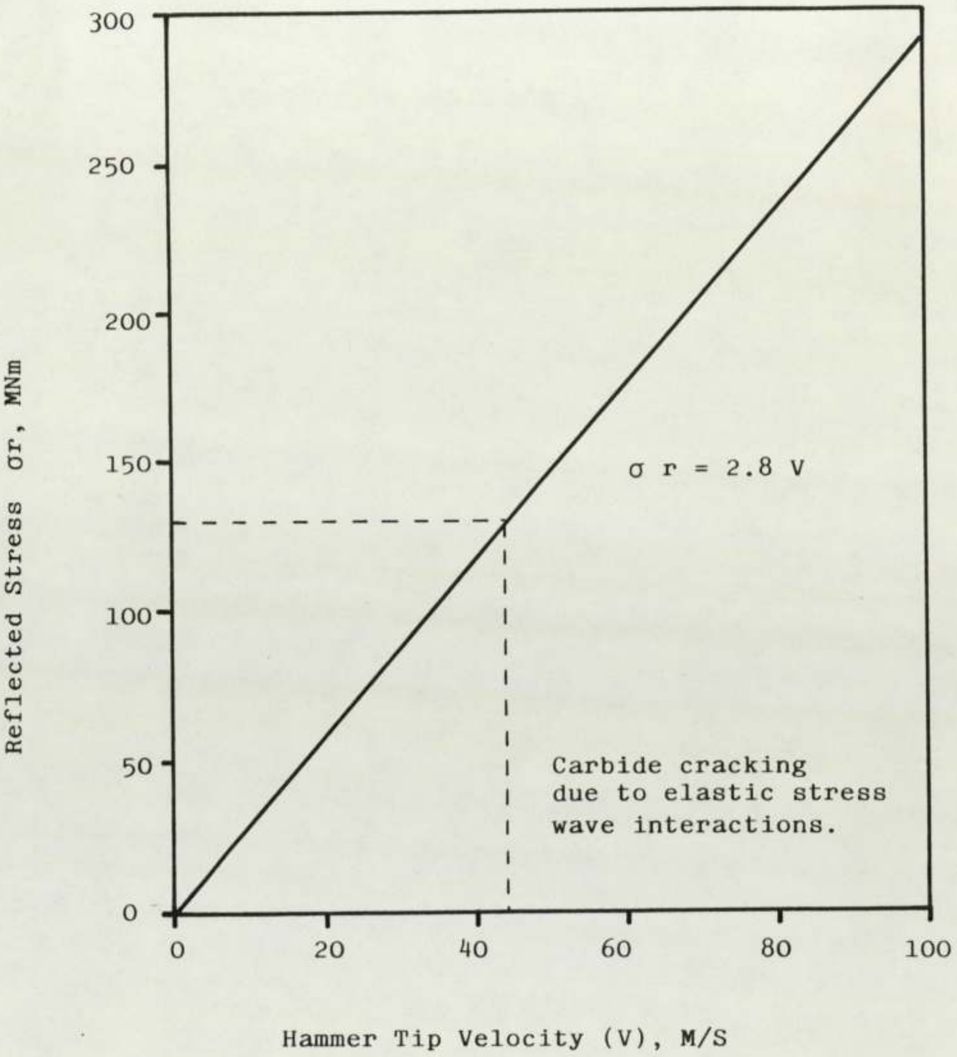

Figure 10.9

Calculated reflected stress wave intensity against hammer tip velocity.

10.5 Fracture Toughness Study.

10.5.1 Fracture Toughness Specimen Preparation.

The machining of high chromium cast irons has been notoriously difficult and until the introduction of cubic boron nitride (C.B.N) cutting tools all metal removal was carried out by grinding. Even with the introduction of C.B.N. tooling operations are restricted by the need to maintain cutting speeds of approximately 60M/minute and the generation of sufficient levels of heat. (279, 280) As yet no techniques for the milling or drilling of these hard irons has been developed.

The fracture toughness specimens have been prepared using an electro discharge machine process. In addition to producing the specimen 'blanks' from the original castings the technique was also used to generate the chevron 'V' notch. A typical fractured specimen has been illustrated in Plate 10.76 where the straight sides and accurate positioning is evident. This accuracy was highlighted by viewing the notch tip and surrounding area in a scanning electron microscope. Plate 10.77. The allignment of the inclined cuts and the acuteness of the notch tip, approximate radius of curvature 20µm, was clearly apparent. The use of a continuous copper wire electrode to produce the chevron notch also had the added benefit of producing a radius root tip as shown in Plate 10.78. The width of the slot produced using a 0.2 mm diameter wire together with the semi-circular root radius enabled Barkers criteria for plain strain conditions to be maintained. (136) Evidence of the production of the radius can be seen in Plate 10.79 which clearly demonstrated this point on a fractured specimen.

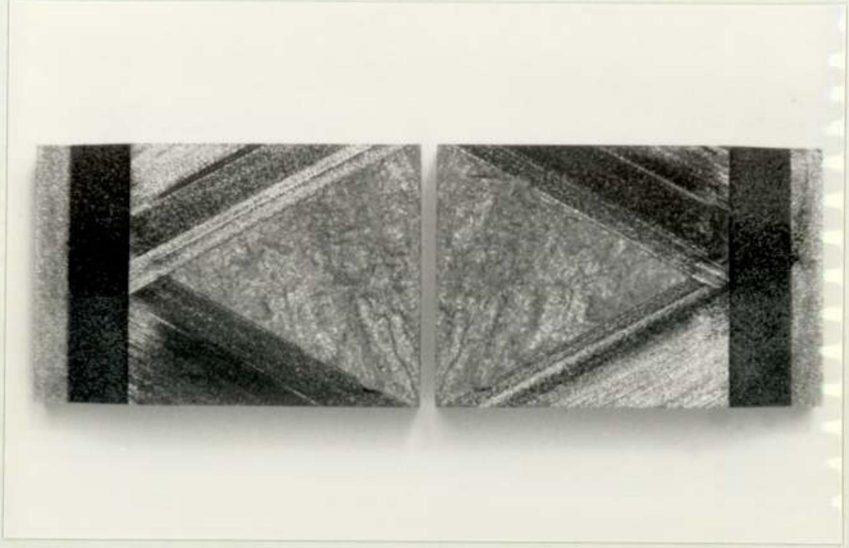

Plate 10.76

Fractured short bar specimen.

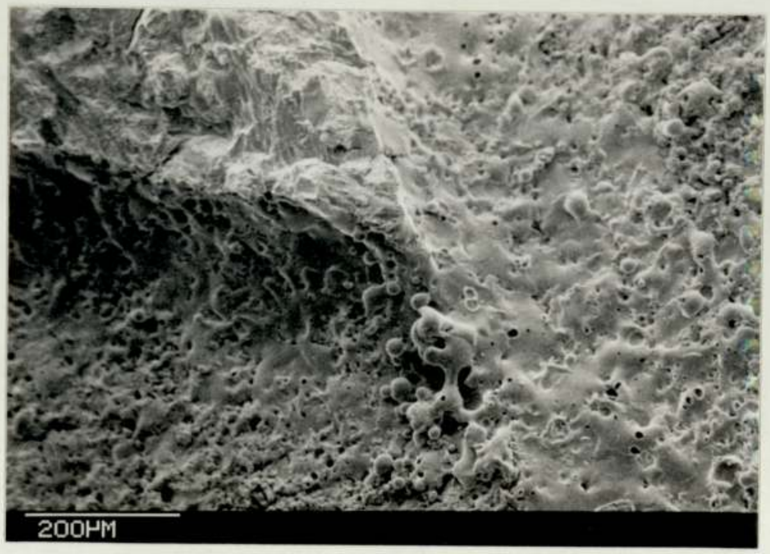

Plate 10.77

Details of chevron notch tip.

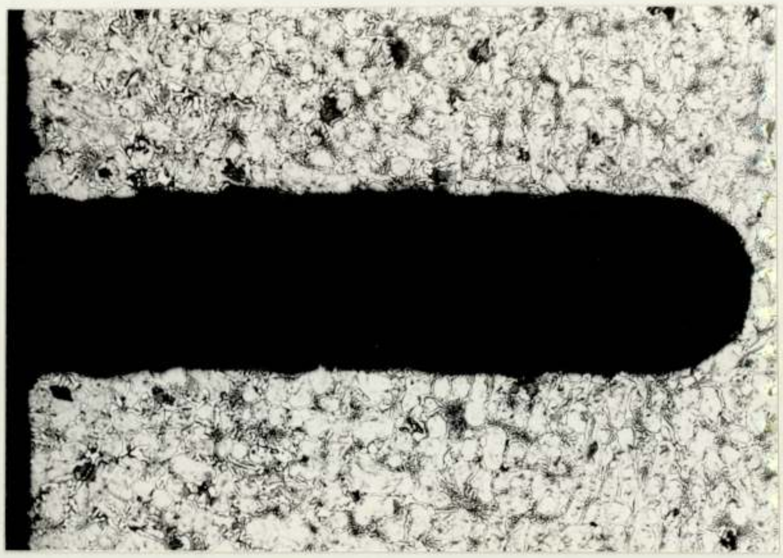

Plate 10.78

Chevron notch tip profile.

Plate 10.79

Chevron notch tip configuration on fractured specimen.

10.5.2 Fracture Appearance of High Chromium Iron.

Typical fracture surfaces of the short bar specimens have been illustrated in Plates 10.80 - 10.90, these include both conventionally treated materials having a martensitic matrix and austenitic matrix vacuum processed structures.

The unused, vacuum treated material exhibited a generally coarse matrix surface of overlapping tongues indicative of a ductile tearing process. (Plates 10.80 - 10.83) The eutectic carbide revealed clear evidence of river markings and cleavage failure however, all fractures did not necessarily show particularly flat surfaces. Some of the carbide fracture faces were curved (Plate 10.83) and comparable with the modified carbide morphology described earlier (Plates 10.44 and 10.45.) As noted by Biner (165) the failure mechanism of the austenitic matrix was presumably due to ductile tearing immediately proceeding void formation around secondary chromium carbides. While being essentially austenitic the matrix did contain some carbide precipitation. Detailed examination of the fracture surface in precipitate rich regions revealed the morphology of the secondary carbides to be prismatic rods approximately 1μm in diameter in excess of 4μm long. (Plate 10.84) This observation was consistent with the findings of the matrix leeching exercise which showed distinct secondary carbides within the matrix of an austenitic alloy. Plate 10.46 and 10.47. The diameter of the precipitates was similar to the reported findings of Durman. (166) No attempt was made to investigate the orientation of these carbides but Maratray(218) has stated that secondary carbide precipitation during the destabilising treatment takes place on three preferred planes.

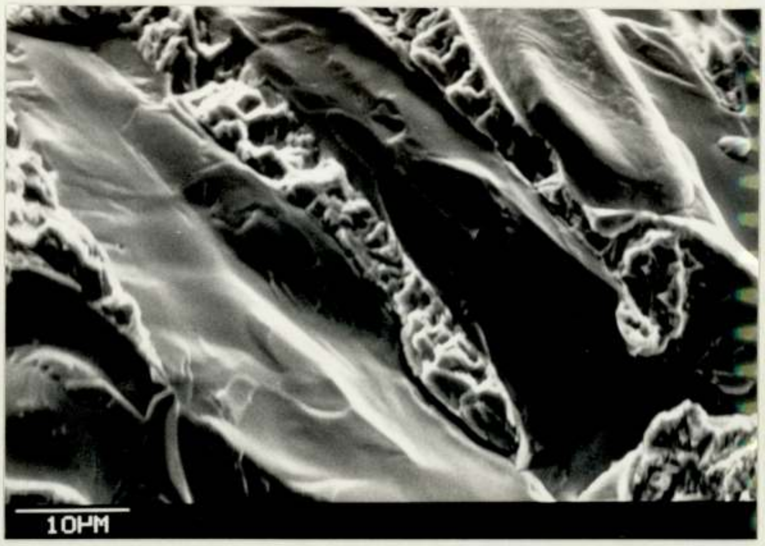

Plate 10.80

Fracture surface of unused vacuum processed material.

Plate 10.81

Fracture surface of unused vacuum processed material.

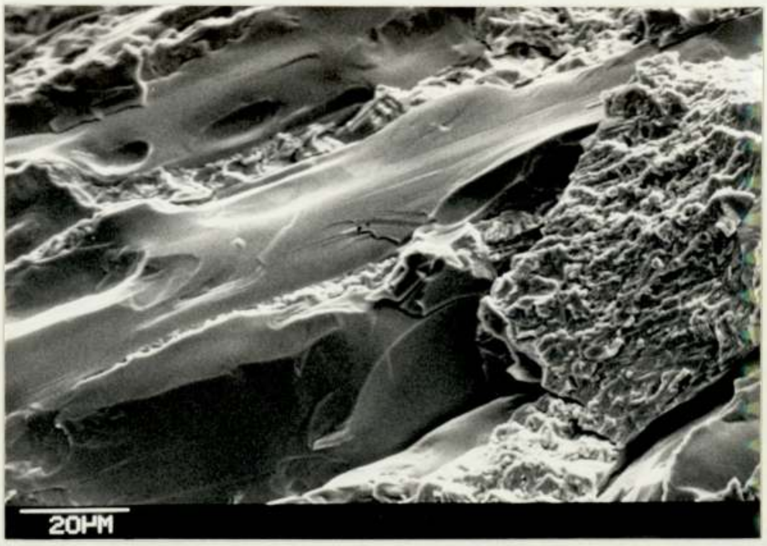

Plate 10.82

Fracture surface of unused vacuum processed material.

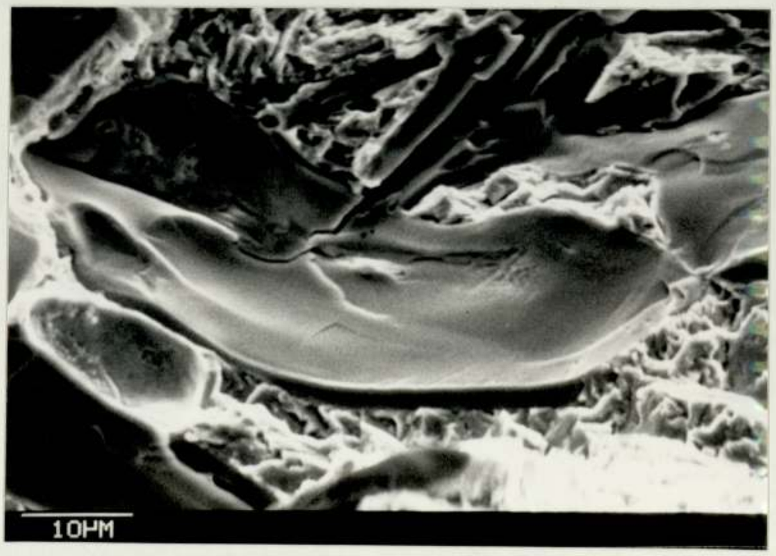

Plate 10.83

Fracture surface of unused vacuum processed material.

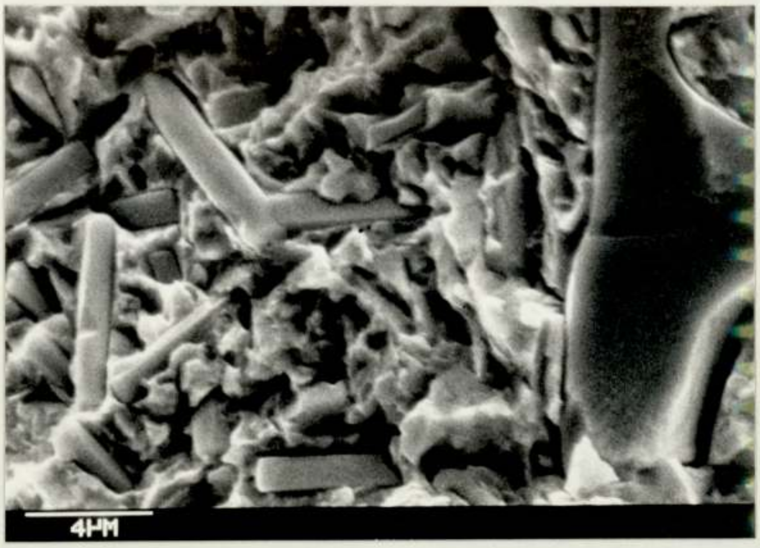

Plate 10.84

Secondary chromium carbides on fracture face of vacuum processed casting.

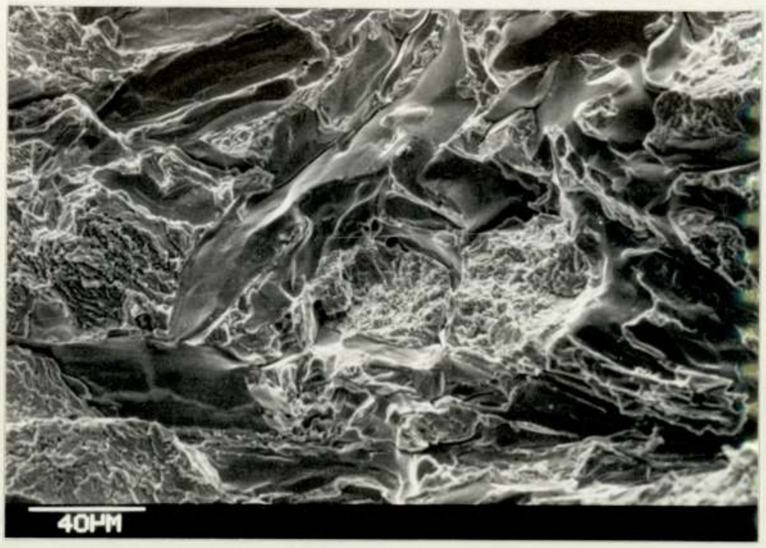

Plate 10.85

Fracture surface of vacuum processed material after 16 months service.

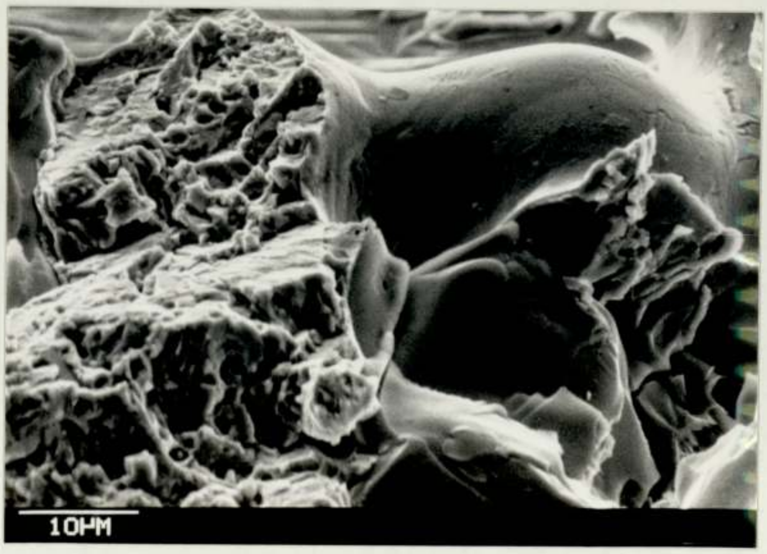

Plate 10.86

Fracture surface of vacuum processed material after 16 months service.

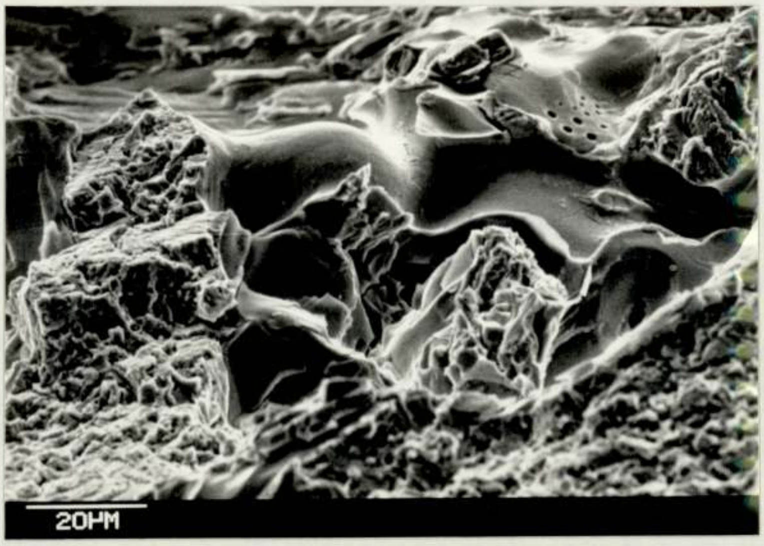

Plate 10.87

Fracture surface of vacuum processed material after 16 months service.

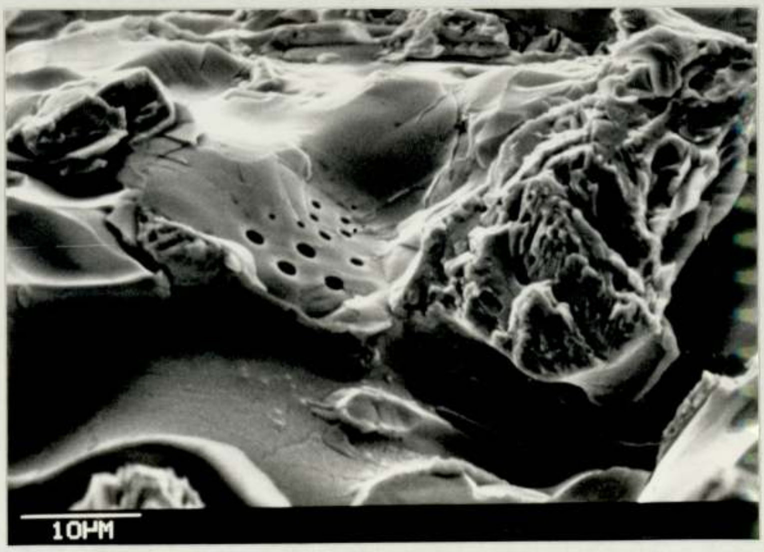

Plate 10.88

Details of fracture surface of vacuum produced material after 16 months service.

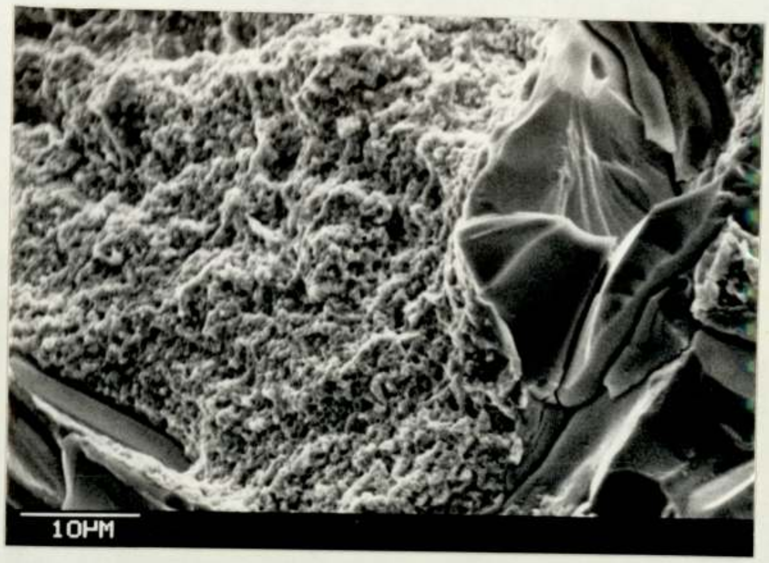

Plate 10.89

Fracture surface of conventionally
heat treated specimen D.

Plate 10.90

Fracture surface of conventionally
heat treated specimen D showing cleavage fracture of carbide.

Examination of the fracture surfaces of specimens from casting E, vacuum processed and 16 months service was generally similar to that previously described, these have been illustrated in Plates 10.85 to 10.87. There was evidence of matrix/carbide decohesion, Plate 10.87, the curved, rounded surface being an extension of the matrix fracture face. The fracture face illustrated in Plate 10.88 appeared to predominantly consist of matrix, either fractured or smooth interfacial boundary. The regular array of voids at the centre of the field was probably a series of secondary carbides, the diameters being comparable with the precipitates in Plate 10.84.

The fracture surfaces of the conventionally hardened and tempered alloy having a martensitic matrix consisted of cleavage fractured eutectic chromium carbides and a dimpled rupture matrix appearance. Compared with the vacuum treated austenitic alloys the matrix fracture was considerably finer and more homogeneous. The individual secondary carbides remained irresolvable at the magnifications used. (see Plates 10.89 - 10.91).

10.5.3 Fracture toughness testing using the short bar specimen geometry.

The short rod/bar specimen geometry as developed by Barker appears to be gaining in acceptance particularly amongst users and producers of relatively low toughness materials. Interest has also been generated by industries having a requirement for large volume fracture toughness assessment in which case the absence of fatigue precracking has obvious cost and time advantages.

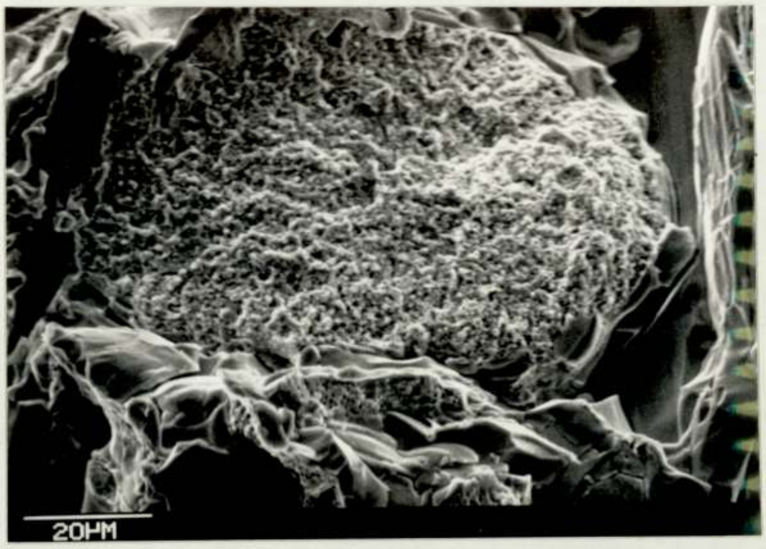

Plate 10.91

Microfracture of carbides in conventionally heat treated specimen D.

The data reported in Tables 9.8 and 9.9 demonstrated the sensitivity of the test to descriminate between the two matrix constituents. The plasticity factor was significantly higher for austenitic materials compared with martensitic structures. This difference was also highlighted in the load displacement records of these structures. Typical records have been illustrated in Figure 10.10. Calculated K_{ICSR} values using the maximum load and zero plasticity criteria have illustrated the generally higher toughness values of the austenitic materials which is in agreement with published literature. As the plasticity factor was able to descriminate between the two matrix structures this could provide a convenient method for the quality assessment of vacuum heat treated components. It is known that some secondary carbide precipitate was present after the specialised processing, however, this was insufficient to achieve solute denundation of the matrix and the austenitic structure was retained to room temperature. If cooling through the critical temperature range, 1180°C to approximately 850°C is achieved at a rate less than 3°C per hour increased precipitation can allow a martensitic reaction to occur. As shown by Biner (165) and Durman (166) the production of a martensitic structure in a high temperature processed alloy results in the reduction of fracture toughness values due to ductile dimple formation around the homogeneously precipitated secondary carbides. The use of the plasticity factor may be capable of identifying precise limits for the amount of secondary precipitation.

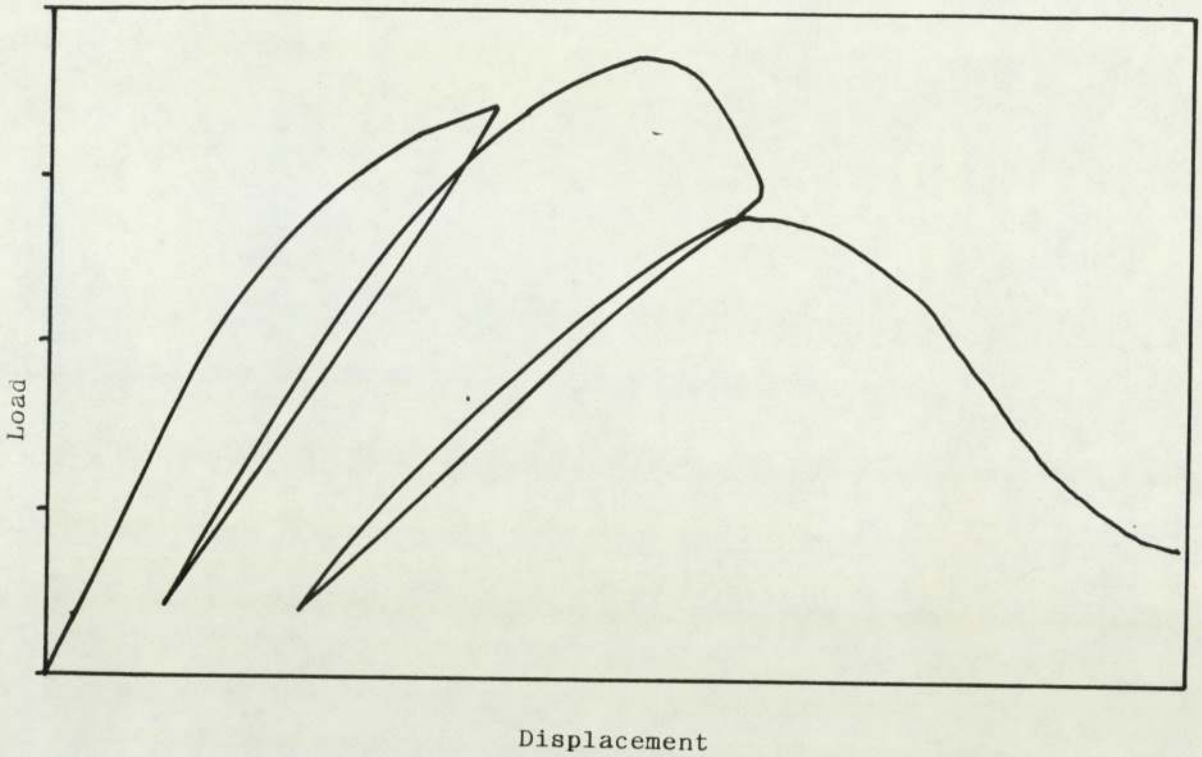

(a) austenitic matrix.

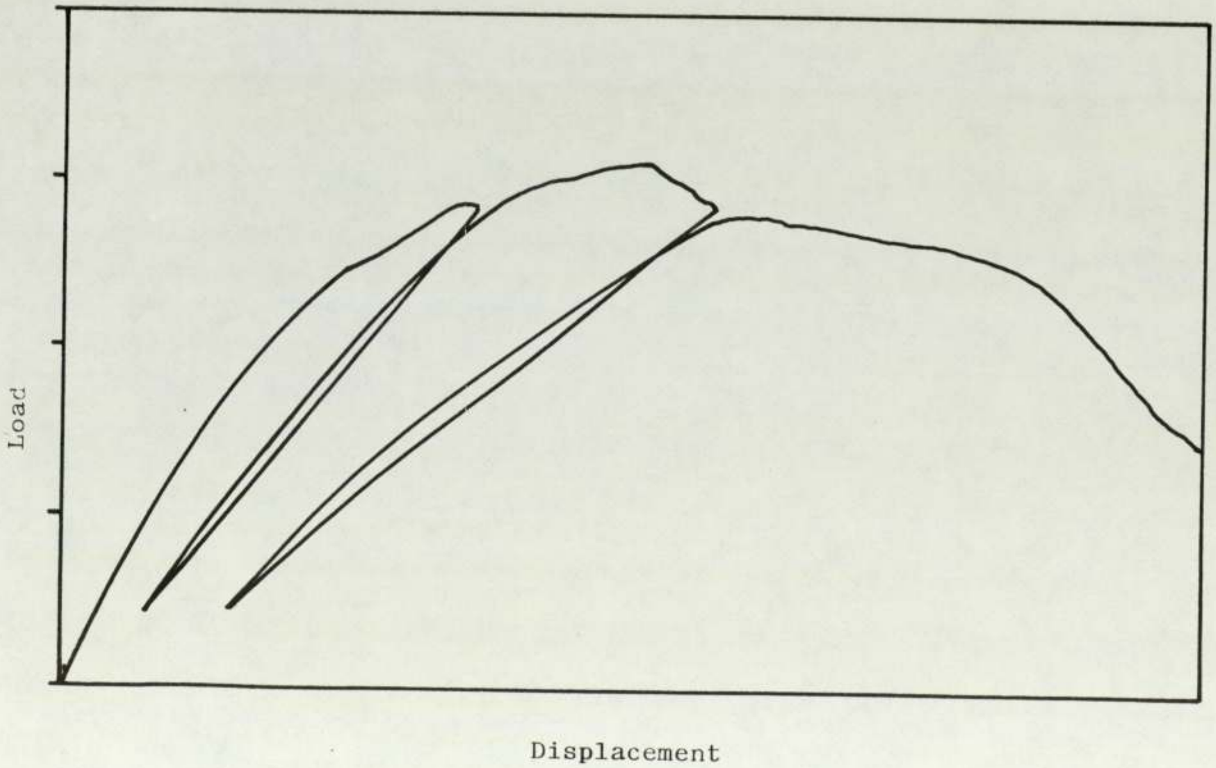

(b) martensitic matrix.

Figure 10.10.

Fracture toughness specimen traces of load against displacement.

10.6 Technical Aspects of Swing Hammer Production.

The production of a new range of cast components involving the novel processing of a recently developed alloy inevitably requires the implementation of a modified processing route. Throughout the course of this work a number of specific details have been identified as being particularly relevant to the production of swing hammers in BF.153S.

10.6.1 Design Considerations.

At the design study stage attention must be paid to the cross sectional area of material on the axial plane of the pivot hole. Furthermore, the requested size tolerance on the pivot hole should be examined and the most suitable core material (e.g. shell, furane or oil sand) selected. Changes in section, for example from shank to head, should be accomplished through the use of generous radii of the order of 25 mm.

10.6.2 Pattern Equipment and Mould Making.

The pattern should allow for a contraction of 1 in 48 and have a moulding taper of about 1 mm per 100 mm. The core must be provided with an adequate 'print' in both the cope and drag. This is to ensure the accurate and rigid location of the core in the mould cavity. As with any casting design a sufficient supply of hot, clean metal must be available to produce a sound casting but ingate or feeder locations should be provided with a breaker core or similar assembly. The removal of excess material by grinding can cause cracking of austenitic alloys.

10.6.3 Heat Treatment Processing.

The heat treatment cycle has been detailed but because of the use of a vacuum process material should be supplied as clean and free of contamination as possible. The heating rates are generally related to casting complexity and the need to avoid cracking castings.

The heat treatment record sheet supplied by the sub contract company should be analysed and treatment times and temperatures checked against the specifications. The quench rate from the holding temperature down to approximately 850°C should be measured and assessed against the requirement of a minimum rate of 3°C per minute. It is believed that at slower quench rates significant secondary carbide precipitation can occur with resultant transformation to martensite.

10.6.4 Inspection Procedure.

A 'first stage' visual inspection should be carried out prior to heat treatment so that no obvious scrap castings are processed. Following the vacuum heat treatment a number of inspection procedures should be carried out. Initially, a visual and dimensional check should confirm conformance with customer specifications. The inside of the pivot hole must be thoroughly inspected for surface defects, e.g. cold laps or cracks. Dye penetrant techniques are useful in detecting cracks in this area and around changes in section. While the destructive examination of a casting is time consuming suitably sized specimens could be heat treated with the castings and used for final metallographic examination. The response of the material to the heat treatment can be assessed using portable hardness and magnetic response equipment. A limited number of historic records have been used to produce Figure 10./12. which is a graph of hardness value against magnetic response. Both areas of this graph are given in terms of an instrument reading number, no attempt has been made to convert these to more meaningful value. The use of this graph, which can be continually updated as more information becomes available, should assist with the rapid identification of unacceptable heat treated castings.

11.0 Future Work.

It is envisaged that future work could be classified into two principle areas, that is material research and product development.

Further clarification of the precise mechanism of spheroidisation is required so that the heat treatment process and perhaps metal chemistry may be further refined. In addition, investigation of the decohesion of the matrix/carbide interface could produce results leading to the development of still tougher alloys. While this, and previous work (165) has been essentially involved with a base 15% chromium, 2% - 3% carbon alloy the principles developed could be applied to other specification ranges. In this way the variation in carbide modification and molybdenum catalysis with metallurgical variables such as carbide volume fraction and chromium/carbon ratio may be studied. As reported, the austenitic matrix material had work hardened during service but the supply of an initially harder component may be advantageous in certain circumstances where impact conditions would be less severe than those encountered during this study. It is considered that the production of a harder matrix either by subcritical heat treatment of subzero quenching could be achieved without a significant reduction in fracture toughness however work to determine the degree of austenite stability and its transformation behaviour would be necessary.

Product development may be subdivided into two groups, that is swing hammer development and development of new markets. Only one specific service trial has been reported, material performance in other environments where higher hammer velocities are encountered together with the crushing of a range of high and low density aggregates should be explored. The full exploitation of the market potential of this development in high chromium cast iron technologhy also requires significant technical and commercial investigation.

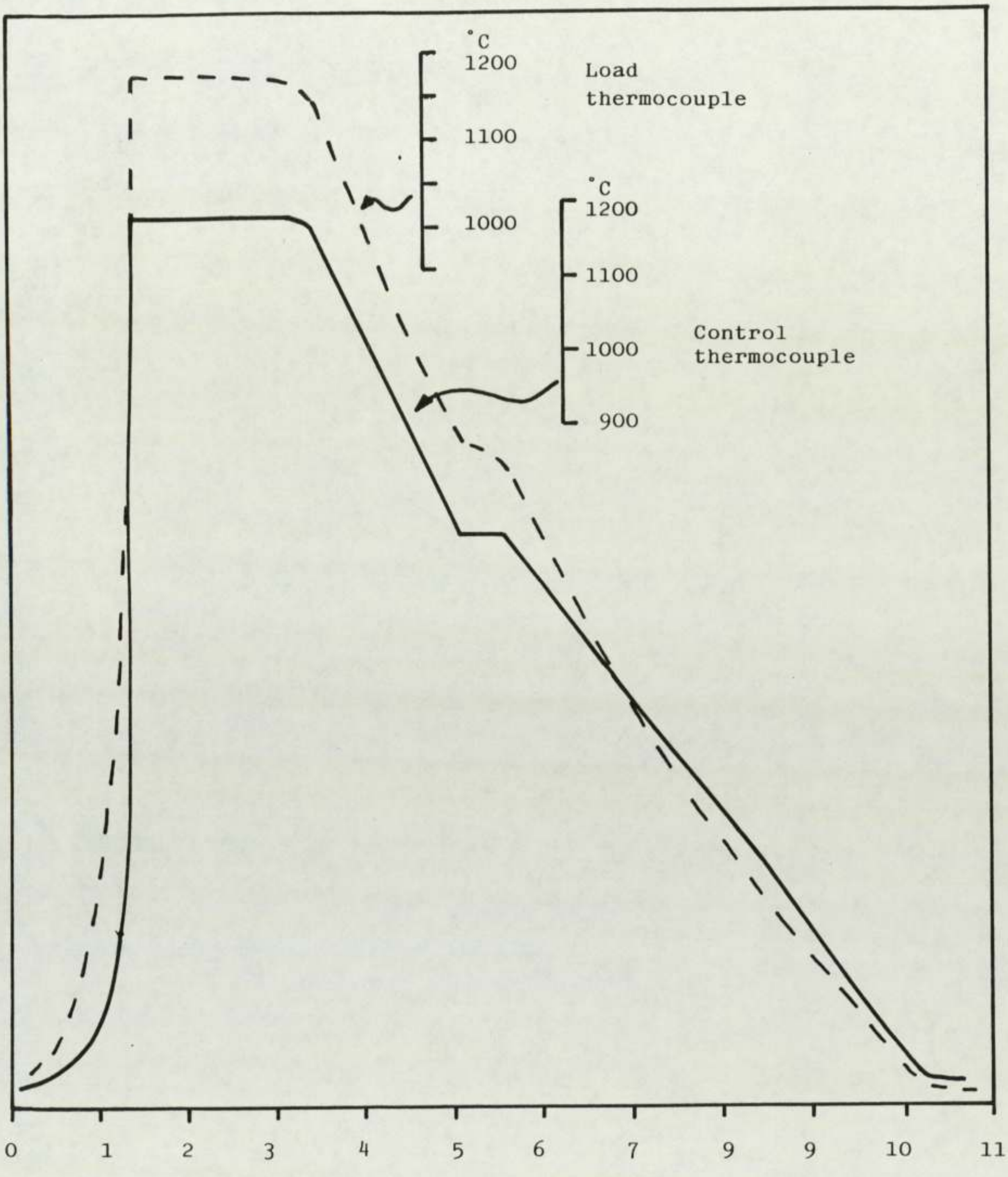

Figure 10.11

Schematic illustration of vacuum heat treated cycle.

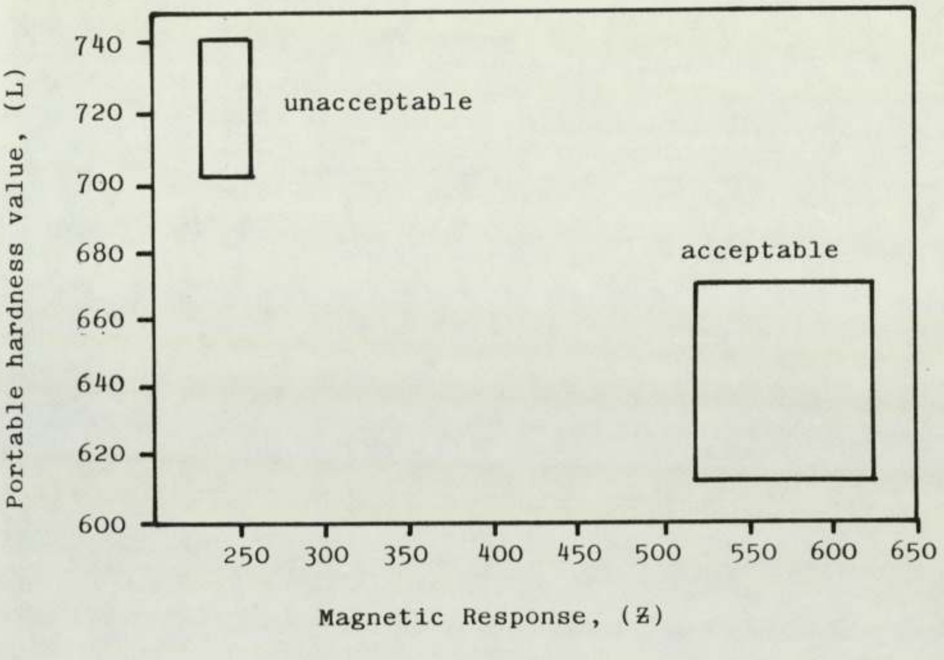

Figure 10.12

Hardness values against magnetic response illustrating acceptable and unacceptable ranges.

12.0 Conclusions.

This work has elucidated some of the mechanisms, metallurgical parameters and production variables which have been shown to be important in the production of a vacuum processed high chromium cast iron of increased fracture toughness.

1. It has been shown that cast components can be successfully produced and processed to achieve increased fracture toughness compared with conventionally alloyed and treated material.

2. The specially treated high toughness cast components have been successfully used in a service environment which was recognised as being too hostile for conventional high chromium cast iron.

3. After service the swing hammers had exhibited work hardening and microstructural transformation of the matrix to a maximum depth of approximately 20 mm.

4. Two distinct micro mechanisms of abrasive wear have been identified and discussed relative to the mechanics of the mill operation.

5. A duplex carbide has been observed of the form M_7C_3, $M_{23}C_6$ and an insitu transformation involving changes in nucleation with temperature/composition have been suggested.

6. A technique for matrix leeching the materials to enable the observation of the three dimensional carbide morphology has been developed. This has enabled the carbide to be observed

at greater depths and in more detail than previously reported.

6. The modification of the eutectic carbide phase due to the high temperature heat treatment has been observed and compared with other conventionally treated material.

7. The use of the short bar fracture toughness specimen has allowed the measurement of fracture toughness at specific sample locations and orientations.

8. No distinct correlation between specimen location, fracture toughness and microstructural parameter has been observed.

9. The fracture toughness tests were sufficiently sensitive to microstructural changes to identify the austenitic and martensitic matrix material.

10. The decohesion of the matrix/carbide interface has been observed in the vacuum processed material.

11. Secondary chromium carbides in the form of prismatic rods have been observed on fracture surfaces and incomplete matrix leeched specimens.

12. The use of a higher molybdenum content alloy given a specialised vacuum treatment has enabled a proposed sequence of the spheroidisation process to be suggested. This involved the necking down of carbides, carbide migration leading to grain boundary formation, exaggerated grain sizes and dissolution of secondary carbides.

Appendix I

Metallographic Examination of a High Molybdenum Vacuum Processed Alloy.

During this study there was an opportunity to examine a sample of vacuum heat treated material which had been produced with a molybdenum content in excess of the recommended level. Although subjected to the suggested vacuum treatment the metallographic structure was considered to be abnormal and unsuitable for service. It is suggested that the structure of this material provided an indication of a possible spheroidisation sequence and helped to explain the observed reduction in fracture values with increasing molybdenum additions or treatment times. The microstructures obtained in a material containing 4% molybdenum have been shown in Plates i. - v. The lower magnification view Plate i. illustrated the presence of a small number of significantly larger matrix grains. The initial stages of the spheroidisation process are illustrated in Plate ii. where the eutectic carbide has begun to neck down in a number of locations. The development of this sequence also identified in Plate ii. and Plate iii. showes the removal of the small carbide globules formed during necking down and the development of a thin grain boundary layer. It is unclear whether the carbide removal is by dissolution into the matrix or by bulk transfer along the boundary. Following the production of these grain boundaries there appears to be a removal of secondary carbides thereby producing a single constituent matrix. The secondary carbide removal could result from dissolution into the matrix. Plates iv. and v. illustrate the relatively coarse austenitic structure and the dividing grain boundary. It is suggested that it is the development of this grain boundary which resulted in the reduction of toughness.

Appendix Plate i.

Sequence of spheroidising process.

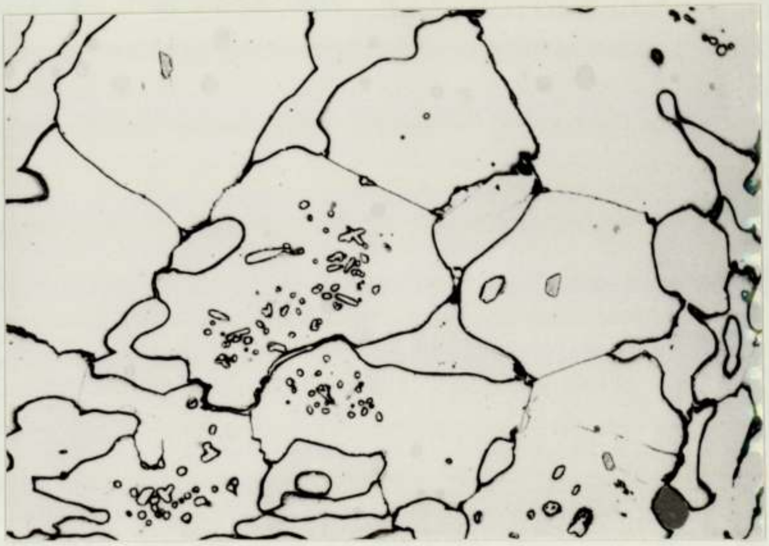

Plate ii

Formation of precipitate free matrix.

Plate iii

Development of carbidic boundry.

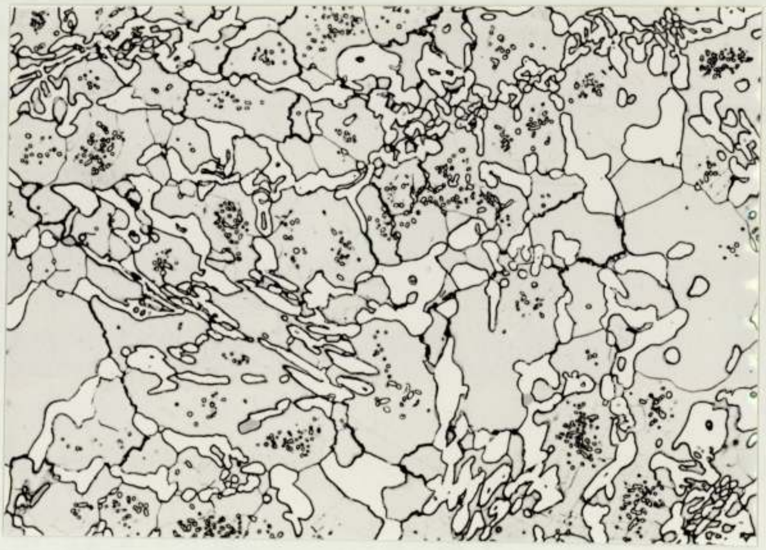

Plate iv

General view illustrating variation in
matrix precipitation.

Plate v.

Breakdown of carbide boundary.

References.

1. Concise Oxford Dictionary. 6th Edition. Oxford University Press-1976.

2. Organisations For Economic Co-operation And Development. Glossary of terms anddefinitions in the field of friction, wear and lubrication. (Tribology) OECD 1969

3. D. Dowson, History of tribology, Longman Group Ltd. 1979.

4. Lubrication (Tribology) Education and Research, D.E.S. Report, 1966 H.M.S.O.

5. J. Halling, Principles of tribology, The MacMillan Press Ltd. 1975.

6. J. T. Burwell, Survey of possible wear mechanisms, Wear, 1957 (1) 119-141.

7. N.P. Suh, The delamination theory of wear, Wear, 1973 (25) 111-124.

8. E. Rabinowicz, Friction and wear of materials, John Wiley and Sons, 1965.

9. J. F. Archard, Contact and rubbing of flat surfaces, Journal of Applied Physics, 1953 (24) 981-988

10. A.E.Miller, Wear in steels, Journal of Materials, 1983 (35) 56-62.

11. J.F. Archard and W. Hirst. The wear of metals under unlubricated conditions, Proc. R. Soc., 1956 (A236) 397-410.

12. C.N.Rowe, Some aspects of the heat of absorption in the function of a boundary lubricant, Trans. Am. Soc. Lub. Engineers, 1966 (9) 100-111.

13. Abrasive Wear - J.965. Report of Iron and Steel Technical Committee 1966 S.A.E. New York.

14. H.S. Avery, The measurement of wear resistance, Wear, 1961 (4) 427.- 429.

15. A. Palmgren, Ball and roller bearing engineering, S.K.F. IndustrialCorp 3rd. Ed. 1959. Philadelphia.

16. M.H. Jones and D,Scott, Industrial tribology - The practical aspects of friction, lubrication and wear, Elsevier Scientific Publishing Co. 1983.

17. R.G.Bager and R.A.Schumacher. On the significance of surface fatigue in sliding wear. Wear, 1968 (12) 173-183.

18. R.G.Bayer. W.C. Clinton. C.W. Nelson and R.A. Schumacher. Engineering model for wear, Wear, 1962 (5) 378-391.

19. R.G.Bayer and T.C. Ku, Analytical design for wear, Plenum, New York 1964.

20. J.G.A. Bitter. A study of erosion phenomena, Wear, 1963 (6) 51-69.

21. I.A. Bucklow and M.Cole, Spark Machining, Metallurgical Reviews, 1969 (14) No. 135.

22. Metals Handbook Volume 3, Machining. 8th Ed. A.S.M. 1967 Metals Park, Ohio.

23. N.P. Suh, An overview of the delamination theory of wear, Wear, 1977 (44) 1-16

24. I.R. Sare, Repeated impact-abrasion of ore-crushing hammers. Wear, 1983 (87) 207-225.

25. K.C. Ludema, Wear debris as an indicator of valid simulation in wear tests, A.S.T.M. S.T.P. 615. Selection and use of wear tests for metals. R.G.Bayer Editor 1976 102-109.

26. R.G.Bayer, As above, 110-111.

27. Private communication.

28. H.Hocke wear resistant lining materials for steelwork chutes. Tribology in Iron and Steel Works. ISI Publication 125. 1970, 17-22.

29. T.E.Norman and C.M. Loeb, Wear tests on grinding balls. American Institute of Mining and Metallurgical Engineers 1948 (176) 490-526.

30. F. Borik, Rubber wheel abrasion test, S.A.E. Combined National Farm, Construction and Industrial Machinery and Powerplant Meetings. Milwaukee U.S.A. Sept. 14 -17 1970.

31. R.D. Haworth JR., The abrasion resistance of metals, Trans. A.S.M. 1949 (41) 819-854.

32. H.S. Avery, Surface protection against wear and corrosion, A.S.M. Monograph 1954 Chapter 3 22-24.

33. F. Borik, Using tests to define the influence of metallurgical variables on abrasion, Metals Engineering Quarterly 1972.

34. D.E. Diesburg and F. Borik, Optimising abrasion resistance and toughness in steels and irons for the mining industry. Vail, Colorado 1974 Symposium - Materials for the Mining Industry. 15-41.

35. Standard practice for conducting dry sand/rubber wheel abrasion tests, A.S.T.M. G 65-80.

36. J. Muscara and M.J. Sinnott, Construction and evaluation of a versatile abrasive wear testing apparatus. Metals Engineering Quarterly 1972 (2) 21-32.

37. F. Borik, and D.L. Sponseller, Gouging abrasion test for materials used in ore and rock crushing. Part 1. Description of the test, Journal of Materials 1971 (6) 576-589.

38. H. Hocke and N.H. Wilkinson, Testing abrasion resistance of slurry pipeline materials, Tribology International 1978 (11) 289-294.

39. J.W. Boyes, Development and use of abrasion testing at B.C.I.R.A., B.C.I.R.A. Journal 1967 (15) 572 - 585.

40. R.W.Durman, Basic metallurgical concepts and the mechanical testing of some abrasion resistant alloys. Foundry Trade Journal 1973 (134) 645 - 651.

41. R. Blickensderfer and J.H.Tylczak, A large scale impact spalling test, Wear 1983 (84) 361-373.

42. J.C. Farge and G.A. Barclay, Properties and performance of cast iron grinding balls, As (34)

43. B.A. Baldwin, Comparison of wear measurements between four ball and Falex wear test machines, Wear 1984 (93) 233-234.

44. A.W.J. de Gee, Comments on above, Wear 1984 (96) 99

45. M.M. Kruschov and M.A. Babichev, Resistance to abrasive wear of structurally in homogeneous materials, Friction Wear Mach. 1958 (12) 5.

46. M.M. Kruschov, Resistance of metals to wear by abrasion as related to hardness, Proc. Int. Conf. Lubrication and Wear. Institution of Mech. Engineers, London 1957.

47. K-H, Zum-Gahr, Abrasive wear on Metallic materials. Proc. Conf. Metallurgical Aspects of Wear. West Germany 1979.

48. Abrasive wear in steel castings. S.C.R.A.T.A. Journal of Research 1983 (63) 69 - 78.

49. N.C.Welsh, The dry wear of steels, Phil. Trans. Roy. Soc. 1965 (257) 31 - 70.

50. A.J.Bedford, A.L.Wingrove and K.R.L. Thompson. The phenomenon of adiabatic shear deformation. Journal Australian Institute of Metals, 1974 (19) 61-73.

51. K - L. Hsu, T.M. Ahn and D.A. Rigney, Friction, wear and microstructure of unlubricated austenitic stainless steels, Wear 1980 (60) 13 - 37.

52. H.N. Farmer, Factors affecting selection and performance of hard facing alloys, As (34) 85-91.

53. R.J.Dawson, S. Shewchuck and J.E. Pritchard, Selection and use of hard facing alloys, Intermountain Minerals Symposium. Vail Colorado 1982 109-120.

54. A.J.Hick, Heat treatment - the present position and future outlook, Metallurgia 1979 (46) 47 - 62.

55. A.J. Hick, Advantages in surface heat treatment processes. The Metallurgist and Materials Technologist 1983 325-330.

56. H.C. Child, S.A. Plumb and G.Reeves. The effect of thermochemical treatments on the properties of tool steels. Materials and Design 1983 (4) 681 - 686.

57. As (56) 1983 (4) 716 - 722.

58. J. Tasker, Austenitic Manganese steel-fact and fallacy. As (53) 3 - 20

59. J. Tasker, Austenitic manganese steel-fact and fallacy. S.C.R.A.T.A. Proc. 28th Annual Conference 1983 paper 15.

60. A. Ball. On the importance of work hardening in the design of wear-resistant materials, Wear 1983 (91) 201 - 207.

61. A.W.J. de Gee, Comments on resistance of pure metals to low stress abrasive wear, Wear 1982 (81) 373 - 374.

62. K. Bhansali and A.E.Miller, Resistance of pure metals to low stress abrasive wear. Wear 1981 (71) 375-379.

63. R.W.K. Honeycomb Steels-microstructure and properties. Edward Arnold 1981.

64. H.T. Angus. Cast iron -- physical and mechanical properties, Butterworths 1976.

65. F.D. Tabor, Moh's hardness scale - a physical interpretation Proc. Phy. Soc. 1954 (67) 249 - 257.

66. R.C.D. Richardson, The wear of metals by hard abrasives. Wear 1967 (10) 291 - 309.

67. P.S. Lane. Trans. Am. Foundrymans Assoc. 1937. (45) 157-199.

68. E.K.Smith. Cast iron cylinder bores. Observations on microstructure, composition, hardness and wear. Trans. Am. Foundrymans Assoc. 1940 (48) 667 - 722.

69. P.C. Nautigal, S. Singhal and J.P. Sharma, Friction and wear processes in piston rings, Tribology International 1983 (16) 43 - 49.

70. V.S.R. Murthy, M.E. Kishore and S. Seshan, Properties of cast iron with compacted graphite. The British Foundryman 1985 (78) 71 - 77.

71. P.A. Blackmore, High strength nodular irons. B.C.I.R.A. Conference, Development for future foundry prosperity. 2 - 4 April 1984. paper 14.

72. J. Dodd and R.B. Gundlach, Advances in process technology and new applications of austempered ductile irons. As (71) Paper 15.

73. R.Q.Barr and J.F. Janowak, Austempered nodular cast irons. Molybdenum Mosaic 1982 (5) 3, 1 - 4.

74. J.F. Janowak and R.B. Gundlach, Development of a ductile iron for commercial austempering, Transactions of the American Foundrymen's Society. 1983 (86) 377 -388.

75. R.H.T. Dixon, Ni - Hard grinding balls far outlive steel. Engineering 1960 (190) 598-599.

76. Wear of nickel-chromium martensitic white irons. International Nickel Co. Ltd., 1965.

77. P.J. Provios, Nickel-chromium white irons for abrasion service, Canadian Mining and Metallurgical Bulletin. 1965 (58) 923 - 930.

78. R.H.T. Dixon, Some effects of heat treatment upon the impact fatigue life of Ni - Hard grinding balls. J.I.S.I. 1961 (197) 40-48.

79. A.J.Rickard, Ni-Hard cast iron an improved material for grinding media, Engineer, 1964 (217) 559-561.

80. N.F. Fiore, J.P.Coyle, S.P. Udvardy, T.H. Kosel and W.A. Konkel, Abrasive wear-microstructural interactions in a nickel-chromium white iron, Wear 1980 (62) 387-404.

81. Bradley and Foster Ltd. Unpublished communication 1985.

82. K - H. Zum Gahr, Abrasive wear of white cast irons, Wear 1980 (64) 175 - 194.

83. R.W.Durman, Abrasion resistant cast iron, British Foundryman 1979 (72) 159 - 163.

84. J.K. Fulcher, T.M. Kosel and N.F. Fiore, The effect of carbide volume fraction on the low stress abrasion resistance of high Cr - Mo white cast iron, Wear 1983 (84) 313 - 325.

85. J.D.Watson, P.J. Mutton and I.R. Sare, Abrasive wear of white cast iron, Metals Forum 1980 (3) 74 - 88.

86. P. Hurricks, Wear resistance of steels, Wear 1973 (26) 285 - 304.

87. I.R. Sare, Abrasion resistance and fracture toughness of white cast iron, Metals Technology 1979 (6) 412-419.

88. S.V. Prasad and T.H. Kosel, A study of carbide removal mechanisms during quartz abrasion. I. In situ scratching test studies, Wear 1983 (92) 253-268.

89. S.V. Prasad and T.H. Kosel, A study of carbide removal mechanisms during quartz abrasion. II. Effect of abrasive particle shape, Wear 1984 (95) 87-102.

90. B. Lawn and R.Wilshaw. Review, indentation fracture: principles and applications, Journal of Materials Science 1975 (10) 1049-1081.

91. B. Lawn and E.R. Fuller, Equilibrium penny-like cracks in indentation fracture, Journal of Materials Science 1975 (10) 2016-2024.

92. A.G.Evans and R.Wilshaw, Quasi-static solid particle damage in brittle solids, I, observations, analysis and implications, Acta Metallurgia 1976 (24) 939-956.

93. B. Lawn and M.V. Swain, Microfracture beneath point indentations in brittle solids, Journal of Material Science 1975 (10) 113-122.

94. B. Lamy, Effect of brittleness index and sliding speed on the morphology of surface scratching in abrasive or erosive processes. Tribology International 1984 (17) 35 - 38.

95. J.M. Bereza, Wear and impact resistant white cast irons. Institute of British Foundrymen 1981 (74) 205-211.

96. R.B. Gundlach, Microstructural, hardness and abrasion resistance of as-cast 17.5% chromium white irons, A.F.S. Transaçtions 1974 (82) 309-316.

97. J.T.H. Pearce, Abrasive wear behaviour of alloy cast irons. Institute of British Foundrymen 1985 (78) 13 - 23.

98. R. B. Gundlach and J.L.Parks. Influence of abrasive hardness on the wear resistance of high chromium irons. Wear 1978 (46) 97 - 108.

99. R.H. Sailors and J. Owens, Cast high chromium media in wet grinding. Intermountain Minerals Symposium Vail, Colorado, August 1982 53-61.

100. Collapse of US 35 Highway Bridge, Point Pleasant West Virginia. NTSB Report No. NTSB-Har-71-1 Dec. 1967.

101. T.Bishop, Fatigue and the Comet disasters. Metal Progress 1955 May 79 - 85

102 C.F.Tipper, The brittle fracture story, Cambridge University Press. New York 1962.

103. A.A. Griffith, The phenomena of rupture and flow in solids. Trans. Royal Soc. London 1920 A - 221.

104. C.E. Inglis. Stress in a plate due to the presence of cracks and sharp corners. Proc. Institute of Naval Architects, 1913, (80)

105. G.R.Irwin, Fracturing dynamics, Fracturing of Metals, A.S.M. Cleveland 1948.

106 E.Orowan 'Fracture strength of solids' Report on progress in physics V.12 Physical Society of London 1949.

107. C.P. Paris and G.C.Sih, Stress analysis of cracks, Fracture toughness testing and its applications, A.S.T.M. S.T.P. 381 Philadelphia 1965.

108. J.T.Barnby, An introduction to fracture mechanics, N.D.T. 1971 Dec. 385-390.

109. J.T. Barnby. Toughness and critical defects size. N.D.T. 1972 Feb. 32-37.

110. A.A. Wells. Unstable crack propagation in metals-cleevage and fast fracture. Cranfield crack propagation symposium, 1961, Sept. 210.

111. D.S. Dugdale. Yielding of steel sheets containing slits. J. Mech. Phys. Solids 1960 (8) 100 - 104.

112. J.E. Rice. A path independent integral and the approximate analysis of strain concentration by notches and cracks. J. of Applied Mech. Trans. ASME 1968 June.

113. J.D. Landes and J.A. Begley. Test resulst from J - integral studies: An attempt to establish a J_{IC} testing procedure. Fracture Analysis A.S.T.M. S.T.P. 560 1974 170-186.

114. ASTM E 813-81. Standard test method for J_{IC}, a measure of fracture toughness. A.S.T.M. Publications Philadelphia.

115. A.S.T.M. E.561-81. Standard practice for R-curve determination. A.S.T.M. Publications Philadelphia.

116. S.R.Novak. Resistance to plane-stress fracture (R-curve behaviour) of A.572 steel. A.S.T.M. S.T.P. 591.

117. R.E. Heyer and D.E. McCabe. Plane stress fracture toughness testing using a crack line loaded specimen. Eng. Frac. Mech. 1972 (4) 393-412.

118. R.E. Heyer and D.E. McCabe. Crack growth resistance in plane-stress fracture testing. Eng. Frac. Mech. 1972 (4) 413-430.

119. D.E. McCabe and R.E. Heyer. R-curve determination using a crack line wedge loaded (CLWL) specimen. A.S.T.M. S.T.P. 527 17 - 35.

120. J.C. Newman Nr. A review of chevron notched fracture specimens. A.S.T.M. S.T.P. 855 5 - 31.

121. J. Nakayama. A bending method for direct measurement of fracture energy of brittle materials Japanese Journal of Applied Physics 1964 (3) 422 - 423.

122. J. Nakayama. Direct measurement of fracture energies of brittle heterogeneous materials. Journal of the American Ceramic Society 1965 (43) 583 - 587.

123. H.G. Tattersall and G. Tappin. The work of fracture and its measurement in metals, ceramics and other materials. Journal of Material Science 1966 (1) 296 - 301.

124. L.P. Pook. An approach to a quality control K_{IC} testpiece. Int. Journal of Fracture Mechanics 1972 (8) 103-104.

125. J.I. Bluhm. Slice synthesis of a three dimensional 'work of fracture' specimen. Engineering Fracture Mechanics 1975 (7) 593-604.

126. D. Munz, R.T. Bubsey and J.E. Stawley. Compliance and stress intensity coefficient for short bar specimens with chevron notches. Int. Journal of Fracture 1980 (16) 359 - 374.

127. L.M. Barker. A simplified method for measuring plane strain fracture toughness. Engineering Fracture Mechanics 1977 (9) 361 - 369.

128. L.M. Barker. Short bar specimens for K_{IC} measurements in Fracture mechanics applied to brittle materials. Proceedings of the 11th national symposium on fracture mechanics. Ed. S.W. Freiman A.S.T.M. S.T.P. 678 1979.

129. L.M. Barker, Development of the Fractometer II system for fracture toughness testing using short rod and short bar specimens. Terratek report TR 79 - 32.

130. L.M. Barker. Theory for determining K_{IC} from small non - LEFM specimens, supported by experiment on aluminium. Terratek Report TR 78 - 6R. Aug. 1978.

131. J.T. Ryder, G.F. Bowie and D.E. Pettit. Recent considerations in experimental compliance calibration of the WOL specimen. Engineering Fracture Mechanics 1977 (9) 901 - 923.

132. S.B. Biner, J.T. Barnby, D.W.J.Elwell. On the use of short-rod/bar test specimens to determine the fracture toughness of metallic materials. Int. Journal of Fracture 1984 (26) 3 - 16.

133. R.T. Bubsey. D. Munz. W.S. Pierce and J.L.Shannon Jr. Compliance calibration of the short rod chevron-notch. Int. Journ. of Fracture 1982 (18) 125-133.

134. J.C. Newman JR. A review of chevron notched fracture specimens. Chevron notched specimens. Testing and stress analysis. A.S.T.M. S.T.P. 855. J.H. Underwood. S.W. Freiman and F.I. Baratta. A.S.T.M. Philadelphia 1984 5 - 31.

135. L.M. Barker. The Fractometer II Systems 4210 and 4211 Owner's Manual. Terratek. Saltlake City Utah. U.S.A.

136. L.M. Barker. Specimen size effects in short-rod fracture toughness measurements. As 135 117 - 133.

137. D. Munz, R.T. Budsey and J.L. Shannon Jr. Performance of chevron notch short bar specimen in determining the fracture toughness of silicon nitride and aluminium oxide. J. Testing and Eval. 1980 (8) 103 - 107.

138 B.C.I.R.A. Broadsheet No. 1. Which Cast Iron. 1985. B.C.I.R.A. Alvechurch, Birmingham.

139. G.N.J. Gilbert. The fracture toughness properties of cast irons: a review. B.C.I.R.A. Report 1446 Nov. 1981.

140. A.G.Glover and G. Pollard. The brittle fracture of grey cast irons. In: Fracture, proceedings of the second International Conference on fracture, Brighton. April 1969, Paper 29 350 - 359.

141. A.G. Glover and G. Pollard. Effect of microstructure on the fracture toughness of grey cast iron. In: Iron and Steel Institute Fracture toughness of high strength materials; theory and practice. London ISI, 1970 90 - 94 ISI publication 120.

142. E. Hornbogen and J.M.Motz. Fracture toughness of grey cast irons. A.F.S. International Cast Metals Journal. 1977 (2) No. 4 31 - 31.

143. T.J.Baker. The fracture resistance of flake graphite cast iron Materials in Engineering Applications 1978 (1) No. 1. 13 - 18.

144. L. Gruter. Crack propagation in cast iron. Thesis Doktor-Ingenieur. Ruhr - University. Bochum 1975.

145. L. Gruter. Prediction of fracture toughness for cast iron alloys. Material Science and Engineering. 1978 (35) 157 - 164.

146. L. Gruter. Fracture toughness of cast iron with flake graphite. Giessereiforschung. 1977 (29) 47 - 57.

147. G.N.J. Gilbert. Fracture toughness data available on cast irons - an essessment. B.C.I.R.A. Report No. 1469 May 1982.

148. D.K.Verma and J.T. Berry Modeling thefracture behaviour of pearlitic grey irons. A.F.S. Transactions. 1981 (93) 849 - 856.

149. W.L. Bradley. Toughness properties of nodular iron. Journal of Metals 1985 January 74 - 76.

150. A. Lazaridis and C.R. Loper. Fracture toughness of ductile cast irons. Trans A.F.S. 1971 (79) 351 - 360.

151. R. K. Nanstad. F. J. Worzala and C.R. Loper. Fracture toughness testing of nodular cast irons. Trans. A.F.S. 1974. (82) 473 - 486.

152. R.K. Nanstad, F.J. Worzala andC.R. Loper. Static and dynamic toughness of ductile cast iron. Trans A.F.S. 1975. (83) 245-256.

153. S.R. Holdsworth and G. Jolley. Fracture toughness tests on pearlitic spheroidal graphite cast iron. British Foundryman 1974 (67) No. 3. 77-82.

154. S.R. Holdsworth and G. Jolley. The influence of graphite nodule number and volume fraction on the fracture toughness of ferritic nodular cast iron In: The Metallurgy of Cast iron: proceedings of the second international symposium Geneva. May 1974. St. Saphorin, Switzerland. Georgi 1975, 809-825.

155. S. R. Holdsworth and G. Jolley. The fracture toughness of pearlitic and ferritic spheroidal graphite cast iron. British Foundryman 1975 (68) No. 6. 169 - 172.

156. K. E. Mckinney. W.L. Bradley and P. C. Gerhardt. Jnr. A comparison of the fracture toughness of ductile iron to cast steel using a modified Charpy test specimen. Trans. A.F.S. 1984.

157. J.O.T. Adewara and C.R. Loper Jr. Crack initiation and propagation in fully ferritic ductile iron. Trans. A.F.S. 1976 (84) 527 - 534.

158. T. Luyendijk and H. Nieswaag. Crack growth and fracture toughness in nodular cast iron. Solidification Technology in the Foundry and Casthouse. The Metals Society, University of Warwick Sept. 1980 Paper 86.

159. R. K. Nanstad, F.J. Wrozala and C.R. Loper Jr. Static and dynamic toughness of ductile cast iron. Modern Castings 1975 (65) 58

160. P.A. Blackmore. The fracture toughness testing of some normalised and austempered nodular irons - a progress report B.C.I.R.A. 1587 July 1984.

161. L. Bingzhe and B.L. Averbach. The effects of heat treatment on fracture toughness and fatigue crack growth rates in 440°C and BG 42 steels. Met. Trans. A. 1983 (14A) 1899 - 1906

162. D.E. Diesburg. Fracture toughness test methods for abrasion-resistant white cast irons using compact specimens. Fracture toughness and slow stable cracking, ASTM STP 559, American Society for Testing and Materials, 1974, 3 - 14.

163. P.A. Blackmore. The fracture-toughness testing of abrasion-resistant white cast irons - a progress report B.C.I.R.A. Journal 1984, Jan. 36 - 43 Report No. 1562.

164. K. H. Zum Gahr and W.G. Scholz. Fracture toughness of white cast irons. Journal of Metals 1980 (32) 38 - 44.

165. S.B. Biner. The effect of metallurgical variables on the mechanical properties of high chromium iron. PhD. Thesis. University of Aston 1979.

166. R.W.Durman. Fracture toughness of a series of high chromium abrasion resistant alloy. Ph.d. Thesis. University of Aston in Birmingham 1970.

167. Kraft. Applied materials research 1964 April 88-91.

168. F. Maratray. Choice of appropriate compositions for chromium-molybdenum white irons. A.F.S. Transactions 1971 (79) 121 - 124.

169. K.H. Zum Gahr and D.V. Doane. Optimizing fracture toughness and abrasion resistance in white cast irons. Metallurgical Transactions A. 1980 (11A) 613-620.

170. I. Katavic. White cast irons with improved properties of toughness and abrasion resistance. International Foundry Congress. Lisbon June 1984 paper 16.

171. G.L.F. Powell and L.S. Heard. Misinterpretation of microstructure in wear resistant alloy white irons.

172. K. Selby. Fracture toughness principles applied to steel castings. Proceedings of 1980 Annual S.C.R.A.T.A. Conference. Paper 4.

173. W.J. Jackson and J.C. Wright. Fracture toughness approach to steel castings quality assurance. Metals Technology. 1977. September 425 - 433.

174. B.C.I.R.A. Broadsheet 235. Fracture mechanics - its relevance to cast iron design stresses. B.C.I.R.A. Alvechurch 1985.

175. E. Hornbogen. The role of fracture toughness in the wear of metals. Wear 1975 (33) 251-259.

176. K. H. Zum Gahr. Relation between abrasive wear rate and the fracture toughness of metallic materials. Z. Metallkde 1978 (69) 643-650.

177. A. G. Atkins. Toughness in wear and grinding Wear 1980 (61) 183 - 190.

178. F. T. Barwell. The contribution of particle analysis to the study of wear of metals. Wear 1983 (90) 167 - 181.

179. D. Andarelli, D. Mavgis and R. Courtel. Observation of dislocation created by friction on aluminium thin foils. Wear 1973 (23) 21 - 31.

180 A. R. Rosenfield. A dislocation theory approach to wear. Wear 1981 (72) 97 - 103.

181. J. P. Scholes. The selection and use of cast irons. Engineering Design Guides No. 31. Oxford University Press 1979.

182. R. Barton. Special cast irons. B.C.I.R.A. Journal 1960 (8) 857 - 882. Report No. 576.

183. R. W. Durman. The application of alloyed white cast irons in crushing, grinding and materials handling processes. British Foundryman 1976 (69) 141 - 149.

184. K. Eriksson. Fracture toughness of hard high speed steels, tool steels and white cast irons. Scandinavian Journal of Metallurgy. 1973 (2) 197 - 203.

185. G.L.F. Powell. Morphology of eutectic M_3C and M_7C_3 in white iron castings. Metals Forum. 1980 (3) No. 1 37 - 46.

186. J. Dodd and D.J. Dunn, High chromium - molybdenum alloy irons for the mining industry. Casting Engineering. 1978 Winter 25 - 32.

187. U.S. Patent 1,245,552,1917.

188. W. Fairhurst and K. Rohrig. Abrasion resistant high chromium white cast irons. Foundry Trade Journal. 1974. (136) 685 - 698.

189. Metals Handbook, 9th Ed. Volume 1. Properties and selection: Irons and Steels. A.S.M. Publications.

190. Engineering properties and applications of Ni-Hard 1978 Inco Durope Ltd. 4th Ed.

191. Abrasion resistant castings for handling coal. Casting Engineering 1978 (10) 14 - 19.

192. T. E. Norman, A. Soloman and D.V. Doane. Martensitic white irons for abrasion resistant castings. Trans A.F.S. 1959 (67) 242 - 256.

193. W. Fairhurst. Chromium - molybdenum white cast irons for abrasive applications. B.C.I.R.A. Journal 1980. 503 - 510 Report No. 1010.

194. B.S. 4844 June 1974. Specification for abrasion resisting white cast irons.

Part 1: Unalloyed and low alloy grades.
Part 2: Nickel-chromium grades.
Part 3: High chromium grades.

British standards Institution, 2 Park St. London.

195. A.S.T.M. A.532 - 80. Standard specification for abrasion resistant cast iron. A.S.T.M. Publications Philadelphia.

196. R. Barton. The influence of alloying elements in cast iron. B.C.I.R.A. Journal. 1960 (8) 567 - 585 Report No. 559.

197. R.M. Kotschi and C.R. Loper. How master and tramp elements affect the structures of cast iron. Metals Progress. 1978. October. 64 - 67.

198. B.C.I.R.A. Broadsheet 26. Additions of chromium to cast iron. B.C.I.R.A. Alvechurch. Birmingham 1971.

199. R.S. Jackson. Metallurgical and production aspects of high chromium cast irons for abrasion resisting applications. British Foundryman. 1974 (67) Feb. 34 - 41.

200 T. Murakami. Tech. Rep. Tokoku. University 1930 (3) 59 - 99.

201. A. Westgren, G. Phragmen and T. Negresco. On the structure of the iron - chromium - carbon system. J.I.S.I. 1928 (117) No. 1 383 - 400.

202. W. Tofaute. C. Kuttner and A. Buttinghaus. Das system Eisen - Chrom - chromkarbid $Cr_7 C_3$ - sementit. Arch. Eisenh. 1935 - 6. (9) 607 - 617.

203. A. B. Kinzel andW. Crafts. The alloys of chromium. Vol. 1. 1937 McGraw-Hill.

204. K. Bungardt. E. Kunze and E. Horn. Untersuchaungenuber den Aufbau des systems Eisen-Chrom-Kohlenstoff. Arch. Eisenh. 1958 (29) 193 - 203.

205. N. R. Griffing, W.D. Forgeng and E. W. Healy. C - Cr - Fe liquidus surface. Trans A.I.M.E. 1962 (148) 148 - 159.

206. R. S. Jackson. The austenite liquidus surface and constitutional diagram for the Fe-Cr-C metastable system. J.I.S.I. 1970 Feb. 163 - 167.

207. M. Hansen. Constitution of binary alloys. 2nd Ed. 1958 McGraw-Hill.

208. R. L. Woodyatt and G. Krauss. Iron - chromium - carbon system at 870°C. Metallurgical Transactions A 1976 (7A) 983 - 989.

209. R. Lundberg. M. Waldenstrom and B. Unrenius. Calphad. 1977 (1) No. 2. 159.

210. F. Maratray. Alloyed abrasion and wear resisting white irons. B.C.I.R.A. Foundry Technology for the 80's. Proc. Conf. April 1979 Paper 7.

211. T. Okamoto, S. Matsuo and K. Kishitake. Dendrite arm spacings in iron - carbon - chromium alloys. Trans. Iron and Steel Institute of Japan 1978 (18) No. 5 289 - 295.

212. H. Fredriksson and B. Remaeus. The solidification and transformation process in white, high chromium cast irons. 44th International Foundry Congress. Firenze 11 - 14 Sept. 1977.

213. J. D. Hunt and K. A. Jackson. Binary eutectic solidification. Trans. Met. Soc. A.I.M.E. 1966 (236) 843 - 852.

214. G. A. Chadwick. Metallography of phase transformations. Butterworths. 1972.

215. P. Dupin, J. Saverna and J. M. Schissler. A structural study of chromium white cast irons. A.F.S. Transactions 1982 (154) 711 - 718.

216. J. D. B. De Mello. M. Durand-Charre and S. Hamar-Thibault. Solidification and solid state transformation during cooling of chromium-molybdenum white cast irons. Metallurgical Transaction A. 1983 (14A) 1793 - 1801.

217. J. Dodd and R.S. Jackson. High chromium cast irons for crushing and grinding machinery. Metallurgia 1967 (76) Sept. 107 - 110.

218. F. Maratray and R. Usseglio-Nonot. Factors affecting the structure of chromium and chromium-molybdenum white irons. Climax Molybdenum Publication.

219. F. Maratray and R. Usseglio-Nonot. Atlas. Climax Molybdenum Publication.

220. B.C.I.R.A. Broadsheet 63. Properties of high chromium cast irons. B.C.I.R.A. Alvechurch. Birmingham.

221. W. A. Johnson and R.F. Mehl. Reaction kinetics in processes of nucleation and growth. Trans A.I.M.E. 1939 (135) 416 - 441.

222. R. W. Christian. Physical Metallurgy. Chapter 10. Phase Transformations. Ed. by R. W. Cahn. North Holland Publishing Co. 1965.

223. R.D. Doherty. Physical Metallurgy. Part 2. Chapter 14. Phase Transformations, Diffusive. Ed. by R.W. Cahn and P. Haasen. North Holland Physics Publishing 1983.

224. Patent specification No. 1218981. Grinding members and steels therefor. 13 Jan. 1977.

225. R. L. Miller. Volume fraction analysis of phases in textured alloys. Trans. A.S.M. 1966 (61) No. 3 592 - 597.

226. C. Kim. X-ray method of measuring retained austenite in heat treated white cast irons. J.Heat Treatment 1979 (1) 43.

227. R. Fillit. H. Bruyas, F. Maratray and A Poulation. Measurement of austenite content in various textured alloys. Private Communication.

228. D. F. LaCount. A production technique for measurement of retained austenite in abrasion resistant irons. A. F.S. Technical Report No. 8001 March 1980.

229. F. Maratray and A. Poulation. Austenite retention in high chromium white irons. A.F.S. Trans. 1982 (27) 795 - 804.

230. J. L. Parks. Characteristics of as-cast and subcritically heat treated high-chromium-molybdenum white irons for thick section castings. Climax. Moly. Publication M-358.

231. G.B. Olsen and M. Cohn. J. Less-Common Metals. 1972 (28) No. 107.

232. H. Onodera. H. Goto and I. Tamura. Suppl. Trans. Japan Inst. Metals 1976 (17) 327.

233. H. Onodera and I. Tamura. Proc. US - Japan Symp. on Mechanical behaviour of metals and alloys associated with displacive transformations. 1979. Rensselaer Polytechnic Inst. Troy. N.Y.

234. G.B. Olsen and M. Cohen Metallurgical Transactions 1976 (7A) 7, 1897, 1905, 1915 - 23. A general mechanism of martensitic Nucleation - Part I General concepts and the FCC - MCP transformation.

235. V.G. Rivlin. Critical review of constitution of carbon-chromium-iron andcarbon-iron-manganese systems. International Metallurgical Reviews. 1984 (29) No. 4 299 - 327.

236. International Patent Application (P.C.T.) Abrasive Resistant White Cast Irons. International Publication No. WO84/00385.

237. W. W. Cias. Austenite transformation kinetics and hardenability of heat treated 17.5% chromium white irons. A.F.S. Transactions 1974 (82) 317 - 328.

238. S. E. Klein. Effect of alloy additions on the hardenability of 12.5% chromium white cast irons. Unpublished work, Climax Molybdenum Co. 1971.

239. J. Dodd and C.E. Gouin. Making abrasion resistant irons. Foundry Management and Technology. 1974. July 102 - 105.

240. I.I. Typsin. M. E. Garber and E.V. Razhava. Hardenability of wear resistant Cr-Mn-Mo cast iron. Translated from Metallovedenie i Terricheskays Obrabot Ra Metallov. 1970 62 - 64.

241. DIN 1695 September 1981. Verschleißbestondiges legiertes Gußeisen.

242. J. Dodd and J.L. Parks. Factors affecting the production and performance of thick section high chromium-molybdenum alloy iron castings. Met Forum 1980 (3) 3-27

243. S. Parent and J.C. Margerie. mechanical properties and wear resistance of white cast irons. A.F.S. Transactions. 1972. 393 - 400.

244. D. M. Stefanescu and S. Craciun. Abrasion resistant cast irons alloyed with chromium and vanadium. 42nd International Foundry Congress. Lisbon 1975.

245. J.V. Dawson. Vanadium in cast iron. B.C.I.R.A. Journal 1982 87 - 102. Report No. 1457.

246. Yu. A. Shulte and M. N. Berkun. Influence of alloying and additive treatments on the properties of high chromium alloys. Russian Casting Production.

247. B.C.I.R.A. Broadsheet 54. Essential features of the production of high chromium cast irons. B.C.I.R.A. Alvechurch. Birmingham.

248. G.A.Fisher and J.H.Woodling. Electric furnace melting and production of abrasion resistant steels and irons. 21st Annual Electric Furnace Conference, Chicago. December 4 1963.

249. Ultrahard materials in industry, machining with Amborite. DeBeers Industrial Diamond Division.

250. D.W.J. Elwell. Unpublished work. Bradley and Foster Ltd. 1981.

251. W. Fairhurst and K. Rohrig. The use of abrasion resistant high chromium molybdenum cast irons in mineral processing. Mine. and Quarry October & December 1976.

252. From Coal to Steam. Published by the Central Electricity Generating Board, Sudbury House, London.

253. Blue Circle Cement Publication 1971.

254. Fuels and Fuel Technology. Second Ed. W. Francis and M.C. Peters. Pergarmon Press 1980.

255. W. Day. Corrision and erosion effects on materials for slurry pumps. Intermountain Minerals Symposium, Vail, Colorado. Aug. 3 - 6 1982 79 - 82.

256. J. Dodd. High chromium - molybdenum alloy iron rolls.

257. Crushing and Grinding. G.C. Lowrison, Butterworths London 1974.

258. Mineral Processing Technology. B.A. Wills Pergamon Press, Oxford.

259. L. A. Adorjan. Mineral Processing. Mining Annual Review. 1982 239 - 280.

260. J. Dodd. Trends in the production, utilization and development of abrasion - resistant alloys in America.

261. P.C. Kemp. Laminated martensitic white irons, properties and applications.

262. B. J. Davies and D. H. Wilding. A composite approach to reducing abrasive wear. Intermountain Minerals Symposium, Vail, Colorado. 3 - 6 August 1982. 105 - 108.

263. P.C. Kemp. New markets through new products. Proceedings of 1981 Annual S.C.R.A.T.A. Conference. Paper 8.

264. R.J. Dawson, S. Shewchuck and J.E. Pritchard. Selection and use of hardfacing alloys. As 262 109 - 120.

265. Data Sheets on the properties of steel castings BS 3100 BW 10, No. 10 Austenitic Manganese Steel Castings. S.C.R.A.T.A. 1977.

266. Sandvik Cast-in-Carbide. A new material for tough, hard, briutal jobs. Sandvik AB, Sweden 1981.

267. Technical Report. Cemented carbides promote power station efficiency. Materials and Design 1982 (3) 523.

268. L. A. Adorjan Mineral Processing 1980. Mining Annual Review 259 - 300.

269. D. W. J. Elwell. Toughness and abrasion resistance of high alloy cast irons. 2nd Annual progress report University of Aston. 1984.

270 W.H. Duda. Cement data - book. Bouverlag GMbH Berlin 1976

271 J.T.H. Pearce. Private communication 1984.

272 J.T.H. Pearce. Ph.D Thesis University of Aston 1982.

273 A. Inoue and T. Masumoto. Carbide reactions (M_3C->M_7C_3->$M_{23}C_6$->M_6C) during tempering of rapidly solidified high carbon Cr-W and Cr-Mo steels. Metallurgical Transactions. 1980 (11A) 739 - 747.

274. C.J.Smithells (Ed) Metals Reference Book, Butterworths, London 5th Ed. 1976.

275 K. Rohrig. Annual Review - White cast iron and roll castings, 1977. Climax Molybdenum Publication.

276. C. Zener and J.M. Hollomon, Effect of strain rate upon plastic flow in steel. J. Appl. Phys. 1944 (15) 22-32

277 A. L. Wingrove, A note on the structure of adiabatic shear bands in steel. J. Aust. Inst. Met. 1971 (16) 67 - 70.

278 D. M. Turley, The nature of the white etching surface layers produced during reaming ultra-high strength steel. Mater. Sci. Eng. 1975 (19) 79 - 86

279 D. Aspinwall, Superhard tooling ten years on Metallworking Production 1984 Nov. 90-98.

280 Anon, Machining abrasion resistant cast irons with Amborite. Casting Engineering and Foundry World 1983 (Fall) 30-39.